

UNIVERSITY OF CALIFORNIA, MERCED

Simulating X-ray spectroscopy using mean-field and correlated many-body theories

DISSERTATION

submitted in partial satisfaction of the requirements
for the degree of

DOCTOR OF PHILOSOPHY

in
Chemistry

by

Abdulrahman Y. Zamani

Dissertation Committee:
Professor Hrant P. Hratchian, Advisor
Professor Aurora Pribram-Jones, Chair
Professor Liang Shi
Professor Lin Tian

2023

Chapters 2 and 4 © 2022-2023 AIP Publishing LLC
Other Chapters © 2023 Abdulrahman Y. Zamani

The dissertation of Abdulrahman Y. Zamani is approved, and it is acceptable in quality and form for publication on microfilm and electronically:

Professor Hrant P. Hratchian, Advisor

Professor Aurora Pribram-Jones, Chair

Professor Liang Shi

Professor Lin Tian



University of California, Merced
Department of Chemistry and Biochemistry
Center for Chemical Computation and Theory

Simulating X-ray spectroscopy using mean-field and correlated many-body theories

Abdulrahman Y. Zamani

Advisor **Professor Hrant P. Hratchian**
Department of Chemistry and Biochemistry
University of California, Merced

Chair **Professor Aurora Pribram-Jones**
Department of Chemistry and Biochemistry
University of California, Merced

Reviewer **Professor Liang Shi**
Department of Chemistry and Biochemistry
University of California, Merced

Reviewer **Professor Lin Tian**
Department of Physics
University of California, Merced

November 30, 2023

Abdulrahman Y. Zamani

Simulating X-ray spectroscopy using mean-field and correlated many-body theories

Dissertation, November 30, 2023

Advisor: Professor Hrant P. Hratchian

Reviewers: Professor Aurora Pribram-Jones, Professor Liang Shi, & Professor Lin Tian

University of California, Merced

Department of Chemistry and Biochemistry
Center for Chemical Computation and Theory
5200 Lake Rd
Merced, CA
95343

Abstract

X-ray spectroscopy provides a great deal of information for analyzing reactivity and characteristic properties of matter by probing the interactions of molecules with their local chemical environment. The nature of core orbitals and elemental specificity of core-level transitions provide an advantage for resolving spectroscopic signatures with continually advancing experimental X-ray techniques. Computational modeling of X-ray processes can be achieved with *ab initio* methods for describing the electronic structure of core-excited states. This dissertation explores quantum chemical models for simulating X-ray photoelectron spectroscopy (XPS), X-ray absorption spectroscopy (XAS), and X-ray emission spectroscopy (XES). Specifically, the following research examines the applicability of Δ -based self-consistent-field (Δ SCF) and Møller-Plesset (MP) perturbation theory (Δ MP) methods and introduces different composite models coupling these techniques with electron propagator theory (EPT) for studying element-specific *K*-shell transitions.

Firstly, as a practical approach, vertical core excitation energies are obtained using a combination of the Δ SCF method and the diagonal second-order self-energy approximation with the inclusion of relativistic effects. For core excitations involving delocalized symmetry orbitals, the applied method improves upon the overestimation of Δ SCF by providing approximate values close to experimental *K*-shell transition energies.

Furthermore, spin projected Δ UHF and Δ UMP $_n$ ($n = 2, 2.5, 3$) methods are also used to calculate vertical core excitation energies. These methods are applied to a set of symmetrical molecules with equivalent atoms. The role of core localization, SCF orbital relaxation, pair correlation, and different relativistic corrections on the accuracy and reliability of the results is examined. Additionally, the limitations of using core-hole reference determinants and complications that may arise in perturbative calculations are addressed.

Lastly, a practical *ab initio* composite method for modeling X-ray absorption and non-resonant X-ray emission is presented. Vertical *K*-edge excitation and emission energies are obtained from core-electron binding energies calculated with spin-projected Δ HF/ Δ MP and outer-core ionization potentials/electron affinities calculated with electron propagator theory. An assessment of the combined methodologies

against experiment is performed for a set of small molecules containing second-row elements. Methods for obtaining transition intensities are applied for reconstructing non-resonant X-ray emission spectra.

Results from the various *ab initio* models examined indicate that sub-electron-volt accuracy can be obtained for core-level energetics while maintaining a satisfactory balance between accuracy and computational cost.

Acknowledgement

I would like to thank Professor Hrant P. Hratchian for providing me the opportunity to perform research in his group and for providing me with the resources to acquire the skills and expertise of a professional scientist.

I would like to thank my colleagues at UC Merced. In particular, I express my gratitude to Dr. Héctor H. Corzo and Dr. Ali Abou Taka for their guidance and friendship.

I would like to thank Professor J. V. Ortiz, Professor Filip Pawłowski, and Ernest Opoku for their insightful discussions on the formulations and methodologies of electron propagator theory.

Additionally, I would like to thank Dr. Yang Ha for enlightening discussions on X-ray science which inspired me to explore different quantum chemical methods for simulating X-ray spectroscopy.

Finally, I would like to thank my family and friends for their immeasurable support during my PhD.

Contents

1	Introduction	1
1.1	Molecular Electronic Structure Theory	1
1.1.1	Hartree-Fock	5
1.1.2	Configuration Interaction	14
1.1.3	Møller-Plesset Perturbation Theory	16
1.1.4	Electron Propagator Theory	20
1.2	Computational X-ray Spectroscopy	26
2	Calculating Vertical Core-Excitation Energies Using ΔSCF + $\Delta\Sigma$	29
2.1	Motivation	29
2.2	Methods	31
2.2.1	Δ SCF + $\Delta\Sigma$ Approach	31
2.2.2	Relativistic Corrections	33
2.3	Results	33
2.4	Conclusion	36
3	Calculating Vertical Core-Excitation Energies Using ΔMP with Spin Projection	41
3.1	Motivation	41
3.2	Methods	42
3.2.1	Spin Projection	43
3.2.2	Projected Hartree-Fock and Møller-Plesset Theory	45
3.2.3	Relativistic Corrections	51
3.2.4	Denominator Control	52
3.3	Results and Discussion	52
3.3.1	Computational Details	52
3.3.2	Δ PUHF and Δ PUMP _n	53
3.4	Conclusion	60
4	Δ-Based Composite Models for Simulating X-ray Absorption and Emission Spectra	75
4.1	Motivation	75

4.2	Methods	77
4.3	Results and Discussion	79
4.4	Conclusion	98
	Bibliography	99
A	Spin-adapted Configuration State Functions	135
A.1	Spin Algebra	135
A.2	Spin Projection	140
A.3	Density Matrices and Operators for Many-Body Systems	145
A.4	S^2 Matrix Elements	152
A.5	Implementation	154

” ... [O]ne might argue that the explanatory success of quantum chemistry throughout successive developmental stages rested on the degree of interlocking among constitutive elements—chemical concepts, mathematical notions, numerical methods, pictorial representations, experimental measurements, virtual experiments—to such an extent that it was not the relative contribution of each component that mattered, but the way in which the whole was reinforced by the cross linking and cross-fertilization of all elements.

— Kostas Gavroglu and Ana Simões

Neither Physics nor Chemistry: A History of Quantum Chemistry

1.1 Molecular Electronic Structure Theory

The ever-growing wealth of chemical research is now routinely complemented and accelerated by computer-driven molecular modeling. Atomistic simulation of chemical reactivity and molecular structure is made possible through the application of the principles of quantum mechanics to many-electron systems. This research enterprise is known as quantum chemistry. The major utility of *ab initio* (from first principles) quantum chemical methodologies is the capacity to abstract information about the electronic structure of a chemical system and to obtain quantities with direct connections to experimental observables. Thus, the ultimate goal of quantum chemistry is to make predictions about natural phenomena by providing physical insight into bonding and many-particle interactions.

Ab initio quantum chemistry methods are typically concerned with finding approximate solutions to the non-relativistic Schrödinger equation.¹ In one dimension, the partial differential wave equation for a single particle reads

$$i\hbar \frac{\partial}{\partial t} \Psi(x, t) = \left[-\frac{\hbar^2}{2m} \frac{\partial^2}{\partial x^2} + V(x, t) \right] \Psi(x, t) \quad (1.1)$$

where i is the imaginary unit, Ψ is the wavefunction of the quantum system, \hbar is the reduced Planck constant, and m is the particle mass.

If the potential does not explicitly depend on time ($V(x, t) \rightarrow V(x)$), one may invoke the separation of variables to simplify the task of finding solutions for $\Psi(x, t)$. The wavefunction can then be expressed as a product of independent functions of position x and time t

$$\Psi(x, t) = \psi(x)\phi(t). \quad (1.2)$$

Using Eq. 1.2, the functions of x and t are isolated on either side of Eq. 1.1 as follows

$$i\hbar \frac{d\phi(t)}{dt} \psi(x) = -\frac{\hbar^2}{2m} \frac{d^2\psi(x)}{dx^2} \phi(t) + V(x)\psi(x)\phi(t). \quad (1.3)$$

Dividing both sides of Eq. 1.3 by $\psi(x)\phi(t)$ yields

$$i\hbar \frac{d\phi(t)}{dt} \frac{1}{\phi(t)} = -\frac{\hbar^2}{2m} \frac{d^2\psi(x)}{dx^2} \frac{1}{\psi(x)} + V(x). \quad (1.4)$$

The left- and right-hand sides of Eq. 1.4 are equal by means of a separation constant E , the energy. This expression can be separated and rearranged into two ordinary differential equations

$$i\hbar \frac{d\phi(t)}{dt} = E\phi(t) \quad (1.5)$$

$$-\frac{\hbar^2}{2m} \frac{d^2\psi(x)}{dx^2} + V(x)\psi(x) = E\psi(x). \quad (1.6)$$

The solution of Eq. 1.5 is $\phi(t) = e^{-iEt/\hbar}$ with constants of integration absorbed. The solution to the time-dependent Schrödinger equation is a stationary state

represented by the total wavefunction $\Psi(x, t) = \psi(x)e^{-iEt/\hbar}$. Depicted in Eq. 1.6 is the time-independent Schrödinger equation. It has general form of

$$H\psi = E\psi. \quad (1.7)$$

where H is the non-relativistic, time-independent Hamiltonian that accounts for the kinetic and potential energies of the system. If the wavefunctions ψ are cast in a finite basis representation, then Eq. 1.7 may be solved with matrix algebra. Since H is a Hermitian (self-adjoint) operator, its eigenvalues are real. The eigenvalues that belong to the spectrum of H correspond to the energies assigned to the eigenvectors ψ .

The Hamiltonian for a molecular system is written as

$$H = - \sum_{i=1}^{N_{elec}} \frac{\hbar^2}{2m_e} \nabla_i^2 - \sum_{A=1}^{N_{nuc}} \frac{\hbar^2}{2M_A} \nabla_A^2 - \sum_{i=1}^{N_{elec}} \sum_{A=1}^{N_{nuc}} \frac{Z_A e^2}{4\pi\epsilon_0 r_{iA}} + \sum_{i=1}^{N_{elec}} \sum_{j>i}^{N_{elec}} \frac{e^2}{4\pi\epsilon_0 r_{ij}} + \sum_{A=1}^{N_{nuc}} \sum_{B>A}^{N_{nuc}} \frac{Z_A Z_B e^2}{4\pi\epsilon_0 R_{AB}} \quad (1.8)$$

where \hbar is the reduced Planck constant, m_e is the mass of an electron, ∇^2 is the Laplacian operator, M_A is the mass of a nucleus, Z_A is the atomic number of a nucleus, $r_{iA} = |r_i - R_A|$ is the distance between an electron and nucleus, $r_{ij} = |r_i - r_j|$ is the distance between two electrons, $R_{AB} = |R_A - R_B|$ is the distance between two nuclei, e is the elementary charge, and $4\pi\epsilon_0$ is the inverse of the Coulomb constant, with ϵ_0 as the vacuum permittivity. Further simplification is achieved when expressing Eq. 1.8 in atomic units (a.u) or Hartrees (Ha), *viz.*:

$$H = - \sum_{i=1}^{N_{elec}} \frac{1}{2} \nabla_i^2 - \sum_{A=1}^{N_{nuc}} \frac{1}{2M_A} \nabla_A^2 - \sum_{i=1}^{N_{elec}} \sum_{A=1}^{N_{nuc}} \frac{Z_A}{r_{iA}} + \sum_{i=1}^{N_{elec}} \sum_{j>i}^{N_{elec}} \frac{1}{r_{ij}} + \sum_{A=1}^{N_{nuc}} \sum_{B>A}^{N_{nuc}} \frac{Z_A Z_B}{R_{AB}} \quad (1.9)$$

Like the molecular Hamiltonian, the molecular wavefunction will depend on the positions of the electrons and nuclei. However, note that the mass of a nucleus is

many times greater than the mass of an electron (i.e. $\rightarrow M_A \gg m_e$). Because kinetic energy is inversely proportional to mass, we can say that the nuclei move at vastly different timescales than electrons and are considered to be nearly motionless with respect to the electrons. Therefore we can decouple the molecular wavefunction into electronic and nuclear parts

$$\Psi_{mol}(\mathbf{r}, \mathbf{R}) = \Psi_{elec}(\mathbf{r}; \mathbf{R}) \Psi_{nuc}(\mathbf{R}). \quad (1.10)$$

This invocation is known as the Born-Oppenheimer approximation.² Under this bold (albeit practical) assumption, the electronic wavefunction only depends parametrically on the nuclear coordinates. The object of interest is then Ψ_{elec} , which should contain all the information pertaining to the electronic structure located within a given set of nuclear coordinates. This is valid reasoning provided one adopts an interpretation of quantum mechanics where the Born rule³ for obtaining probabilities of observed eigenstates is essential. Since the nuclei appear fixed, we can simplify the Hamiltonian further by setting the nuclear kinetic energy to zero. The nuclear-nuclear repulsion term V_{NN} remains constant for each stationary state.

$$H = - \sum_{i=1}^{N_{elec}} \frac{1}{2} \nabla_i^2 - \sum_{A=1}^{N_{nuc}} \frac{1}{2M_A} \nabla_A^2 - \sum_{i=1}^{N_{elec}} \sum_{A=1}^{N_{nuc}} \frac{Z_A}{r_{iA}} + \sum_{i=1}^{N_{elec}} \sum_{j>i}^{N_{elec}} \frac{1}{r_{ij}} + \sum_{A=1}^{N_{nuc}} \sum_{B>A}^{N_{nuc}} \frac{Z_A Z_B}{R_{AB}} \quad (1.11)$$

$\nearrow 0$
 $\nearrow V_{NN}$

We now have what is known as the electronic Hamiltonian plus V_{NN} :

$$H = \underbrace{- \sum_{i=1}^{N_{elec}} \frac{1}{2} \nabla_i^2}_{T_{elec}} - \underbrace{\sum_{i=1}^{N_{elec}} \sum_{A=1}^{N_{nuc}} \frac{Z_A}{r_{iA}}}_{V_{elec-nuc}} + \underbrace{\sum_{i=1}^{N_{elec}} \sum_{j>i}^{N_{elec}} \frac{1}{r_{ij}}}_{V_{elec-elec}} + V_{NN} \quad (1.12)$$

H then becomes the sum of the electronic kinetic energy term T_{elec} , the electron-nucleus attraction term $V_{elec-nuc}$, the electron-electron repulsion term $V_{elec-elec}$, and the nuclear-nuclear repulsion term V_{NN} .

For many-electron systems, analytic solutions to the Schrödinger equation become inaccessible due to the electron-electron interaction term which requires knowledge of all electron pair coordinates. Without complete information of the initial conditions, the wavefunction, and, subsequently, the probability distribution function (from the density), numerical approximations aided by computational implementations are required to accurately model many-electron interactions or correlations. Decades of research have culminated in development of many methods of addressing electron correlation and its significance in field of chemistry. The following sections will briefly highlight the quantum chemical methods relevant to the work featured in this dissertation.

1.1.1 Hartree-Fock

The Hartree-Fock method⁴⁻⁶ (HF) is an approximate approach to solve Eq. 1.7.ⁱ It includes Fermi correlation, or the effect of exchange interactions that arise due to the antisymmetry principle. This is a quantum mechanical effect with no classical analogue. As a rule for indistinguishable fermions, the wavefunction must be antisymmetric under the exchange of two electrons

$$\Psi(\mathbf{x}_1, \mathbf{x}_2, \dots, \mathbf{x}_N) = -\Psi(\mathbf{x}_2, \mathbf{x}_1, \dots, \mathbf{x}_N). \quad (1.13)$$

If two electrons were to possess the same spatial and spin coordinates (i.e. $\mathbf{x}_1 = \mathbf{x}_2$) the wavefunction would vanish and the probability of two electrons being of the same quantum state (orbital) would be zero. Specifically, for many-electron atoms, no two electrons can share the same quantum numbers. Thus, the Pauli exclusion principle is said to be a direct consequence of the antisymmetry principle.

An antisymmetric N -electron wavefunction $|\Psi\rangle$, expressed in Dirac notation, can be generated using a Slater determinant⁹

ⁱSection 1.1.1 is based on a set of notes written by the author, notes by C. D. Sherrill⁷, and the textbook *Modern Quantum Chemistry*⁸

$$|\Psi\rangle = \frac{1}{\sqrt{N!}} \begin{vmatrix} \chi_1(\mathbf{x}_1) & \chi_2(\mathbf{x}_1) & \cdots & \chi_N(\mathbf{x}_1) \\ \chi_1(\mathbf{x}_2) & \chi_2(\mathbf{x}_2) & \cdots & \chi_N(\mathbf{x}_2) \\ \vdots & \vdots & \ddots & \vdots \\ \chi_1(\mathbf{x}_N) & \chi_2(\mathbf{x}_N) & \cdots & \chi_N(\mathbf{x}_N) \end{vmatrix} \quad (1.14)$$

where the spin-orbital χ is a function of spin ω and spatial \mathbf{r} coordinates

$$\chi(\mathbf{x}) = \psi(\mathbf{r})\sigma(\omega). \quad (1.15)$$

χ can be expanded in terms of an "approximately" complete basis set. The atomic orbital (AO) representation of the single particle functions can take the mathematical form of a Slater-type orbital¹⁰ (STO) with the Kato's cusp condition¹¹

$$\phi_{abc}^{STO}(x, y, z) = \mathcal{N} x^a y^b z^c e^{-\zeta r} \quad (1.16)$$

or a Gaussian-type orbital¹² (GTO) with a convenient product theorem

$$\phi_{abc}^{GTO}(x, y, z) = \mathcal{N} x^a y^b z^c e^{-\zeta r^2} \quad (1.17)$$

where \mathcal{N} is a normalization constant and $a+b+c$ give the orbital angular momentum l . The exponent is composed of ζ , an orbital width parameter, and a radial variable r^2 (or $\sqrt{r^2}$) that is related to the equation of a sphere with an origin centered at Cartesian coordinates x, y, z . In molecules, a linear combination of atomic orbitals (LCAO) gives rise to molecular orbitals (MOs)

$$|i\rangle = \sum_{\mu} c_{\mu i} |\mu\rangle. \quad (1.18)$$

Greek letters (μ, ν, λ, \dots) denote functions in the AO basis $\{|\mu\rangle\}$ and Latin letters (i, j, k, \dots) to denote functions in the MO basis $\{|i\rangle\}$.

Coefficients $c_{\mu i}$ and orbital energies ϵ_i can be obtained from the Hartree-Fock method. Moving forward, we refer to the Roothaan-Hartree-Fock method¹³ for single configuration wavefunctions as, simply, HF since it is important to distinguish it from the multiconfigurational Hartree-Fock (MCHF) method for atomic structure calculations.¹⁴

In molecular electronic structure theory, variational optimization of the orbitals is achieved through iterative solution of the Roothaan-Hall equations

$$\mathbf{FC} = \mathbf{SC}\epsilon. \quad (1.19)$$

Here, \mathbf{F} is the Fock matrix, \mathbf{C} is the coefficient matrix, \mathbf{S} is the AO overlap matrix, and ϵ is the set of orbital energies. The HF wavefunction, orbital energies, and total energy are invariant to unitary transformation or rotation of the occupied orbital subspace. We can employ Löwdin symmetric orthogonalization to transform Eq. 1.19 into a proper eigensystem.

The transformation matrix \mathbf{X} is Hermitian and is built from the unitary transformation that diagonalizes the inverse square root of the AO overlap matrix $\mathbf{S}^{-1/2}$.

$$\mathbf{X} = \mathbf{U}\mathbf{s}^{-1/2}\mathbf{U}^\dagger \quad (1.20)$$

The matrix $\mathbf{s}^{-1/2}$ is a diagonal matrix whose elements are inverse square roots of overlap integrals. Since \mathbf{S} is Hermitian, $\mathbf{S}^{-1/2}$ is also Hermitian. Due to the properties of unitary matrices, the transformation matrix \mathbf{X} becomes conveniently equal to $\mathbf{S}^{-1/2}$

$$\mathbf{X} = \mathbf{S}^{-1/2}. \quad (1.21)$$

The following definitions based on Eq. 1.21 are used to define how the MO coefficient matrix is orthogonalized

$$\mathbf{C}' = \mathbf{X}^{-1}\mathbf{C} = (\mathbf{S}^{-1/2})^{-1}\mathbf{C} \quad \text{and} \quad \mathbf{C} = \mathbf{X}\mathbf{C}' = \mathbf{S}^{-1/2}\mathbf{C}'. \quad (1.22)$$

We substitute the new expression of \mathbf{C} in the Roothaan-Hall equations

$$\mathbf{F}\mathbf{S}^{-1/2}\mathbf{C}' = \mathbf{S}\mathbf{S}^{-1/2}\mathbf{C}'\epsilon. \quad (1.23)$$

Left multiplying by $\mathbf{S}^{-1/2}$ yields

$$\underbrace{\mathbf{S}^{-1/2}\mathbf{F}\mathbf{S}^{-1/2}}_{\mathbf{F}'}\mathbf{C}' = \underbrace{\mathbf{S}^{-1/2}\mathbf{S}\mathbf{S}^{-1/2}}_{\mathbf{1}}\mathbf{C}'\epsilon \quad (1.24)$$

and the canonical HF equations

$$\mathbf{F}'\mathbf{C}' = \mathbf{C}'\epsilon \quad (1.25)$$

The transformed Fock matrix \mathbf{F}' and coefficient matrix \mathbf{C}' that diagonalizes it yields the unchanged MO energies ϵ . The Fock operator, for a closed-shell system, is

$$\mathcal{F} = h + \sum_i^{N_{occ}/2} [2\mathcal{J}_i - \mathcal{K}_i]. \quad (1.26)$$

Here, h is the one-electron Hamiltonian containing the T_{elec} and $V_{elec-nuc}$ terms. Representing the $V_{elec-elec}$ potential are the Coulomb operator \mathcal{J} and the exchange operator \mathcal{K} . The action of these operators on a spin-orbital $\chi_i(\mathbf{x}_1)$ is shown below

$$\mathcal{J}_j(\mathbf{x}_1) |\chi_i(\mathbf{x}_1)\rangle = \langle \chi_j(\mathbf{x}_2) | \frac{1}{r_{12}} | \chi_j(\mathbf{x}_2)\rangle | \chi_i(\mathbf{x}_1)\rangle \quad (1.27)$$

$$= \int \left[\chi_j^*(\mathbf{x}_2) \frac{1}{r_{12}} \chi_j(\mathbf{x}_2) d\mathbf{x}_2 \right] \chi_i(\mathbf{x}_1), \quad (1.28)$$

$$\mathcal{K}_j(\mathbf{x}_1) |\chi_i(\mathbf{x}_1)\rangle = \langle \chi_j(\mathbf{x}_2) | \frac{1}{r_{12}} |\chi_i(\mathbf{x}_2)\rangle |\chi_j(\mathbf{x}_1)\rangle \quad (1.29)$$

$$= \int \left[\chi_j^*(\mathbf{x}_2) \frac{1}{r_{12}} \chi_i(\mathbf{x}_2) d\mathbf{x}_2 \right] \chi_j(\mathbf{x}_1). \quad (1.30)$$

The local interaction in \mathcal{J} represents the potential from the average charge distribution of spin orbitals $\chi_j(\mathbf{x}_2)$ experienced by $\chi_i(\mathbf{x}_1)$. The non-local interaction in \mathcal{K} lacks a classical interpretation of a potential defined at some specific coordinate \mathbf{x}_1 and appears due to the antisymmetric nature of the wavefunction. Note that these operators must also remain invariant under unitary transformation.

In HF, two-electron interactions are modeled with effective one-electron operators describing the average interaction of each electron with average potential of the other electrons in the system. As such, HF is often regarded as a mean-field theory since the interactions concerning other electronic degrees of freedom are averaged. Explicit electron-electron correlation terms other than exchange are left out of HF formalism and can be recovered with post-HF methods, some of which are detailed in later in this chapter.

Turning back to Eq. 1.26, one can obtain a Fock matrix element representation by projecting onto a basis $\{|\mu\rangle\}$

$$\langle \mu | \mathcal{F} | \nu \rangle = \langle \mu | h | \nu \rangle + \langle \mu | \sum_i^{N_{occ}/2} [2\mathcal{J}_i - \mathcal{K}_i] | \nu \rangle \quad (1.31)$$

and expanding further, using Eqs. 1.27 and 1.29, gives

$$F_{\mu\nu} = h_{\mu\nu} + \sum_i^{N_{occ}/2} \left[2(\mu\nu|ii) - (\mu i|i\nu) \right] \quad (1.32)$$

where the spatial electron repulsion integrals (ERI) are in chemists' notation. Each MO i is expanded as a linear combination of AOs, leading to

$$F_{\mu\nu} = h_{\mu\nu} + \sum_{\lambda\sigma}^{N_{basis}} \left[\sum_i^{N_{occ}/2} c_{\sigma i}^* c_{\lambda i} \right] \left[2(\mu\nu|\lambda\sigma) - (\mu\sigma|\lambda\nu) \right]. \quad (1.33)$$

The charge density matrix in the AO basis $P_{\lambda\sigma}$ is:

$$P_{\lambda\sigma} = 2 \sum_i^{N_{occ}/2} c_{\sigma i}^* c_{\lambda i} \quad (1.34)$$

and is inserted into Eq. 1.33

$$F_{\mu\nu} = h_{\mu\nu} + \sum_{\lambda\sigma}^{N_{basis}} P_{\lambda\sigma} \left[(\mu\nu|\lambda\sigma) - \frac{1}{2}(\mu\sigma|\lambda\nu) \right]. \quad (1.35)$$

The two-electron part of Eq. 1.35 is sometimes bundled into a single term $G_{\mu\nu}$, leading to

$$F_{\mu\nu} = h_{\mu\nu} + G_{\mu\nu}. \quad (1.36)$$

An expectation value for the electronic energy is obtained by contraction with the density matrix

$$E_{elec} = \frac{1}{2} \sum_{\mu\nu}^{N_{basis}} P_{\mu\nu} \left[h_{\mu\nu} + \sum_{\lambda\sigma}^{N_{basis}} P_{\lambda\sigma} \left[(\mu\nu|\lambda\sigma) - \frac{1}{2}(\mu\sigma|\lambda\nu) \right] \right] \quad (1.37)$$

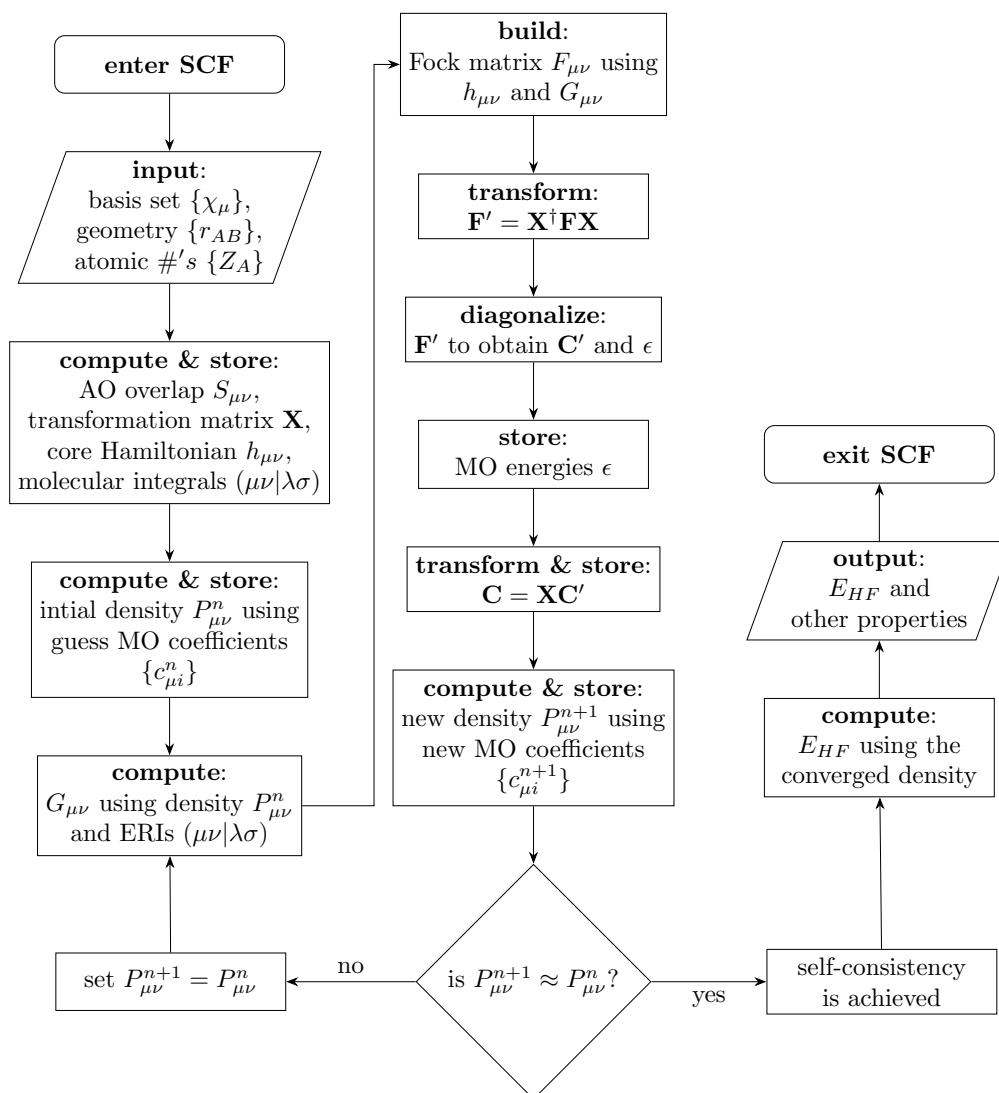
or simply

$$E_{HF} = \frac{1}{2} \sum_{\mu\nu}^{N_{basis}} P_{\mu\nu} \left[h_{\mu\nu} + G_{\mu\nu} \right]. \quad (1.38)$$

The total energy is the sum of the electronic energy and V_{NN}

$$E = \frac{1}{2} \sum_{\mu\nu}^{N_{basis}} P_{\mu\nu} \left[h_{\mu\nu} + G_{\mu\nu} \right] + V_{NN}. \quad (1.39)$$

Fig. 1.1.: Flowchart for a Hartree-Fock SCF procedure



The HF equations are solved in an iterative manner via the self-consistent-field (SCF) procedure. Self-consistency is achieved when a certain threshold criteria is met for the changes in the total energy and density. Satisfying the commutator relation $[\mathbf{F}, \mathbf{P}] = 0$ between the Fock matrix \mathbf{F} and density matrix \mathbf{P} is also an indication of self-consistency. A workflow for the SCF process is depicted in Fig. 1.1

Using a trial wavefunction $|\tilde{\Psi}\rangle$, say a HF determinant, an approximation to the ground state energy can be obtained with the variational method guided by the variational principle,

$$\frac{\langle \tilde{\Psi} | \hat{H} | \tilde{\Psi} \rangle}{\langle \tilde{\Psi} | \tilde{\Psi} \rangle} \geq E_0 \quad (1.40)$$

which states that the approximate energy, a functional of $|\tilde{\Psi}\rangle$, is an upper bound to the true ground state energy E_0 .

There are versions of the HF method that vary the types of restrictions made on the orbital basis. Designations for HF methods with varying symmetry constraints for achieving different levels of variational flexibility have been established.^{15,16} So far, in the formulations above, it is assumed that the spatial components for electrons with either up α and down β spin are the same. This constraint on the SCF procedure leads to the restricted Hartree-Fock (RHF) method for closed-shell systems. RHF maintains perfect electron pairing and good intrinsic spin quantum numbers. For systems with unpaired electrons, there are restricted open-shell (ROHF) approaches that conserve total spin through the preservation of proper S^2 eigenvalues.¹⁷ There are many discussions on the physical meaning of stand-alone ROHF solutions, ambiguity of ROHF orbital energies, and methods of improving ROHF.^{18–22}

The use of different orbitals for different spins is a feature of the unrestricted Hartree-Fock (UHF) scheme,

$$\psi_i^\alpha(\mathbf{r}) = \sum_{\mu}^N c_{\mu i}^\alpha \phi_{\mu}(\mathbf{r}) \quad \psi_i^\beta(\mathbf{r}) = \sum_{\mu}^N c_{\mu i}^\beta \phi_{\mu}(\mathbf{r}) \quad (1.41)$$

which requires the solution of a pair of HF equations called the Pople–Nesbet equations^{23,24}

$$\mathbf{F}^\alpha \mathbf{C}^\alpha = \mathbf{S} \mathbf{C}^\alpha \epsilon^\alpha \quad \mathbf{F}^\beta \mathbf{C}^\beta = \mathbf{S} \mathbf{C}^\beta \epsilon^\beta. \quad (1.42)$$

UHF relieves the constraint that the wavefunction should be an eigenstate of S^2 . At the Coulson-Fischer point²⁵, the RHF solution can break symmetry and collapse to a lower energy UHF solution. In the closed-shell case of single bond dissociation, the UHF solution will be a mixture of singlet and triplet states, resulting in spin contamination. The presence of such a solution is determined by an instability

identified in the orbital Hessian.²⁶ The UHF method is often employed to obtain a qualitatively improved potential energy surface PES topology in the bond-breaking regime.

The general Hartree-Fock (GHF) method^{27,28} avoids satisfying the conditions of proper spin symmetry by adopting a spinor basis

$$\chi_i(\mathbf{x}) = \psi_i^\alpha(\mathbf{r}) + \psi_i^\beta(\mathbf{r}) \quad (1.43)$$

where

$$\psi_i^\alpha(\mathbf{r}) = \sum_{\mu}^N c_{\mu i}^{\alpha} \phi_{\mu}(\mathbf{r}) \quad \text{and} \quad \psi_i^\beta(\mathbf{r}) = \sum_{\mu}^N c_{\mu i}^{\beta} \phi_{\mu}(\mathbf{r}) \quad (1.44)$$

Confinement to the S_z quantization axis is then lifted in GHF. When either set of $c_{\mu i}^{\alpha}$ or $c_{\mu i}^{\beta}$ is zero for all μ of each orbital χ_i , the UHF scenario is recovered and, if $c_{\mu i}^{\alpha}$ and $c_{\mu i}^{\beta}$ happen to be the same, one gets the RHF scenario. Hence, RHF and UHF are regarded as special cases of GHF.

GHF thus allows for noncollinear spin, which is useful for modeling magnetic properties of strongly correlated materials such as (geometrically) spin frustrated systems. Greater variational flexibility is achieved by switching from real (r) to complex (c) orbitals, which increasing the degrees of freedom in the SCF solution.

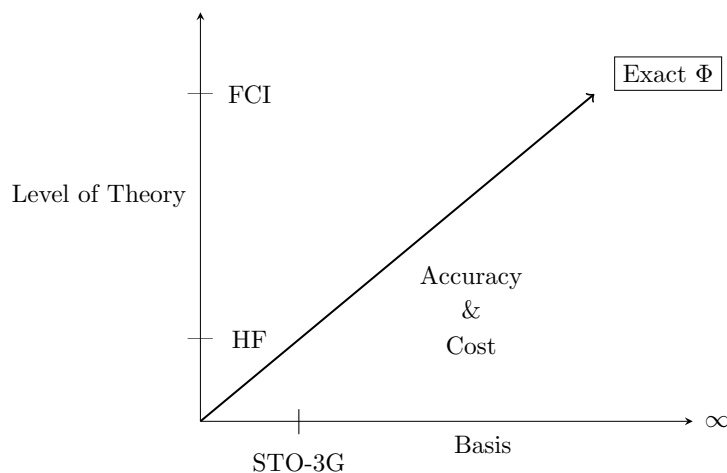
	S^2	S_z
RHF	✓	✓
ROHF	✓	✓
UHF	✗	✓
GHF	✗	✗

Fig. 1.2.: Table of spin symmetry constraints for RHF, ROHF, UHF, and GHF.

Deciding whether or not to break symmetry in the pursuit of finding global minima is a hallmark of the so-called symmetry dilemma.²⁹ The extended Hartree-Fock (EHF) method was developed to find the optimal orbitals that minimize the SCF energy corresponding to a spin-pure wavefunction.³⁰⁻³² Such a wavefunction is obtained with projection operators and related techniques^{30,33-39}. Details on the construction of spin eigenfunctions and related quantities are presented in Appendix A. Basic techniques from the EHF method are introduced in Chapter 3.

The HF method is a practical foundation for quantum chemical modeling, yet requires much improvement due to its deficiencies in capturing the effects of instantaneous correlated movement of electrons (dynamic correlation) and multiconfigurational character of an electronic state for which a single HF determinant is insufficient (static correlation). An accurate description of electronic structure beyond the HF approximation requires a more explicit treatment of electron correlation found in correlated wavefunction and many-body methods.

Fig. 1.3.: A Pople diagram for computational quantum chemistry



1.1.2 Configuration Interaction

The method of configuration interaction⁴⁰⁻⁴⁴ (CI) is a linear variational approach for solving the Schrödinger equation where the wavefunction is a superposition of configurations.

$$H\Phi^{CI} = E\Phi^{CI} \quad (1.45)$$

The CI wavefunction $|\Phi\rangle^{CI}$ may be a linear combination of configuration state functionsⁱⁱ (CSF) or Slater determinants. In the basis of determinants, $|\Phi\rangle^{CI}$ is represented, in cluster form⁴⁵, by the ground state $|\Psi_0\rangle$ and substituted (or “excited”) electronic configurations

ⁱⁱSee Appendix A

$$|\Phi^{CI}\rangle = d_0 |\Psi_0\rangle + \sum_{ia} d_i^a |\Psi_i^a\rangle + \sum_{\substack{i<j \\ a<b}} d_{ij}^{ab} |\Psi_{ij}^{ab}\rangle + \sum_{\substack{i<j<k \\ a<b<c}} d_{ijk}^{abc} |\Psi_{ijk}^{abc}\rangle + \dots \quad (1.46)$$

where i, j, k, \dots are occupied orbital indices and a, b, c, \dots are unoccupied (virtual) orbital indices. The components $|\Psi_i^a\rangle$ (singles), $|\Psi_{ij}^{ab}\rangle$ (doubles), $|\Psi_{ijk}^{abc}\rangle$ (triples), \dots are the substituted determinants. The inclusion of all possible configurations in the expansion of $|\Phi^{CI}\rangle$ in Eq. 1.45 is called full CI (FCI). An approximation to the ground state wavefunction $|\Psi_0\rangle$ is usually a HF determinant, which can be obtained via SCF theory. Then, a ground state CI wavefunction $|\Phi_0\rangle$ can be normalized with $\langle\Psi_0|\Phi_0\rangle = 1$ (intermediate normalization). The exact, non-relativistic ground state energy E_0 is given by the following expectation value

$$\langle\Phi_0|H|\Phi_0\rangle = E_0. \quad (1.47)$$

The difference between this energy and the HF energy at the basis set limit is what is known as the correlation energy⁴¹

$$e_{corr} = E_0 - E_{HF}. \quad (1.48)$$

The value of e_{corr} is simply the electronic interaction energy that is absent in mean-field approximations such as HF. If $|\Psi_0\rangle$ is a HF wavefunction, then expectation values of the class $\langle\Phi_0|H|\Psi_i^a\rangle$ will be zero according to Brillouin's theorem. Similarly, expectation values between the reference $|\Psi_0\rangle$ and substituted determinants that differ by three or more orbitals go to zero in accordance with the Slater-Condon rules. The correlation energy e_{corr} is then dependent on the amplitudes of the doubly substituted determinants d_{ij}^{ab} of a CI wavefunction that has undergone intermediate normalization. However, linear variation of the doubles amplitudes are affected by the amplitudes of other determinants in the wavefunction expansion. To get the "exact" energy E_0 , all configurations or a special selection^{44,46-57} of important configurations must be included.

A conventional FCI wavefunction expanded over all substituted determinants would grow factorially with the number of electrons and basis functions. The incredibly steep scaling of such an approach can be cost-prohibitive for large molecular systems

and high-dimensional electronic structure problems. The desire to approach the accuracy of FCI is the impetus for the development of post-SCF quantum chemistry methodologies.

1.1.3 Møller-Plesset Perturbation Theory

Møller-Plesset (MP) perturbation theory^{58,59} is used to improve upon the HF approach by incorporating electron correlation effects. MP theory is a specific application of Rayleigh–Schrödinger perturbation theory where the exact time-independent Hamiltonian H is represented by an unperturbed zeroth-order Hamiltonian H_0 with an additional small perturbation V controlled by a parameter λ between 0 and 1

$$H = H_0 + \lambda V. \quad (1.49)$$

Inserting the perturbed Hamiltonian into Eq. 1.7 gives

$$(H_0 + \lambda V)\Psi_i = E_i\Psi_i \quad (1.50)$$

for i eigenstates Ψ_i with energies E_i . Assuming Ψ_i and E_i are functions of λ starting at $\lambda = 0$, we expand these as a power series to n^{th} order

$$\Psi_i = \Psi_i^{(0)} + \lambda\Psi_i^{(1)} + \lambda^2\Psi_i^{(2)} + \lambda^3\Psi_i^{(3)} + \dots \quad (1.51)$$

$$E_i = E_i^{(0)} + \lambda E_i^{(1)} + \lambda^2 E_i^{(2)} + \lambda^3 E_i^{(3)} + \dots \quad (1.52)$$

Rewriting Eq. 1.50 using Eqs. 1.51 and 1.52 gives

$$\begin{aligned} (H_0 + \lambda V) & \left[\Psi_i^{(0)} + \lambda\Psi_i^{(1)} + \lambda^2\Psi_i^{(2)} + \lambda^3\Psi_i^{(3)} + \dots \right] \\ & = \left[E_i^{(0)} + \lambda E_i^{(1)} + \lambda^2 E_i^{(2)} + \lambda^3 E_i^{(3)} + \dots \right] \\ & \times \left[\Psi_i^{(0)} + \lambda\Psi_i^{(1)} + \lambda^2\Psi_i^{(2)} + \lambda^3\Psi_i^{(3)} + \dots \right]. \end{aligned} \quad (1.53)$$

Equating the λ factors lead to the following perturbative expansions for each order:

$$n = 0 \quad H_0 \Psi_i^{(0)} = E_i^{(0)} \Psi_i^{(0)} \quad (1.54)$$

$$n = 1 \quad H_0 \Psi_i^{(1)} + V \Psi_i^{(0)} = E_i^{(0)} \Psi_i^{(1)} + E_i^{(1)} \Psi_i^{(0)} \quad (1.55)$$

$$n = 2 \quad H_0 \Psi_i^{(2)} + V \Psi_i^{(1)} = E_i^{(0)} \Psi_i^{(2)} + E_i^{(1)} \Psi_i^{(1)} + E_i^{(2)} \Psi_i^{(0)} \quad (1.56)$$

$$n = 3 \quad \dots$$

\vdots

Using intermediate normalization $\langle \Psi_i^{(0)} | \Psi_i \rangle = 1$, with $\langle \Psi_i^{(0)} | \Psi_i^{(0)} \rangle = 1$, begets the orthogonality relation $\langle \Psi_i^{(0)} | \Psi_i^n \rangle = 0$. The energy using the zeroth-order unperturbed Hamiltonian H_0 is

$$E_i^{(0)} = \langle \Psi_i^{(0)} | H_0 | \Psi_i^{(0)} \rangle \quad (1.57)$$

and the contributions to the total perturbed energy up to n^{th} order ($n > 0$) are

$$E_i^{(n)} = \langle \Psi_i^{(0)} | V | \Psi_i^{(n-1)} \rangle. \quad (1.58)$$

The zeroth-order energy and the first-order energy correction depend just on $\Psi_i^{(0)}$, which can be known. The first-order wavefunction is seemingly unknown but can be written in terms of a linear expansion of known eigenstates of H_0

$$|\Psi_i^{(1)}\rangle = \sum_Q c_Q^{(1)} |Q\rangle \quad (1.59)$$

with amplitudes

$$c_Q^{(1)} = \langle Q | \Psi_i^{(1)} \rangle. \quad (1.60)$$

Recall the orthogonality between normalized eigenstates of H_0 and (intermediate normalized) perturbed wavefunction corrections. One can use the resolution of the identity for a change of basis representation

$$|\Psi_i^{(1)}\rangle = \sum_{Q \neq i} |Q\rangle \langle Q|\Psi_i^{(1)}\rangle \quad (1.61)$$

Taking Eq. 1.55 and applying $\langle Q|$

$$\langle Q|V|\Psi_i^{(0)}\rangle = (E_i^{(0)} - E_Q^{(0)}) \langle Q|\Psi_i^{(1)}\rangle \quad (1.62)$$

then using Eq. 1.58 for $n = 2$, an expression for the second-order energy correction is produced

$$E_0^{(2)} = \sum_{Q \neq i} \frac{\langle \Psi_i^{(0)}|V|Q\rangle \langle Q|V|\Psi_i^{(0)}\rangle}{(E_i^{(0)} - E_Q^{(0)})}. \quad (1.63)$$

Higher-order energy contributions require knowledge of the previous $(n - 1)$ wavefunction corrections and the preceding general approach can be applied to non-degenerate eigenstates.

One can partition H using the Fock operator ($H_0 \equiv F$) and a perturbationⁱⁱⁱ

$$V = r_{12}^{-1} - v_{HF}. \quad (1.64)$$

where V is defined as the Coulomb operator minus the HF potential. This is called Møller-Plesset partitioning.

Since a HF wavefunction Ψ_0 is an eigenfunction of F , following Eq. 1.54, the zeroth-order correction for the ground state energy is

ⁱⁱⁱThe term fluctuation potential is also used describe deviations or perturbations away from the average electrostatic potential

$$E_0^{(0)} = \sum_p^{occ} \epsilon_p \quad (1.65)$$

which are the molecular orbital energies. Following Eq. 1.55 and Eq. 1.64, the first-order correction for the ground state energy is

$$E_0^{(1)} = -\frac{1}{2} \sum_{pq}^{occ} \langle pq || pq \rangle \quad (1.66)$$

where the “double-bar” integral for Coulomb and exchange interactions is in the MO basis $\{p\}$. Combining the zeroth- and first-order corrections

$$E_{HF} = E_0^{(0)} + E_0^{(1)} \quad (1.67)$$

gives the HF electronic energy. The correlation energy through MP n is then

$$e_{corr} = E_0^{(2)} + E_0^{(3)} + E_0^{(4)} + E_0^{(5)} + \dots \quad (1.68)$$

Correlation corrections to the Hartree-Fock energy thus begins at second-order

$$E_0^{(2)} = \frac{1}{4} \sum_{ijab} \frac{|\langle ij || ab \rangle|^2}{\epsilon_i + \epsilon_j - \epsilon_a - \epsilon_b}. \quad (1.69)$$

The correction $E_0^{(2)}$ accounts for pair correlations through interaction terms between uncoupled doubles substitutions and the ground state. This approach is known as MP2 and is the most basic many-body method to include dynamical correlation effects with a HF reference. MP2 is an affordable method to employ since conventional implementations only require an overhead of AO to MO integral transformation with a computational complexity of $\sim \mathcal{O}(N^5)$.

1.1.4 Electron Propagator Theory

The electron propagator formalism^{60–67} provides a systematic framework for the inclusion of correlation in the one-electron picture of molecular electronic structure. EPT calculations generate Dyson orbitals as well as correlated binding and detachment energies without the need for determining wavefunctions and eigenvalues of total electronic states. The electron propagator, or one-electron Green’s function, provides an approach for obtaining both qualitative and quantitative descriptions of chemical bonding and interpretation of spectra. In this section, we will briefly cover the basics of EPT.

Beginning with the Møller–Plesset partitioning of the non-relativistic molecular Hamiltonian H

$$H = H_0 + V \quad (1.70)$$

where H_0 is taken to be the Fock operator and the fluctuation potential V is approximated as an energy dependent effective potential $\Sigma(E)$, coined the “self-energy”, which can be expanded as a perturbative series to arbitrary order. We aim to solve the inverse Dyson equation for the electron propagator matrix $\mathbf{G}(E)$

$$(\mathbf{G}(E))^{-1} = (\mathbf{G}_0(E))^{-1} - \Sigma(E) \quad (1.71)$$

By taking the Fock operator resolvent $\mathbf{G}_0(E)$ (the HF Green’s function), in a spin-orbital basis,

$$\mathbf{G}_0(E) = (E\mathbb{1} - H_0)^{-1} \quad (1.72)$$

one can obtain the real-valued simple poles of the propagator. The poles, or energies where the singularities of one-electron Green’s function $\mathbf{G}_0(E)$ lie, occur at the HF eigenvalues ϵ . By requiring $(\mathbf{G}(E))^{-1} = 0$, we can recast the problem into a system of linear equations and solve

$$\det((E\mathbf{1} - \epsilon - \Sigma(E)) = 0 \quad (1.73)$$

Since the lowest-order corrections to the orbital energies ϵ_i involve only the diagonal elements of the self-energy matrix, the above simplifies to

$$\prod_i ((E - \epsilon_i - \Sigma_{ii}(E)) = 0 \quad (1.74)$$

For each correction to ϵ_i , we solve for E

$$E = \epsilon_i + \Sigma_{ii}(E) \quad (1.75)$$

This is done iteratively by first evaluating $\Sigma_{ii}(E)$ at a guess pole $E = \epsilon_i$. The corrected HF orbital energies are thus

$$\omega = \epsilon_i + \Sigma_{ii}(E) \quad (1.76)$$

$\Sigma_{ii}(E)$ is evaluated at ω and Eq. (1.76) is solved iteratively until the convergence criteria is met. When the i^{th} orbital is occupied, ω is an electron detachment energy; when it is unoccupied, ω is an electron attachment energy. The energies obtained arise from the diagonal quasiparticle equation

$$[\mathbf{F} + \Sigma_{ii}(E_i)] C_i^{Dyson} = C_i^{Dyson} \omega_i \quad (1.77)$$

The minimum approximation to the self-energy that recovers the qualitative correlation correction to Koopmans' theorem is performed at diagonal second-order, $\Sigma_{ii}^{(2)}(E)$. Explicit matrix elements of $\Sigma_{ii}^{(2)}(E)$ are generated through electron field operator couplings. The manifold, \mathbf{h} , of elements from the linear space of field operators separated into two orthogonal subspaces, \mathbf{a}^\dagger (primary) and \mathbf{f} (secondary), is applied to superoperator energy matrix \mathbf{H} using Löwdin's partitioning method.⁶⁸ The elements of $\mathbf{G}(E)$ for the primary space are then

$$\mathbf{G}(E) \equiv \langle\langle \mathbf{a}; \mathbf{a}^\dagger \rangle\rangle_E = \left(\mathbf{a}^\dagger | (E\mathbf{1} - \mathbf{H})^{-1} \mathbf{a}^\dagger \right) \quad (1.78)$$

Through inner projection of \mathbf{h} , we obtain another form of the propagator matrix

$$\mathbf{G}(E) = \left(\mathbf{a}^\dagger | \mathbf{h} \right) \left(\mathbf{h} | (E\mathbf{1} - \mathbf{H}) \mathbf{h} \right)^{-1} \left(\mathbf{h} | \mathbf{a}^\dagger \right) \quad (1.79)$$

The partitioned form of the propagator matrix becomes

$$\mathbf{G}(E) = \begin{bmatrix} \left(\mathbf{a}^\dagger | \mathbf{a}^\dagger \right) & \left(\mathbf{a}^\dagger | \mathbf{f} \right) \end{bmatrix} \begin{bmatrix} \left(\mathbf{a}^\dagger | (E\mathbf{1} - \mathbf{H}) \mathbf{a}^\dagger \right) & \left(\mathbf{a}^\dagger | (E\mathbf{1} - \mathbf{H}) \mathbf{f} \right) \\ \left(\mathbf{f} | (E\mathbf{1} - \mathbf{H}) \mathbf{a}^\dagger \right) & \left(\mathbf{f} | (E\mathbf{1} - \mathbf{H}) \mathbf{f} \right) \end{bmatrix}^{-1} \begin{bmatrix} \left(\mathbf{a}^\dagger | \mathbf{a}^\dagger \right) \\ \left(\mathbf{a}^\dagger | \mathbf{f} \right) \end{bmatrix} \quad (1.80)$$

Given the orthogonality conditions $\left(\mathbf{a}^\dagger | \mathbf{f} \right) = 0$, this simplifies to

$$\mathbf{G}(E) = \begin{bmatrix} \mathbf{1} & 0 \end{bmatrix} \begin{bmatrix} E\mathbf{1} - \left(\mathbf{a}^\dagger | \mathbf{H} \mathbf{a}^\dagger \right) & - \left(\mathbf{a}^\dagger | \mathbf{H} \mathbf{f} \right) \\ - \left(\mathbf{f} | \mathbf{H} \mathbf{a}^\dagger \right) & \left(\mathbf{f} | \mathbf{H} \mathbf{f} \right) \end{bmatrix}^{-1} \begin{bmatrix} \mathbf{1} \\ 0 \end{bmatrix} \quad (1.81)$$

The poles of the electron propagator, occurring at values $E = \omega$, are determined through the following eigensystem

$$\mathbf{U}\omega = \mathbf{H}\mathbf{U} \quad (1.82)$$

Here, \mathbf{H} is the superoperator Hamiltonian matrix and \mathbf{U} contain the residues connected to the j^{th} pole ω_j . The matrix elements of \mathbf{U} can be used to compute the Dyson orbitals of a particular pole

$$\phi_j^{\text{Dyson}} = \sum_i \phi_i U_{ij}^* \quad (1.83)$$

The probability factor, or pole strength, is given by

$$\pi_j = \sum_i |U_{ij}|^2 \quad (1.84)$$

In the diagonal approximation, a value of $\pi \geq 0.85$ is typically taken as an indication that the HF orbitals are a good reference for the Dyson orbitals.⁶⁹

Again, due to the orthogonality between primary and secondary spaces, the diagonal of $(\mathbf{h}|(E\mathbf{1} - \mathbf{H})\mathbf{h})^{-1}$ is needed. The inverse propagator matrix is given by

$$(\mathbf{G}(E))^{-1} = (\mathbf{a}^\dagger|(E\mathbf{1} - \mathbf{H})\mathbf{a}^\dagger) - (\mathbf{a}^\dagger|\mathbf{H}\mathbf{f}) (\mathbf{f}|(E\mathbf{1} - \mathbf{H})\mathbf{f})^{-1} (\mathbf{f}|\mathbf{H}\mathbf{a}^\dagger) \quad (1.85)$$

which reduces further to

$$(\mathbf{G}(E))^{-1} = E\mathbf{1}_a - \mathbf{H}_{aa} - \mathbf{H}_{af} (E\mathbf{1}_a - \mathbf{H}_{ff})^{-1} \mathbf{H}_{fa} \quad (1.86)$$

The set $\{\mathbf{f}_n\}$ represent vectors of length n containing creation operators exceeding annihilation operators by one for either particles (p) or holes (h). For example, with general orbital indices p, q, r, s, t, \dots , we have $\mathbf{f}_1 \equiv a_p^\dagger$ (h/p), $\mathbf{f}_3 \equiv a_p^\dagger a_q^\dagger a_r$ (2hp/2ph), $\mathbf{f}_5 \equiv a_p^\dagger a_q^\dagger a_r^\dagger a_s a_t$ (3h2p/3p2h), and so on. These operator “strings” generate the $N \pm 1$ states in a type of configuration interaction expansion in Hilbert space.

The set of field operators in the primary subspace \mathbf{a}^\dagger can be taken to be the creation operator product \mathbf{f}_1 acting on the HF vacuum to generate a HF reference. Because one can choose the basis representation of the primary subspace, the first two terms in Eq. (1.86) result in the inverse HF Green’s function $(\mathbf{G}(E))_0^{-1}$. The final term is thus the energy dependent part of the self-energy matrix $\sigma(E)$ and the total self-energy is

$$\Sigma(E) = \sigma(E) + \Sigma(\infty) \quad (1.87)$$

As $E \rightarrow \infty$, $\sigma(E)$ vanishes to leave the constant, or energy independent, form of the self-energy

$$\Sigma(\infty)_{pq} = \sum_{rs} \langle pr || qs \rangle \rho_{rs}^c \quad (1.88)$$

where ρ^c is the correction to the HF one-particle density ρ^{HF} .

The simplest approximation to the self-energy within EPT selects the \mathbf{f}_3 operators to constitute the secondary space. This first-order approximation leads to the second-order self-energy matrix

$$\Sigma^{(2)}(E) = (\mathbf{a}|\mathbf{H}\mathbf{f}_3)^{(1)} \left(E\mathbf{1} - (\mathbf{f}_3|\mathbf{H}\mathbf{f}_3)^{(0)} \right)^{-1} (\mathbf{f}_3|\mathbf{H}\mathbf{a})^{(1)} \quad (1.89)$$

The superscripts represent the n^{th} order correction to the self-energy. The first correction $n = 1$ thus begins at second-order perturbation theory. Diagonalizing the superoperator Hamiltonian, \mathbf{H}

$$\mathbf{H}^{(1)} = \begin{bmatrix} (\mathbf{a}|\mathbf{H}\mathbf{a})^{(0)} & (\mathbf{a}|\mathbf{H}\mathbf{f}_3)^{(1)} \\ (\mathbf{f}_3|\mathbf{H}\mathbf{a})^{(1)} & (\mathbf{f}_3|\mathbf{H}\mathbf{f}_3)^{(0)} \end{bmatrix} \quad (1.90)$$

gives the poles of $\Sigma^{(2)}(E)$. Note that the matrix elements $(\mathbf{a}|\mathbf{H}\mathbf{a})^{(0)}$ and $(\mathbf{f}_3|\mathbf{H}\mathbf{f}_3)^{(0)}$ rely on just the Fock operator. Terms in the primary-secondary coupling blocks that also rely on the Fock operator are omitted to preserve the Hermiticity of $\mathbf{H}^{(1)}$; otherwise, these spurious terms will vanish as the reference configuration is improved to a sufficient order. Algebraic or diagrammatic derivation of the second-order self energy-matrix elements yields

$$\Sigma_{pq}^{(2)}(E) = \frac{1}{2} \sum_{aij} \frac{\langle ij || qa \rangle \langle pa || ij \rangle}{E + \epsilon_a - \epsilon_i - \epsilon_j} + \frac{1}{2} \sum_{iab} \frac{\langle pi || ab \rangle \langle ab || qi \rangle}{E + \epsilon_i - \epsilon_a - \epsilon_b} \quad (1.91)$$

The hole indices $\{i, j, \dots\}$ represent occupied spin-orbitals and particle indices $\{a, b, \dots\}$ represent virtual spin-orbitals. The first and second summations of Eq. (1.91) are the 2hp and 2ph terms. If the canonical HF orbitals are sufficient approximations to the Dyson orbitals, we only need to evaluate the diagonal of $\Sigma^{(2)}(E)$ by requiring pole index $p = q$

$$\Sigma_{pp}^{(2)}(E) = \frac{1}{2} \sum_{aij} \frac{|\langle pa || ij \rangle|^2}{E + \epsilon_a - \epsilon_i - \epsilon_j} + \frac{1}{2} \sum_{iab} \frac{|\langle pi || ab \rangle|^2}{E + \epsilon_i - \epsilon_a - \epsilon_b} \quad (1.92)$$

If we take the second sum in Eq. (1.91) and separate terms with no dependency on E and set either a or b equal to i , we recover the contribution of single-particle excitations in the second-order energy. These singles substitutions are meant to improve the occupied space of the $N - 1$ system towards a more optimal set of one-electron orbitals. This amounts to the orbital relaxation term

$$\Sigma_{pp}^{R(2)} = \sum_{ai} \frac{|\langle ap || ip \rangle|^2}{\epsilon_a - \epsilon_i} \quad (1.93)$$

Note that $a \neq i$. The relaxation term $\Sigma_{pp}^{R(2)}$ is the second-order contribution to the ionization energy of orbital p from a Δ SCF calculation

$$-I_p(\Delta\text{SCF}) = E_{HF}(N) - E_{HF}^p(N-1) \quad (1.94)$$

A generalization of relaxation contribution to the binding energy of orbital p at the Δ SCF level is presented as a correction to the HF eigenvalue ϵ_p

$$-I_p(\Delta\text{SCF}) \simeq \epsilon_p - \Sigma_{pp}^{R(2)} \quad (1.95)$$

Additionally, the correlation part of the diagonal second-order self-energy can be extracted as follows

$$\Sigma_{pp}^{C(2)}(E) = \Sigma_{pp}^{(2)}(E) - \Sigma_{pp}^{R(2)} \quad (1.96)$$

which can be rewritten as

$$\Sigma_{pp}^{C(2)}(E) = \frac{1}{2} \sum_a \sum_{i \neq p} \sum_{j \neq p} \frac{|\langle pa || ij \rangle|^2}{E + \epsilon_a - \epsilon_i - \epsilon_j} + \frac{1}{2} \sum_{i \neq p} \sum_a \sum_b \frac{|\langle pi || ab \rangle|^2}{E + \epsilon_i - \epsilon_a - \epsilon_b} \quad (1.97)$$

The first term in Eq. (1.97) describes the correlation contribution of pair interactions of occupied i, j orbitals with unoccupied orbital a and the new virtual p , which is analogous to orbital relaxation but for the $N - 1$ state. The second term in Eq. (1.97), related to typical second-order HF perturbation theory for the N -particle system, contains the correlation effects of losing pairwise interactions due to the removal of orbital p .^{8,60} Turning to Eq. 1.92, we see that the second term in the diagonal second-order self-energy approximation (D2) leads to an arithmetic scaling of $\mathcal{O}(OV^2)$ for each pole search after performing the integral transformation to the MO basis.

1.2 Computational X-ray Spectroscopy

High resolution X-ray spectroscopy is widely used to obtain insights into the electronic and geometric structure of condensed and gaseous matter.⁷⁰⁻⁷⁷ Advances in experimental techniques, such as X-ray photoelectron spectroscopy (XPS), X-ray absorption spectroscopy (XAS), and inner-shell electron energy loss spectroscopy (ISEELS), have facilitated analysis of atom-specific core-level ionizations and excitations, both of which provide information relevant for “molecular fingerprinting” and probing the photophysics of materials. The spectroscopic signatures of an inner-shell photodetachment or excitation is dependent on the nature of the core-hole state, its sensitivity to the local environment, and the electronic structure of the final states.

Growing research in X-ray science has led to the increasing availability of high resolution experimental data. This has motivated the development of theoretical and computational approaches for simulating X-ray spectroscopy. Thus, in corroboration with experiment, the identification of chemical shifts and potential mechanisms for ultra-fast reactivity drives the need for accurate and predictive models.

Detailed accounts of many successful *ab initio* methods for modeling excitations and ionizations of core electrons are present in the literature.⁷⁸⁻⁸⁶ Early studies on core-ionizations of small molecules utilized the difference of self-consistent-field solutions (Δ SCF) obtained with the Roothaan-Hartree-Fock (HF) method.⁸⁷⁻⁹¹ Developed around the same time, Slater’s $X\alpha$ method⁹² gave reasonable results for optical transitions by X-ray absorption in molecules and solids. Slater’s $X\alpha$ became

the progenitor of transition potential and transition operator methods through its use of fractional orbital occupation numbers.^{93–103} Methods based on Kohn-Sham density functional theory (DFT), modified extensions of time-dependent density functional theory (TD-DFT), and variations of the static-exchange (STEX) method have shown viability for accurate, low-cost computation of core spectra.^{104–120} More recent examples of single determinant DFT methods include the restricted open-shell Kohn–Sham (ROKS) approach^{121,122} and the direct application of ionization potential (IP) corrected exchange correlation functionals.^{123–125} State-of-the-art, systematically improvable approximations based on many-body response theories offer highly accurate intensities and energies for assignments of X-ray spectra. Under this description spans variations of the *GW* approximation^{126–133}, the algebraic diagrammatic construction^{134–139} (ADC), the class of equation-of-motion coupled cluster (EOM-CC) methods^{140–146}, and related propagator methods.^{147,148} Methods for combining Δ SCF with quasiparticle corrections for orbital eigenvalues have been tested recently.^{149,150}

Wavefunction theories have also been tailored for X-ray spectroscopy. These include multireference configuration interaction^{151–154} (MRCI), Monte Carlo configuration interaction¹⁵⁵ (MCCI), excited state mean field (ESMF) theory^{156,157}, non-orthogonal configuration interaction^{158–160} (NOCI), restricted open configuration interaction with singles^{161–163} (ROCIS), and multiconfigurational self-consistent field (MCSCF) methods.^{164–168}

For most post-SCF calculations, core-excited states are accessed by limiting the excitation space of substituted determinants or by employing the core-valence separation (CVS) approximation.^{134,169–171} Weak electrostatic interactions between core and valence electrons justify the exclusion of certain types of configurations or Coulomb repulsion integrals, resulting in very minor effects on *K*-edge excitation energies for light atoms.¹⁷² Due to the nuclear proximity of core electrons, scalar relativistic and perturbative spin-orbit treatments are typically performed.^{173–177} Additionally, relativistic multicomponent methods have been applied to core-excitations.^{178–183}

Development of theories and computational models for X-ray spectroscopy is ongoing and bountiful as evidenced by the vast buffet of methodologies available. When perusing through the assortment of the different flavors of methods, one may be inclined to seek out an à la carte selection of methods that are cost-effective, accurate, and conceptually accessible. The work featured in Chapters 2–4 will examine low-to-modest scaling mean-field and many-body approaches simulating for single particle X-ray transitions.

Calculating Vertical Core-Excitation Energies Using $\Delta\text{SCF} + \Delta\Sigma$

” ...[W]e define the correlation energy as the difference between the energy calculated in the Hartree-Fock approximation and that calculated using any better approximation.

— D. Pines

Electron Interaction in Metals.

Solid State Physics 1, 367-450 (1955)

This chapter is based on the following:

A.Y. Zamani and H.P. Hratchian. “Assessing the performance of ΔSCF and the diagonal second-order self-energy approximation for calculating vertical core excitation energies” *J. Chem. Phys.* 157, 084115 (2022)

2.1 Motivation

X-ray spectroscopy is a powerful experimental technique for elucidating the excited-state physics of materials.^{73,184–192} The features of the observed spectral profile create a “fingerprint” characteristic of the atom or molecule under optical excitation. In particular, X-ray absorption spectroscopy (XAS) is used to probe element specific core-excited state properties in the soft X-ray region. Interpretations of X-ray spectra often rely on calculations based on *ab initio* quantum chemical methods. As such, approaches based on density functional and wavefunction theories have been developed for the accurate simulation of various X-ray spectroscopies.⁷⁸

The nature of a core-hole state generated by the excitation of a K-shell electron must be described by dynamical quantum many-body effects within the local electronic structure. The challenge for accurate and predictive simulation of these core-excited states is properly accounting for orbital relaxation and correlation.

State-of-the-art methods for the direct computation of core excitation energies such as the algebraic diagrammatic construction^{134,139,193} (ADC) and coupled cluster^{143,194} (EOM-CC,CCn), in the core-valence separation (CVS) approximation, can reproduce X-ray spectra to a high degree of accuracy. Recent developments of excited state mean field theory¹⁵⁶ (ESMF) and non-orthogonal configuration interaction singles¹⁵⁸ (NOCIS) have produced viable results for K-edge excitation energies at reasonable cost. Multireference configuration interaction calculations have been used to accurately describe core excitations in small molecules.^{151–153} Additionally, the multiconfigurational self-consistent field (MCSCF) class of methods along with perturbative spin-orbit treatments has also seen successful application in this area.^{195–197} However, the steep computational scaling involved with such methods often limits their applicability to a small set of modest sized systems. For this reason, the computational cost of self-consistent field (SCF) methods is especially attractive and Δ SCF based models remain quite popular in computational studies of core-excited states.

Historically, the Δ SCF approach with Hartree-Fock (HF) had been employed in the computation of ionization energies.^{88,91,198,199} In recent years, Δ SCF has been used in conjunction with maximum overlap methods for computing core excitation energies and core binding energies due to the simplicity of separately optimizing the MOs of two reference states.^{200,201} For weakly correlated systems, SCF determinants are often a good approximation for the ground electronic state. The reference orbitals of a good HF wavefunction are a viable guess basis for an excited SCF calculation. Through Δ SCF, much of the orbital relaxation is accounted for—quite evidently so with localized core ionizations and excitations.^{60,202,203} What remains to be accounted for is the many-body correlation via two (or more) particle interactions.

With HF lacking correlation one may be inclined to use Kohn-Sham DFT. However, the sensitivity to the approximate functional makes it difficult to control the inclusion of correlation in a Δ DFT calculation—possibly leading to inconsistent results. Systems involving degenerate configurations and transitions beyond a non-degenerate HOMO-LUMO gap can also be challenging for DFT. The restricted open-shell Kohn-Sham (ROKS) approach has been employed by Hait and Head-Gordon for obtaining accurate vertical core excitation energies.^{204,205} Alternatively, we propose the adoption of Hartree-Fock solutions as a fundamental, parameter-free starting point for computing excitation gaps.

This work presents a composite model for computing vertical core excitation energies with Δ HF and diagonal second-order correlation corrections to Koopmans' theorem for ionization potentials using electron propagator theory (EPT). For a

brief overview of EPT, see Chapter 1 Section 1.1.4. The combination of Δ SCF and post-HF methods in the context of core-excited states is seldom explored. However, an analogous method for computing binding energies was developed and tested some time ago.^{206,207} It was proposed that the total relaxation effects contained within the Δ SCF result between the N and $N - 1$ determinants and that the correlation contributions are contained in the second-order self-energy for an electron detachment. With that observation in mind, this work explores the potential for a similar reasoning applied to N -conserving electronic excitations. As shown below, the quality of excitation energies using this compound model chemistry approach depends on the quality of EPT results for the core orbital. It is also shown that the locality of core orbitals and non-equivalency of neighboring atoms often lead to accurate results using only Δ HF.

2.2 Methods

To compute core excitation energies, we propose a composite model combining quantum chemical methods with Δ SCF that treat dynamical correlation, corrected spin state energetics from an approximate spin projection method, and relativistic effects.

2.2.1 Δ SCF + $\Delta\Sigma$ Approach

Following the detailed protocol by Pickup and Goscinski⁶⁰ together with developments in EPT^{206,207} by Öhrn, Ortiz, and others, one can recover an expression for the lowest-order correction to Koopmans' theorem

$$-I = -I_p(\Delta\text{SCF}) + \Sigma_{pp}^{C(2)}(E) \quad (2.1)$$

This interpretation of the true binding energy retains a complete second-order description of relaxation and correlation contributions.

What has yet to be explored in great detail is the application of this concept to excitation energies for one-electron transitions. Following from the discussion above, we propose an approximation of the excitation energy ω_X given by

$$\omega_X \simeq E(\Delta\text{SCF}) + \Delta\Sigma^{C(2)}(E) \quad (2.2)$$

$$\simeq [E_{p \rightarrow r}(N) - E_0(N)] + [\Sigma_{rr}^{C(2)}(E_{N+1}) - \Sigma_{pp}^{C(2)}(E_{N+1})] \quad (2.3)$$

where $E(\Delta\text{SCF})$ is the difference between the excited ($E_{p \rightarrow r}$) and ground state (E_0) HF energies. $\Delta\Sigma^{C(2)}(E)$ is the difference between the correlation corrections to ϵ_r and ϵ_p . These terms are computed for the $N + 1$ determinant, the propagator reference, where orbitals p and r are both occupied. This anionic species is used to provide a model configuration for obtaining correlation energy gaps.

Since core-hole configurations are often subject to variational collapse in the SCF procedure, we make use of a maximum overlap algorithm to obtain representative single determinant excited-state solutions of the desired configuration. Here, we have chosen the projected initial maximum overlap method (PIMOM).²⁰⁸ The SCF excited-states are unrestricted Hartree-Fock (UHF) solutions obtained after an occupied-virtual orbital rotation.

As a consequence of the symmetry dilemma,²⁰⁹ these excited-state solutions often break spin and electronic state symmetry in exchange for a lower energy. For closed-shell initial states, the core excitation process should involve a linear combination of open-shell configurations, since either the up-spin or down-spin electron can be substituted. With a single unrestricted determinant, an estimate for the energy of a proper spin eigenstate for the excited state is computed using approximate projection (AP) according to²¹⁰⁻²¹²

$$E_{AP} = aE_{LS} + (1 - a)E_{HS} \quad (2.4)$$

where the weight or single annihilation parameter a is

$$a = \frac{\langle \mathcal{S}_{HS}^2 \rangle - S_{z,LS}(S_{z,LS} + 1)}{\langle \mathcal{S}_{HS}^2 \rangle - \langle \mathcal{S}_{LS}^2 \rangle} \quad (2.5)$$

E_{LS} is the energy of the spin contaminated core-hole configuration and E_{HS} is the energy of its $S + 1$ counterpart. AP is then applied for excited-state ΔSCF calculations.

2.2.2 Relativistic Corrections

To attain a proper description of core electron physics, relativistic effects need to be considered. Bethe and Salpeter defined the relativistic shift in the ionization potential for a two-electron atom as²¹³

$$E_J = \alpha^2 \left[-\frac{1}{8}Z^4 + \frac{1}{4}\langle p_1^4 \rangle - \pi Z \langle \delta^{(3)}(\mathbf{r}_1) \rangle - \pi \langle \delta^{(3)}(\mathbf{r}_{12}) \rangle \right] - E_2. \quad (2.6)$$

Extensions of this model to higher Z and formulas for the expectation values above have been provided by Perekis, Silverman, and Scherr.^{214,215} For consistency, E_J for a particular atom is included in our model in an ad hoc fashion to the computed non-relativistic core excitation energy to obtain ω_X . Following this protocol, our calculated corrections for C, N, O, and F are 0.1 eV, 0.2 eV, 0.4 eV, and 0.7 eV respectively. We note that these values agree with those previously reported.^{134,216}

2.3 Results

A test set has been selected from the CGB data set, which has been reported in prior publications.^{217,218} These structures were optimized using the CCSD(T)/aug-cc-pVTZ model chemistry. Additional molecules were selected from the NIST CCCBDB²¹⁹ and were optimized using the same level of theory. All calculations were performed with a development version of GAUSSIAN.²²⁰ Reference single-point SCF calculations used the aug-cc-pVTZ basis. Diagonal second-order (D2) calculations used the cc-pVTZ basis with a full MO integral transformation window. Neutral and anion reference determinants were generally eigenstates of the total spin-squared operator S^2 , except for the heterocyclic molecules. Furan, imidazole, tetrazine, pyridine, and thiophene anions possess $\langle S^2 \rangle$ values that deviate from $S(S+1)$ by $\sim 10\%$ to 18% . Mean pole strengths for core and valence electron detachments are 0.73 and 0.92 respectively.

Table 2.1 reports the vertical excitation energies obtained with only Δ SCF. The absence of degenerate or quasi-degenerate core orbitals for a particular atom tends to minimize the interactions of configurations relevant for describing the excited state, meaning the correlation contribution to the energy is much less than the orbital relaxation in these cases. As such, it is not surprising that the computed Δ SCF energies with relativistic corrections are well in the vicinity of experimental

values (see Table 2.2) since the atomic cores of interest are unique and other core orbitals belonging to atoms of the same bonding class are not present. The differences in the measure of errors between excitation energies computed with (MAE: 0.6 eV, RMSE: 0.8 eV) and without relativistic effects (MAE: 0.6 eV, RMSE: 0.7 eV) are shown to be minimal for this data set.

Systems for which core excitations are poorly described using ΔSCF are thus candidates for treatment with EPT based models. To avoid double counting of orbital relaxation recovered with ΔSCF , $\Delta\Sigma^{R(2)}$ must be removed from the self-energy correction to binding energies obtained with Koopmans' theorem. Results using the $\Delta\text{SCF} + \Delta\Sigma^{C(2)}$ method are given in Tables 2.3 and 2.4. ΔSCF results for core excitations in the set of molecules with equivalent atoms highly overestimate experimental values—with errors exceeding 10 eV. Significant improvements are made when $\Delta\Sigma^{C(2)}$ is added along with relativistic corrections for each atom type (MAE: 1.3 eV, RMSE: 1.7 eV). Errors here slightly increase when relativistic effects are ignored.

Although the ΔSCF method is satisfactory for the molecules in Table 2.1, an evaluation of changes in the data with the introduction of D2 self energy corrections is performed for completeness and summarized in Tables 2.5 and 2.6. The addition of $\Delta\Sigma^{C(2)}$ consistently underestimates experiment and overcorrects ΔSCF energies. This is a residual, nonphysical effect of using the difference in the correlation terms of the D2 approximation for two independent ionizations in the anions.

Reducing point group symmetry or applying effective core potentials (ECP) can localize the core orbital and improve estimates to ω_X . Table 2.7 contains energies computed with ΔSCF alone for the data set in Table 2.3 but with broken molecular symmetry. For molecules with $D_{\infty h}$, D_{3d} , or D_{2h} symmetry, multi-electron Wood-Boring ECPs (MWB2) are applied to all atoms except hydrogen and the atom of interest. For all other molecules, the symmetries are reduced to C_1 . With this pragmatic approach, errors (see Table 2.8) are reduced to about half of an electron volt (MAE: 0.5 eV, RMSE: 0.5 eV). This remarkable, but well-known effect ameliorates the problems that arise from quasi-degeneracy and delocalization at the cost of losing symmetry and its usefulness for theoretical assignment spectral signatures.

A qualitative effect of adding correlation corrections to Hartree-Fock energy gaps is apparent. However, quantitative predictions of vertical core excitation energies with this method can vary as there are multiple factors at play. For example, modeling excited states of neutral molecules through electron detachments within the $N + 1$ configurations lacks a one-to-one correspondence with respect to the relaxation of

the target N electron core-hole state. For errors that manifest in Δ SCF calculations, different non-Aufbau SCF solutions representing an excited state configuration can be obtained depending on basis projections, overlap metrics, and convergence criteria—all of which can alter the Δ SCF result. Since the quality of the poles is dependent on the quality of the reference determinant, it is important to note an additional layer of error is present when there is spin contamination in the anions. Whenever possible, propagator references with good intrinsic spin quantum numbers are preferred.^{221,222}

Lastly, the choice of relativistic correction may vary the magnitude of ω_X significantly with increasing atomic number and heightened many-electron correlation in the core region. In addition to the technique applied in this study, there many other methods in relativistic quantum chemistry to choose from.^{173–175} Nonetheless, the composite model introduced here provides a reasonable estimate to core excitation energies and appears to balance static and dynamic correlation effects well with affordable computational cost.

The qualitative utility of the Δ SCF + $\Delta\Sigma$ model for predicting vertical core excitation energies is reflected in the moderate deviations from experimental values. The “relaxation error” is pronounced for K-shell ionizations or excitations, more so when the core orbitals are delocalized, and the relative importance of relaxation Σ^R and correlation Σ^C contributions varies between the core and valence regimes.^{242,243} For ionizations of local, non-equivalent cores, Δ SCF recovers the bulk of the relaxation effects.^{90,244}

Lone pairs and double bonds between equivalent atoms (which give rise to degenerate orbitals) enhance the correlation effects involving the interaction of degenerate configurations. In cases of strong correlation, Δ HF tends to overestimate the excitation energy. Cederbaum and Domcke²⁴⁵ have explained that when there are no degenerate or closely degenerate core orbitals, the correlation energy becomes very small in comparison to the relaxation energy found in $\Sigma_{pp}^{(2)}(E)$. In the case of homonuclear diatomics (e.g. N_2), they have shown that the degeneracy of the delocalized orbitals with *gerade* and *ungerade* symmetry, σ_g and σ_u , causes the correlation contribution to the self energy to become competitive in magnitude to the relaxation component. With two delocalized, symmetry orbitals close in energy, Δ HF results will not include the now increased correlation effects.

If one lifts the symmetry constraints (i.e. reduce the molecular symmetry) and localizes the basis for the cores, the total SCF relaxation energy becomes a mixture of orbital relaxation and pair correlation in the relaxed $N - 1$ state. This explains why Δ SCF for K-shell electron detachments often yields good agreement with experiment

when the core orbitals are localized. However, by breaking symmetry, the admixture of orbital relaxation and correlation effects in the excited SCF solutions obtained with HF or KS-DFT limits systematic improvements with perturbation theory. More recent studies have further explored the errors that arise from using localized/delocalized core orbitals with a variety of methods for modeling x-ray spectroscopies.²⁴⁶

Computing core excitation energies using $\Delta\text{SCF} + \Delta\Sigma^{C(2)}$ requires a balanced treatment of orbital relaxation and correlation effects. Correlation corrections to ΔSCF are heavily modulated by the quality of the pole of the excited core orbital. Higher-order approximations to the self-energy beyond D2 may be needed to obtain accurate core binding energies. Computing self-energy gaps with electron affinities starting from a core-hole cation reference state may be an alternative to an ionization-based approach. Although, some precautions must be taken to deal with numerical instabilities that may accompany a non-Aufbau core-hole reference with post-HF methods.²⁴⁷ Additionally, varying the occupation number of the target core orbital via the transition operator method^{93,96} may also be a relevant approach towards increasing the quality of the self-energy.

2.4 Conclusion

We have presented computational results for core excitation energies using ΔHF and the diagonal second-order self-energy approximation. The efficacy of obtaining accurate excitation energies with only ΔHF when core orbitals are localized is reaffirmed. Without reducing molecular symmetry, the results calculated with the proposed $\Delta\text{SCF} + \Delta\Sigma$ composite method for chemical species with degenerate C, N, O, and F core orbitals are in good agreement with experimental energies. Separating the orbital relaxation energy recovered with ΔSCF and correlation energy gaps determined with the D2 self-energy approximation provides a step towards a systematic approach for estimating vertical core excitation energies. With a limiting step of generating the MO integrals, the $\mathcal{O}(OV^2)$ arithmetic scaling of diagonal second-order EPT is indeed a low-cost choice as a post-HF method to be used with ΔSCF for calculating core-excitation energies.

Studies of K- and L-edge transitions beyond second period elements and computation of cross-sections for simulating spectra will be important diagnostics for this model and will be examined in future work. Further exploration of practical, low-scaling composite models for computing excitation energies with different electron propagator methods is also underway.

Tab. 2.1.: Δ SCF vertical excitation energies ω_X for the lowest symmetry-allowed core to valence transition.

Molecule	Core	Δ SCF (eV)	ω_X (eV)	Exp. (eV)
Acetone	C (C-O)	287.3	287.4	286.4 ²²³
Acetone	O	531.0	531.4	531.4 ²²³
Acrolein	C (C-O)	286.7	286.8	286.1 ²²⁴
Acrolein	O	530.2	530.6	530.6 ²²⁴
CH4	C	289.8	289.9	288.0 ²²⁵
CO	C	288.4	288.5	287.4 ²²⁶
CO	O	533.7	534.1	534.2 ²²⁶
Furan	O	535.1	535.5	535.2 ²²⁷
H ₂ CO	C	286.5	286.6	285.6 ²²⁸
H ₂ CO	O	530.6	531.0	530.8 ²²⁸
H ₂ O	O	534.3	534.7	534.0 ²²⁵
HF	F	687.3	688.0	687.4 ²²⁹
NH ₃	N	401.1	401.3	400.8 ²²⁵
Pyridine	N	398.8	399.0	398.8 ²³⁰
CO ₂	C	292.4	292.5	290.8 ²³¹
Imidazole	N (N-H)	403.2	403.4	402.3 ²³²
Imidazole	N	400.4	400.6	399.9 ²³²
N ₂ O	N (N-N)	401.2	401.4	401.0 ²³¹
N ₂ O	N (N-O)	404.7	404.9	404.6 ²³¹
N ₂ O	O	534.1	534.5	534.6 ²³¹
HCN	C	286.9	287.0	286.4 ²³³
HCN	N	400.0	400.2	399.7 ²³³
CF ₂ O	C	292.2	292.3	290.9 ²³⁴
CF ₂ O	O	532.7	533.1	532.7 ²³⁴
NO	N	400.0	400.2	399.7 ²³⁵
NO	O	532.2	532.6	532.7 ²³⁵
CH ₃ OH	C	289.0	289.1	288.1 ²³⁶
CH ₃ OH	O	534.3	534.7	534.1 ²²³
CH ₃ NH ₂	C	288.2	288.3	287.5 ²³⁶
CH ₃ NH ₂	N	401.2	401.4	400.6 ²³⁶

Tab. 2.2.: Mean absolute error (MAE) and root-mean-square error (RMSE) in eV.

	Δ SCF with rel.	Δ SCF
MAE	0.6	0.6
RMSE	0.8	0.7

Tab. 2.3.: $\Delta\text{SCF} + \Delta\Sigma^{C(2)}$ vertical excitation energies ω_X for the lowest symmetry-allowed core to valence transition.

Molecule	Core	ΔSCF (eV)	$\Delta\Sigma^{C(2)}$ (eV)	ω_X (eV)	Exp. (eV)
C ₂ H ₂	C	294.0	-9.3	284.8	285.9 ²³⁷
C ₂ H ₄	C	293.0	-9.2	283.8	284.7 ²³⁷
C ₂ H ₆	C	294.5	-8.6	286.0	286.9 ²³⁷
C ₂ N ₂	C	293.3	-8.5	284.9	286.3 ²³³
C ₂ N ₂	N	410.4	-11.6	398.9	398.9 ²³³
F ₂	F	695.2	-13.5	682.3	682.2 ²²⁹
N ₂	N	410.5	-10.5	400.2	400.9 ²³⁸
O ₂	O	542.0	-11.9	530.5	530.8 ²³⁵
Pyridine	C	294.6	-9.7	285.0	285.3 ²³⁰
Tetrazine	N	413.6	-14.4	399.4	398.8 ²³⁹
Tetrazine	C	293.8	-7.6	286.3	285.2 ²³⁹
Thiophene	C (C-S)	294.4	-8.5	286.0	285.4 ²⁴⁰
CO ₂	O	546.6	-14.4	532.6	535.4 ²³¹
Furan	C	295.8	-8.2	287.7	286.6 ²²⁷
CF ₂ O	F	700.9	-16.4	685.3	689.2 ²³⁴
C ₂ F ₄	C	298.7	-10.8	287.9	290.1 ²⁴¹
C ₂ F ₄	F	708.4	-21.8	687.3	690.7 ²⁴¹

Tab. 2.4.: Mean absolute error (MAE) and root-mean-square error (RMSE) in eV.

	$\Delta\text{SCF} + \Delta\Sigma^{C(2)}$ with rel.	$\Delta\text{SCF} + \Delta\Sigma^{C(2)}$	ΔSCF with rel.	ΔSCF
MAE	1.3	1.4	10.6	10.4
RMSE	1.7	1.9	11.0	10.7

Tab. 2.5.: $\Delta\text{SCF} + \Delta\Sigma^{C(2)}$ vertical excitation energies ω_X for the lowest symmetry-allowed core to valence transition.

Molecule	Core	ΔSCF (eV)	$\Delta\Sigma^{C(2)}$ (eV)	ω_X (eV)	Exp. (eV)
Acetone	C (C-O)	287.3	-3.5	283.9	286.4 ²²³
Acetone	O	531.0	-1.6	529.8	531.4 ²²³
Acrolein	C (C-O)	286.7	-3.4	283.5	286.1 ²²⁴
Acrolein	O	530.2	-2.2	528.4	530.6 ²²⁴
CH ₄	C	289.8	-3.5	286.3	288.0 ²²⁵
CO	C	288.4	-3.5	285.1	287.4 ²²⁶
CO	O	533.7	-2.5	531.6	534.2 ²²⁶
Furan	O	535.1	-2.4	533.1	535.2 ²²⁷
H ₂ CO	C	286.5	-4.5	282.1	285.6 ²²⁸
H ₂ CO	O	530.6	-3.1	527.8	530.8 ²²⁸
H ₂ O	O	534.3	-5.2	529.5	534.0 ²²⁵
HF	F	687.3	-5.5	682.6	687.4 ²²⁹
NH ₃	N	401.1	-2.7	398.6	400.8 ²²⁵
Pyridine	N	398.8	-3.6	395.3	398.8 ²³⁰
CO ₂	C	292.4	-5.3	287.2	290.8 ²³¹
Imidazole	N (N-H)	403.2	-1.4	402.0	402.3 ²³²
Imidazole	N	400.4	-2.5	398.1	399.9 ²³²
N ₂ O	N (N-N)	401.2	-1.5	399.9	401.0 ²³¹
N ₂ O	N (N-O)	404.7	-2.4	402.5	404.6 ²³¹
N ₂ O	O	534.1	-1.4	533.1	534.6 ²³¹
HCN	C	286.9	-3.2	283.8	286.4 ²³³
HCN	N	400.0	-2.6	397.6	399.7 ²³³
CF ₂ O	C	292.2	-4.7	287.6	290.9 ²³⁴
CF ₂ O	O	532.7	-4.7	528.4	532.7 ²³⁴
NO	N	400.0	-3.2	397.0	399.7 ²³⁵
NO	O	532.2	-2.1	530.4	532.7 ²³⁵
CH ₃ OH	C	289.0	-3.6	285.4	288.1 ²³⁶
CH ₃ OH	O	534.3	-4.6	530.1	534.1 ²²³
CH ₃ NH ₂	C	288.2	-3.1	285.1	287.5 ²³⁶
CH ₃ NH ₂	N	401.2	-3.7	397.7	400.6 ²³⁶

Tab. 2.6.: Mean absolute error (MAE) and root-mean-square error (RMSE) in eV.

	$\Delta\text{SCF} + \Delta\Sigma^{C(2)}$ with rel.	$\Delta\text{SCF} + \Delta\Sigma^{C(2)}$	ΔSCF with rel.	ΔSCF
MAE	2.6	2.9	0.6	0.6
RMSE	2.8	3.1	0.8	0.7

Tab. 2.7.: Δ SCF vertical excitation energies ω_X for the lowest symmetry-allowed core to valence transition with core localization.

Molecule	Core	Δ SCF (eV)	ω_X (eV)	Exp. (eV)
C ₂ H ₂	C	286.0	286.1	285.9 ²³⁷
C ₂ H ₄	C	285.0	285.1	284.7 ²³⁷
C ₂ H ₆	C	287.2	287.3	286.9 ²³⁷
C ₂ N ₂	C	286.3	286.4	286.3 ²³³
C ₂ N ₂	N	398.6	398.8	398.9 ²³³
F ₂	F	680.7	681.4	682.2 ²²⁹
N ₂	N	400.7	400.9	400.9 ²³⁸
O ₂	O	530.9	531.3	530.8 ²³⁵
Pyridine	C	285.9	286.0	285.3 ²³⁰
Tetrazine	N	398.2	398.4	398.8 ²³⁹
Tetrazine	C	286.2	286.3	285.2 ²³⁹
Thiophene	C (C-S)	286.1	286.2	285.4 ²⁴⁰
CO ₂	O	535.1	535.5	535.4 ²³¹
Furan	C	287.0	287.1	286.6 ²²⁷
CF ₂ O	F	689.2	689.9	689.2 ²³⁴
C ₂ F ₄	C	290.5	290.6	290.1 ²⁴¹
C ₂ F ₄	F	690.4	691.1	690.7 ²⁴¹

Tab. 2.8.: Mean absolute error (MAE) and root-mean-square error (RMSE) in eV.

	Δ SCF with rel.	Δ SCF
MAE	0.5	0.4
RMSE	0.5	0.6

Calculating Vertical Core-Excitation Energies Using Δ MP with Spin Projection

” *One of the big difficulties which was still remaining after one understood the single electron problem was that when you considered a problem concerning two or more electrons, you had to assume that the spins all set themselves parallel or anti-parallel, so that one had a definite value for the total spin. Then one found that the energy levels depended very much on the value of the total spin.*

— **P.A.M. Dirac**

An Historical Perspective of Spin. Proceedings of the Summer Studies on High-energy Physics with Polarized Beams. Argonne National Laboratory (1974)

This chapter is based on the following:

A.Y. Zamani and H.P. Hratchian. “Estimating vertical core-excitation energies from Møller-Plesset theory with spin projection” *in prep* (2023)

3.1 Motivation

The formation of a core-hole is accompanied by a significant reorganization of the atomic or molecular electronic structure. In quantum chemistry, this particular effect can be characterized by orbital relaxation (ORX). It is known that Δ SCF with HF is able to capture ORX effects for core-level transitions when the core orbital is localized on one atom.^{60,202,203,244,248} However, when molecular symmetry is present, core orbitals are delocalized over equivalent atoms as symmetry adapted linear combinations. One prototypical example is the $1s\sigma_g^{-1}$ or $1s\sigma_u^{-1}$ hole-state

of N_2 . The reorganization or relaxation energy is then representative of the screening potential induced by the charge distribution of valence electrons in the presence of a vacant core.^{249,250} Picturing this case as a simple two-site point charge model, the screened interaction energy of a delocalized core-hole is half of what it would be with a localized core-hole. Δ SCF calculations for ionizations in diatomics from either σ_g or σ_u produce only about half of the ORX energy²⁴⁵, but when the core orbitals are strongly localized (i.e. as a 1s orbital on either atom), most of the ORX energy is recovered. It follows that the ORX energy is inversely proportional to number of equivalent atomic sites that the core-hole orbitals are delocalized over.²⁴⁴ If one chooses not to abandon orbital symmetry, correlation energy contributions describing pair interactions involving the delocalized core-holes must be incorporated. By using many-body perturbation theory (MBPT) to construct a response function⁸ that contains information about the hole state, one will find that fluctuation potential/self-energy expressions contain terms corresponding to correlation that will become competitive, energetically, with terms for relaxation when symmetry is present.^{60,206,245,248} With localization, the position of the core-hole is inherently correlated with the coordinates of the redistributed electron charge density that contributes to the screening potential, and thus, the “concepts of relaxation and correlation become inseparable”.^{251,252} The accurate performance of Δ SCF calculations on local core-holes is a direct result of effectively mixing ORX and correlation effects.²⁴⁵

We have merely stated simple, historically established ideas on the physical effects that must be incorporated in theoretical models for understanding molecular X-ray physics. One can take the approach of explicit orbital optimization of two reference determinants to model ORX.²⁵³ Alternatively, one can adopt a variational coupled cluster *ansatz* to include infinite order relaxation effects.²⁵⁴ Similarly, correlation effects can be added arbitrarily through Δ DFT or systematically with MBPT(n) to n^{th} order. In this study, we opt for a spin-conserving composition of both SCF and Møller-Plesset (MP) perturbation theory with scalar relativistic corrections. The performance of these methods on the computation vertical K-edge excitation energies is assessed.

3.2 Methods

Spin-projected UHF and UMP n ($n = 2, 2.5, 3$) calculations are performed with different basis sets, pseudopotentials, and relativistic corrections. A protocol for orbital index restrictions according to specified thresholds for suppressing errors due

to small denominators is applied. This section is composed of largely self-contained explanations of the theoretical and computational procedures herein.

3.2.1 Spin Projection

For generating an initial SCF wavefunction, HF is selected as fundamental, parameter-free starting point in order to mitigate delocalization errors, self-interaction errors, and the task of curating of density functional approximations.^{255–259} The maximum overlap method^{208,260–263} (MOM) is used to locate a non-Aufbau, unrestricted Hartree-Fock (UHF) solution representing a core-hole state. This method avoids variational collapse to the ground state, although other efficient algorithms are also applicable.^{122,264,265} The excited state singlet is ideally a linear combination of open-shell configurations since the promotion of either an up-spin α or down-spin β electron from the same core orbital to some virtual orbital is equally probable. Since the chosen model is constrained to a monodeterminantal framework, the core-hole UHF solution will suffer from artificial spin contamination as a consequence of breaking spin-symmetry in exchange for a lower energy.^{209,266–268}

To obtain correct spin-state energetics starting from a broken-symmetry solution, one can employ projection-after-variation techniques. One such method is approximate projection (AP).^{210–212} A limitation of AP is that calculation of additional $(s + 1)$ spin states (themselves susceptible to spin contamination) is required if more than one contaminant is present—highlighting an insufficiency in the two-state model. Another drawback is that AP alone does not correct the wavefunction.

Furthermore, a UHF wavefunction after a single annihilation may exhibit an anomalous increase²⁶⁹ in the value of the total spin-squared expectation value $\langle S^2 \rangle$ away from its true $s(s + 1)$ eigenvalue or, in some circumstances, $\langle S^2 \rangle$ can even become negative.²⁷⁰ As such, it may become necessary to remove multiple contaminants of higher spin. Determining the weighted contributions from higher spin states will require information about higher moments m of $\langle S^2 \rangle$ —the values of $\langle S^{2m} \rangle$. To initiate spin purification of the broken-symmetry UHF solution, the wavefunction must be corrected.

Projected HF (PHF) wavefunctions are constructed by re-coupling intrinsic electronic spin using projection operator^{30,33–35} or group-theoretical^{36,271–274} techniques. PHF wavefunctions are multiconfigurational spin eigenfunctions and include the necessary nondynamical correlation in the many-electron system. Here, we employ Löwdin's spin projection operator \mathcal{O}_k

$$\mathcal{O}_k = \prod_{s \neq k} \frac{S^2 - s(s+1)}{k(k+1) - s(s+1)} \quad (3.1)$$

where k is the spin of the target spin state and s is the spin of the higher state to project out. The operator \mathcal{O}_k can resolve a vector in Hilbert space into its component along the axis for k spin via orthogonal projection.²⁷⁵ In addition to its commutation with the spin-free non-relativistic Hamiltonian \mathcal{H} , this projector satisfies characteristic properties of idempotency and completeness. \mathcal{O}_k is a product of annihilation operators \mathcal{A}_k , which are not idempotent.²⁷⁶ Applying all possible annihilators for obtaining the entire manifold of configuration state functions (CSF) is analogous to performing full CI (FCI), so truncation becomes necessary.

The many-electron total spin-squared operator⁴⁰ is then

$$S^2 = -\frac{N(N-4)}{4} + \sum_{i>j} \mathcal{P}_{ij}^{\zeta} \quad \zeta = \frac{N!}{2!(N-2)!} \quad (3.2)$$

where ζ is the number of unique two-index spin transposition generators \mathcal{P}_{ij} of the symmetric group S_N containing N particles.²⁷⁷ Application of \mathcal{O}_k on some reference wavefunction Ψ_0 gives a CSF Φ_k that is a linear combination of Slater determinants D_j that span the subspace of basis vectors with M_k quantum numbers

$$|\Phi_k\rangle = \sum_j c_j |D_j\rangle \quad (3.3)$$

such that

$$S^2 |\Phi_k\rangle = k(k+1) |\Phi_k\rangle. \quad (3.4)$$

The configuration weights c_j are sometimes referred to as the Sanibel coefficients.²⁷⁸ The PHF wavefunction, its energy, and spin properties should correspond to an electronic state of a particular multiplicity. The solution of the PHF equations constitutes a variation-after-projection (VAP) approach if the projected wavefunction

itself variationally optimized at the beginning.^{279,280} This kind of approach is a hallmark of the extended Hartree-Fock (EHF) method.^{30,31} Projection-after-variation (PAV) assumes one optimizes a UHF determinant and subsequently performs spin-projection. This is known as projected UHF or PUHF^{32,281,282} which falls under the category of EHF schemes.²⁸³ We take advantage of the robustness of modern SCF solvers and fast convergence of single reference SCF densities to optimize UHF wavefunctions for subsequent spin projection. What is absent from the PUHF model is dynamical correlation.

3.2.2 Projected Hartree-Fock and Møller-Plesset Theory

To introduce information about electron-electron correlations, we treat many-body interactions perturbatively via Møller-Plesset partitioning⁵⁸ of \mathcal{H} into the zeroth-order Hamiltonian \mathcal{H}_0 and perturbation operator \mathcal{V} :

$$\mathcal{H} = \mathcal{H}_0 + \mathcal{V}. \quad (3.5)$$

At second order, a minimal description of pair correlation corrections to the HF energy are brought about through connected doubles substitution operators \mathcal{X}_{ij}^{ab} . The set of \mathcal{X}_{ij}^{ab} correlators are said to have isolated effects in that there is no coupling between double substitutions. In the context of core-hole states, the second-order $\langle \text{OO} || \text{VV} \rangle$ terms allow for pairwise core-core, core-valence, and valence-valence Coulomb and exchange interactions. Brumboiu and Fransson have performed MP2 energy decomposition analysis for core IPs.²⁴⁶ Their findings indicate very large energy contributions from core-valence corrections with delocalized symmetry orbitals (see Fig. 7 of Ref. [246]). This is significant in regards to the SCF picture of an ionization of a delocalized core orbital because, in a sense, one is removing only “half” the core electron density. In N_2 , for example, the ORX energy of a core-ionized state formed by a detachment of $1s\sigma_u$ must be complemented by the correlation energies that describe pair-removal and pair correlations that involve both $1s\sigma_u$ and $1s\sigma_g$ —quantities that ΔSCF lacks. This reasoning translates to core-excitations as well. Take a single orbital rotation of $1s\sigma_u$ and $2p\pi_g$. ΔSCF does not have the very large core-valence corrections involving $1s\sigma_u^{-1}$ or the remaining occupied $1s\sigma_g$. Another interesting point in the study of Brumboiu and Fransson is the large contributions of opposite spin $\alpha\beta$ and same spin $\beta\beta$ terms in the core-valence MP2 corrections for the ionization of a delocalized α core orbital. An earlier work by

Kosugi²⁸⁴ also signifies the occurrence of large core-valance exchange integrals for core-hole states in diatomics (see Table 2 of Ref. [284]). The physical basis of this observation along with the considerable β ORX discourages the use of spin-component-scaled MP methods. The spin polarization in the final state will result in a high degree of spin contamination in the UHF reference, which is a cause for severe errors in the UMP $_n$ series.²⁸⁵ We propose, quite simply, that PUMP2 and PUHF can be chosen to remedy spin-symmetry breaking.

Because MP2 usually exaggerates the pair correlation energy, MP3 is said to offer a more realistic description of that energy.⁵⁹ It may be reasonable to suggest roughly extrapolating the perturbation series by adding some fraction of the third-order correction to the second-order total energy. Methods that rely on the arithmetic mean of second- and third-order corrections have shown promising results for modeling non-covalent interactions^{286,287}, reactivity²⁸⁸, and spectroscopy²⁸⁹. Since we are concerned with excitation gaps, we desire more direct information about total energies through Δ PUHF, Δ PUMP2, and Δ PUMP3. In this paper, we adopt the formulations for spin projection outlined by Schlegel.²⁹⁰

The energy for some projected reference wavefunction Ψ is given by

$$\frac{\langle \mathcal{O}_k \Psi | \mathcal{H} | \mathcal{O}_k \Psi \rangle}{\langle \mathcal{O}_k \Psi | \mathcal{O}_k \Psi \rangle}. \quad (3.6)$$

Since

$$[\mathcal{H}, \mathcal{O}_k] = 0, \quad (3.7)$$

the following matrix elements are equivalent:

$$\frac{\langle \Psi | \mathcal{O}_k^\dagger \mathcal{H} \mathcal{O}_k | \Psi \rangle}{\langle \Psi | \mathcal{O}_k^\dagger \mathcal{O}_k | \Psi \rangle} = \frac{\langle \mathcal{O}_k \Psi | \mathcal{H} | \mathcal{O}_k \Psi \rangle}{\langle \mathcal{O}_k \Psi | \mathcal{O}_k \Psi \rangle}. \quad (3.8)$$

To formulate projected energy expressions, Löwdin suggested that expectation values be evaluated for a composite Hamiltonian^{30,283}

$$\Omega = \mathcal{O}_k^\dagger \mathcal{H} \mathcal{O}_k \quad (3.9)$$

which can be reduced to

$$\mathcal{O}_k^\dagger \mathcal{H} \mathcal{O}_k = \mathcal{H} \mathcal{O}_k \quad (3.10)$$

because

$$\mathcal{O}_k = \mathcal{O}_k^\dagger \mathcal{O}_k \quad \mathcal{O}_k^\dagger = \mathcal{O}_k. \quad (3.11)$$

The projected energy is then

$$\frac{\langle \mathcal{O}_k \Psi | \mathcal{H} | \mathcal{O}_k \Psi \rangle}{\langle \mathcal{O}_k \Psi | \mathcal{O}_k \Psi \rangle} = \frac{\langle \Psi | \mathcal{H} \mathcal{O}_k | \Psi \rangle}{\langle \Psi | \mathcal{O}_k \Psi \rangle}. \quad (3.12)$$

The PUHF energy expression using a zeroth-order wavefunction Ψ_0 is

$$E_{\text{PUHF}} = \frac{\langle \Psi_0 | \mathcal{H} \mathcal{O}_k | \Psi_0 \rangle}{\langle \Psi_0 | \mathcal{O}_k \Psi_0 \rangle}. \quad (3.13)$$

To incorporate systematic, order-by-order correlation effects, a projection operator⁶⁸ that spans the subspace of substituted determinants ψ_q is inserted in Eq. 3.13

$$\mathcal{Q} = \sum_q |\psi_q\rangle \langle \psi_q| \quad (3.14)$$

This secondary orthogonal space couples to the primary model space represented by a HF wavefunction. This provides CI-like matrix elements in the perturbative expansion pertinent to n^{th} order wavefunction and energy corrections.

Using \mathcal{Q} , we resolve the identity:

$$E_{\text{PUHF}} = \sum_q \frac{\langle \Psi_0 | \mathcal{H} | \psi_q \rangle \langle \psi_q | \mathcal{O}_k | \Psi_0 \rangle}{\langle \Psi_0 | \mathcal{O}_k | \Psi_0 \rangle}. \quad (3.15)$$

By Brillouin's theorem, $\langle \Psi_0 | \mathcal{H} | \psi_i^a \rangle = 0$ and since \mathcal{H} contains at most two-electron operators, only $\langle \Psi_0 | \mathcal{H} | \psi_{ij}^{ab} \rangle$ elements are needed. Expanding Eq. 3.15 gives

$$E_{\text{PUHF}} = \langle \Psi_0 | \mathcal{H}_0 | \Psi_0 \rangle + \sum_{\substack{i < j \\ a < b}} \frac{\langle \Psi_0 | \mathcal{V} | \psi_{ij}^{ab} \rangle \langle \psi_{ij}^{ab} | \mathcal{O}_k | \Psi_0 \rangle}{\langle \Psi_0 | \mathcal{O}_k | \Psi_0 \rangle}. \quad (3.16)$$

Determination of E_{PUHF} is straightforward since Ψ_0 can be readily computed with a known set of single-particle basis functions. The projected wavefunction with the \mathcal{Q} basis is:

$$\mathcal{O}_k | \Psi_0 \rangle = | \Psi_0 \rangle + \sum_q \frac{|\psi_q\rangle \langle \psi_q | \mathcal{O}_k | \Psi_0 \rangle}{\langle \Psi_0 | \mathcal{O}_k | \Psi_0 \rangle} \quad (3.17)$$

$$= | \Psi_0 \rangle + | \tilde{\Psi}_0 \rangle. \quad (3.18)$$

The correction to the UHF wavefunction from spin projection is then

$$\tilde{\Psi}_0 = \sum_{\substack{i < j \\ a < b}} \frac{|\psi_{ij}^{ab}\rangle \langle \psi_{ij}^{ab} | \mathcal{O}_k | \Psi_0 \rangle}{\langle \Psi_0 | \mathcal{O}_k | \Psi_0 \rangle}. \quad (3.19)$$

However, for the n^{th} order projected energy, the wavefunction corrections up to Ψ_{n-1} will involve substitutions beyond singles ψ_i^a and doubles ψ_{ij}^{ab} due to the evaluation of $\langle S^2 \rangle$ by modified Slater-Condon rules.^{291,292}

The projected UMP $_n$ energy is

$$E_{\text{PUMP}n} = \langle \Psi_0 | \mathcal{H}_0 | \Psi_0 \rangle + \sum_q \frac{\langle \Psi_0 | \mathcal{V} | \psi_q \rangle \langle \psi_q | \mathcal{O}_k | \Psi_0 + \Psi_1 + \dots + \Psi_{n-1} \rangle}{\langle \Psi_0 | \mathcal{O}_k | \Psi_0 + \Psi_1 + \dots + \Psi_{n-1} \rangle}. \quad (3.20)$$

Allowing \mathcal{O}_k and \mathcal{H} to commute, we get expressions for $E_{\text{PUMP}2}$ and $E_{\text{PUMP}3}$:

$$E_{\text{PUMP}2} = \left(\langle \Psi_0 | \mathcal{O}_k | \Psi_0 \rangle \langle \Psi_0 | \mathcal{H}_0 | \Psi_0 + \Psi_1 \rangle + \sum_q \langle \Psi_0 | \mathcal{O}_k | \psi_q \rangle \langle \psi_q | \mathcal{V} | \Psi_0 + \Psi_1 \rangle \right) / \langle \Psi_0 | \mathcal{O}_k | \Psi_0 + \Psi_1 \rangle \quad (3.21)$$

$$E_{\text{PUMP}3} = \left(\langle \Psi_0 | \mathcal{O}_k | \Psi_0 \rangle \langle \Psi_0 | \mathcal{H}_0 | \Psi_0 + \Psi_1 + \Psi_2 \rangle + \sum_q \langle \Psi_0 | \mathcal{O}_k | \psi_q \rangle \langle \psi_q | \mathcal{V} | \Psi_0 + \Psi_1 + \Psi_2 \rangle \right) / \langle \Psi_0 | \mathcal{O}_k | \Psi_0 + \Psi_1 + \Psi_2 \rangle. \quad (3.22)$$

Equations 3.21 and 3.22 are advantageous since one can directly control of the number \mathcal{A}_k operators. Typically, spin purification is achieved after applying \mathcal{A}_{k+1} and \mathcal{A}_{k+2} , but projection of $s > 3$ spins may still be necessary.²⁹³ If there is only one spin contaminant, the approximation $\mathcal{O}_k \approx \mathcal{A}_{k+1}$ holds and ψ_q would contain only ψ_i^a and $\alpha\beta \psi_{ij}^{ab}$ excitations. For each \mathcal{A}_k , there is an instance of \mathcal{S}^2 . Thus, m projections requires matrix elements for $\langle \mathcal{S}^{2m} \rangle$ that involve Ψ_0 , ψ_{ij}^{ab} , and higher excitations in Eq. 3.20. The less-sparse \mathcal{S}^{2m} matrix for more than one annihilator reaches a spatial complexity of $\sim O^4 V^4$. This approach is not very practical beyond MP2. In Eqs. 3.21 and 3.22, one only needs $\langle \Psi_0 | \mathcal{S}^2 | \psi_q \rangle$ where ψ_q runs over ψ_i^a and ψ_{ij}^{ab} , but at the cost of computing $\langle \psi_q | \mathcal{H} | \Psi_{n-1} \rangle$ with ψ_q going up to quadruples for PUMP2 and hexuples for PUMP3.²⁹⁰

In either forms of $E_{\text{PUMP}n}$, the computation of \mathcal{S}^{2m} and \mathcal{H} matrix elements is similar to that of a FCI approach. Approximations to the spin projected projected energies can be made via Gram–Schmidt orthogonalization of perturbative corrections Ψ_n .

$$\tilde{\Psi}_n = \Psi_n - \frac{\tilde{\Psi}_0 \langle \Psi_n | \tilde{\Psi}_0 \rangle}{\langle \tilde{\Psi}_0 | \tilde{\Psi}_0 \rangle}. \quad (3.23)$$

The contributions of spin projection and configurations already contained in Ψ_n are removed from the spin-projection correction of the UHF reference $\tilde{\Psi}_0$ to avoid double counting. We require, for annihilating m higher spins s ,

$$\mathcal{A}_{s+m} = \frac{\mathcal{S}^2 - (s+m)(s+m+1)}{\langle \tilde{\Psi}_0 | \mathcal{S}^2 | \tilde{\Psi}_0 \rangle - (s+m)(s+m+1)} \quad (3.24)$$

to ensure intermediate normalization: $\langle \tilde{\Psi}_0 | \mathcal{A}_{s+m} \tilde{\Psi}_0 \rangle = 1$.²⁹⁴ Here, we see that \mathcal{O}_k is not directly applied to each Ψ_n . Rather, $\tilde{\Psi}_n$ are found using the overlaps of $\langle \Psi_n | \tilde{\Psi}_0 \rangle$.

For the limit as the set of Ψ_n and its corrections $\tilde{\Psi}_n$ approaches the exact wavefunction Ψ , the projected energy is

$$\begin{aligned} E_{\text{PUMP}n} &= \langle \tilde{\Psi}_0 | \mathcal{H} | \tilde{\Psi}_0 + \tilde{\Psi}_1 + \tilde{\Psi}_2 + \dots + \tilde{\Psi}_{n-1} \rangle \\ &= \langle \tilde{\Psi}_0 | \mathcal{H} | \tilde{\Psi}_0 + \tilde{\Psi}_1 + \dots + \tilde{\Psi}_{n-1} \rangle + \\ &\quad \langle \tilde{\Psi}_0 | \mathcal{H} | \tilde{\Psi}_0 \rangle \left(\frac{1 - \langle \tilde{\Psi}_0 | \tilde{\Psi}_1 + \tilde{\Psi}_2 + \dots + \tilde{\Psi}_{n-1} \rangle}{\langle \tilde{\Psi}_0 | \tilde{\Psi}_0 \rangle} \right) \end{aligned} \quad (3.25)$$

The projected energies can be written in terms of UMP n energies combined with projected wavefunction correction terms

$$\begin{aligned} E_{\text{PUMP}n} &= E_{\text{UMP}n} + \\ &\quad \delta E_{\text{PUHF}} \left(\frac{1 - \langle \tilde{\Psi}_0 | \tilde{\Psi}_1 + \tilde{\Psi}_2 + \dots + \tilde{\Psi}_{n-1} \rangle}{\langle \tilde{\Psi}_0 | \tilde{\Psi}_0 \rangle} \right) \end{aligned} \quad (3.26)$$

where

$$\delta E_{\text{PUHF}} = \sum_{\substack{i < j \\ a < b}} \frac{\langle \Psi_0 | \mathcal{V} | \psi_{ij}^{ab} \rangle \langle \psi_{ij}^{ab} | \mathcal{S}^2 | \Psi_0 \rangle}{\langle \Psi_0 | \mathcal{S}^2 | \Psi_0 \rangle - (s+m)(s+m+1)} \quad (3.27)$$

is obtained from Eq. 3.16. The expressions for this estimation at second and third order are

$$\tilde{E}_{\text{PUMP2}} \simeq E_{\text{UMP2}} + \delta E_{\text{PUHF}} \left(\frac{1 - \langle \Psi_1 | \tilde{\Psi}_0 \rangle}{\langle \tilde{\Psi}_0 | \tilde{\Psi}_0 \rangle} \right) \quad (3.28)$$

and

$$\tilde{E}_{\text{PUMP3}} \simeq E_{\text{UMP3}} + \delta E_{\text{PUHF}} \left(\frac{1 - \langle \Psi_1 + \Psi_2 | \tilde{\Psi}_0 \rangle}{\langle \tilde{\Psi}_0 | \tilde{\Psi}_0 \rangle} \right). \quad (3.29)$$

The approximation to PUMP3, in the \mathcal{Q} space of singles, doubles, and quadruples, conventionally scales $O(M^6)$ for M basis with the additional overhead of generating $\langle \mathcal{S}^2 \rangle$ for each annihilation. Results for UMP4 also accompany those for projected third order, but with the omission of ψ_{ijk}^{abc} terms.²⁹⁵ Contributions from three-body correlations would otherwise present a steep cost of $O(M^7)$. In this work, we make use of implementations based on Eqs. 3.16 and 3.28-3.29.

3.2.3 Relativistic Corrections

Scalar relativistic effects for C, N, O, and F atoms are included as a *post hoc* correction to ΔHF and ΔMP excitation energies. We examine two procedures. The first is based on the relativistic shift in the ionization potential for a two-electron atom defined by Bethe and Salpeter.²¹³

$$E_J = \alpha^2 \left[-\frac{1}{8} Z^4 + \frac{1}{4} \langle p_1^4 \rangle - \pi Z \langle \delta^{(3)}(\mathbf{r}_1) \rangle - \pi \langle \delta^{(3)}(\mathbf{r}_{12}) \rangle \right] - E_2 \quad (3.30)$$

Expectation values in E_J for atomic number $Z > 2$ are available in works by Perekis, Silverman, and Scherr.^{214,215} A different correction scheme for C, N, O, and F was developed by Chong and coworkers²⁹⁶⁻²⁹⁸, leading to the following formula

$$C_{rel} = \mathcal{A}I_{nr}^{\mathcal{B}} \quad (3.31)$$

where the correction C_{rel} (in eV) is found with $\mathcal{A} = 2.198 \times 10^{-7}$, $\mathcal{B} = 2.178$, and the calculated non-relativistic core IP I_{nr} (in eV). The corrections of Perekis $C_{Perekis}$ for atomic ions isoelectronic to helium lack valence screening present in molecules. The values of $C_{Perekis}$ are then larger than those of C_{Chong} by a factor of ~ 2 . In lieu of performing Δ SCF calculations for Eq. 3.31, we abide by this heuristic. The relativistic corrections used in this work for C, N, O, and F are 0.1, 0.2, 0.4, 0.7 eV under $C_{Perekis}$ and 0.05, 0.1, 0.2, 0.35 eV under C_{Chong} , respectively.

3.2.4 Denominator Control

The MP2 energy denominator with a core-hole reference ($\epsilon_i + \epsilon_j - \epsilon_a - \epsilon_b$) may become very small. The addition of a core-hole orbital ϵ_a with a large negative eigenvalue with a lower-lying occupied valence ϵ_i may nearly cancel the addition of another valence ϵ_j with a high-lying virtual ϵ_b that possesses a large, positive eigenvalue. Similarly, a core-hole ϵ_a plus another negative, high-energy core orbital ϵ_i combined with a valence orbital ϵ_j plus a low-lying virtual ϵ_b can lead to a very small denominator. In these cases, identical atoms can lead to greater instances of coupling between core-holes and occupied cores. Also, basis sets with many polarization functions of high angular momentum spawn the presence of higher-lying virtual orbitals with eigenvalues that are similar in magnitude but opposite in sign to the core-orbitals. These small denominators introduce numerical instabilities in the perturbation series.^{142,246,299} A recent protocol by Dreuw and Fransson²⁴⁷, suggests a denominator threshold of 0.1 a.u. for freezing orbital indices for correlation. We adopt this threshold τ_L and switch on a tighter (0.02 a.u.) threshold τ_T when the frozen orbital window with τ_L still exceeds 5% of the total orbital count.

3.3 Results and Discussion

3.3.1 Computational Details

Vertical K -edge excitation energies ω_X for symmetry-allowed transitions are computed using Δ UHF and Δ UMP n ($n = 2, 2.5, 3$) with and without spin projection

Tab. 3.1.: Set of symmetrical molecules and experimental core-excitation energies at the C, N, O, and F K-edge.

Mol.	Exp.	Mol.	Exp.	Mol.	Exp.
C ₂ H ₂	285.9 ³⁰⁰	N ₂	400.9 ³⁰¹	F ₂	682.2 ³⁰²
C ₂ H ₄	284.7 ³⁰⁰	<i>cis</i> -Diazene	398.4 ³⁰³	C ₂ F ₄	690.7 ³⁰⁴
C ₂ H ₆	286.9 ³⁰⁰	C ₂ N ₂	398.9 ³⁰⁵	CF ₂ O	689.2 ³⁰⁶
C ₂ N ₂	286.3 ³⁰⁵	Hydrazine	401.5 ³⁰⁷	CH ₂ CF ₂	690.3 ³⁰⁴
Cyclopropane	287.7 ³⁰⁸	Urea	402.0 ³⁰⁹	<i>cis</i> -CH ₂ CF ₂	689.3 ³⁰⁴
C ₂ F ₄	290.1 ³⁰⁴	N ₃ ⁻ (N=N=N)	399.6 ³⁰³	OF ₂	683.8 ³¹⁰
Furan (C-O)	286.6 ²²⁷	Tetrazine	398.8 ^{230,311}	NF ₃	687.4 ³¹²
Allene (C=C=C)	285.4 ³¹³	O ₃ (O=O-O)	529.1 ³¹⁴		
Cyclobutane	287.4 ³⁰⁸	H ₂ O ₂	533.0 ³¹⁵		
C ₂	285.9 ^{300,316}	CO ₂	535.4 ³¹⁷		
Acetone (C-C=O)	288.4 ³¹⁸	O ₂	530.8 ³¹⁹		
Pyridine (C-N)	285.3 ²³⁰				
Tetrazine	285.2 ³¹¹				
Benzene	285.2 ³²⁰				
Pyrrrole (C-NH)	286.3 ³²¹				

for various combinations of basis sets. Relativistic corrections for C, N, O, and F are added to the individual energy differences. The Pople and Dunning basis sets are taken from the Basis Set Exchange.³²⁵ Multi-electron Wood-Boring (MWB2) effective core potentials (ECP) on non-target atoms sans hydrogen are used for core-localization. The basis sets for second-row atoms are also 1s uncontracted for a more optimal core orbital. Redundant functions in the core-uncontracted Dunning basis are removed.

An assortment of symmetrical molecules with equivalent atoms listed in Table 3.1 were taken from the Chong-Gritsenko-Baerends (CGB) dataset²¹⁸ and the NIST CCCBDB.²¹⁹ Optimized geometries with CCSD(T)/aug-cc-pVTZ are reported in a prior publication²¹⁷ and in the CCCBDB. The structure for OF₂ was optimized locally at the same level of theory. Molecules in the test set are closed shell except O₂.

All calculations were performed with a development version of Gaussian.²²⁰ For calculations without ECPs, integral symmetry with Abelian groups is used.

3.3.2 Δ PUHF and Δ PUMP_{*n*}

The mean absolute error (MAE) and root-mean-square error (RMSE) between calculated ω_X values and experimental values are reported. Histograms with the

MAE for Δ PUHF and Δ PUMP $_n$ using $\mathcal{C}_{\text{Chong}}$ are provided in this section. Detailed information about the overall data, $\langle \mathcal{S}_{\text{UHF}}^2 \rangle$ and the measure of errors are available in the Supplementary Material. Spin contamination is removed from core-excited states after annihilation of spin states up to $s + 3$ or $s + 4$.

The performance of Δ UHF and Δ PUHF is shown in Figure 3.1. As Δ SCF methods, there is a stark difference of ~ 10 eV in the MAE between basis sets with and without core localization by ECP. The results for Δ PUHF are similar to Δ UHF without ECPs across the standard contracted basis sets. A notable decrease in MAE occurs when going from (u)6-311G(d) to (u)6-311+G(2df) and from (u)cc-pVTZ to (u)aug-cc-pVTZ—owing to the increased variational flexibility in the SCF solutions. Localized core Δ UHF and Δ PUHF calculations offer a MAE ~ 0.5 – 1.0 eV and RMSE ~ 1 eV. No significant difference between contracted or uncontracted basis sets are observed for this data. We observe that Δ PUHF+ECP energies are equal to or slightly higher than Δ UHF+ECP. This may be due to the non-variational nature of the correction to the excited state E_{UHF} , quality of the SCF+ECP solution, or simply a consequence of the symmetry dilemma.

In Figure 3.2, we have results for Δ UMP2 and Δ PUMP2. We find that second-order energies underestimate experiment by a range of $\sim 1 - 5$ eV (see Supplementary Material). This is not unexpected as MP2 usually overestimates the correlated two-body corrections. The results for Δ UMP2+ECP and Δ PUMP2+ECP are slightly lower, more varied and less uniform than the same results without ECPs. Uncontracting the 1s basis function in this dataset appears to slightly increase the deviation from experiment, except for (u)cc-pvtz+ECP where it decreases considerably.

Figure 3.3 shows results for Δ UMP3 and Δ PUMP3. The third order ω_X values generally overestimate experiment. For calculations on delocalized cores, the MAE and RMSE can reach up to ~ 4 eV and ~ 5 eV respectively. The MAE for Δ PUMP3 at 6-311G(d) that is about two times smaller than the others in its class is merely coincidental. The errors for Δ UMP3+ECP and Δ PUMP3+ECP are generally equal to or lower than their second-order counterparts. The behavior of uncontracted versus contracted results in this dataset is inconsistent: slightly higher in some cases or slightly lower in others. The energies of both the second- and third-order methods coupled with ECPs are essentially lower than those without across basis sets.

The results for Δ UMP2.5 and Δ PUMP2.5 are featured in Figure 3.4. For the retention of molecular symmetry, the inclusion of 50% third-order corrections ameliorates some of the deficiencies of MP2 and MP3 energies by providing ω_X values approximately halfway between. Cancellation of errors becomes less fortuitous here as ECP calculations are generally higher than the delocalized core dataset. The projected

energies are typically lower across all bases except ucc-pVTZ+ECP in the core-localized set and 6-311+G(2df) in the delocalized set. What is noteworthy is the good cost-performance of just (u)6-311+G(2df) (Tables 3.10–3.11) and (u)cc-pVTZ (Tables 3.12–3.13) without breaking the orbital symmetry. The method statistics for these basis sets are depicted in Tables 3.4–3.7. The overall data suggests no cost-benefit preference for the larger diffuse Dunning basis sets. In benzene, for example, the dimensions of M basis reaches beyond 400 with (u)aug-cc-pVTZ. Additional results for (u)6-311G(d) and (u)aug-cc-pVTZ can be viewed in the Supplementary Material. Finally, there appears to be very little difference in the effect of C_{Perekis} versus C_{Chong} except for the F 1s results. For the F K -edge, C_{Perekis} is nearly a half of an eV larger than C_{Chong} . The smaller corrections by Chong are probably more realistic for molecules.

The first core-excitation, particularly those to orbitals of π character, do not typically require spatially expansive basis functions. Higher transitions to Rydberg orbitals, aptly described in a one-electron picture, would require at least doubly augmented diffuse functions to yield accurate energies.¹⁹⁴ Demonstrative calculations for the first few core-level transitions in N_2 are featured in Table 3.14. $\Delta\text{PUMP2.5}$ produces viable results for these states.

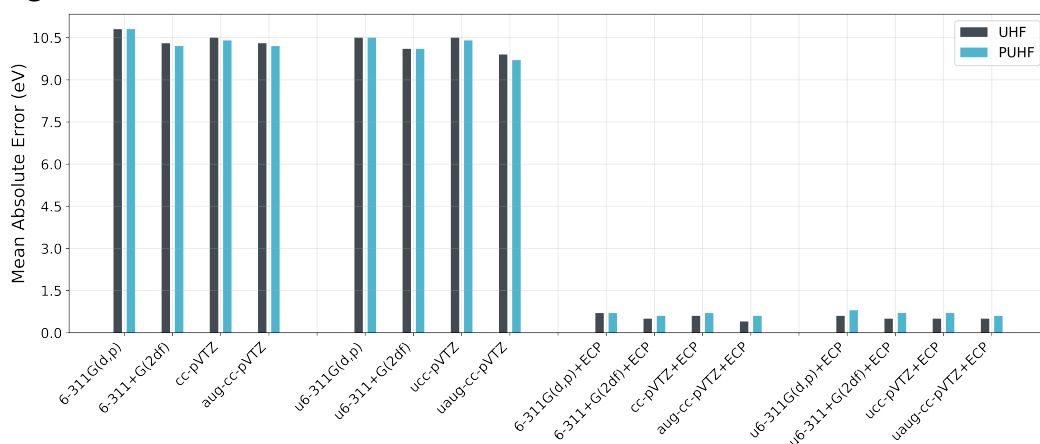
When applied to K -edge ionizations and excitations, the Pople basis sets augmented with additional polarization and diffuse functions are known to offer a balance between accuracy and computational cost.^{326,327} This observation is further substantiated in this work. The optimal performance u6-311+G(2df) is exemplified for $\Delta\text{PUMP2.5}$ results with symmetry retained. Core-localized ΔPUHF results are sufficient with (u)6-311+G(2df)+ECP. Other basis sets designed for improved core orbitals could have been chosen.³²⁸ Instead, we sought to examine the effect of decontracting standard basis sets.

Considering the modern-day experimental precision in spectral measurements, the $\Delta\text{PUMP2.5}$ method for estimating vertical excitation energies is very useful since spin, ORX, and quasi-extrapolated correlation corrections are accounted for. The validity of ΔSCF is also once again apparent for when one adopts a localized picture of core orbitals. To ensure that energies correspond to states with good spin quantum numbers, spin projection is necessary if the UHF wavefunction breaks symmetry. For chemical species with multireference character, such as C_2 and O_3 , single determinant Δ -methods are inadequate. This is reflected in the notable deviations of ΔPUHF from experiment. Additionally, when molecules undergo an adiabatic transition, the vertical ω_X values will normally be larger than what is observed. In the assortment of molecules selected, allene and CO_2 experience

Jahn-Teller/Renner-Teller distortions^{329,330}, so vertical ω_X values for the principle transition are also expected to be less accurate. Transitions associated with fine vibrational structure in core spectra are not accounted for either.

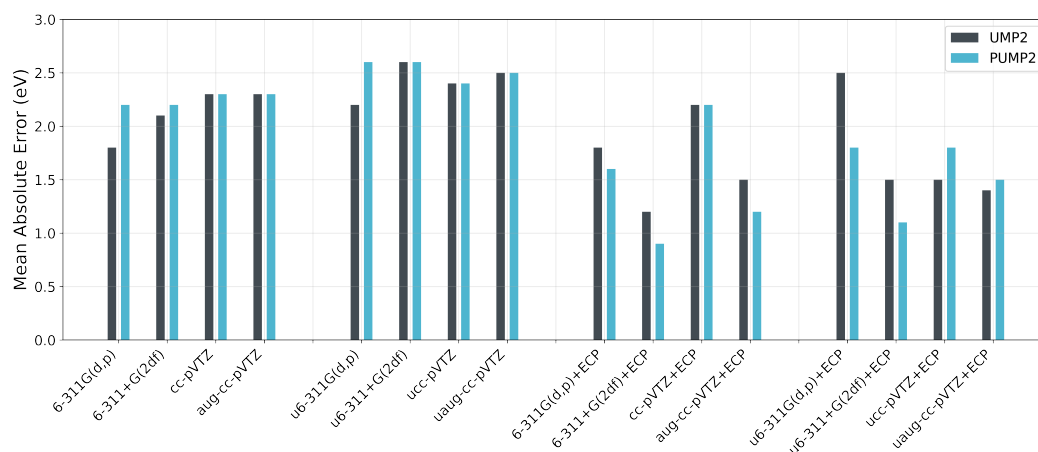
The mixed portrait of ORX and correlation inherent in a localized core-hole reference makes Δ SCF a satisfactory approach—especially for molecules with nonequivalent, asymmetrical atomic sites. The parallel approach of delegating the labor of modeling ORX to Δ SCF and separately recovering correlations through $n = 2, 3$ or 2.5 order MP perturbation theory is also a theoretically sound model for symmetrical molecules. Preserving the orbital symmetry and applying the latter method would assist with spectral assignments. One can also break symmetry, use Δ SCF, and rely on visual inspection of the orbitals involved if the spatial character of said orbitals are known *a priori*. In both approaches, spin projection is necessary for obtaining an approximately right answer for the right reason.

Fig. 3.1.: Mean absolute errors (eV) of UHF and PUHF for various basis set combinations.^a



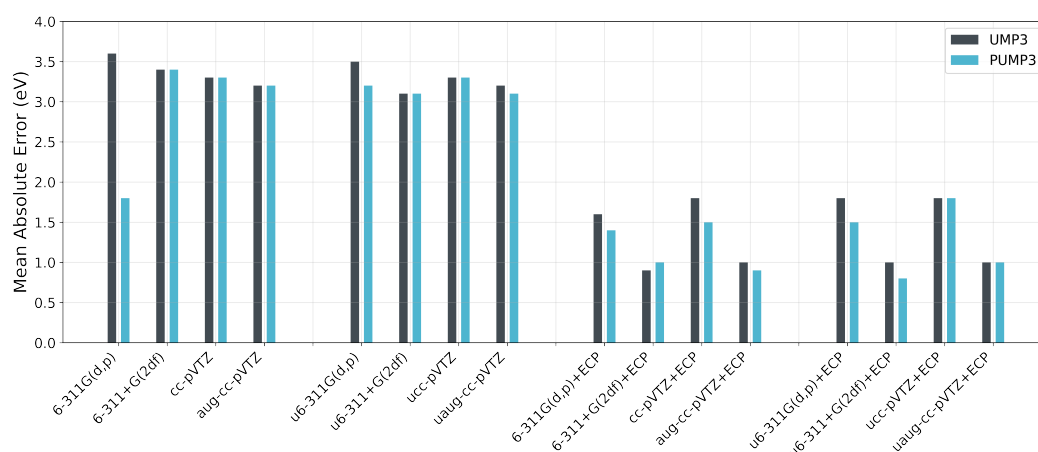
^aResults obtained with tight threshold τ_T , relativistic correction B (C_{Chong}), and with outlier cases removed.

Fig. 3.2.: Mean absolute errors (eV) of UMP2 and PUMP2 for various basis set combinations.^a



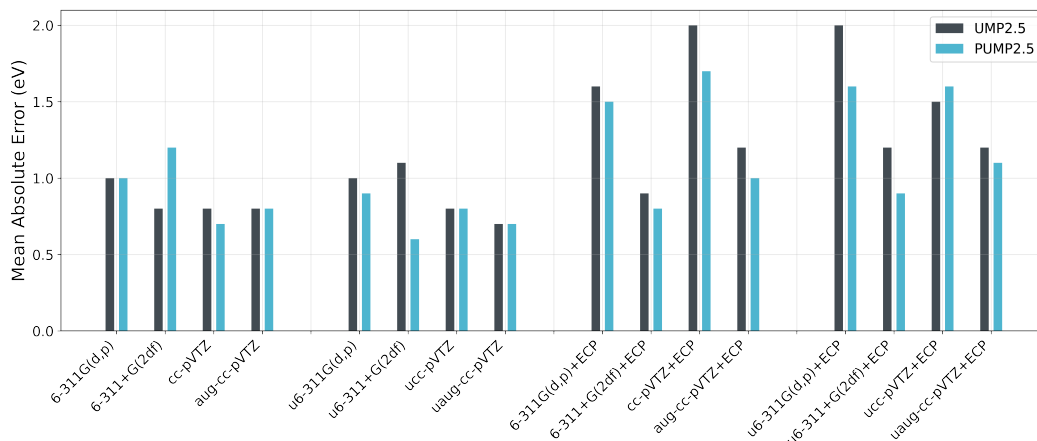
^aResults obtained with tight threshold τ_T , relativistic correction B (C_{Chong}), and with outlier cases removed.

Fig. 3.3.: Mean absolute errors (eV) of UMP3 and PUMP3 for various basis set combinations.^a



^aResults obtained with tight threshold τ_T , relativistic correction B (C_{Chong}), and with outlier cases removed.

Fig. 3.4.: Mean absolute errors (eV) of UMP2.5 and PUMP2.5 for various basis set combinations.^a



^aResults obtained with tight threshold τ_T , relativistic correction B (C_{Chong}), and with outlier cases removed.

Although the quantum chemistry problem is established clearly and addressed quite well with the methods introduced, there are numerical complications and idiosyncrasies that accompany the use of single determinant core-hole with perturbation theory. The issues are delineated as follows:

1. The PUHF and PUMP n variants employed here involve PAV, so the projected energies and wavefunctions do not necessarily correspond to a proper eigenstate of \mathcal{H} . Alternatively, VAP spin projection methods can be applied for locating PUHF stationary states along with extensions thereof to include dynamic correlation.^{331,332}
2. The monodeterminantal non-Aufbau reference is not an excited state wavefunction that transforms under the proper molecular electronic symmetry operations. It is an SCF solution that can only provide a representative charge density that, in principle, corresponds to a single target non-Aufbau configuration. With solutions found with guided SCF solvers (e.g. MOM), there is no guarantee the particle-hole pair orbitals will resemble the ones of the ground state. The SCF orbital optimization process will attempt to converge any solution given the overlap metric or level-shifting directive. The core-hole solution may then give a meaningful energy with respect to the ground state, but its core-hole and/or newly occupied valence orbitals may be distorted. A deformed core-hole density can lead to poor Δ MP energies and loss of an intuitive molecular orbital picture. We encounter this problem in C_2N_2 and C_2F_4 for calculations using some basis sets in tandem with ECPs. At times, these “excited-state” solutions can only converge with basis set projections

from other calculations. This situation can give rise to multiple SCF solutions with similar energies that are difficult to distinguish by orbital shape and occupation.

3. The use of the MWB2 ECPs seems to interfere with the correlation consistency of the Dunning basis, so different pseudopotentials could prove to be more viable.³³³ Another possibility is to apply the Edmiston-Ruedenberg³³⁴ or Boys³³⁵ localization to break the core orbital symmetry. Localization lacks the advantage ECPs have for reducing the number of non-target occupied core orbitals that may contribute to occurrence of small denominators.
4. The convergence behavior of the MP series is mainly understood for ground state references. For references other than the ground state, the situation is less predictable.^{336,337} The most prominent errors in the perturbative calculations with core-hole references comes from (a) divergence in MP3 and (b) different orbital correlation windows between the ground and excited states due to index freezing. Orbitals indices are only frozen in the core excited-state to mitigate the small denominators. Divergence at third-order may be avoided, but the correlation corrections are not summed over the same indices of the ground state. This leads to an imbalanced treatment of correlation. These errors are most pronounced in the ω_X computed with Δ MP3 and Δ MP2.5 as the third-order correction is not stable. Often, the presence of basis sets with higher angular momentum functions or nearly degenerate orbitals eventually lead to a greater amount of frozen indices. The tighter threshold τ_T reduces this amount and improves the energies but, in some cases, $\sim 40 - 60\%$ of the orbital window remains frozen. This problem doesn't appear to correlate with the size of the molecule, as benzene with uaug-cc-pVTZ required just two orbitals to be removed at τ_L . It is unclear how to maintain a 1:1 mapping between ground and excited SCF orbitals due to the large relaxation that occurs. To resolve this, perhaps a reduced set of compact, local virtual orbitals can be found and passed to the ground and excited state MP calculations.

Conventional implementations of projected MP can be cost-prohibitive for very large molecules. Density-fitting or resolution of the identity methods could be used to accelerate the evaluation of UMP_n contributions to the projected energy.^{338,339} Even though the methods are well-grounded for single reference molecules, the results in this study have proven to be very sensitive to calculation setup.

3.4 Conclusion

Vertical core-excitation energies at the C, N, O, and F K -edge are obtained with Δ PUHF and Δ PUMP $_n$ for a set of symmetrical molecules with equivalent atoms. The methods employed inherit old quantum chemistry concepts for modeling the electronic structure of core-holes. The historical foundations of the validity and efficiency of Δ SCF with core-localization is reaffirmed. Second-order Møller-Plesset perturbation theory recovers a large fraction of the missing correlation in Δ SCF for molecules with equivalent atomic sites. Averaged corrections from PUMP2 and PUMP3 combined with PUHF, for a select assortment of basis sets, provides the best performance when molecular symmetry is present. The results are heavily influenced by the quality of the SCF solutions and the number of indices removed to avoid divergences in the MP energies. The effect of the scalar relativistic corrections incorporated in this work on the overall statistics do not vary between corrections schemes except in F 1s excitations. The relativistic IP shift in the two-electron atomic model is too high for F and atoms with higher Z . For the K -edge ω_X values computed here, $\mathcal{C}_{\text{Chong}}$ is preferred. A more complete relativistic description of molecules with heavier atoms is needed. Single reference Δ -based approaches are probably not widely applicable to L -edge due to high degeneracy and multiplet structure of the final states.

Nevertheless, for an excitation defined by a canonical particle-hole pair, the quantitative performance of Δ PMP2.5 or Δ PUHF limits the need for significant empirical shifting. Step-wise reproduction and assignment of spectra is doable provided transition dipole strengths are obtained using the projected UHF or PUMP density corrections. Data from each calculation could be concatenated to generate the spectra up to the IP. Auger cascading and shake-related processes involve the correlated, physical motion of two- or many- electrons not described in single configuration mean-field theory. One must then turn to more accurate methods that contain information on the two-particle density matrix and Feynman-Dyson amplitudes for computing energies and transition strengths.^{340,341}

Tab. 3.2.: Measure of errors w.r.t. experiment for symmetry-allowed vertical K-edge excitation energies (eV) computed without spin projection using different combinations of the 6-311G(d,p) basis set.^{a,b}

	$\langle \bar{S}_{\text{UHF}}^2 \rangle_{S=0^c}$	UHF	UMP2	UMP3	UMP2.5
<u>6-311G(d,p)^d</u>	1.040				
τ_T -A-MAE		10.9 (11.0)	1.6 (1.6)	3.9 (3.8)	1.2 (1.2)
τ_L -A-MAE		10.9 (11.0)	1.7 (1.7)	4.3 (4.0)	1.6 (1.4)
τ_T -A-RMSE		11.2 (11.2)	2.0 (2.1)	4.3 (4.2)	1.6 (1.5)
τ_L -A-RMSE		11.2 (11.2)	2.1 (2.1)	4.9 (4.6)	2.4 (2.1)
τ_T -B-MAE		10.8 (10.8)	1.7 (1.8)	3.8 (3.6)	1.1 (1.0)
τ_L -B-MAE		10.8 (10.8)	1.8 (1.8)	4.2 (3.9)	1.5 (1.3)
τ_T -B-RMSE		11.0 (11.0)	2.2 (2.2)	4.2 (4.0)	1.4 (1.4)
τ_L -B-RMSE		11.0 (11.0)	2.2 (2.2)	4.8 (4.5)	2.3 (2.0)
<u>6-311G(d,p) & ECP^e</u>	0.215				
τ_T -A-MAE		0.8 (0.8)	2.0 (1.9)	1.6 (1.7)	1.8 (1.8)
τ_L -A-MAE		0.8 (0.8)	1.8 (1.8)	1.5 (1.5)	1.6 (1.6)
τ_T -A-RMSE		1.0 (1.0)	2.4 (2.4)	2.0 (2.1)	2.2 (2.2)
τ_L -A-RMSE		1.1 (1.0)	2.2 (2.2)	1.8 (1.9)	2.0 (2.0)
τ_T -B-MAE		0.8 (0.7)	1.8 (1.8)	1.5 (1.6)	1.6 (1.6)
τ_L -B-MAE		0.8 (0.7)	1.7 (1.7)	1.4 (1.4)	1.5 (1.5)
τ_T -B-RMSE		1.0 (0.9)	2.3 (2.3)	1.9 (2.0)	2.1 (2.1)
τ_L -B-RMSE		1.0 (0.9)	2.1 (2.1)	1.7 (1.7)	1.9 (1.9)
<u>u6-311G(d,p)^d</u>	1.039				
τ_T -A-MAE		10.7 (10.7)	2.1 (2.1)	3.6 (3.5)	0.9 (0.8)
τ_L -A-MAE		10.7 (10.7)	2.1 (2.0)	4.0 (3.7)	1.2 (1.0)
τ_T -A-RMSE		10.9 (10.9)	2.5 (2.5)	4.0 (3.8)	1.2 (1.2)
τ_L -A-RMSE		10.9 (10.9)	2.5 (2.4)	4.6 (4.2)	2.0 (1.7)
τ_T -B-MAE		10.5 (10.6)	2.2 (2.2)	3.5 (3.3)	0.9 (0.8)
τ_L -B-MAE		10.5 (10.5)	2.2 (2.2)	3.8 (3.5)	1.2 (1.0)
τ_T -B-RMSE		10.8 (10.8)	2.7 (2.7)	3.8 (3.7)	1.2 (1.1)
τ_L -B-RMSE		10.8 (10.8)	2.6 (2.6)	4.4 (4.1)	1.9 (1.6)
<u>u6-311G(d,p) & ECP^d</u>	0.216				
τ_T -A-MAE		0.7 (0.6)	2.3 (2.3)	1.9 (1.9)	2.1 (2.1)
τ_L -A-MAE		0.7 (0.6)	2.3 (2.3)	1.9 (2.0)	2.1 (2.1)
τ_T -A-RMSE		0.9 (0.8)	2.6 (2.6)	2.2 (2.2)	2.4 (2.4)
τ_L -A-RMSE		0.9 (0.8)	2.6 (2.6)	2.2 (2.2)	2.4 (2.4)
τ_T -B-MAE		0.7 (0.6)	2.2 (2.5)	1.8 (1.8)	2.0 (2.0)
τ_L -B-MAE		0.7 (0.6)	2.2 (2.2)	1.8 (1.8)	2.0 (2.0)
τ_T -B-RMSE		1.0 (0.9)	2.2 (2.4)	2.1 (2.1)	2.3 (2.2)
τ_L -B-RMSE		1.0 (0.9)	2.5 (2.4)	2.1 (2.1)	2.3 (2.3)

^aEntries in parenthesis are statistics for the dataset excluding two species with multireference character.

^bMAE and RMSE with relativistic correction A (C_{Perekis}) and B (C_{Chong}). ^cAverage excited state $\langle S_{\text{UHF}}^2 \rangle$ for singlets. ^dOne outlier excluded for τ_T and/or τ_L . ^eUp to two outliers excluded for τ_T and/or τ_L .

Tab. 3.3.: Measure of errors w.r.t. experiment for symmetry-allowed vertical K-edge excitation energies (eV) computed with spin projection using different combinations of the 6-311G(d,p) basis set.^{a,b}

	$\langle \bar{S}_{\text{UHF}}^2 \rangle_{S=0^c}$	PUHF	PUMP2	PUMP3	PUMP2.5
<u>6-311G(d,p)^d</u>	1.040				
τ_T -A-MAE		10.9 (11.0)	1.6 (1.6)	1.7 (1.7)	1.2 (1.2)
τ_L -A-MAE		10.9 (11.0)	1.7 (1.7)	4.3 (4.0)	1.6 (1.4)
τ_T -A-RMSE		11.2 (11.2)	2.0 (2.0)	2.1 (2.1)	1.6 (1.5)
τ_L -A-RMSE		11.2 (11.2)	2.1 (2.0)	5.0 (4.6)	2.4 (2.1)
τ_T -B-MAE		10.8 (10.8)	1.7 (2.2)	1.8 (1.8)	1.1 (1.0)
τ_L -B-MAE		10.8 (10.8)	1.8 (1.8)	4.2 (3.9)	1.5 (1.3)
τ_T -B-RMSE		11.0 (11.0)	1.7 (2.2)	2.2 (2.2)	1.4 (1.4)
τ_L -B-RMSE		11.0 (11.0)	2.2 (2.1)	4.8 (4.5)	2.3 (1.9)
<u>6-311G(d,p) & ECP^e</u>	0.215				
τ_T -A-MAE		0.8 (0.7)	1.7 (1.7)	1.4 (1.5)	1.5 (1.6)
τ_L -A-MAE		0.8 (0.7)	1.6 (1.5)	1.3 (1.4)	1.4 (1.4)
τ_T -A-RMSE		1.0 (0.9)	2.1 (2.2)	1.9 (1.9)	2.0 (2.0)
τ_L -A-RMSE		1.0 (0.9)	1.9 (1.9)	1.7 (1.7)	1.7 (1.8)
τ_T -B-MAE		0.8 (0.7)	1.6 (1.6)	1.4 (1.4)	1.4 (1.5)
τ_L -B-MAE		0.8 (0.7)	1.4 (1.4)	1.3 (1.3)	1.3 (1.3)
τ_T -B-RMSE		1.0 (0.9)	2.0 (2.0)	1.8 (1.8)	1.9 (1.9)
τ_L -B-RMSE		1.1 (0.9)	1.8 (1.8)	1.6 (1.6)	1.6 (1.7)
<u>u6-311G(d,p)^d</u>	1.039				
τ_T -A-MAE		10.6 (10.6)	2.1 (2.1)	3.6 (3.5)	0.9 (0.8)
τ_L -A-MAE		10.7 (10.6)	2.1 (2.0)	3.6 (3.4)	1.2 (1.0)
τ_T -A-RMSE		10.8 (10.9)	2.5 (2.5)	4.0 (3.8)	1.2 (1.1)
τ_L -A-RMSE		10.9 (10.9)	2.4 (2.4)	4.0 (3.7)	2.0 (1.7)
τ_T -B-MAE		10.5 (10.7)	2.2 (2.2)	3.5 (3.3)	0.8 (0.7)
τ_L -B-MAE		10.5 (10.5)	2.2 (2.6)	3.5 (3.2)	1.1 (0.9)
τ_T -B-RMSE		10.5 (10.7)	2.7 (2.7)	3.8 (3.7)	1.1 (1.1)
τ_L -B-RMSE		10.7 (10.7)	2.2 (2.6)	3.8 (3.5)	1.9 (1.6)
<u>u6-311G(d,p) & ECP^d</u>	0.216				
τ_T -A-MAE		0.8 (0.8)	1.9 (1.9)	1.6 (1.6)	1.8 (1.8)
τ_L -A-MAE		0.8 (0.8)	1.9 (1.9)	1.6 (1.6)	1.8 (1.8)
τ_T -A-RMSE		1.1 (1.0)	2.2 (2.2)	1.9 (1.9)	2.0 (2.0)
τ_L -A-RMSE		1.1 (1.0)	2.2 (2.2)	1.9 (1.9)	2.0 (2.0)
τ_T -B-MAE		0.9 (0.8)	1.8 (1.8)	1.5 (1.5)	1.6 (1.6)
τ_L -B-MAE		0.9 (0.8)	1.8 (1.8)	1.5 (1.5)	1.6 (1.7)
τ_T -B-RMSE		1.2 (1.0)	2.1 (2.0)	1.8 (1.7)	1.9 (1.9)
τ_L -B-RMSE		1.2 (1.0)	2.1 (2.1)	1.8 (1.7)	1.9 (1.9)

^aEntries in parenthesis are statistics for the dataset excluding two species with multireference character.

^bMAE and RMSE with relativistic correction A ($\mathcal{C}_{\text{Perekis}}$) and B ($\mathcal{C}_{\text{Chong}}$). ^cAverage excited state ($\langle S_{\text{UHF}}^2 \rangle$) for singlets. ^dOne outlier excluded for τ_T and/or τ_L . ^eUp to two outliers excluded for τ_T and/or τ_L .

Tab. 3.4.: Measure of errors w.r.t. experiment for symmetry-allowed vertical K-edge excitation energies (eV) computed without spin projection using different combinations of the 6-311+G(2df) basis set.^{a,b}

	$\langle \overline{S}_{\text{UHF}}^2 \rangle_{S=0^c}$	UHF	UMP2	UMP3	UMP2.5
<u>6-311+G(2df)^d</u>	1.043				
τ_T -A-MAE		10.4 (10.4)	2.0 (2.0)	3.7 (3.5)	1.0 (1.0)
τ_L -A-MAE		10.4 (10.5)	1.9 (1.8)	4.2 (4.0)	1.6 (1.4)
τ_T -A-RMSE		10.8 (10.8)	2.3 (2.3)	4.1 (4.0)	1.4 (1.3)
τ_L -A-RMSE		10.8 (10.9)	2.3 (2.1)	4.8 (4.6)	2.3 (2.0)
τ_T -B-MAE		10.3 (10.3)	2.1 (2.1)	3.5 (3.4)	0.9 (0.8)
τ_L -B-MAE		10.3 (10.3)	2.0 (1.9)	4.1 (3.8)	1.5 (1.2)
τ_T -B-RMSE		10.6 (10.6)	2.4 (2.5)	4.0 (3.8)	1.2 (1.2)
τ_L -B-RMSE		10.6 (10.7)	2.4 (2.2)	4.7 (4.5)	2.2 (1.9)
<u>6-311+G(2df) & ECP^d</u>	0.217				
τ_T -A-MAE		0.7 (0.6)	1.0 (1.0)	0.9 (0.8)	0.8 (0.8)
τ_L -A-MAE		0.6 (0.5)	1.4 (1.3)	0.9 (0.9)	1.1 (1.0)
τ_T -A-RMSE		0.8 (0.7)	1.3 (1.2)	1.0 (1.0)	1.0 (1.0)
τ_L -A-RMSE		0.8 (0.6)	1.7 (1.6)	1.1 (1.1)	1.4 (1.3)
τ_T -B-MAE		0.7 (0.6)	1.0 (0.9)	0.9 (0.9)	0.8 (0.8)
τ_L -B-MAE		0.6 (0.5)	1.3 (1.2)	0.9 (0.8)	1.0 (0.9)
τ_T -B-RMSE		0.9 (0.7)	1.2 (1.1)	1.0 (1.0)	1.0 (1.0)
τ_L -B-RMSE		0.7 (0.6)	1.6 (1.5)	1.1 (1.1)	1.3 (1.2)
<u>u6-311+G(2df)^d</u>	1.039				
τ_T -A-MAE		10.2 (10.2)	2.4 (2.4)	3.4 (3.2)	0.8 (0.8)
τ_L -A-MAE		10.2 (10.3)	2.2 (2.1)	4.0 (3.8)	1.4 (1.2)
τ_T -A-RMSE		10.6 (10.6)	2.8 (2.8)	3.8 (3.7)	1.1 (1.1)
τ_L -A-RMSE		10.6 (10.7)	2.6 (2.4)	4.6 (4.4)	2.2 (1.9)
τ_T -B-MAE		10.1 (10.1)	2.6 (2.6)	3.2 (3.1)	0.8 (0.7)
τ_L -B-MAE		10.1 (10.2)	2.3 (2.2)	3.8 (3.6)	1.3 (1.2)
τ_T -B-RMSE		10.5 (10.5)	2.9 (2.9)	3.7 (3.5)	1.1 (1.0)
τ_L -B-RMSE		10.5 (10.6)	2.7 (2.5)	4.5 (4.3)	2.1 (1.7)
<u>u6-311+G(2df) & ECP^d</u>	0.218				
τ_T -A-MAE		0.5 (0.4)	1.6 (1.6)	1.1 (1.1)	1.3 (1.3)
τ_L -A-MAE		0.5 (0.4)	1.6 (1.6)	1.1 (1.1)	1.3 (1.3)
τ_T -A-RMSE		0.7 (0.5)	2.2 (2.2)	1.4 (1.4)	1.8 (1.8)
τ_L -A-RMSE		0.7 (0.5)	2.2 (2.2)	1.4 (1.4)	1.8 (1.8)
τ_T -B-MAE		0.5 (0.5)	1.5 (1.5)	1.0 (1.0)	1.2 (1.2)
τ_L -B-MAE		0.5 (0.5)	1.5 (1.5)	1.1 (1.0)	1.2 (1.2)
τ_T -B-RMSE		0.8 (0.6)	2.1 (2.1)	1.4 (1.4)	1.7 (1.7)
τ_L -B-RMSE		0.8 (0.6)	2.1 (2.1)	1.4 (1.4)	1.7 (1.7)

^aEntries in parenthesis are statistics for the dataset excluding two species with multireference character. ^bMAE and RMSE with relativistic correction A (C_{Perekis}) and B (C_{Chong}). ^cAverage excited state $\langle \overline{S}_{\text{UHF}}^2 \rangle$ for singlets. ^dOne outlier excluded for τ_T and/or τ_L .

Tab. 3.5.: Measure of errors w.r.t. experiment for symmetry-allowed vertical K-edge excitation energies (eV) computed with spin projection using different combinations of the 6-311+G(2df) basis set.^{a,b}

	$\langle \bar{S}_{\text{UHF}}^2 \rangle_{S=0^c}$	PUHF	PUMP2	PUMP3	PUMP2.5
<u>6-311+G(2df)^d</u>	1.043				
τ_T -A-MAE		10.4 (10.4)	2.0 (2.0)	3.7 (3.5)	1.0 (1.0)
τ_L -A-MAE		10.4 (10.5)	1.9 (1.8)	4.2 (3.9)	1.6 (1.4)
τ_T -A-RMSE		10.8 (10.8)	2.3 (2.3)	4.1 (4.0)	1.4 (1.3)
τ_L -A-RMSE		10.8 (10.9)	2.3 (2.0)	4.8 (4.6)	2.3 (2.0)
τ_T -B-MAE		10.3 (10.2)	2.1 (2.2)	3.5 (3.4)	0.9 (0.8)
τ_L -B-MAE		10.3 (10.3)	2.0 (1.9)	4.0 (3.8)	1.4 (1.2)
τ_T -B-RMSE		10.6 (10.6)	2.4 (2.5)	4.0 (3.8)	1.2 (1.2)
τ_L -B-RMSE		10.6 (10.7)	2.4 (2.2)	4.7 (4.5)	2.2 (1.8)
<u>6-311+G(2df) & ECP^d</u>	0.217				
τ_T -A-MAE		0.6 (0.5)	1.3 (1.3)	1.0 (1.0)	1.0 (1.0)
τ_L -A-MAE		0.7 (0.6)	1.0 (1.0)	0.8 (0.8)	0.8 (0.8)
τ_T -A-RMSE		0.7 (0.6)	1.6 (1.6)	1.2 (1.2)	1.3 (1.3)
τ_L -A-RMSE		0.8 (0.7)	1.3 (1.3)	1.0 (1.0)	1.1 (1.0)
τ_T -B-MAE		0.6 (0.5)	1.2 (1.2)	0.9 (0.9)	1.0 (0.9)
τ_L -B-MAE		0.7 (0.6)	1.0 (0.9)	0.8 (0.8)	0.8 (0.8)
τ_T -B-RMSE		0.7 (0.6)	1.5 (1.5)	1.2 (1.2)	1.2 (1.2)
τ_L -B-RMSE		0.9 (0.7)	1.2 (1.2)	1.0 (1.0)	1.0 (1.0)
<u>u6-311+G(2df)^d</u>	1.039				
τ_T -A-MAE		10.2 (10.2)	2.5 (2.5)	3.4 (3.2)	0.8 (0.7)
τ_L -A-MAE		10.2 (10.3)	2.2 (2.1)	3.9 (3.7)	1.4 (1.1)
τ_T -A-RMSE		10.6 (10.6)	2.8 (2.8)	3.8 (3.7)	1.1 (1.1)
τ_L -A-RMSE		10.6 (10.7)	2.6 (2.4)	4.6 (4.4)	2.2 (1.8)
τ_T -B-MAE		10.1 (10.1)	2.6 (2.6)	3.2 (3.1)	0.7 (0.6)
τ_L -B-MAE		10.1 (10.1)	2.3 (2.2)	3.8 (3.6)	1.3 (1.0)
τ_T -B-RMSE		10.4 (10.5)	3.0 (3.0)	3.6 (3.5)	1.0 (1.0)
τ_L -B-RMSE		10.5 (10.5)	2.7 (2.5)	4.5 (4.3)	2.1 (1.7)
<u>u6-311+G(2df) & ECP^d</u>	0.218				
τ_T -A-MAE		0.7 (0.6)	1.2 (1.2)	0.9 (0.8)	1.0 (1.0)
τ_L -A-MAE		0.7 (0.6)	0.9 (0.8)	0.9 (0.8)	1.0 (1.0)
τ_T -A-RMSE		1.0 (0.8)	1.8 (1.8)	1.1 (1.1)	1.4 (1.4)
τ_L -A-RMSE		0.9 (0.8)	1.1 (1.1)	1.1 (1.1)	1.5 (1.5)
τ_T -B-MAE		0.8 (0.7)	1.1 (1.1)	0.9 (0.8)	1.0 (0.9)
τ_L -B-MAE		0.8 (0.7)	0.9 (0.8)	0.9 (0.8)	1.0 (1.0)
τ_T -B-RMSE		1.0 (0.9)	1.7 (1.8)	1.1 (1.1)	1.4 (1.4)
τ_L -B-RMSE		1.0 (0.9)	1.1 (1.1)	1.1 (1.1)	1.4 (1.4)

^aEntries in parenthesis are statistics for the dataset excluding two species with multireference character. ^bMAE and RMSE with relativistic correction A (C_{Perekis}) and B (C_{Chong}). ^cAverage excited state $\langle S_{\text{UHF}}^2 \rangle$ for singlets.

^dOne outlier excluded for τ_T and/or τ_L .

Tab. 3.6.: Measure of errors w.r.t. experiment for symmetry-allowed vertical K-edge excitation energies (eV) computed without spin projection using different combinations of the cc-pVTZ basis set.^{a,b}

	$\langle \bar{S}_{\text{UHF}}^2 \rangle_{S=0^c}$	UHF	UMP2	UMP3	UMP2.5
<u>cc-pVTZ^d</u>	1.038				
τ_T -A-MAE		10.5 (10.6)	2.2 (2.1)	3.7 (3.5)	1.0 (0.8)
τ_L -A-MAE		10.5 (10.5)	2.1 (2.0)	4.3 (4.0)	1.7 (1.5)
τ_T -A-RMSE		10.9 (11.0)	2.6 (2.5)	4.1 (3.9)	1.6 (1.3)
τ_L -A-RMSE		10.9 (10.9)	2.6 (2.4)	5.0 (4.7)	2.7 (2.3)
τ_T -B-MAE		10.4 (10.5)	2.3 (2.3)	3.5 (3.3)	1.0 (0.8)
τ_L -B-MAE		10.4 (10.4)	2.2 (2.1)	4.1 (3.9)	1.6 (1.4)
τ_T -B-RMSE		10.7 (10.8)	2.8 (2.7)	3.9 (3.7)	1.5 (1.2)
τ_L -B-RMSE		10.7 (10.7)	2.7 (2.5)	4.9 (4.5)	2.6 (2.2)
<u>cc-pVTZ & ECP^d</u>	0.213				
τ_T -A-MAE		0.7 (0.6)	2.4 (2.4)	1.9 (2.0)	2.2 (2.2)
τ_L -A-MAE		0.7 (0.6)	2.4 (2.4)	2.0 (2.0)	2.2 (2.2)
τ_T -A-RMSE		0.9 (0.8)	2.7 (2.7)	2.2 (2.2)	2.4 (2.4)
τ_L -A-RMSE		0.9 (0.8)	2.7 (2.7)	2.2 (2.2)	2.5 (2.5)
τ_T -B-MAE		0.6 (0.6)	2.3 (2.2)	1.8 (1.8)	2.0 (2.0)
τ_L -B-MAE		0.6 (0.6)	2.3 (2.6)	1.8 (1.8)	2.1 (2.1)
τ_T -B-RMSE		0.9 (0.8)	2.5 (2.5)	2.1 (2.1)	2.3 (2.3)
τ_L -B-RMSE		0.9 (0.8)	2.3 (2.6)	2.1 (2.1)	2.3 (2.3)
<u>ucc-pVTZ^d</u>	1.039				
τ_T -A-MAE		10.5 (10.6)	2.3 (2.3)	3.7 (3.5)	1.0 (0.8)
τ_L -A-MAE		10.5 (10.6)	2.3 (2.2)	4.3 (4.1)	1.6 (1.5)
τ_T -A-RMSE		11.0 (11.1)	2.8 (2.7)	4.2 (4.0)	1.7 (1.4)
τ_L -A-RMSE		11.0 (11.1)	2.7 (2.5)	5.1 (5.0)	2.7 (2.5)
τ_T -B-MAE		10.4 (10.5)	2.5 (2.4)	3.5 (3.3)	1.0 (0.8)
τ_L -B-MAE		10.4 (10.5)	2.4 (2.3)	4.1 (3.9)	1.6 (1.4)
τ_T -B-RMSE		10.8 (10.9)	2.9 (2.8)	4.1 (3.9)	1.6 (1.3)
τ_L -B-RMSE		10.8 (10.9)	2.8 (2.6)	4.9 (4.8)	2.6 (2.4)
<u>ucc-pVTZ & ECP^d</u>	0.213				
τ_T -A-MAE		0.6 (0.5)	1.6 (1.6)	1.9 (1.9)	1.7 (1.7)
τ_L -A-MAE		0.6 (0.5)	1.6 (1.6)	1.9 (2.0)	1.7 (1.7)
τ_T -A-RMSE		0.8 (0.7)	2.1 (2.1)	2.2 (2.2)	2.0 (2.1)
τ_L -A-RMSE		0.8 (0.7)	2.2 (2.2)	2.3 (2.3)	2.1 (2.2)
τ_T -B-MAE		0.6 (0.5)	1.5 (1.5)	1.7 (1.8)	1.5 (1.5)
τ_L -B-MAE		0.6 (0.5)	1.6 (1.5)	1.8 (1.8)	1.6 (1.6)
τ_T -B-RMSE		0.9 (0.8)	2.0 (2.0)	2.1 (2.1)	1.9 (1.9)
τ_L -B-RMSE		0.9 (0.8)	2.1 (2.1)	2.2 (2.2)	2.0 (2.0)

^aEntries in parenthesis are statistics for the dataset excluding two species with multireference character.

^bMAE and RMSE with relativistic correction A ($\mathcal{C}_{\text{Perekis}}$) and B ($\mathcal{C}_{\text{Chong}}$). ^cAverage excited state

$\langle \bar{S}_{\text{UHF}}^2 \rangle$ for singlets. ^dOne outlier excluded for τ_T and/or τ_L .

Tab. 3.7.: Measure of errors w.r.t. experiment for symmetry-allowed vertical K-edge excitation energies (eV) computed with spin projection using different combinations of the cc-pVTZ basis set.^{a,b}

	$\langle \bar{S}_{\text{UHF}}^2 \rangle_{S=0^c}$	PUHF	PUMP2	PUMP3	PUMP2.5
<u>cc-pVTZ^d</u>	1.038				
τ_T -A-MAE		10.5 (10.6)	2.2 (2.1)	3.6 (3.4)	1.0 (0.8)
τ_L -A-MAE		10.5 (10.5)	2.1 (2.0)	4.3 (4.0)	1.7 (1.4)
τ_T -A-RMSE		10.9 (11.0)	2.6 (2.5)	4.1 (3.8)	1.6 (1.2)
τ_L -A-RMSE		10.9 (10.9)	2.6 (2.4)	5.0 (4.7)	2.7 (2.3)
τ_T -B-MAE		10.4 (10.4)	2.4 (2.3)	3.5 (3.3)	0.9 (0.7)
τ_L -B-MAE		10.4 (10.3)	2.2 (2.1)	4.1 (3.8)	1.5 (1.3)
τ_T -B-RMSE		10.7 (10.8)	2.8 (2.7)	3.9 (3.7)	1.5 (1.1)
τ_L -B-RMSE		10.7 (10.7)	2.7 (2.5)	4.9 (4.5)	2.6 (2.2)
<u>cc-pVTZ & ECP^d</u>	0.213				
τ_T -A-MAE		0.7 (0.7)	2.0 (2.0)	1.6 (1.6)	1.8 (1.8)
τ_L -A-MAE		0.7 (0.7)	2.0 (2.0)	1.6 (1.7)	1.8 (1.8)
τ_T -A-RMSE		1.0 (0.8)	2.3 (2.3)	1.9 (1.9)	2.1 (2.1)
τ_L -A-RMSE		1.0 (0.8)	2.3 (2.4)	1.9 (2.0)	2.1 (2.2)
τ_T -B-MAE		0.8 (0.7)	1.9 (2.2)	1.5 (1.5)	1.7 (1.7)
τ_L -B-MAE		0.8 (0.7)	1.9 (1.9)	1.5 (1.5)	1.7 (1.7)
τ_T -B-RMSE		1.0 (0.9)	1.9 (2.2)	1.8 (1.8)	2.0 (2.0)
τ_L -B-RMSE		1.0 (0.9)	2.2 (2.2)	1.8 (1.8)	2.0 (2.0)
<u>ucc-pVTZ^d</u>	1.039				
τ_T -A-MAE		10.5 (10.6)	2.4 (2.3)	3.6 (3.4)	1.0 (0.8)
τ_L -A-MAE		10.5 (10.6)	2.3 (2.2)	4.2 (4.0)	1.6 (1.4)
τ_T -A-RMSE		10.9 (11.1)	2.8 (2.7)	4.2 (4.0)	1.7 (1.3)
τ_L -A-RMSE		11.0 (11.1)	2.7 (2.5)	5.1 (5.0)	2.7 (2.4)
τ_T -B-MAE		10.4 (10.4)	2.5 (2.4)	3.5 (3.3)	1.0 (0.8)
τ_L -B-MAE		10.4 (10.4)	2.4 (2.3)	4.1 (3.9)	1.5 (1.3)
τ_T -B-RMSE		10.8 (10.9)	2.9 (2.8)	4.1 (3.9)	1.6 (1.3)
τ_L -B-RMSE		10.8 (10.9)	2.8 (2.6)	5.0 (4.8)	2.6 (2.3)
<u>ucc-pVTZ & ECP^d</u>	0.213				
τ_T -A-MAE		0.8 (0.7)	2.0 (2.0)	1.6 (1.6)	1.8 (1.8)
τ_L -A-MAE		0.8 (0.7)	2.0 (2.0)	1.6 (1.6)	1.8 (1.8)
τ_T -A-RMSE		1.0 (0.9)	2.3 (2.3)	1.9 (1.9)	2.1 (2.1)
τ_L -A-RMSE		1.0 (0.9)	2.4 (2.4)	2.0 (2.0)	2.2 (2.2)
τ_T -B-MAE		0.8 (0.7)	1.8 (1.8)	1.4 (1.8)	1.6 (1.6)
τ_L -B-MAE		0.8 (0.7)	1.9 (1.9)	1.5 (1.5)	1.7 (1.7)
τ_T -B-RMSE		1.1 (0.9)	2.2 (2.2)	1.4 (1.8)	2.0 (2.0)
τ_L -B-RMSE		1.1 (0.9)	2.2 (2.2)	1.9 (1.9)	2.0 (2.1)

^aEntries in parenthesis are statistics for the dataset excluding two species with multireference character.

^bMAE and RMSE with relativistic correction A (C_{Perekis}) and B (C_{Chong}). ^cAverage excited state $\langle S_{\text{UHF}}^2 \rangle$

for singlets. ^dOne outlier excluded for τ_T and/or τ_L .

Tab. 3.8.: Measure of errors w.r.t. experiment for symmetry-allowed vertical K-edge excitation energies (eV) computed without spin projection using different combinations of the aug-cc-pVTZ basis set.^{a,b}

	$\langle \bar{S}_{\text{UHF}}^2 \rangle_{S=0^c}$	UHF	UMP2	UMP3	UMP2.5
<u>aug-cc-pVTZ^d</u>	1.040				
τ_T -A-MAE		10.3 (10.4)	2.3 (2.2)	3.5 (3.3)	1.0 (0.9)
τ_L -A-MAE		10.3 (10.3)	2.4 (2.3)	4.2 (3.9)	1.7 (1.5)
τ_T -A-RMSE		10.7 (10.8)	2.6 (2.5)	4.1 (3.9)	1.6 (1.4)
τ_L -A-RMSE		10.7 (10.7)	2.8 (2.6)	5.2 (4.7)	2.9 (2.4)
τ_T -B-MAE		10.2 (10.3)	2.4 (2.3)	3.4 (3.2)	1.0 (0.8)
τ_L -B-MAE		10.2 (10.1)	2.5 (2.4)	4.1 (3.7)	1.6 (1.4)
τ_T -B-RMSE		10.6 (10.7)	2.7 (2.7)	4.0 (3.8)	1.5 (1.3)
τ_L -B-RMSE		10.6 (10.5)	2.8 (2.7)	5.0 (4.6)	2.7 (2.3)
<u>aug-cc-pVTZ & ECP^d</u>	0.214				
τ_T -A-MAE		0.5 (0.4)	1.6 (1.6)	1.1 (1.1)	1.3 (1.3)
τ_L -A-MAE		0.5 (0.4)	1.6 (1.6)	1.0 (1.1)	1.3 (1.3)
τ_T -A-RMSE		0.7 (0.6)	2.0 (2.0)	1.4 (1.4)	1.7 (1.7)
τ_L -A-RMSE		0.7 (0.6)	1.9 (1.9)	1.3 (1.3)	1.6 (1.6)
τ_T -B-MAE		0.5 (0.4)	1.5 (1.5)	1.0 (1.0)	1.2 (1.2)
τ_L -B-MAE		0.5 (0.4)	1.5 (1.5)	0.9 (1.0)	1.2 (1.2)
τ_T -B-RMSE		0.7 (0.6)	1.9 (1.9)	1.4 (1.4)	1.6 (1.6)
τ_L -B-RMSE		0.7 (0.6)	1.8 (1.8)	1.2 (1.2)	1.5 (1.5)
<u>uaug-cc-pVTZ^d</u>	1.040				
τ_T -A-MAE		9.8 (10.1)	2.4 (2.3)	3.5 (3.3)	1.0 (0.8)
τ_L -A-MAE		9.8 (10.1)	2.7 (2.4)	4.3 (4.0)	1.8 (1.5)
τ_T -A-RMSE		10.6 (10.7)	2.9 (2.7)	4.1 (3.9)	1.6 (1.2)
τ_L -A-RMSE		10.6 (10.7)	3.3 (2.7)	5.3 (5.0)	3.2 (2.6)
τ_T -B-MAE		9.7 (9.9)	2.6 (2.5)	3.4 (3.2)	0.9 (0.7)
τ_L -B-MAE		9.7 (9.9)	2.7 (2.5)	4.1 (3.8)	1.8 (1.5)
τ_T -B-RMSE		10.4 (10.6)	3.0 (2.9)	3.9 (3.7)	1.5 (1.1)
τ_L -B-RMSE		10.4 (10.6)	3.3 (2.8)	5.2 (4.9)	3.1 (2.5)
<u>uaug-cc-pVTZ & ECP</u>	0.213				
τ_T -A-MAE		0.5 (0.4)	1.5 (1.5)	1.0 (1.1)	1.2 (1.3)
τ_L -A-MAE		0.5 (0.4)	1.6 (1.6)	1.1 (1.2)	1.3 (1.4)
τ_T -A-RMSE		0.7 (0.6)	1.9 (1.9)	1.4 (1.4)	1.6 (1.6)
τ_L -A-RMSE		0.7 (0.6)	2.1 (2.1)	1.5 (1.6)	1.8 (1.8)
τ_T -B-MAE		0.5 (0.5)	1.4 (1.4)	1.0 (1.0)	1.2 (1.2)
τ_L -B-MAE		0.5 (0.5)	1.5 (1.5)	1.1 (1.1)	1.3 (1.3)
τ_T -B-RMSE		0.8 (0.6)	1.8 (1.8)	1.3 (1.4)	1.5 (1.6)
τ_L -B-RMSE		0.8 (0.6)	2.0 (2.0)	1.5 (1.5)	1.7 (1.7)

^aEntries in parenthesis are statistics for the dataset excluding two species with multireference character.

^bMAE and RMSE with relativistic correction A (C_{Perekis}) and B (C_{Chong}). ^cAverage excited state $\langle S_{\text{UHF}}^2 \rangle$

for singlets. ^dOne outlier excluded for τ_T and/or τ_L .

Tab. 3.9.: Measure of errors w.r.t. experiment for symmetry-allowed vertical K-edge excitation energies (eV) computed with spin projection using different combinations of the aug-cc-pVTZ basis set.^{a,b}

	$\langle \bar{S}_{\text{UHF}}^2 \rangle_{S=0^c}$	PUHF	PUMP2	PUMP3	PUMP2.5
<u>aug-cc-pVTZ^d</u>	1.040				
τ_T -A-MAE		10.3 (10.4)	2.3 (2.2)	3.5 (3.3)	1.0 (0.8)
τ_L -A-MAE		10.3 (10.2)	2.4 (2.3)	4.2 (3.8)	1.7 (1.5)
τ_T -A-RMSE		10.7 (10.8)	2.6 (2.5)	4.1 (3.9)	1.6 (1.3)
τ_L -A-RMSE		10.7 (10.7)	2.8 (2.6)	5.2 (4.8)	2.8 (2.4)
τ_T -B-MAE		10.2 (10.2)	2.4 (2.3)	3.4 (3.2)	0.9 (0.8)
τ_L -B-MAE		10.2 (10.1)	2.5 (2.4)	4.0 (3.7)	1.6 (1.4)
τ_T -B-RMSE		10.6 (10.6)	2.7 (2.7)	4.0 (3.8)	1.5 (1.2)
τ_L -B-RMSE		10.6 (10.5)	2.8 (2.7)	5.0 (4.6)	2.7 (2.3)
<u>aug-cc-pVTZ & ECP^d</u>	0.214				
τ_T -A-MAE		0.6 (0.5)	1.3 (1.3)	0.9 (0.9)	1.0 (1.0)
τ_L -A-MAE		0.6 (0.5)	1.3 (1.3)	0.9 (0.9)	1.0 (1.0)
τ_T -A-RMSE		0.8 (0.7)	1.7 (1.7)	1.2 (1.3)	1.4 (1.4)
τ_L -A-RMSE		0.9 (0.7)	1.6 (1.6)	1.1 (1.1)	1.3 (1.3)
τ_T -B-MAE		0.7 (0.6)	1.2 (1.2)	0.9 (0.9)	1.0 (1.0)
τ_L -B-MAE		0.7 (0.6)	1.1 (1.1)	0.8 (0.8)	0.9 (0.9)
τ_T -B-RMSE		0.9 (0.8)	1.6 (1.6)	1.2 (1.2)	1.3 (1.3)
τ_L -B-RMSE		0.9 (0.8)	1.5 (1.5)	1.1 (1.1)	1.2 (1.2)
<u>uaug-cc-pVTZ^d</u>	1.040				
τ_T -A-MAE		9.6 (9.9)	2.5 (2.3)	3.5 (3.3)	1.0 (0.8)
τ_L -A-MAE		9.8 (10.0)	2.7 (2.4)	4.2 (3.9)	1.8 (1.5)
τ_T -A-RMSE		10.5 (10.7)	2.9 (2.7)	4.1 (3.9)	1.6 (1.2)
τ_L -A-RMSE		10.5 (10.7)	3.3 (2.7)	5.3 (5.0)	3.2 (2.5)
τ_T -B-MAE		9.5 (9.7)	2.6 (2.5)	3.3 (3.1)	0.9 (0.7)
τ_L -B-MAE		9.6 (9.9)	2.7 (2.5)	4.1 (3.8)	1.7 (1.4)
τ_T -B-RMSE		10.3 (10.5)	3.0 (2.8)	3.9 (3.7)	1.5 (1.1)
τ_L -B-RMSE		10.4 (10.6)	3.3 (2.7)	5.2 (4.8)	3.1 (2.4)
<u>uaug-cc-pVTZ & ECP</u>	0.213				
τ_T -A-MAE		0.7 (0.6)	1.3 (1.3)	1.0 (1.0)	1.1 (1.1)
τ_L -A-MAE		0.7 (0.6)	1.4 (1.4)	1.1 (1.1)	1.2 (1.2)
τ_T -A-RMSE		0.9 (0.8)	1.6 (1.6)	1.2 (1.2)	1.4 (1.4)
τ_L -A-RMSE		0.9 (0.8)	1.8 (1.8)	1.4 (1.4)	1.6 (1.6)
τ_T -B-MAE		0.7 (0.6)	1.2 (1.5)	1.0 (1.0)	1.1 (1.1)
τ_L -B-MAE		0.7 (0.6)	1.3 (1.3)	1.1 (1.1)	1.1 (1.2)
τ_T -B-RMSE		1.0 (0.9)	1.2 (1.5)	1.2 (1.2)	1.3 (1.3)
τ_L -B-RMSE		1.0 (0.9)	1.7 (1.8)	1.4 (1.4)	1.5 (1.5)

^aEntries in parenthesis are statistics for the dataset excluding two species with multireference character.

^bMAE and RMSE with relativistic correction A (C_{Perekis}) and B (C_{Chong}). ^cAverage excited state $\langle S_{\text{UHF}}^2 \rangle$

for singlets. ^dOne outlier excluded for τ_T and/or τ_L .

Tab. 3.10.: Vertical K -edge excitation energies (eV) using u6-311+G(2df) without spin projection.^a

Molecule	K-Edge	UHF	UMP2	UMP3	UMP2.5	Exp.
N ₂	N	409.7	397.6	403.5	400.5	400.9 ³⁰¹
<i>cis</i> -Diazene	N	407.6	396.1	400.5	398.3	398.4 ³⁰³
C ₂ H ₂	C	293.4	283.9	287.3	285.6	285.9 ³⁰⁰
C ₂ H ₄	C	292.5	283.6	285.7	284.7	284.7 ³⁰⁰
C ₂ H ₆	C	294.8	285.5	287.9	286.7	286.9 ³⁰⁰
F ₂	F	694.1	678.3	684.8	681.5	682.2 ³⁰²
O ₃ (O=O-O)	O	540.0	525.7	533.6	529.6	529.1 ³¹⁴
H ₂ O ₂	O	543.8	529.4	535.6	532.5	533.0 ³¹⁵
CO ₂	O	546.5	531.8	540.0	535.9	535.4 ³¹⁷
O ₂	O	542.0	526.8	534.2	530.5	530.8 ³¹⁹
C ₂ N ₂	C	293.6	286.2	287.8	287.0	286.3 ³⁰⁵
C ₂ N ₂	N	409.8	393.1	403.5	398.3	398.9 ³⁰⁵
Cyclopropane	C	295.4	285.9	288.7	287.3	287.7 ³⁰⁸
C ₂ F ₄	C	297.9	293.2	294.2	293.7	290.1 ³⁰⁴
C ₂ F ₄	F	708.6	685.1	697.2	691.2	690.7 ³⁰⁴
CF ₂ O	F	701.0	688.2	694.7	691.4	689.2 ³⁰⁶
CH ₂ CF ₂	F	701.5	687.8	694.4	691.1	690.3 ³⁰⁴
<i>cis</i> -CH ₂ CF ₂	F	700.9	685.3	692.4	688.9	689.3 ³⁰⁴
Hydrazine	N	411.4	399.0	404.0	401.5	401.5 ³⁰⁷
Furan (C-O)	C	295.3	285.3	289.0	287.2	286.6 ²²⁷
OF ₂	F	696.6	680.1	688.9	684.5	683.8 ³¹⁰
Urea	N	411.9	400.4	406.0	403.2	402.0 ³⁰⁹
N ₃ ⁻ (N=N=N)	N	410.3	394.4	405.5	399.9	399.6 ³⁰³
Allene (C=C=C)	C	286.8	286.6	286.5	286.6	285.4 ³¹³
Cyclobutane	C	299.3	286.0	288.4	287.2	287.4 ³⁰⁸
C ₂	C	295.4	284.3	292.1	288.2	285.9 ^{300,316}
Acetone (C-C=O)	C	295.8	286.0	289.3	287.6	288.4 ²²³
Pyridine (C-N)	C	294.4	283.8	288.0	285.9	285.3 ²³⁰
Tetrazine	C	295.0	284.2	289.0	286.6	285.2 ³¹¹
Tetrazine	N	413.1	396.6	404.1	400.3	398.8 ^{230,311}
Benzene	C	297.6	283.2	286.9	285.0	285.2 ³²⁰
Pyrrrole (C-NH)	C	295.2	284.7	288.7	286.7	286.3 ³²¹
NF ₃	F	700.6	684.3	692.7	688.5	687.4 ³¹²

^aResults using τ_T and C_{Chong} .

Tab. 3.11.: Vertical *K*-edge excitation energies (eV) using u6-311+G(2df) with spin projection.^a

Molecule	K-Edge	PUHF	PUMP2	PUMP3	PUMP2.5	Exp.
N ₂	N	410.0	397.9	403.8	400.8	400.9 ³⁰¹
cis-Diazene	N	407.9	396.3	400.8	398.5	398.4 ³⁰³
C ₂ H ₂	C	293.5	284.0	287.4	285.7	285.9 ³⁰⁰
C ₂ H ₄	C	292.6	283.7	285.9	284.8	284.7 ³⁰⁰
C ₂ H ₆	C	294.7	285.4	287.8	286.6	286.9 ³⁰⁰
F ₂	F	694.7	678.9	685.4	682.2	682.2 ³⁰²
O ₃ (O=O-O)	O	539.9	525.5	533.4	529.4	529.1 ³¹⁴
H ₂ O ₂	O	544.3	530.0	536.1	533.0	533.0 ³¹⁵
CO ₂	O	546.5	531.8	540.0	535.9	535.4 ³¹⁷
O ₂	O	541.9	526.7	534.2	530.5	530.8 ³¹⁹
C ₂ N ₂	C	292.9	285.5	287.1	286.3	286.3 ³⁰⁵
C ₂ N ₂	N	409.7	393.0	403.4	398.2	398.9 ³⁰⁵
Cyclopropane	C	295.3	285.8	288.6	287.2	287.7 ³⁰⁸
C ₂ F ₄	C	298.2	293.5	294.5	294.0	290.1 ³⁰⁴
C ₂ F ₄	F	708.4	685.0	697.1	691.0	690.7 ³⁰⁴
CF ₂ O	F	700.9	688.0	694.5	691.2	689.2 ³⁰⁶
CH ₂ CF ₂	F	701.3	687.5	694.2	690.8	690.3 ³⁰⁴
cis-CH ₂ CF ₂	F	700.8	685.2	692.2	688.7	689.3 ³⁰⁴
Hydrazine	N	411.4	398.9	403.9	401.4	401.5 ³⁰⁷
Furan (C-O)	C	295.3	285.3	289.0	287.1	286.6 ²²⁷
OF ₂	F	696.8	680.2	689.0	684.6	683.8 ³¹⁰
Urea	N	411.9	400.4	406.0	403.2	402.0 ³⁰⁹
N ₃ ⁻ (N=N=N)	N	410.2	394.2	405.3	399.8	399.6 ³⁰³
Allene (C=C=C)	C	286.4	286.2	286.1	286.1	285.4 ³¹³
Cyclobutane	C	299.2	285.9	288.3	287.1	287.4 ³⁰⁸
C ₂	C	295.6	284.5	292.3	288.4	285.9 ^{300,316}
Acetone (C-C=O)	C	295.7	285.9	289.2	287.5	288.4 ²²³
Pyridine (C-N)	C	294.1	283.5	287.7	285.6	285.3 ²³⁰
Tetrazine	C	295.0	284.2	289.0	286.6	285.2 ³¹¹
Tetrazine	N	412.9	396.4	403.9	400.2	398.8 ^{230,311}
Benzene	C	297.4	283.0	286.7	284.8	285.2 ³²⁰
Pyrrrole (C-NH)	C	295.2	284.6	288.7	286.7	286.3 ³²¹
NF ₃	F	700.7	684.4	692.8	688.6	687.4 ³¹²

^aResults using τ_T and $\mathcal{C}_{\text{Chong}}$.

Tab. 3.12.: Vertical K -edge excitation energies (eV) using ucc-pVTZ without spin projection.^a

Molecule	K-Edge	UHF	UMP2	UMP3	UMP2.5	Exp.
N ₂	N	409.7	397.6	403.4	400.5	400.9 ³⁰¹
<i>cis</i> -Diazene	N	407.6	396.1	400.5	398.3	398.4 ³⁰³
C ₂ H ₂	C	293.4	284.0	287.3	285.7	285.9 ³⁰⁰
C ₂ H ₄	C	292.4	283.7	285.8	284.7	284.7 ³⁰⁰
C ₂ H ₆	C	295.5	286.2	288.6	287.4	286.9 ³⁰⁰
F ₂	F	694.2	678.5	684.8	681.6	682.2 ³⁰²
O ₃ (O=O-O)	O	540.1	525.8	533.5	529.7	529.1 ³¹⁴
H ₂ O ₂	O	543.8	529.6	535.6	532.6	533.0 ³¹⁵
CO ₂	O	546.5	531.8	540.1	535.9	535.4 ³¹⁷
O ₂	O	542.0	526.9	534.2	530.5	530.8 ³¹⁹
C ₂ N ₂	C	293.6	286.0	287.6	286.8	286.3 ³⁰⁵
C ₂ N ₂	N	409.8	394.7	404.8	399.7	398.9 ³⁰⁵
Cyclopropane	C	296.1	286.3	289.3	287.8	287.7 ³⁰⁸
C ₂ F ₄	C	297.9	294.9	296.4	295.6	290.1 ³⁰⁴
C ₂ F ₄	F	708.6	683.9	695.8	689.9	690.7 ³⁰⁴
CF ₂ O	F	701.2	688.6	694.5	691.6	689.2 ³⁰⁶
CH ₂ CF ₂	F	701.6	686.8	693.5	690.2	690.3 ³⁰⁴
<i>cis</i> -CH ₂ CF ₂	F	700.9	685.3	692.3	688.8	689.3 ³⁰⁴
Hydrazine	N	411.7	399.2	404.3	401.7	401.5 ³⁰⁷
Furan (C-O)	C	295.3	285.3	289.0	287.1	286.6 ²²⁷
OF ₂	F	696.7	680.3	688.9	684.6	683.8 ³¹⁰
Urea	N	412.5	402.7	407.8	405.3	402.0 ³⁰⁹
N ₃ ⁻ (N=N=N)	N	410.3	394.8	405.1	400.0	399.6 ³⁰³
Allene (C=C=C)	C	286.9	286.7	286.6	286.6	285.4 ³¹³
Cyclobutane	C	300.3	286.6	289.3	287.9	287.4 ³⁰⁸
C ₂	C	295.4	284.4	292.1	288.2	285.9 ^{300,316}
Acetone (C-C=O)	C	296.5	285.8	289.2	287.5	288.4 ²²³
Pyridine (C-N)	C	294.4	283.7	287.9	285.8	285.3 ²³⁰
Tetrazine	C	295.0	283.6	288.4	286.0	285.2 ³¹¹
Tetrazine	N	413.1	399.2	406.3	402.7	398.8 ^{230,311}
Benzene	C	297.5	283.2	287.0	285.1	285.2 ³²⁰
Pyrrrole (C-NH)	C	295.3	284.6	288.6	286.6	286.3 ³²¹
NF ₃	F	705.4	684.5	696.6	690.5	687.4 ³¹²

^aResults using τ_T and C_{Chong} .

Tab. 3.13.: Vertical K -edge excitation energies (eV) using ucc-pVTZ with spin projection.^a

Molecule	K-Edge	UHF	UMP2	UMP3	UMP2.5	Exp.
N ₂	N	410.0	397.9	403.7	400.8	400.9 ³⁰¹
cis-Diazene	N	407.9	396.4	400.7	398.5	398.4 ³⁰³
C ₂ H ₂	C	293.5	284.1	287.4	285.8	285.9 ³⁰⁰
C ₂ H ₄	C	292.5	283.8	285.9	284.8	284.7 ³⁰⁰
C ₂ H ₆	C	295.4	286.1	288.5	287.3	286.9 ³⁰⁰
F ₂	F	694.8	679.1	685.4	682.3	682.2 ³⁰²
O ₃ (O=O-O)	O	539.9	525.6	533.3	529.5	529.1 ³¹⁴
H ₂ O ₂	O	544.3	530.1	536.1	533.1	533.0 ³¹⁵
CO ₂	O	546.5	531.8	540.0	535.9	535.4 ³¹⁷
O ₂	O	542.0	526.8	534.2	530.5	530.8 ³¹⁹
C ₂ N ₂	C	292.9	285.2	286.8	286.0	286.3 ³⁰⁵
C ₂ N ₂	N	409.9	394.7	404.8	399.8	398.9 ³⁰⁵
Cyclopropane	C	296.0	286.2	289.2	287.7	287.7 ³⁰⁸
C ₂ F ₄	C	298.2	295.2	296.7	296.0	290.1 ³⁰⁴
C ₂ F ₄	F	708.4	683.7	695.6	689.6	690.7 ³⁰⁴
CF ₂ O	F	701.0	688.5	694.4	691.4	689.2 ³⁰⁶
CH ₂ CF ₂	F	701.5	686.7	693.3	690.0	690.3 ³⁰⁴
cis-CH ₂ CF ₂	F	700.7	685.1	692.0	688.6	689.3 ³⁰⁴
Hydrazine	N	411.6	399.2	404.2	401.7	401.5 ³⁰⁷
Furan (C-O)	C	295.3	285.3	289.0	287.1	286.6 ²²⁷
OF ₂	F	696.9	680.5	689.1	684.8	683.8 ³¹⁰
Urea	N	412.5	402.8	407.9	405.3	402.0 ³⁰⁹
N ₃ ⁻ (N=N=N)	N	410.2	394.7	405.0	399.8	399.6 ³⁰³
Allene (C=C=C)	C	286.4	286.2	286.2	286.2	285.4 ³¹³
Cyclobutane	C	300.2	286.5	289.2	287.8	287.4 ³⁰⁸
C ₂	C	295.6	284.6	292.3	288.4	285.9 ^{300,316}
Acetone (C-C=O)	C	296.4	285.7	289.1	287.4	288.4 ²²³
Pyridine (C-N)	C	294.0	283.3	287.5	285.4	285.3 ²³⁰
Tetrazine	C	295.1	283.6	288.4	286.0	285.2 ³¹¹
Tetrazine	N	413.0	399.0	406.1	402.6	398.8 ^{230,311}
Benzene	C	297.3	283.0	286.8	284.9	285.2 ³²⁰
Pyrrrole (C-NH)	C	295.2	284.5	288.5	286.5	286.3 ³²¹
NF ₃	F	705.3	684.5	696.6	690.5	687.4 ³¹²

^aResults using τ_T and $\mathcal{C}_{\text{Chong}}$.

Tab. 3.14.: Core-level valence and Rydberg transitions (eV) of N₂.^a

State	Excitation	PUHF	PUMP2	PUMP3	PUMP2.5	Exp. ^c	Exp. ^d
¹ Π _u	(1sσ _u ⁻¹)(2pπ _g) ¹	410.0 ^b	397.8	403.6	400.9	400.9	400.8
¹ Σ _u ⁺	(1sσ _u ⁻¹)(3sσ _g) ¹	415.7	400.9	410.8	406.0	406.2	405.6
¹ Π _u	(1sσ _g ⁻¹)(3pπ _u) ¹	416.6	401.8	411.8	407.0	407.1	406.5
¹ Σ _u ⁺	(1sσ _g ⁻¹)(3pσ _u) ¹	416.8	402.0	412.1	407.2	407.3	406.7
	<i>K</i> -Edge IP	419.1	404.6	414.4	409.7	409.9	409.5

^audaug-cc-pVTZ, C_{Chong}, full orbital window. ^bUp-projected from ucc-pVTZ. ^cRef.³²² ^dRefs.^{323,324}

Δ -Based Composite Models for Simulating X-ray Absorption and Emission Spectra

“ ...[W]e believe that the results of theoretical computations are going to compete more and more strongly with experiment from now on.

— **R.S.Mulliken and C.C.J.Roothaan**

Broken Bottlenecks and the Future of Molecular Quantum Mechanics.
Proc. Natl. Acad. Sci. U.S.A. 45 (3) 394-398 (1959)

This chapter is based on the following:

A.Y. Zamani and H.P. Hratchian. “Assessing the performance of Δ SCF and the diagonal second-order self-energy approximation for calculating vertical core excitation energies” *J. Chem. Phys.* Accepted (2023)

4.1 Motivation

Spectroscopic analysis using X-ray and electron sources provides rich information on the characteristic properties of materials.^{342–344} Techniques such as X-ray photoelectron spectroscopy (XPS) probe the valence and core-level energy signatures for a local chemical environment via ionization. Core-excited states are accessed with X-ray absorption spectroscopy (XAS) and inner-shell electron energy loss spectroscopy (ISEELS). Non-resonant X-ray emission spectroscopy (XES) measures the radiative decay of an outer-core electron into a core-hole formed upon ionization. Advances in X-ray techniques such as these have seen ancillary development of theoretical methods for interpreting core spectra, which is critical for studying ultrafast chemical reactivity and dynamics.^{72–75}

Historically, quantum chemical methods for modeling core-ionization often used the difference of self-consistent-field solutions (Δ SCF) for the N and $N - 1$ states (where N is the number of electrons).^{88,89} Early computation of X-ray emission energies used a two-step model involving the difference between the detachment energy, or ionization potential (IP), of the K -shell electron and the valence IPs of the neutral species.¹⁴⁷ The formula for the non-resonant emission energy \mathcal{E}_X is

$$\mathcal{E}_X = \text{IP}_{\text{core}} - \text{IP}^f \quad (4.1)$$

where IP^f is the energy to reach a particular final state configuration in which a higher occupied orbital reoccupies the ionized core (see Figure 4.1). Specialized methods using equation of motion coupled cluster singles and doubles (EOM-CCSD), algebraic diagrammatic construction (ADC) schemes, GW +BSE, and time-dependent density functional theory (TD-DFT) have been applied to studies of XES.^{108,138,345,346} Similarly, the X-ray absorption energy is obtained through the difference of IP_{core} and the electron affinity (EA) of a virtual orbital in the core-ionized system. The excitation energy ω_X is

$$\omega_X = \text{IP}_{\text{core}} - \text{EA}_{\text{core}}^f \quad (4.2)$$

where $\text{EA}_{\text{core}}^f$ is the energy to attach an electron, in the presence of the core-hole, to an orbital that is occupied in the final neutral excited state configuration (see Figure 4.2). This is analogous to approaches based on the static-exchange approximation (STEX) where excitation energies are estimated through EAs obtained from configuration interaction singles (CIS) calculations with an optimized core-hole reference.^{119,347,348} Recent extensions of STEX to time-dependent density functional theory (TD-DFT) are able to produce highly accurate K -edge excitation energies.³⁴⁹ Related approaches for computing core excitation and ionization energies from coupled cluster (CC) theory such as electron attachment equation-of-motion (EA-EOM-CC) and Δ -based CC methods are also shown to be very accurate and amenable to systematic improvements.^{145,146,299,350,351}

It is well-known that Δ SCF captures the orbital relaxation (ORX) effects that accompany the formation of the core-hole state.^{60,200,244,352} This reasoning supports its viability for obtaining good estimates for IP_{core} which can be further refined with Møller-Plesset (MP) perturbation theory. The values for outer-valence IPs in addition to EAs of unoccupied levels can be accurately computed with one-particle Green's function methods.^{67,353-355}

In this study, we propose and examine composite models that incorporate Δ SCF and Δ MP methods with self-energy $\Sigma(E)$ corrections to the eigenvalues of the Fock

operator F . The computational protocol for obtaining representative single-reference solutions is delineated and results for vertical K -edge excitation and emission energies are presented.

4.2 Methods

In this section, we describe the individual procedural components of the composite models. These include SCF reference calculations, computation of core-hole intermediates, spin projection schemes, determination of IPs and EAs with a post-SCF response method, and additional capabilities for estimating emission intensities.

The value of IP_{core} can be approximated by subtracting the N and $N - 1$ total energies obtained from Hartree-Fock (HF) calculations. The representative core-hole state can be generated by applying projection operators or level-shifting in a modified SCF algorithm.^{261,264} In this work, the non-Aufbau solutions are converged using the projected initial maximum overlap method.²⁰⁸ To include correlation effects in the initial neutral the final ionized states not contained in ΔHF , a series of ΔMP_n ($n = 2, 2.5, 3$) methods are employed. Numerical issues may arise when using core-hole reference determinants with MP expansions. Certain orbital indices coupled to the core-hole can lead to near-zero denominators and instabilities reflected in divergent MP energies. Procedures described in recent literature²⁴⁷ are adopted to mitigate this effect. This involves removing orbital indices contributing to second-order energy denominators below a 0.02 a.u. threshold.

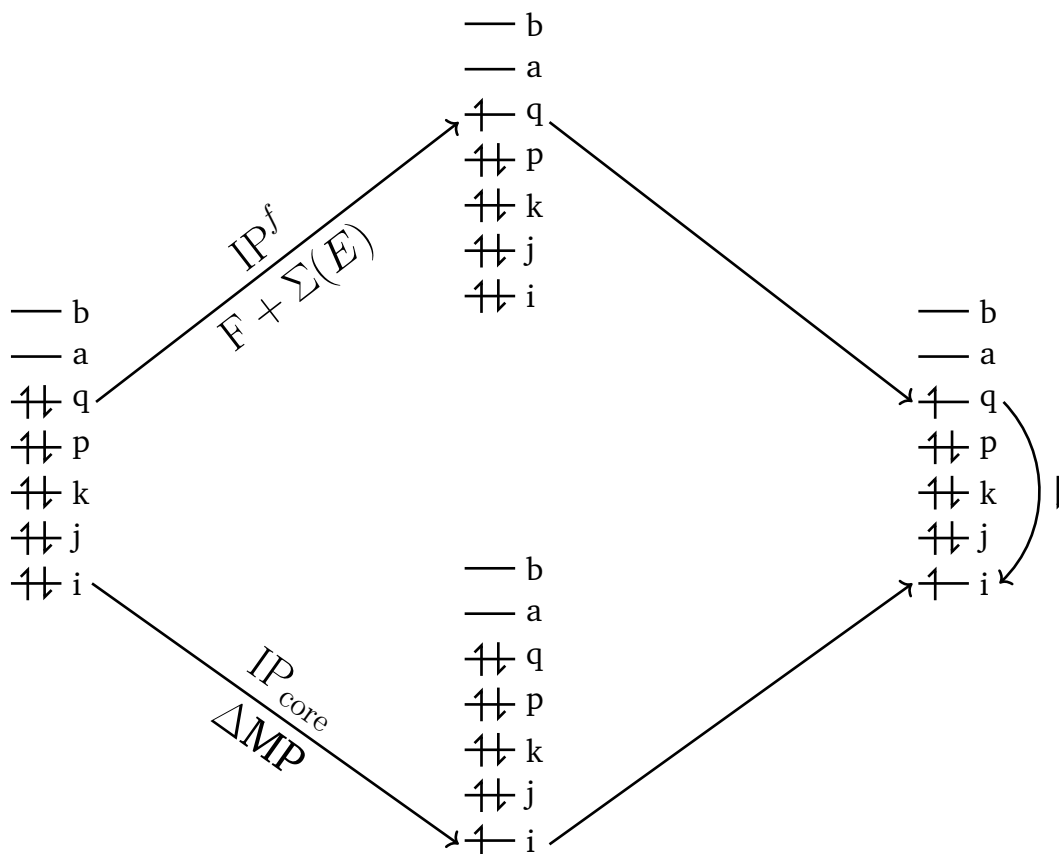
For ionization in closed-shell species, the unrestricted Hartree-Fock (UHF) result for the core-hole doublet typically exhibits minor spin polarization due to the spatial contraction of the electronic structure influenced by the increased effective nuclear charge. The spin contamination is typically low but not always negligible. Often, conceptual deficiencies of broken-symmetry solutions can be remedied with spin projection. Spin-projected energies are calculated perturbatively through a composite Hamiltonian^{30,283} under a class of approximate projection-after-variation (PAV) methods.^{290,291,293} The spin-projected methods are denoted as PUHF and PUMP $_n$.

Electron propagator theory (EPT) is a formalism for the one-electron Green's function that provides a foundation for the direct calculation of IPs, EAs, and Dyson orbitals from first principles.⁶⁶ Systematic improvements to self-energy approximations have been formulated and thoroughly assessed.³⁵⁶⁻³⁵⁹ Its advantage as a correlated one-electron theory is reflected in the inclusion of important many-body interactions

that follow a physical change in particle number while still retaining the intuitive utility of orbital concepts routinely used in molecular quantum chemistry. The renormalized partial third-order (P3+) method is a diagonal quasiparticle approximation for accurate determination of vertical IPs and EAs.³⁶⁰ The overestimation of correlation contributions typical of second-order corrections and exaggerated final-state relaxation effects offered at base third-order are ameliorated with P3+. P3+ is also selected as an optimal, cost-effective approach for its modest arithmetic bottleneck of $\mathcal{O}(O^2V^3)$ (where O and V give the number of occupied and virtual molecular orbitals (MOs)) and for its reduced storage requirements for generating the largest transformed integral subset of type $\langle OV || VV \rangle$ needed to calculate IPs. Symmetry-adapted implementations can then accelerate the time-to-solution for each pole search. The probability factors or pole strengths (PS) that accompany the quasiparticle corrections are the norms of the Dyson orbitals. A PS above 0.85 indicates that the Dyson orbital is dominated by a single canonical MO and that qualitative one-electron concepts for interpreting the $N \pm 1$ states hold.^{361,362}

Since core emission spectra typically resemble the photoelectron spectrum of the valence electrons that will undergo de-excitation, intensities or photoionization cross sections can be inferred from the proportional PS values. Relative emission intensities can also be obtained with transition dipole moments evaluated in the frozen orbital approximation.^{363–365} From the assumption that the core orbital is highly localized and that de-excitations involve valence MOs built from local atomic contributions, population analysis of the 2p character in the neutral-state valence MOs can be used to approximate the relative intensities for one-particle core-hole decay for second-row elements.^{366–368} The squares of the 2p components of the MO coefficients are summed over the atomic center(s) to reconstruct main-line non-resonant emission spectra for N₂, H₂O, and C₂H₄.

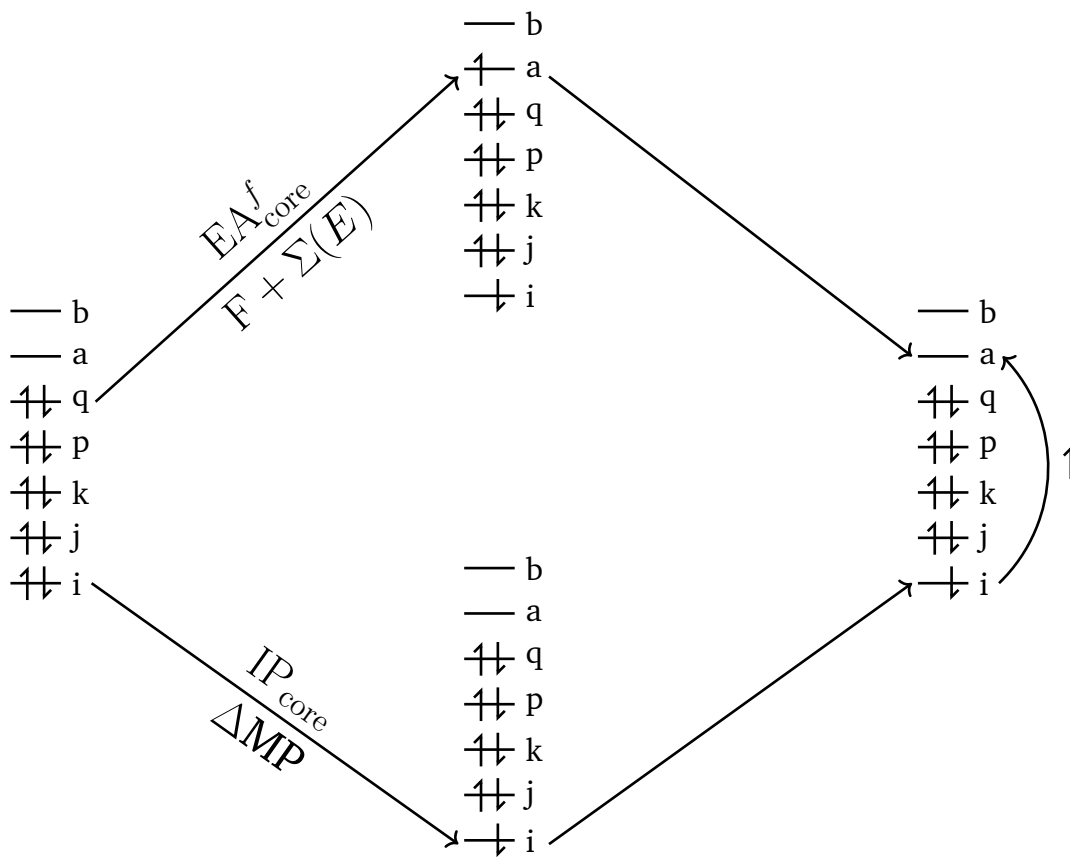
Fig. 4.1.: Model schematic for non-resonant XES with a closed shell reference.



4.3 Results and Discussion

Two sets of molecules are examined for the evaluation of \mathcal{E}_X . The first test set contains results for C, N, O, and Ne K -edge. $\Delta PUHF$ and $\Delta PUMP_n$ values for IP_{core} are computed using the aug-cc-pCVTZ basis with modification. For hydrogen, the cc-pVTZ basis is used. For post-SCF denominator control in this set, f-functions are removed to reduce or remove instances of high-energy virtual MOs spawned from atomic orbitals with high angular momentum. The second group of molecules is composed of fluoromethanes, for which IP_{core} is computed using the full aug-cc-pCVTZ basis set. The IP_{core} estimates for a selection of molecules from the first set, along with H_2O_2 , are used for evaluations of ω_X . When applying Δ -based methods for ionizations of symmetry-equivalent atomic cores, an effective-core-potential (ECP) is applied to all other atoms except the target site and any hydrogen atoms.

Fig. 4.2.: Model schematic for XAS with a closed shell reference.



The average percent deviation of $\langle S^2 \rangle_{\text{UHF}}$ for the entire set of core-hole doublets is 17%. The two core-hole spin channels for NO consist of a singlet and triplet with $\langle S^2 \rangle_{\text{UHF}}$ values of 1.241 and 2.578 respectively. Spin contamination is removed through successive annihilation up to $S + 4$ with projected MP.

Relativistic effects are incorporated using methodologies previously reported in the literature. Specifically, molecular relativistic corrections for C, N, O, and F are 0.05, 0.1, 0.2, and 0.35 eV respectively.²⁹⁶ The atomic relativistic correction for Ne is 1.2 eV.^{214,215}

Propagator calculations for IP^f using the P3+ method on neutral species are performed with the cc-pVTZ basis set. Many transitions beyond the lowest unoccupied orbital exhibit Rydberg character and increasing orbital angular momentum l —requiring additional diffuse and polarization functions for accurate excitation energies.¹⁹⁴ The d-aug-cc-pV6Z basis truncated at $l = 3$ is then used for computing bound-state (positive) $\text{EA}_{\text{core}}^f$ values with P3+. This approach is chosen for consistency and as an expedient approach towards customized basis set saturation. The core-hole reference for computing EAs is simulated with a $Z + 1$ model where the number of electrons is conserved and the atomic number Z of the target atom is increased by one.³⁶⁹ When the core orbitals of interest are delocalized by symmetry, the +1 charge is distributed evenly among equivalent atoms.

Geometries are obtained from the NIST CCCBDB²¹⁹ and Ranasinghe et al.²¹⁷ Structures are optimized at the CCSD(T)/aug-cc-pVTZ level except CF_4 which is optimized at the $\omega\text{B97X-D/aug-cc-pVTZ}$ level of theory. ΔPUHF , ΔPUMP_n and EPT calculations were performed with a development version of the Gaussian suite of programs.³⁷⁰ Integral symmetry with Abelian groups is used when applicable. Basis sets are acquired from the Basis Set Exchange.³²⁵

Experimental values for non-resonant valence-to-core emission energies available in the literature are reported from direct XES measurements or inferred from differences in photoelectron spectra. Observed excitation energies are taken from XAS and ISEELS experimental data. Experimental emission spectra are traced using WebPlotDigitizer.³⁷¹

Tab. 4.1.: Vertical C-N-O-Ne K -edge emission energies \mathcal{E}_X computed with projected, Δ UHF, Δ MP n , and EPT [P3+].

Molecule	Core	Orbital	Δ PUHF[P3+]	Δ PUMP2[P3+]	Δ PUMP2.5[P3+]	Δ PUMP3[P3+]	Exp.
CO	C	5σ	281.1 (-1.0)	282.5 (0.4)	282.4 (0.3)	282.4 (0.3)	282.1 ³⁷²
	C	1π	278.3 (-0.9)	279.7 (0.5)	279.7 (0.5)	279.6 (0.4)	279.2 ³⁷²
	O	1π	524.3 (-1.2)	525.9 (0.4)	525.7 (0.2)	525.5 (0.0)	525.5 ³⁷²
	O	4σ	521.5 (-1.1)	523.2 (0.6)	523.0 (0.4)	522.8 (0.2)	522.6 ³⁷²
N ₂	N	$3\sigma_g$	393.1 (-1.2)	395.2 (0.9)	394.9 (0.6)	394.5 (0.2)	394.3 ³⁷²
	N	$1\pi_u$	391.6 (-1.3)	393.7 (0.8)	393.3 (0.4)	393.0 (0.1)	392.9 ³⁷²
NO	N (S=0)	2π	402.7 (0.6)	403.0 (0.9)	403.0 (0.9)	403.0 (0.9)	402.1 ³⁷²
	N (S=1)	5σ	392.8 (-1.0)	394.8 (1.0)	394.6 (0.8)	394.4 (0.6)	393.8 ³⁷²
	N (S=0)	5σ	394.8 (1.3)	395.1 (1.6)	395.1 (1.6)	395.1 (1.6)	393.5 ³⁷²
H ₂ O	O	$1b_2$	520.3 (-0.1)	521.4 (1.0)	521.4 (1.0)	521.4 (1.0)	520.4 ³⁷³
	O	$3a_1$	524.4 (-0.7)	525.5 (0.4)	525.5 (0.4)	525.5 (0.4)	525.1 ³⁷³
	O	$1b_1$	526.7 (-0.1)	527.8 (1.0)	527.8 (1.0)	527.7 (0.9)	526.8 ³⁷³
CH ₃ OH	C	$2a''$	281.2 (0.0)	281.8 (0.6)	281.7 (0.5)	281.6 (0.4)	281.2 ³⁷⁴
	C	$7a'$	279.4 (0.0)	280.0 (0.6)	279.9 (0.5)	279.8 (0.4)	279.4 ³⁷⁴
	C	$6a'$	277.1 (-0.3)	277.6 (0.2)	277.5 (0.1)	277.4 (0.0)	277.4 ³⁷⁴

	O	$2a''$	527.1 (-0.7)	528.4 (0.6)	528.2 (0.4)	528.0 (0.2)	527.8 ³⁷⁴
	O	$7a'$	525.3 (-0.9)	526.6 (0.4)	526.4 (0.2)	526.2 (0.0)	526.2 ³⁷⁴
	O	$6a'$	522.9 (-0.9)	524.3 (0.5)	524.0 (0.2)	523.8 (0.0)	523.8 ³⁷⁴
CH ₄	C	$1t_2$	276.2 (-0.1)	276.6 (0.3)	276.7 (0.4)	276.7 (0.4)	276.3 ³⁷⁵
CO ₂	C	$1\pi_u$	280.9 (1.4)	279.2 (-0.4)	279.7 (0.2)	280.3 (0.7)	279.6 ³⁷⁶
	C	$3\sigma_u$	280.6 (1.1)	278.9 (-0.7)	279.4 (-0.1)	280.0 (0.4)	279.6 ³⁷⁶
	O	$1\pi_g$	526.8 (-1.5)	528.9 (0.6)	528.1 (-0.2)	527.3 (-1.0)	528.3 ³⁷⁶
	O	$1\pi_u$	522.7 (-1.7)	524.7 (0.3)	524.0 (-0.4)	523.2 (-1.2)	524.4 ³⁷⁶
	O	$3\sigma_u$	522.4 (-2.0)	524.5 (0.1)	523.7 (-0.7)	522.9 (-1.5)	524.4 ³⁷⁶
NH ₃	N	$3a_1$	394.4 (-0.7)	395.1 (0.1)	395.1 (0.1)	395.2 (0.1)	395.1 ³⁷⁷
	N	$1e$	388.6 (-0.2)	389.4 (0.6)	389.4 (0.6)	389.5 (0.7)	388.8 ³⁷⁷
Ne	Ne	$2p$	848.5 (0.0)	849.9 (1.4)	849.8 (1.3)	849.8 (1.3)	848.5 ³⁷⁸
N ₂ O	NN	2π	394.4 (-1.2)	395.8 (0.2)	395.7 (0.1)	395.6 (0.0)	395.6 ³⁷⁷
	NO	1π	391.9 (-2.9)	394.8 (0.0)	394.4 (-0.4)	393.9 (-0.9)	394.8 ³⁷⁷
	NN	7σ	390.6 (-1.7)	392.0 (-0.3)	391.9 (-0.4)	391.8 (-0.5)	392.3 ³⁷⁷
	NN	1π	388.6 (-2.0)	390.0 (-0.6)	389.9 (-0.7)	389.8 (-0.8)	390.6 ³⁷⁷
	O	2π	527.0 (-1.8)	529.4 (0.6)	529.1 (0.3)	528.7 (-0.1)	528.8 ³⁷⁷
	O	1π	521.1 (-2.8)	523.6 (-0.3)	523.3 (-0.6)	522.9 (-1.0)	523.9 ³⁷⁷

	O	7σ	523.1 (-1.8)	525.6 (0.7)	525.3 (0.4)	524.9 (0.0)	524.9 ³⁷⁹
	O	6σ	519.8 (-1.3)	522.3 (1.1)	522.0 (0.8)	521.6 (0.4)	521.2 ³⁷⁹
	NO	7σ	393.9 (-2.2)	396.8 (0.7)	396.4 (0.3)	395.9 (-0.2)	396.1 ³⁷⁹
	NO	6σ	390.6 (-1.8)	393.5 (1.2)	393.1 (0.7)	392.7 (0.3)	392.4 ³⁷⁹
	NN	6σ	387.3 (-1.2)	388.7 (0.2)	388.6 (0.1)	388.5 (0.0)	388.5 ³⁷⁹
C ₂ H ₄	C	$1b_{3u}$	279.7 (-0.2)	280.4 (0.5)	280.1 (0.2)	279.7 (-0.2)	279.9 ³⁸⁰
	C	$1b_{3g}$	277.2 (-0.5)	277.9 (0.2)	277.6 (-0.1)	277.3 (-0.4)	277.7 ³⁸⁰
	C	$3a_g$	275.4 (-0.4)	276.1 (0.3)	275.7 (-0.1)	275.4 (-0.4)	275.8 ³⁸⁰
	C	$1b_{2u}$	274.1 (-0.4)	274.8 (0.3)	274.5 (0.0)	274.2 (-0.3)	274.5 ³⁸⁰
	C	$2b_{1u}$	270.7 (-0.6)	271.5 (0.2)	271.1 (-0.2)	270.8 (-0.5)	271.3 ³⁸⁰
PS _{min}	0.84	MAE	1.0	0.6	0.5	0.5	
PS _{ave}	0.90	RMSE	1.3	0.7	0.6	0.6	

Tab. 4.2.: Vertical C-F K -edge emission energies \mathcal{E}_X computed with projected Δ UHF, Δ MP n and EPT [P3+].

Molecule	Core	Orbital	Δ PUHF[P3+]	Δ PUMP2[P3+]	Δ PUMP2.5[P3+]	Δ PUMP3[P3+]	Exp.
CF ₄	C	$2t_2$	261.7 (-0.1)	261.9 (0.1)	261.9 (0.1)	261.9 (0.1)	261.8 ³⁸¹

	C	$3t_2$	280.1 (0.6)	280.3 (0.8)	280.3 (0.8)	280.3 (0.8)	279.5 ³⁸¹
	C	$4t_2$	284.8 (0.4)	285.0 (0.6)	285.0 (0.6)	285.0 (0.6)	284.4 ³⁸¹
	C	$4a_1$	277.1 (0.1)	277.2 (0.2)	277.2 (0.2)	277.2 (0.2)	277.0 ³⁷⁵
	F	$1e$	676.4 (-0.2)	676.1 (-0.5)	675.9 (-0.7)	675.7 (-0.9)	676.6 ^{382,383}
	F	$4t_2$	677.3 (-0.3)	677.0 (-0.6)	676.8 (-0.8)	676.6 (-1.0)	677.6 ^{382,383}
	F	$1t_1$	678.5 (-0.3)	678.2 (-0.6)	678.0 (-0.8)	677.8 (-1.0)	678.8 ^{382,383}
CH ₃ F	F	$1e$	674.5 (-1.1)	676.2 (0.6)	676.1 (0.5)	675.9 (0.3)	675.6 ³⁷⁵
	F	$5a_1$	674.4 (-1.2)	676.0 (0.4)	675.9 (0.3)	675.8 (0.2)	675.6 ³⁷⁵
	F	$2e$	678.1 (-0.5)	679.7 (1.1)	679.6 (1.0)	679.5 (0.9)	678.6 ³⁷⁵
	F	$4a_1$	667.6 (-1.4)	669.2 (0.2)	669.1 (0.1)	669.0 (0.0)	669.0 ³⁷⁵
	C	$1e$	276.5 (0.3)	276.9 (0.7)	276.9 (0.7)	276.9 (0.7)	276.2 ³⁸¹
	C	$5a_1$	276.3 (0.1)	276.7 (0.5)	276.7 (0.5)	276.8 (0.6)	276.2 ³⁸¹
	C	$2e$	280.1 (0.1)	280.4 (0.4)	280.5 (0.5)	280.5 (0.5)	280.0 ³⁸¹
	C	$4a_1$	269.5 (-0.5)	269.9 (-0.1)	269.9 (-0.1)	269.9 (-0.1)	270.0 ³⁸¹
CH ₂ F ₂	F	$4a_1$	668.4 (-1.0)	668.4 (-1.0)	668.1 (-1.3)	667.9 (-1.5)	669.4 ³⁷⁵
	F	$1b_2$	673.5 (-0.9)	673.6 (-0.8)	673.3 (-1.1)	673.0 (-1.4)	674.4 ³⁷⁵
	F	$5a_1$	673.7 (-0.7)	673.7 (-0.7)	673.4 (-1.0)	673.2 (-1.2)	674.4 ³⁷⁵
	F	$3b_1$	673.8 (-0.6)	673.9 (-0.5)	673.6 (-0.8)	673.3 (-1.1)	674.4 ³⁷⁵

	F	$1a_2$	677.0 (-0.4)	677.1 (-0.3)	676.8 (-0.6)	676.5 (-0.9)	677.4 ³⁷⁵
	F	$4b_1$	677.7 (0.3)	677.8 (0.4)	677.5 (0.1)	677.2 (-0.2)	677.4 ³⁷⁵
	F	$6a_1$	677.3 (-0.1)	677.4 (0.0)	677.1 (-0.3)	676.8 (-0.6)	677.4 ³⁷⁵
	F	$2b_2$	679.2 (-0.8)	679.3 (-0.7)	679.0 (-1.0)	678.7 (-1.3)	680.0 ³⁷⁵
	C	$1b_2$	277.1 (0.0)	277.4 (0.3)	277.4 (0.3)	277.4 (0.3)	277.1 ³⁸¹
	C	$5a_1$	277.3 (0.2)	277.6 (0.5)	277.6 (0.5)	277.6 (0.5)	277.1 ³⁸¹
	C	$3b_1$	277.5 (0.4)	277.7 (0.6)	277.7 (0.6)	277.7 (0.6)	277.1 ³⁸¹
	C	$4a_1$	272.0 (0.0)	272.3 (0.3)	272.3 (0.3)	272.3 (0.3)	272.0 ³⁸¹
	C	$6a_1$	280.9 (0.3)	281.2 (0.6)	281.2 (0.6)	281.2 (0.6)	280.6 ³⁸¹
	C	$4b_1$	281.3 (0.7)	281.6 (1.0)	281.6 (1.0)	281.6 (1.0)	280.6 ³⁸¹
	C	$2b_2$	282.9 (0.5)	283.1 (0.7)	283.1 (0.7)	283.1 (0.7)	282.4 ³⁸¹
CHF ₃	C	$4a_1$	274.5 (0.3)	274.7 (0.5)	274.6 (0.4)	274.6 (0.4)	274.2 ³⁸¹
	C	$5a_1$	278.2 (0.0)	278.3 (0.1)	278.3 (0.1)	278.3 (0.1)	278.2 ³⁸¹
	C	$3e$	278.7 (0.5)	278.9 (0.7)	278.9 (0.7)	278.9 (0.7)	278.2 ³⁸¹
	C	$4e$	282.2 (0.4)	282.3 (0.5)	282.3 (0.5)	282.3 (0.5)	281.8 ³⁸¹
	C	$6a_1$	284.3 (0.0)	284.5 (0.2)	284.5 (0.2)	284.4 (0.1)	284.3 ³⁸¹
	F	$4a_1$	668.9 (-1.1)	668.8 (-1.2)	668.5 (-1.5)	668.2 (-1.8)	670.0 ³⁷⁵
	F	$5a_1$	672.6 (-1.0)	672.5 (-1.1)	672.2 (-1.4)	671.9 (-1.7)	673.6 ³⁷⁵

F ₂	F	3e	673.2 (-0.4)	673.0 (-0.6)	672.7 (-0.9)	672.4 (-1.2)	673.6 ³⁷⁵
	F	4e	676.6 (-0.1)	676.5 (-0.2)	676.2 (-0.5)	675.9 (-0.8)	676.7 ³⁷⁵
	F	5e	677.7 (-0.5)	677.5 (-0.6)	677.2 (-0.9)	676.9 (-1.2)	678.1 ^{375,383,384}
	F	1a ₂	678.3 (0.2)	678.2 (0.0)	677.8 (-0.3)	677.5 (-0.6)	678.1 ^{375,383,384}
	F	6a ₁	678.7 (0.6)	678.6 (0.5)	678.3 (0.2)	678.0 (-0.1)	678.1 ^{375,383,384}
	F	1π _g	679.3 (-1.6)	681.9 (1.0)	681.4 (0.6)	681.0 (0.1)	680.8 ^{385,386}
	F	1π _u	676.1 (-1.8)	678.7 (0.8)	678.3 (0.4)	677.8 (-0.1)	677.9 ^{385,386}
	F	3σ _g	673.7 (-1.9)	676.3 (0.7)	675.9 (0.3)	675.4 (-0.2)	675.6 ^{385,386}
PS _{min}	0.84	MAE	0.5	0.5	0.6	0.7	
PS _{ave}	0.91	RMSE	0.7	0.6	0.7	0.8	

Tab. 4.3.: Vertical C-N-O *K*-edge excitation energies ω_X computed with projected Δ UHF, Δ M P_n and EPT [P3+].

Molecule	Core	Orbital	Δ PUHF[P3+]	Δ PUMP2[P3+]	Δ PUMP2.5[P3+]	Δ PUMP3[P3+]	Exp.
CO	C	2pπ*	285.8 (-1.6)	287.2 (-0.2)	287.1 (-0.3)	287.1 (-0.3)	287.4 ³⁸⁷
	C	3sσ	291.6 (-0.8)	292.9 (0.6)	292.9 (0.5)	292.9 (0.5)	292.4 ³⁸⁷
	C	3pπ	292.6 (-0.7)	294.0 (0.7)	293.9 (0.6)	293.9 (0.6)	293.3 ³⁸⁷

	C	$4s\sigma$	292.7 (-2.1)	294.0 (-0.8)	294.0 (-0.8)	293.9 (-0.9)	294.8 ³⁸⁸
	C	$3d\sigma$	293.6 (-1.2)	295.0 (0.2)	295.0 (0.2)	294.9 (0.1)	294.8 ³⁸⁸
	C	$4p\pi$	293.9 (-0.9)	295.2 (0.5)	295.2 (0.4)	295.2 (0.4)	294.8 ³⁸⁷
	C	$5p\pi$	294.1 (-1.2)	295.5 (0.2)	295.5 (0.2)	295.4 (0.1)	295.3 ³⁸⁷
	C	$3d\pi$	293.9 (-0.7)	295.3 (0.7)	295.2 (0.6)	295.2 (0.6)	294.6 ³⁸⁷
	C	$6p\pi$	294.9 (-0.7)	296.3 (0.7)	296.3 (0.7)	296.2 (0.6)	295.6 ³⁸⁷
	O	$2p\pi^*$	532.7 (-1.5)	534.3 (0.1)	534.1 (-0.1)	533.9 (-0.3)	534.2 ³⁸⁹
	O	$3s\sigma$	537.6 (-1.4)	539.2 (0.3)	539.0 (0.1)	538.8 (-0.1)	538.9 ³⁹⁰
	O	$4s\sigma$	538.7 (-2.1)	540.3 (-0.5)	540.1 (-0.7)	539.9 (-0.9)	540.8 ³⁹⁰
	O	$3d\sigma$	539.6 (-1.4)	541.2 (0.2)	541.0 (0.0)	540.8 (-0.2)	541.0 ³⁹⁰
	O	$3p\pi$	538.7 (-1.2)	540.3 (0.4)	540.1 (0.2)	539.9 (0.0)	539.9 ³⁹⁰
	O	$4p\pi$	539.8 (-1.4)	541.5 (0.2)	541.3 (0.0)	541.1 (-0.2)	541.3 ³⁹⁰
	O	$5p\pi$	540.2 (-1.6)	541.8 (0.0)	541.6 (-0.2)	541.4 (-0.4)	541.8 ³⁹⁰
	O	$6p\pi$	540.9 (-1.1)	542.5 (0.5)	542.3 (0.3)	542.1 (0.1)	542.0 ³⁹⁰
	O	$3d\pi$	539.9 (-1.2)	541.5 (0.4)	541.3 (0.2)	541.1 (0.0)	541.0 ³⁹⁰
N ₂	N	$2p\pi_g$	399.7 (-1.3)	401.7 (0.7)	401.4 (0.4)	401.0 (0.0)	401.0 ³⁹¹
	N	$3s\sigma_g$	405.1 (-1.0)	407.2 (1.1)	406.8 (0.7)	406.5 (0.4)	406.1 ³⁹¹
	N	$3p\pi_u$	406.1 (-0.9)	408.2 (1.2)	407.9 (0.9)	407.5 (0.5)	407.0 ³⁹¹

	N	$3p\sigma_u$	406.2 (-1.1)	408.3 (1.0)	407.9 (0.6)	407.6 (0.3)	407.3 ³⁹¹
	N	$3d\sigma_g$	407.2 (-0.8)	409.3 (1.3)	408.9 (0.9)	408.6 (0.6)	408.0 ³⁹¹
	N	$3d\pi_g$	407.4 (-0.9)	409.5 (1.2)	409.1 (0.8)	408.8 (0.5)	408.3 ³⁹¹
NO ^a	N	$2p\pi^*$	398.1 (-1.6)	400.0 (0.3)	399.8 (0.1)	399.7 (0.0)	399.7 ²³⁵
	N	$3s\sigma$	405.5 (-1.1)	407.4 (0.8)	407.3 (0.7)	407.1 (0.5)	406.6 ³⁹²
	N	$3p\sigma$	406.6 (-1.2)	408.5 (0.8)	408.3 (0.6)	408.2 (0.4)	407.8 ³⁹²
	N	$3p\pi$	406.6 (-1.1)	408.5 (0.9)	408.4 (0.7)	408.2 (0.5)	407.7 ³⁹²
	N	$4s\sigma$	408.0 (-0.5)	410.0 (1.5)	409.8 (1.3)	409.6 (1.1)	408.5 ³⁹²
	N	$3d\pi$	407.8 (-0.9)	409.8 (1.0)	409.6 (0.9)	409.5 (0.7)	408.8 ³⁹²
	N	$4p\pi$	408.2 (-0.8)	410.1 (1.2)	410.0 (1.0)	409.8 (0.9)	408.9 ³⁹²
H ₂ O	O	$3sa_1$	532.9 (-1.1)	533.9 (-0.1)	533.9 (-0.1)	533.9 (-0.1)	534.0 ³⁹³
	O	$3pb_2$	535.1 (-0.8)	536.2 (0.3)	536.2 (0.3)	536.2 (0.3)	535.9 ³⁹³
	O	$3pa_1$	536.3 (-0.8)	537.4 (0.3)	537.4 (0.3)	537.4 (0.3)	537.1 ³⁹³
	O	$3pb_1$	536.2 (-0.9)	537.3 (0.2)	537.3 (0.2)	537.3 (0.2)	537.1 ³⁹³
CH ₄	C	$3sa_1$	285.8 (-1.2)	286.2 (-0.8)	286.3 (-0.8)	286.3 (-0.7)	287.0 ³⁹⁴
	C	$3pt_2$	287.7 (-0.7)	288.1 (-0.3)	288.2 (-0.2)	288.2 (-0.2)	288.4 ³⁹⁴
	C	$4pt_2$	288.6 (-1.1)	289.0 (-0.7)	289.1 (-0.6)	289.1 (-0.5)	289.7 ³⁹⁴
	C	$4sa_1$	288.7 (-0.4)	289.1 (0.0)	289.2 (0.1)	289.3 (0.1)	289.1 ³⁹⁴

	C	$5pt_2$	289.3 (-0.7)	289.7 (-0.3)	289.7 (-0.3)	289.8 (-0.2)	290.0 ³⁹⁴
	C	$6pt_2$	290.2 (-0.1)	290.6 (0.3)	290.7 (0.3)	290.8 (0.4)	290.4 ³⁹⁴
NH ₃	N	$3sa_1$	399.6 (-1.0)	400.3 (-0.3)	400.4 (-0.3)	400.4 (-0.2)	400.7 ³⁹⁴
	N	$3pe$	401.8 (-0.5)	402.6 (0.2)	402.6 (0.3)	402.7 (0.3)	402.3 ³⁹⁴
	N	$3pa_1$	402.4 (-0.4)	403.2 (0.3)	403.2 (0.4)	403.3 (0.4)	402.9 ³⁹⁴
	N	$4sa_1$	403.2 (-0.4)	403.9 (0.3)	403.9 (0.4)	404.0 (0.4)	403.6 ³⁹⁴
	N	$4pe$	403.2 (-0.9)	403.9 (-0.2)	404.0 (-0.2)	404.0 (-0.1)	404.2 ³⁹⁴
	N	$5pe$	403.7 (-0.9)	404.4 (-0.2)	404.5 (-0.1)	404.5 (-0.1)	404.6 ³⁹³
	N ₂ O	NN	$2p\pi^*$	399.8 (-1.2)	401.2 (0.2)	401.1 (0.1)	401.1 (0.1)
NN		$3s\sigma$	402.4 (-1.5)	403.8 (0.0)	403.7 (-0.1)	403.6 (-0.2)	403.8 ³⁹⁵
NO		$2p\pi$	402.4 (-2.2)	405.3 (0.7)	404.9 (0.3)	404.4 (-0.2)	404.6 ³⁹⁵
NN		$3p\pi$	404.9 (-0.9)	406.3 (0.6)	406.3 (0.5)	406.2 (0.4)	405.8 ³⁹⁵
NN		$4s\sigma$	405.2 (-1.1)	406.6 (0.4)	406.5 (0.3)	406.4 (0.2)	406.2 ³⁹⁵
NN		$3d\pi$	406.3 (-0.7)	407.7 (0.8)	407.6 (0.7)	407.5 (0.6)	406.9 ³⁹⁵
NN		$4p\pi$	406.1 (-1.0)	407.5 (0.4)	407.4 (0.3)	407.3 (0.2)	407.1 ³⁹⁵
NN		$3d\sigma$	405.3 (-1.9)	406.7 (-0.5)	406.6 (-0.6)	406.5 (-0.7)	407.2 ³⁹⁵
NO		$3s\sigma$	406.5 (-0.9)	409.5 (2.0)	409.0 (1.5)	408.6 (1.1)	407.5 ³⁹⁵
O		$2p\pi^*$	533.6 (-1.0)	536.1 (1.5)	535.8 (1.2)	535.4 (0.8)	534.6 ³⁹⁵

H ₂ O ₂	O	3sσ	534.7 (-1.9)	537.2 (0.6)	536.8 (0.2)	536.5 (-0.1)	536.6 ³⁹⁵
	O	3pπ	537.5 (-1.3)	540.0 (1.2)	539.7 (0.9)	539.3 (0.5)	538.8 ³⁹⁵
	O	4sσ	537.7 (-1.4)	540.2 (1.1)	539.8 (0.7)	539.5 (0.4)	539.1 ^{395,396}
	O	σ*	531.5 (-1.5)	533.0 (0.0)	532.8 (-0.2)	532.6 (-0.4)	533.0 ³⁹⁷
	O	σ*	534.8 (-0.5)	536.3 (1.0)	536.1 (0.8)	535.9 (0.6)	535.3 ³⁹⁷
	O	σ*	536.1 (0.8)	537.6 (2.3)	537.3 (2.0)	537.1 (1.8)	535.3 ³⁹⁷
	O	3s	537.2 (0.4)	538.7 (1.9)	538.4 (1.6)	538.2 (1.4)	536.8 ³⁹⁷
C ₂ H ₄	O	3p	537.2 (-1.1)	538.7 (0.4)	538.4 (0.1)	538.2 (-0.1)	538.3 ³⁹⁷
	C	π*	283.9 (-0.7)	284.6 (0.0)	284.3 (-0.4)	284.0 (-0.7)	284.7 ³⁸⁷
	C	3s	286.6 (-0.7)	287.3 (0.1)	287.0 (-0.3)	286.6 (-0.6)	287.2 ³⁸⁷
	C	3p	287.4 (-0.5)	288.1 (0.2)	287.8 (-0.1)	287.4 (-0.4)	287.9 ³⁸⁷
	C	4p	288.8 (-0.6)	289.5 (0.1)	289.1 (-0.3)	288.8 (-0.6)	289.4 ³⁸⁷
	C	5p	288.9 (-1.0)	289.6 (-0.3)	289.3 (-0.6)	289.0 (-1.0)	289.9 ³⁸⁷
PS _{min}	0.89	MAE	1.0	0.6	0.5	0.4	
PS _{ave}	0.98	RMSE	1.1	0.8	0.6	0.5	

^a ²Δ – ³Π channel.

Vertical emission energies at the C, N, O, and Ne K -edge are reported in Table 4.1. The average pole strength for this set PS_{ave} is 0.90 which suggests that the canonical MOs are a good approximation for the Dyson orbitals. The lowest or minimum value PS_{min} for this set is 0.84 and is reflected in low PS values corresponding to inner-valence electron detachments in N_2O and C_2H_4 . It is not unexpected that ionizations from inner-valence orbitals involve many-body effects of quantitative importance even though a single MO can be designated in the qualitative picture of electron detachment. Spin-projection of the UHF states ensures that the total energies used to determine IP_{core} correspond to eigenstates of S^2 . The errors for ΔPUHF with P3+ imply that additional electron correlation effects can be important in the initial state, core-hole ion, final state, or all of the these. ΔPUMP_n ($n = 2, 2.5, 3$) should provide similar estimates for IP_{core} for localized core orbitals. This is evident in the consistent measure of errors for each method. We briefly note that NO has an open-shell ground state with two core-ionization channels: $^3\Pi$ and $^1\Pi$. A removal of a down-spin β electron in the N_{1s} orbital yields a triplet final-state configuration $^3\Pi$ whereas a removal of an up-spin α electron results in the singlet $^1\Pi$. Valence-to-core decay in either scenario leads to even more electronic states and complex spectral features.

\mathcal{E}_X results for the set of fluoromethanes are given in Table 4.2. Similar assessments for results featured in Table 4.1 can be made for the performance of each composite method here. PS_{min} is 0.84 as well and corresponds to the $2t_2$ detachment in CF_4 .

Vertical core-excitation energies at the C, N, O K -edge are displayed in Table 4.3. Beyond transitions into the lowest unoccupied π^* or σ^* lie a series of Rydberg states of increasing principal and azimuthal quantum numbers. A higher-lying orbital is diffuse and to attach an electron requires a sufficient basis set describing its large radial extent. High-energy Rydberg states are largely independent from the occupied electronic structure and appear quasi-hydrogenic. A PS_{ave} that is effectively equal to 1 again suggests that the Dyson orbital is sufficiently described by the canonical MO and the computed value for EA_{core}^f should also be reasonable. In relation to this, the excited-state Rydberg series can also be directly characterized with molecular quantum defect analysis and EPT.^{399,400} The results for C, N, O K -edge excitations are comparable to those of emission in that the errors for ΔPUMP_n are less than 1 eV. ΔPUHF still confers a mean-absolute-error (MAE) and root-mean-square-error (RMSE) that are ~ 1 eV. The computational results for vertical core-to-valence and valence-to-core transitions indicate that both self-energy corrections and Δ -driven recovery of core-hole ORX are jointly modeling the correct physics.

Fig. 4.3.: Simulated emission spectra for N_2 . IP_{core} computed with $\Delta PUMP3$. EPT results and relative intensities obtained with a HF/cc-pVTZ reference. Experimental spectrum reprinted from Robert E. LaVilla, *J. Chem. Phys.* **56**, 2345–2349 (1972), Ref. [398], with the permission of AIP Publishing.

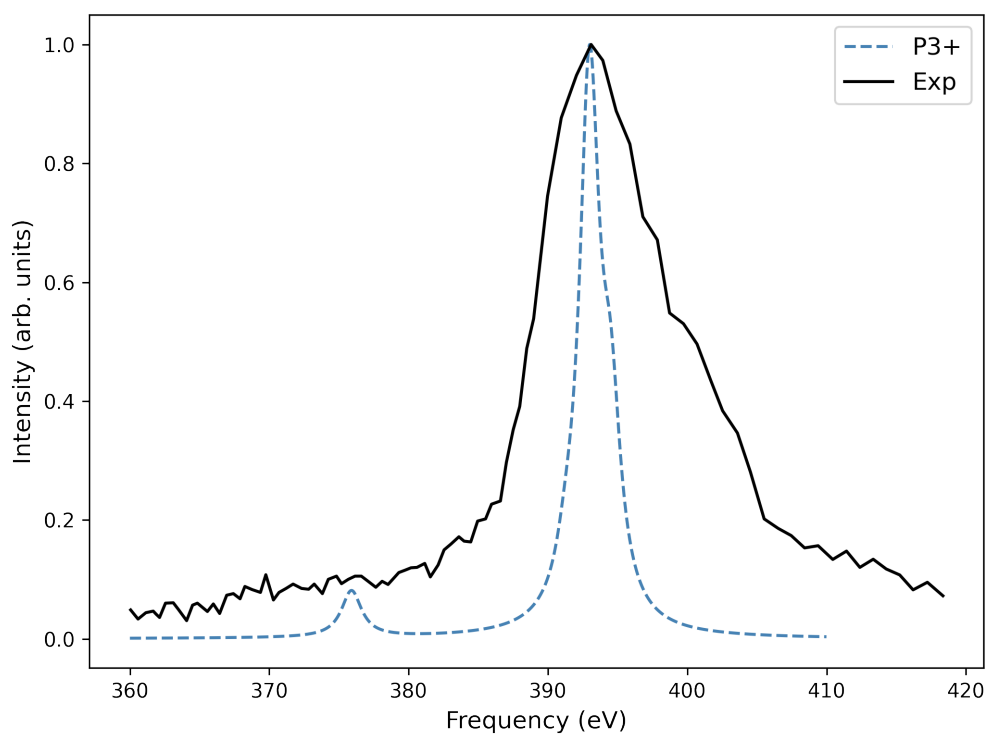


Fig. 4.4.: Simulated emission spectra for C_2H_4 . IP_{core} computed with $\Delta PUMP3$. EPT results obtained with a HF/cc-pVTZ reference. Relative intensities are obtained with an extended Hückel reference. Experimental spectrum reprinted from Rolf Manne, *J. Chem. Phys.* **52**, 5733–5739 (1970), Ref. [366], with the permission of AIP Publishing.

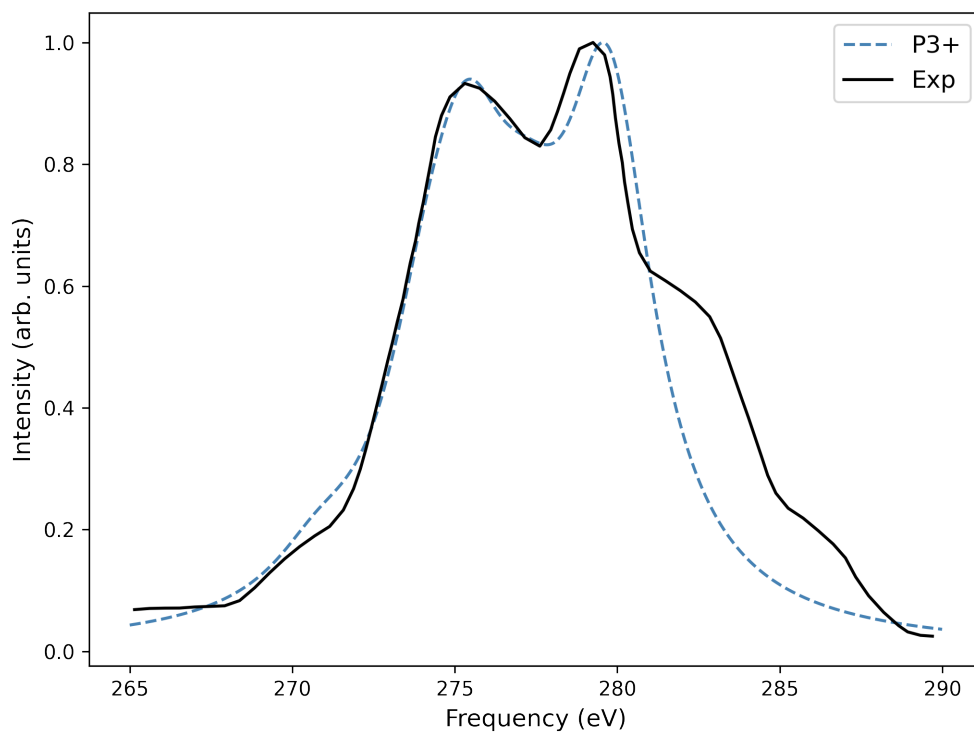
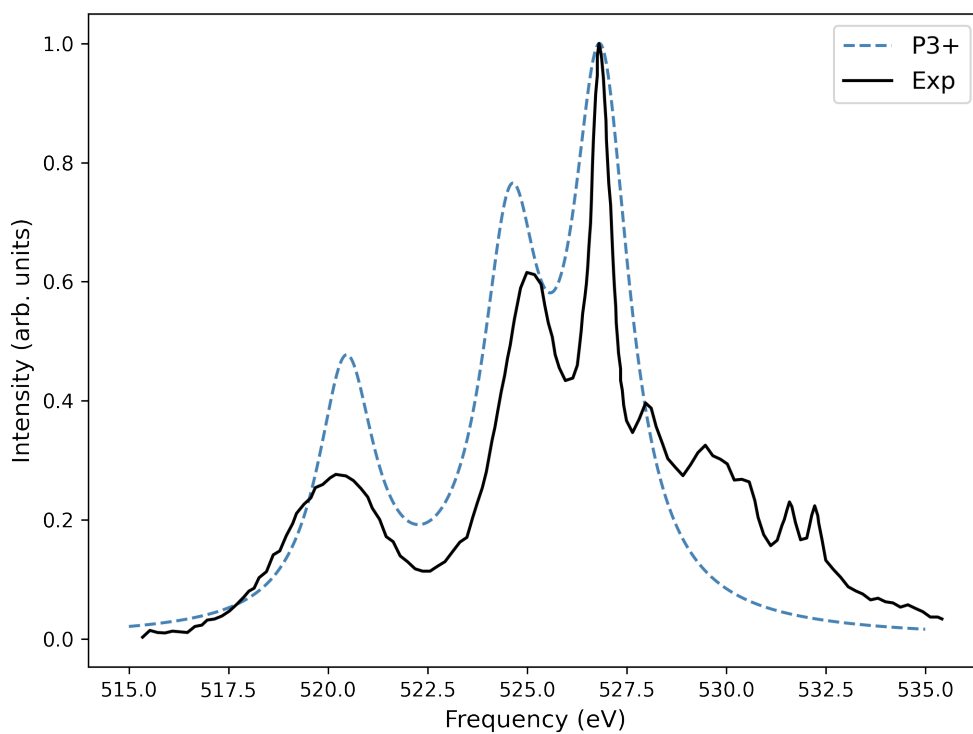


Fig. 4.5.: Simulated emission spectra for H_2O . IP_{core} computed with ΔPUMP3 . EPT results and relative intensities obtained with a HF/cc-pVTZ reference. An alignment shift of -0.9 eV is applied to the simulated spectra. Experimental spectrum reprinted from Jan-Erik Rubensson, Lennart Petersson, Nial Wassdahl, Mats Bäckström, Joseph Nordgren, Olav M. Kvalheim, and Rolf Manne, *J. Chem. Phys.* **82**, 4486–4491 (1985), Ref. [373], with the permission of AIP Publishing.



There are a few important caveats to the types of excited states accessible with single-reference methods. We again turn to the NO example. The $1s \rightarrow 2p\pi^*$ excitation leads to multiple electronic states: $^4\Sigma^-$, $^2\Sigma^-$, $^2\Delta$, and $^2\Sigma^+$. The high-spin quartet $^4\Sigma^-$ and a $^2\Delta$ state in the core open-shell, valence-paired configuration can be approximated by a single Slater determinant. However, the $^2\Sigma^-$ and $^2\Sigma^+$ doublet states with three unpaired spins in $1s$ and $2p\pi^*$ orbitals must be spin-adapted. States that require the recoupling of spin angular momenta and recovery of opposite-spin correlation effects are not directly accessible with single determinant SCF. Determination of excited electronic spin states will require information contained in multi-configurational wavefunctions.

Additionally, this study only examines vertical transitions from ground state geometries. Molecular X-ray spectra may exhibit fine vibrational structure for core-excitations or Jahn-Teller splitting following core-ionization.^{114,401} Furthermore, the two-state Δ -based methods employed here are quantitatively valid only for transitions involving one electron or one particle-hole pair. These approaches are not immediately applicable for describing two-electron processes inherent in resonant inelastic x-ray scattering (RIXS) and Auger spectra. For coherent processes in molecules with equivalent atoms, the convenient option of core-hole localization is no longer viable since decay into specific delocalized core orbitals is necessary to guarantee proper final-state symmetries and spectral patterns.⁴⁰² Koopmans-like interpretations fail to describe shake-processes and satellite structure in the instance of strong configuration interaction (CI) and large ORX. Diagonal quasiparticle methods with uncorrelated HF orbitals fall short in this category, and thus, non-diagonal self-energy approximations are typically applied.^{403–405} To capture the important many-body effects, response theories can be tailored to model X-ray transitions involving two electrons.^{340,341,345,406–410}

The inadequacies of single-reference methods are also pronounced in molecules with multi-reference open-shell character. For example, multi-configurational Δ SCF IP_{core} estimates⁹⁰ of the $^4\Sigma^-$ and $^2\Sigma^-$ states of O_2^+ with orbital optimization, Slater-type basis sets, and core-localization still deviate ~ 1 -2 eV from experiment.²³⁵ Improved accuracy is not expected from projected energies beginning with one HF determinant, especially considering the non-variational nature of the chosen PAV method. Thus, the limits of mean-field methods become apparent when electron correlation is strong. Very accurate vertical IPs for open-shell or strongly correlated molecules, such as O_2 , can be realized with spin-adapted multi-configurational propagator methods^{221,411} and alternative choices of the reference wavefunction.⁴¹²

Some demonstrative examples for simulating non-resonant XES are shown in Figures 4.3-4.5. Peak positions and relative intensities for main-line transitions are adequately reproduced with P3+ and population analysis of the ground state MOs. In the theoretical spectra for N₂, the low PS (0.608) for the 2σ_g orbital leads to a shift in the low intensity peak towards the main peak by about 3 eV. This result is not atypical for inner-valence IPs where considerable relaxation effects are present and better accounted for in higher-order self-energy approximations. For all other transitions depicted in the calculated XES spectra of N₂, C₂H₄, and H₂O, the canonical Hartree-Fock orbitals are sufficient representations of the Dyson orbitals (PS > 0.85) with the selected diagonal method. Characterization of satellite structure necessitates a more detailed analysis with non-diagonal self-energy approximations or CI methods.^{404,413}

Oscillator strengths for X-ray absorption, particularly for Rydberg transitions, can be evaluated through quantum defect analysis with EPT or ΔSCF for reconstructing spectra.⁴¹⁴⁻⁴¹⁶ Alternatively, intensities for *N*-conserving excitations may be calculated directly with projected dipole moments between the orbital-optimized ground state and core-excited state wavefunctions. The scope of these methodologies warrant a separate study.

The overall results presented here highlight the accuracy of Δ-based models using HF, MP, and EPT for computing *K*-shell excitation and non-resonant emission energies of molecules containing second-row p-block elements. The single-reference models used here are deemed appropriate within the one-electron portrait of X-ray transitions. Composite methods, like those featured in this work, are advantageous since they are modular and allow for specific observable quantities to be approximated independently at the desired levels of theory. Extensions of composite models to treat two-electron processes and simulate satellite structure can be made possible with two-electron Green's functions and non-diagonal self-energy approximations. Finally, the inclusion of accurate relativistic effects is of greater importance to the overall spectral profile and shift in IP_{core} with increasing *Z*. For describing inner-shell transitions in heavier elements, the use of relativistic Hamiltonians is preferred over atom-specific *ad hoc* corrections based on two-electron ions or semi-empirical fits used here.^{85,205,417-419}

4.4 Conclusion

We have examined Δ -based composite models for computing K -edge emission and excitation energies. The models' construction and performance are comparable to modern STEX methods and a practical approach for estimating core-level energetics for one-electron processes is established. The models employed here appear to be competitive with ADC, EOM-CCSD, and TD-DFT for one-particle transitions. Notwithstanding the additive propagation of errors and reliance on cancellation of such errors in Δ -based approaches, the combination of projected SCF, MP, and propagator theories afford accurate results with reasonable computational cost.

Bibliography

- [1]E. Schrödinger. “Quantisierung als Eigenwertproblem”. In: *Annalen der Physik* 384.4 (1926), pp. 361–376 (cit. on p. 1).
- [2]M. Born and R. Oppenheimer. “Zur Quantentheorie der Molekeln”. In: *Annalen der Physik* 389.20 (1927), pp. 457–484 (cit. on p. 4).
- [3]Max Born. “Quantenmechanik der Stoßvorgänge”. In: *Zeitschrift für Physik* 38.11-12 (1926), pp. 803–827 (cit. on p. 4).
- [4]D. R. Hartree. “The Wave Mechanics of an Atom with a Non-Coulomb Central Field. Part II. Some Results and Discussion”. In: *Mathematical Proceedings of the Cambridge Philosophical Society* 24.1 (1928), pp. 111–132 (cit. on p. 5).
- [5]J. C. Slater. “Note on Hartree’s Method”. In: *Phys. Rev.* 35 (2 1930), pp. 210–211 (cit. on p. 5).
- [6]V. Fock. “Näherungsmethode zur Lösung des quantenmechanischen Mehrkörperproblems”. In: *Zeitschrift für Physik* 61.1 (1930), pp. 126–148 (cit. on p. 5).
- [7]C. D. Sherrill. URL: <http://vergil.chemistry.gatech.edu/notes/> (cit. on p. 5).
- [8]Attila Szabo and Neil S Ostlund. *Modern Quantum Chemistry: Introduction to Advanced Electronic Structure Theory*. Dover Books on Chemistry. Mineola, NY: Dover Publications, 1996 (cit. on pp. 5, 26, 42).
- [9]J. C. Slater. “The Theory of Complex Spectra”. In: *Phys. Rev.* 34 (10 1929), pp. 1293–1322 (cit. on p. 5).
- [10]J. C. Slater. “Atomic Shielding Constants”. In: *Phys. Rev.* 36 (1 1930), pp. 57–64 (cit. on p. 6).
- [11]Tosio Kato. “On the eigenfunctions of many-particle systems in quantum mechanics”. In: *Communications on Pure and Applied Mathematics* 10.2 (1957), pp. 151–177 (cit. on p. 6).
- [12]S. F. Boys and Alfred Charles Egerton. “Electronic wave functions - I. A general method of calculation for the stationary states of any molecular system”. In: *Proceedings of the Royal Society of London. Series A. Mathematical and Physical Sciences* 200.1063 (1950), pp. 542–554 (cit. on p. 6).
- [13]C. C. J. Roothaan. “New Developments in Molecular Orbital Theory”. In: *Rev. Mod. Phys.* 23 (2 1951), pp. 69–89 (cit. on p. 7).
- [14]Charlotte Froese Fischer. “A multi-configuration Hartree-Fock program”. In: *Computer Physics Communications* 1.3 (1970), pp. 151–166 (cit. on p. 7).

- [15]Hideo Fukutome. “Unrestricted Hartree–Fock theory and its applications to molecules and chemical reactions”. In: *International Journal of Quantum Chemistry* 20.5 (1981), pp. 955–1065 (cit. on p. 12).
- [16]J. L. Stuber and J. Paldus. “Symmetry Breaking in the Independent Particle Model”. In: *Fundamental World of Quantum Chemistry*. Springer Netherlands, 2003, pp. 67–139 (cit. on p. 12).
- [17]C. C. J. Roothaan. “Self-Consistent Field Theory for Open Shells of Electronic Systems”. In: *Rev. Mod. Phys.* 32 (2 1960), pp. 179–185 (cit. on p. 12).
- [18]Takashi Tsuchimochi and Gustavo E. Scuseria. “Communication: ROHF theory made simple”. In: *The Journal of Chemical Physics* 133.14 (2010), p. 141102 (cit. on p. 12).
- [19]Kurt R. Glaesemann and Michael W. Schmidt. “On the Ordering of Orbital Energies in High-Spin ROHF”. In: *The Journal of Physical Chemistry A* 114.33 (2010), pp. 8772–8777 (cit. on p. 12).
- [20]B. N. Plakhutin, E. V. Gorelik, and N. N. Breslavskaya. “Koopmans’ theorem in the ROHF method: Canonical form for the Hartree-Fock Hamiltonian”. In: *The Journal of Chemical Physics* 125.20 (2006), p. 204110 (cit. on p. 12).
- [21]Boris N. Plakhutin and Ernest R. Davidson. “Koopmans’ Theorem in the Restricted Open-Shell Hartree-Fock Method. 1. A Variational Approach”. In: *The Journal of Physical Chemistry A* 113.45 (2009), pp. 12386–12395 (cit. on p. 12).
- [22]Boris N. Plakhutin and Ernest R. Davidson. “Canonical form of the Hartree-Fock orbitals in open-shell systems”. In: *The Journal of Chemical Physics* 140.1 (2014), p. 014102 (cit. on p. 12).
- [23]G. Berthier. “Configurations électroniques incomplètes - Partie I. La Méthode du Champ Moléculaire Self-Consistent et l’Etude des Etats à Couches Incomplètes”. In: *Journal de Chimie Physique* 51 (1954), pp. 363–371 (cit. on p. 12).
- [24]J. A. Pople and R. K. Nesbet. “Self-Consistent Orbitals for Radicals”. In: *The Journal of Chemical Physics* 22.3 (1954), pp. 571–572 (cit. on p. 12).
- [25]C. A. Coulson and I. Fischer. “XXXIV. Notes on the molecular orbital treatment of the hydrogen molecule”. In: *The London, Edinburgh, and Dublin Philosophical Magazine and Journal of Science* 40.303 (1949), pp. 386–393 (cit. on p. 12).
- [26]J. Čížek and J. Paldus. “Stability Conditions for the Solutions of the Hartree–Fock Equations for Atomic and Molecular Systems. Application to the Pi-Electron Model of Cyclic Polyenes”. In: *The Journal of Chemical Physics* 47.10 (1967), pp. 3976–3985 (cit. on p. 13).
- [27]Per-Olov Löwdin and István Mayer. “Some Studies of the General Hartree-Fock Method”. In: ed. by Per-Olov Löwdin. Vol. 24. *Advances in Quantum Chemistry*. Academic Press, 1992, pp. 79–114 (cit. on p. 13).
- [28]Sharon Hammes-Schiffer and Hans C. Andersen. “The advantages of the general Hartree–Fock method for future computer simulation of materials”. In: *The Journal of Chemical Physics* 99.3 (1993), pp. 1901–1913 (cit. on p. 13).

- [29]P. Lykos and G. W. Pratt. “Discussion on The Hartree-Fock Approximation”. In: *Rev. Mod. Phys.* 35 (3 1963), pp. 496–501 (cit. on p. 13).
- [30]Per-Olov Löwdin. “Quantum Theory of Many-Particle Systems. III. Extension of the Hartree-Fock Scheme to Include Degenerate Systems and Correlation Effects”. In: *Phys. Rev.* 97 (6 1955), pp. 1509–1520 (cit. on pp. 13, 43, 45, 46, 77, 140).
- [31]István Mayer. “The Spin-Projected Extended Hartree-Fock Method”. In: ed. by Per-Olov Löwdin. Vol. 12. *Advances in Quantum Chemistry*. Academic Press, 1980, pp. 189–262 (cit. on pp. 13, 45).
- [32]Carlos F. Bunge. “Unrestricted Projected Hartree-Fock Solutions for Two-Electron Systems”. In: *Phys. Rev.* 154 (1 1967), pp. 70–79 (cit. on pp. 13, 45).
- [33]Newton M. Gray and Lawrence A. Wills. “Note on the Calculation of Zero Order Eigenfunctions”. In: *Phys. Rev.* 38 (2 1931), pp. 248–254 (cit. on pp. 13, 43).
- [34]George W. Pratt. “Eigenfunctions of S^2 by a Spin Operator Method”. In: *Phys. Rev.* 92 (2 1953), pp. 278–288 (cit. on pp. 13, 43).
- [35]A. Rotenberg. “Calculation of Exact Eigenfunctions of Spin and Orbital Angular Momentum Using the Projection Operator Method”. In: *The Journal of Chemical Physics* 39.3 (1963), pp. 512–517 (cit. on pp. 13, 43).
- [36]William A. Goddard. “Improved Quantum Theory of Many-Electron Systems. I. Construction of Eigenfunctions of \hat{S}^2 Which Satisfy Pauli’s Principle”. In: *Phys. Rev.* 157 (1 1967), pp. 73–80 (cit. on pp. 13, 43).
- [37]Jr. Smith V. H. “Construction of Exact Spin Eigenfunctions”. In: *The Journal of Chemical Physics* 41.1 (1964), pp. 277–278 (cit. on pp. 13, 144).
- [38]F Berencz and R Pauncz. “Construction of S^2 Eigenfunctions by the Method of Spin Operators I: General Theory”. In: *Proceedings of the Physical Society* 71.2 (1958), p. 145 (cit. on p. 13).
- [39]Fukashi Sasaki and Kimio Ohno. “Spin-Component Analysis of Single-Determinant Wavefunctions”. In: *Journal of Mathematical Physics* 4.9 (1963), pp. 1140–1147 (cit. on p. 13).
- [40]Per-Olov Löwdin. “Quantum Theory of Many-Particle Systems. I. Physical Interpretations by Means of Density Matrices, Natural Spin-Orbitals, and Convergence Problems in the Method of Configurational Interaction”. In: *Phys. Rev.* 97 (6 1955), pp. 1474–1489 (cit. on pp. 14, 44, 140, 145).
- [41]Per-Olov Löwdin. “Correlation Problem in Many-Electron Quantum Mechanics I. Review of Different Approaches and Discussion of Some Current Ideas”. In: *Advances in Chemical Physics*. John Wiley & Sons, Ltd, 1958. Chap. 7, pp. 207–322 (cit. on pp. 14, 15).
- [42]ISALAH SHAVITT. “The history and evolution of configuration interaction”. In: *Molecular Physics* 94.1 (1998), pp. 3–17 (cit. on p. 14).

- [43]C. David Sherrill and Henry F. Schaefer. “The Configuration Interaction Method: Advances in Highly Correlated Approaches”. In: ed. by Per-Olov Löwdin, John R. Sabin, Michael C. Zerner, and Erkki Brändas. Vol. 34. *Advances in Quantum Chemistry*. Academic Press, 1999, pp. 143–269 (cit. on p. 14).
- [44]Carlos F. Bunge. “Chapter One - Present Status of Selected Configuration Interaction With Truncation Energy Error”. In: *Novel Electronic Structure Theory: General Innovations and Strongly Correlated Systems*. Ed. by Philip E. Hoggan. Vol. 76. *Advances in Quantum Chemistry*. Academic Press, 2018, pp. 3–34 (cit. on pp. 14, 15).
- [45]R. K. Nesbet. “Brueckner’s Theory and the Method of Superposition of Configurations”. In: *Phys. Rev.* 109 (5 1958), pp. 1632–1638 (cit. on p. 14).
- [46]Carlos F. Bunge. “Electronic Wave Functions for Atoms. I. Ground State of Be”. In: *Phys. Rev.* 168 (1 1968), pp. 92–103 (cit. on p. 15).
- [47]Norm M. Tubman, Joonho Lee, Tyler Y. Takeshita, Martin Head-Gordon, and K. Birgitta Whaley. “A deterministic alternative to the full configuration interaction quantum Monte Carlo method”. In: *The Journal of Chemical Physics* 145.4 (2016), p. 044112 (cit. on p. 15).
- [48]Paul M. Zimmerman. “Incremental full configuration interaction”. In: *The Journal of Chemical Physics* 146.10 (2017), p. 104102 (cit. on p. 15).
- [49]Vibin Abraham and Nicholas J. Mayhall. “Selected Configuration Interaction in a Basis of Cluster State Tensor Products”. In: *Journal of Chemical Theory and Computation* 16.10 (2020), pp. 6098–6113 (cit. on p. 15).
- [50]Annik Bunge. “Electronic Wavefunctions for Atoms. III. Partition of Degenerate Spaces and Ground State of C”. In: *The Journal of Chemical Physics* 53.1 (1970), pp. 20–28 (cit. on p. 15).
- [51]Carlos F. Bunge. “Selected configuration interaction with truncation energy error and application to the Ne atom”. In: *The Journal of Chemical Physics* 125.1 (2006), p. 014107 (cit. on p. 15).
- [52]P. S. Bagus, N. Bessis, and C. M. Moser. “Multiconfiguration Hartree-Fock Calculations. II. Calculation of the Lowest 3P , 1D , and 1S States of the Carbon Atom”. In: *Phys. Rev.* 179 (1 1969), pp. 39–43 (cit. on p. 15).
- [53]Charles F. Bender and Ernest R. Davidson. “Studies in Configuration Interaction: The First-Row Diatomic Hydrides”. In: *Phys. Rev.* 183 (1 1969), pp. 23–30 (cit. on p. 15).
- [54]B. Huron, J. P. Malrieu, and P. Rancurel. “Iterative perturbation calculations of ground and excited state energies from multiconfigurational zeroth-order wavefunctions”. In: *The Journal of Chemical Physics* 58.12 (1973), pp. 5745–5759 (cit. on p. 15).
- [55]Robert J. Harrison. “Approximating full configuration interaction with selected configuration interaction and perturbation theory”. In: *The Journal of Chemical Physics* 94.7 (1991), pp. 5021–5031 (cit. on p. 15).
- [56]Jean-Pierre Daudey, Jean-Louis Heully, and Jean-Paul Malrieu. “Size-consistent self-consistent truncated or selected configuration interaction”. In: *The Journal of Chemical Physics* 99.2 (1993), pp. 1240–1254 (cit. on p. 15).

- [57]Adam A. Holmes, Norm M. Tubman, and C. J. Umrigar. “Heat-Bath Configuration Interaction: An Efficient Selected Configuration Interaction Algorithm Inspired by Heat-Bath Sampling”. In: *Journal of Chemical Theory and Computation* 12.8 (2016), pp. 3674–3680 (cit. on p. 15).
- [58]Chr. Møller and M. S. Plesset. “Note on an Approximation Treatment for Many-Electron Systems”. In: *Phys. Rev.* 46 (7 1934), pp. 618–622 (cit. on pp. 16, 45).
- [59]Dieter Cremer. “Møller-Plesset perturbation theory: from small molecule methods to methods for thousands of atoms”. In: *Wiley Interdiscip. Rev. Comput. Mol. Sci.* 1.4 (2011), pp. 509–530 (cit. on pp. 16, 46).
- [60]B.T. Pickup and O. Goscinski. “Direct calculation of ionization energies”. In: *Mol. Phys.* 26.4 (1973), pp. 1013–1035 (cit. on pp. 20, 26, 30, 31, 41, 42, 76).
- [61]Y. Öhrn and G. Born. “Molecular Electron Propagator Theory and Calculations”. In: ed. by Per-Olov Löwdin. Vol. 13. *Advances in Quantum Chemistry*. Academic Press, 1981, pp. 1–88 (cit. on p. 20).
- [62]Ricardo Longo, Benoît Champagne, and Yngve Öhrn. “Electron propagator theory and application”. In: *Theor. Chim. Acta* 90.5 (1995), pp. 397–419 (cit. on p. 20).
- [63]J. V. Ortiz. “The Electron Propagator Picture of Molecular Electronic Structure”. In: vol. Volume 2. *Computational Chemistry: Reviews of Current Trends*. World Scientific, 1997, pp. 1–61 (cit. on p. 20).
- [64]J. V. Ortiz. “Quasiparticle approximations and electron propagator theory”. In: *Int. J. Quantum Chem.* 95.4-5 (2003), pp. 593–599 (cit. on p. 20).
- [65]Yngve Öhrn and J.V. Ortiz. “The electron propagator”. In: *Mol. Phys.* 108.21-23 (2010), pp. 2871–2875 (cit. on p. 20).
- [66]Joseph Vincent Ortiz. “Electron propagator theory: an approach to prediction and interpretation in quantum chemistry”. In: *Wiley Interdiscip. Rev. Comput. Mol. Sci.* 3.2 (2013), pp. 123–142 (cit. on pp. 20, 77).
- [67]Héctor H. Corzo and J. Vince Ortiz. “Chapter Thirteen - Electron Propagator Theory: Foundations and Predictions”. In: *Advances in Quantum Chemistry*. Vol. 74. Löwdin Volume. Academic Press, 2017, pp. 267–298 (cit. on pp. 20, 76).
- [68]Per-Olov Löwdin. “Studies in Perturbation Theory. IV. Solution of Eigenvalue Problem by Projection Operator Formalism”. In: *J. Math. Phys* 3.5 (1962), pp. 969–982 (cit. on pp. 21, 47).
- [69]Manuel Díaz-Tinoco, Héctor H. Corzo, Filip Pawłowski, and J. V. Ortiz. “Do Dyson Orbitals resemble canonical Hartree–Fock orbitals?” In: *Molecular Physics* 117.17 (2018), pp. 2275–2283 (cit. on p. 23).
- [70]A.P. Hitchcock. “Electron-energy-loss-based spectroscopies: A molecular viewpoint”. In: *Ultramicroscopy* 28.1 (1989), pp. 165–183 (cit. on p. 26).
- [71]Adam P Hitchcock. “Core Excitation and Ionization of Molecules”. In: *Phys. Scr.* 1990.T31 (1990), p. 159 (cit. on p. 26).

- [72]Peter M. Kraus, Michael Zürich, Scott K. Cushing, Daniel M. Neumark, and Stephen R. Leone. “The ultrafast X-ray spectroscopic revolution in chemical dynamics”. In: *Nat. Rev. Chem.* 2.6 (2018), pp. 82–94 (cit. on pp. 26, 75).
- [73]L. X. Chen, X. Zhang, and M. L. Shelby. “Recent advances on ultrafast X-ray spectroscopy in the chemical sciences”. In: *Chem. Sci.* 5.11 (2014), pp. 4136–4152 (cit. on pp. 26, 29, 75).
- [74]Christian Bressler and Majed Chergui. “Ultrafast X-ray Absorption Spectroscopy”. In: *Chem. Rev.* 104.4 (2004), pp. 1781–1812 (cit. on pp. 26, 75).
- [75]Christian Bressler and Majed Chergui. “Molecular Structural Dynamics Probed by Ultrafast X-Ray Absorption Spectroscopy”. In: *Annu. Rev. Phys. Chem.* 61.1 (2010), pp. 263–282 (cit. on pp. 26, 75).
- [76]Frank de Groot. “High-Resolution X-ray Emission and X-ray Absorption Spectroscopy”. In: *Chem. Rev.* 101.6 (2001), pp. 1779–1808 (cit. on p. 26).
- [77]Adam P. Hitchcock. “Near Edge Electron Energy Loss Spectroscopy: Comparison to X-ray Absorption”. In: *Jpn. J. Appl. Phys.* 32.S2 (1993), p. 176 (cit. on p. 26).
- [78]Patrick Norman and Andreas Dreuw. “Simulating X-ray Spectroscopies and Calculating Core-Excited States of Molecules”. In: *Chem. Rev.* 118.15 (2018), pp. 7208–7248 (cit. on pp. 26, 29).
- [79]Kiran Mathew, Chen Zheng, Donald Winston, et al. “High-throughput computational X-ray absorption spectroscopy”. In: *Sci. Data* 5.1 (2018) (cit. on p. 26).
- [80]Jeroen A Van Bokhoven and Carlo Lamberti. *X-ray absorption and X-ray emission spectroscopy: Theory and applications*. Vol. 1. John Wiley & Sons, 2016 (cit. on p. 26).
- [81]Thomas Fransson, Yoshihisa Harada, Nobuhiro Kosugi, et al. “X-ray and Electron Spectroscopy of Water”. In: *Chem. Rev.* 116.13 (2016), pp. 7551–7569 (cit. on p. 26).
- [82]Paul S. Bagus, Eugene S. Ilton, and Connie J. Nelin. “The interpretation of XPS spectra: Insights into materials properties”. In: *Surf. Sci. Rep.* 68.2 (2013), pp. 273–304 (cit. on p. 26).
- [83]Paul S Bagus, Francesc Illas, Gianfranco Pacchioni, and Fulvio Parmigiani. “Mechanisms responsible for chemical shifts of core-level binding energies and their relationship to chemical bonding”. In: *J. Electron Spectrosc. Relat. Phenom.* 100.1 (1999), pp. 215–236 (cit. on p. 26).
- [84]F.M.F. de Groot. “X-ray absorption of transition metal oxides: An overview of the theoretical approaches”. In: *J. Electron Spectrosc. Relat. Phenom.* 62.1 (1993), pp. 111–130 (cit. on p. 26).
- [85]Joseph M. Kasper, Torin F. Stetina, Andrew J. Jenkins, and Xiaosong Li. “Ab initio methods for L-edge x-ray absorption spectroscopy”. In: *Chem. Phys. Rev.* 1.1 (2020), p. 011304 (cit. on pp. 26, 97).
- [86]Nicholas A. Besley. “Modeling of the spectroscopy of core electrons with density functional theory”. In: *Wiley Interdiscip. Rev. Comput. Mol. Sci.* 11.6 (2021), e1527 (cit. on p. 26).

- [87]C. C. J. Roothaan. “New Developments in Molecular Orbital Theory”. In: *Rev. Mod. Phys.* 23 (2 1951), pp. 69–89 (cit. on p. 26).
- [88]P. S. Bagus. “Self-Consistent-Field Wave Functions for Hole States of Some Ne-Like and Ar-Like Ions”. In: *Phys. Rev.* 139 (3A 1965), A619–A634 (cit. on pp. 26, 30, 76).
- [89]Paul S. Bagus and III Schaefer Henry F. “Direct Near-Hartree–Fock Calculations on the 1s Hole States of NO⁺”. In: *J. Chem. Phys.* 55.3 (1971), pp. 1474–1475 (cit. on pp. 26, 76).
- [90]Paul S. Bagus and III Schaefer Henry F. “Localized and Delocalized 1s Hole States of the O₂⁺ Molecular Ion”. In: *J. Chem. Phys.* 56.1 (1972), pp. 224–226 (cit. on pp. 26, 35, 96).
- [91]R. Manne and T. Åberg. “Koopmans’ theorem for inner-shell ionization”. In: *Chem. Phys. Lett.* 7.2 (1970), pp. 282–284 (cit. on pp. 26, 30).
- [92]J. C. Slater and K. H. Johnson. “Self-Consistent-Field $X\alpha$ Cluster Method for Polyatomic Molecules and Solids”. In: *Phys. Rev. B* 5 (3 1972), pp. 844–853 (cit. on p. 26).
- [93]J.V. Ortiz, R. Basu, and Y. Öhrn. “Electron-propagator calculations with a transition-operator reference”. In: *Chem. Phys. Lett.* 103.1 (1983), pp. 29–34 (cit. on pp. 27, 36).
- [94]Georg S. Michelitsch and Karsten Reuter. “Efficient simulation of near-edge x-ray absorption fine structure (NEXAFS) in density-functional theory: Comparison of core-level constraining approaches”. In: *J. Chem. Phys.* 150.7 (2019), p. 074104 (cit. on p. 27).
- [95]Benedikt P Klein, Samuel J Hall, and Reinhard J Maurer. “The nuts and bolts of core-hole constrained *ab initio* simulation for *K*-shell x-ray photoemission and absorption spectra”. In: *J. Phys. Condens. Matter* 33.15 (2021), p. 154005 (cit. on p. 27).
- [96]Roberto Flores-Moreno, V. G. Zakrzewski, and J. V. Ortiz. “Assessment of transition operator reference states in electron propagator calculations”. In: *J. Chem. Phys.* 127.13 (2007), p. 134106 (cit. on pp. 27, 36).
- [97]Subrata Jana and John M. Herbert. “Fractional-Electron and Transition-Potential Methods for Core-to-Valence Excitation Energies Using Density Functional Theory”. In: *J. Chem. Theory Comput.* 19.13 (2023), pp. 4100–4113 (cit. on p. 27).
- [98]Subrata Jana and John M. Herbert. “Slater transition methods for core-level electron binding energies”. In: *J. Chem. Phys.* 158.9 (2023), p. 094111 (cit. on p. 27).
- [99]Kimihiro Hiraio, Takahito Nakajima, Bun Chan, and Ho-Jin Lee. “The core ionization energies calculated by delta SCF and Slater’s transition state theory”. In: *J. Chem. Phys.* 158.6 (2023), p. 064112 (cit. on p. 27).
- [100]Gabriel L. S. Rodrigues, Elias Diesen, Johannes Voss, Patrick Norman, and Lars G. M. Pettersson. “Simulations of x-ray absorption spectra for CO desorbing from Ru(0001) with transition-potential and time-dependent density functional theory approaches”. In: *Struct. Dyn.* 9.1 (2022), p. 014101 (cit. on p. 27).

- [101]L. Triguero, L. G. M. Pettersson, and H. Ågren. “Calculations of near-edge x-ray-absorption spectra of gas-phase and chemisorbed molecules by means of density-functional and transition-potential theory”. In: *Phys. Rev. B* 58 (12 1998), pp. 8097–8110 (cit. on p. 27).
- [102]Christopher Ehlert and Tillmann Klamroth. “PSIXAS: A Psi4 plugin for efficient simulations of X-ray absorption spectra based on the transition-potential and Δ -Kohn–Sham method”. In: *J. Comput. Chem.* 41.19 (2020), pp. 1781–1789 (cit. on p. 27).
- [103]Matteo Cavalleri, Michael Odelius, Dennis Nordlund, Anders Nilsson, and Lars G. M. Pettersson. “Half or full core hole in density functional theory X-ray absorption spectrum calculations of water?” In: *Phys. Chem. Chem. Phys.* 7 (15 2005), pp. 2854–2858 (cit. on p. 27).
- [104]Nicholas A. Besley. “Density Functional Theory Based Methods for the Calculation of X-ray Spectroscopy”. In: *Acc. Chem. Res.* 53.7 (2020), pp. 1306–1315 (cit. on p. 27).
- [105]Yu Zhang, Jason D. Biggs, Daniel Healion, Niranjana Govind, and Shaul Mukamel. “Core and valence excitations in resonant X-ray spectroscopy using restricted excitation window time-dependent density functional theory”. In: *J. Chem. Phys.* 137.19 (2012), p. 194306 (cit. on p. 27).
- [106]K. Lopata, B. E. Van Kuiken, M. Khalil, and N. Govind. “Linear-Response and Real-Time Time-Dependent Density Functional Theory Studies of Core-Level Near-Edge X-Ray Absorption”. In: *J. Chem. Theory Comput.* 8.9 (2012), pp. 3284–3292 (cit. on p. 27).
- [107]Nicholas A. Besley. “Fast Time-Dependent Density Functional Theory Calculations of the X-ray Absorption Spectroscopy of Large Systems”. In: *J. Chem. Theory Comput.* 12.10 (2016), pp. 5018–5025 (cit. on p. 27).
- [108]Jack D. Wadey and Nicholas A. Besley. “Quantum Chemical Calculations of X-ray Emission Spectroscopy”. In: *J. Chem. Theory Comput.* 10.10 (2014), pp. 4557–4564 (cit. on pp. 27, 76).
- [109]Magnus W. D. Hanson-Heine, Michael W. George, and Nicholas A. Besley. “Kohn-Sham density functional theory calculations of non-resonant and resonant x-ray emission spectroscopy”. In: *J. Chem. Phys.* 146.9 (2017), p. 094106 (cit. on p. 27).
- [110]Kevin Carter-Fenk, Leonardo A. Cunha, Juan E. Arias-Martinez, and Martin Head-Gordon. “Electron-Affinity Time-Dependent Density Functional Theory: Formalism and Applications to Core-Excited States”. In: *J. Phys. Chem. Lett.* 13.41 (2022), pp. 9664–9672 (cit. on p. 27).
- [111]Nicholas A. Besley, Michael J. G. Peach, and David J. Tozer. “Time-dependent density functional theory calculations of near-edge X-ray absorption fine structure with short-range corrected functionals”. In: *Phys. Chem. Chem. Phys.* 11.44 (2009), p. 10350 (cit. on p. 27).
- [112]Megan L. Shelby, Patrick J. Lestrangle, Nicholas E. Jackson, et al. “Ultrafast Excited State Relaxation of a Metalloporphyrin Revealed by Femtosecond X-ray Absorption Spectroscopy”. In: *J. Am. Chem. Soc.* 138.28 (2016), pp. 8752–8764 (cit. on p. 27).

- [113]Eric A. Haugen, Diptarka Hait, Valeriu Scutelnic, et al. “Ultrafast X-ray Spectroscopy of Intersystem Crossing in Hexafluoroacetylacetone: Chromophore Photophysics and Spectral Changes in the Face of Electron-Withdrawing Groups”. In: *J. Phys. Chem. A* 127.3 (2023), pp. 634–644 (cit. on p. 27).
- [114]Enrico Ridente, Diptarka Hait, Eric A. Haugen, et al. “Femtosecond symmetry breaking and coherent relaxation of methane cations via x-ray spectroscopy”. In: *Science* 380.6646 (2023), pp. 713–717 (cit. on pp. 27, 96).
- [115]Noèlia Pueyo Bellafont, Paul S. Bagus, Carmen Sousa, and Francesc Illas. “Assessing the ability of DFT methods to describe static electron correlation effects: CO core level binding energies as a representative case”. In: *J. Chem. Phys.* 147.2 (2017), p. 024106 (cit. on p. 27).
- [116]Benjamin G. Janesko. “Projected Hybrid Density Functionals: Method and Application to Core Electron Ionization”. In: *J. Chem. Theory Comput.* 19.3 (2023), pp. 837–847 (cit. on p. 27).
- [117]J. Matthias Kahk, Georg S. Michelitsch, Reinhard J. Maurer, Karsten Reuter, and Johannes Lischner. “Core Electron Binding Energies in Solids from Periodic All-Electron Δ -Self-Consistent-Field Calculations”. In: *J. Phys. Chem. Lett.* 12.38 (2021), pp. 9353–9359 (cit. on p. 27).
- [118]Woojin Park, Marc Alías-Rodríguez, Daeheum Cho, et al. “Mixed-Reference Spin-Flip Time-Dependent Density Functional Theory for Accurate X-ray Absorption Spectroscopy”. In: *J. Chem. Theory Comput.* 18.10 (2022), pp. 6240–6250 (cit. on p. 27).
- [119]Hans Ågren, Vincenzo Carravetta, Olav Vahtras, and Lars G.M. Pettersson. “Direct, atomic orbital, static exchange calculations of photoabsorption spectra of large molecules and clusters”. In: *Chem. Phys. Lett.* 222.1 (1994), pp. 75–81 (cit. on pp. 27, 76).
- [120]Diptarka Hait, Katherine J. Oosterbaan, Kevin Carter-Fenk, and Martin Head-Gordon. “Computing x-ray absorption spectra from linear-response particles atop optimized holes”. In: *J. Chem. Phys.* 156.20 (2022), p. 201104 (cit. on p. 27).
- [121]Diptarka Hait and Martin Head-Gordon. “Highly Accurate Prediction of Core Spectra of Molecules at Density Functional Theory Cost: Attaining Sub-electronvolt Error from a Restricted Open-Shell Kohn–Sham Approach”. In: *J. Phys. Chem. Lett.* 11.3 (2020), pp. 775–786 (cit. on p. 27).
- [122]Diptarka Hait, Eric A. Haugen, Zheyue Yang, et al. “Accurate prediction of core-level spectra of radicals at density functional theory cost via square gradient minimization and recoupling of mixed configurations”. In: *J. of Chem. Phys.* 153.13 (2020), p. 134108 (cit. on pp. 27, 43).
- [123]Prakash Verma and Rodney J. Bartlett. “Increasing the applicability of density functional theory. V. X-ray absorption spectra with ionization potential corrected exchange and correlation potentials”. In: *J. Chem. Phys.* 145.3 (2016), p. 034108 (cit. on p. 27).
- [124]Yifan Jin and Rodney J. Bartlett. “Accurate computation of X-ray absorption spectra with ionization potential optimized global hybrid functional”. In: *J. Chem. Phys.* 149.6 (2018), p. 064111 (cit. on p. 27).

- [125] Young Choon Park, Ajith Perera, and Rodney J. Bartlett. “Density functionals for core excitations”. In: *J. Chem. Phys.* 157.9 (2022), p. 094107 (cit. on p. 27).
- [126] Yi Yao, Dorothea Golze, Patrick Rinke, Volker Blum, and Yosuke Kanai. “All-Electron BSE@GW Method for *K*-Edge Core Electron Excitation Energies”. In: *J. Chem. Theory Comput.* 18.3 (2022), pp. 1569–1583 (cit. on p. 27).
- [127] Dorothea Golze, Levi Keller, and Patrick Rinke. “Accurate Absolute and Relative Core-Level Binding Energies from *GW*”. In: *The Journal of Physical Chemistry Letters* 11.5 (2020), pp. 1840–1847 (cit. on p. 27).
- [128] J. Vinson, J. J. Rehr, J. J. Kas, and E. L. Shirley. “Bethe-Salpeter equation calculations of core excitation spectra”. In: *Phys. Rev. B* 83 (11 2011), p. 115106 (cit. on p. 27).
- [129] J. Vinson and J. J. Rehr. “Ab initio Bethe-Salpeter calculations of the x-ray absorption spectra of transition metals at the *L*-shell edges”. In: *Phys. Rev. B* 86 (19 2012), p. 195135 (cit. on p. 27).
- [130] Dorothea Golze, Marc Dvorak, and Patrick Rinke. “The *GW* Compendium: A Practical Guide to Theoretical Photoemission Spectroscopy”. In: *Front. Chem.* 7 (2019) (cit. on p. 27).
- [131] K. Gilmore, John Vinson, E.L. Shirley, et al. “Efficient implementation of core-excitation Bethe–Salpeter equation calculations”. In: *Comput. Phys. Commun.* 197 (2015), pp. 109–117 (cit. on p. 27).
- [132] Ramón L. Panadés-Barrueta and Dorothea Golze. *Accelerating core-level GW calculations by combining the contour deformation approach with the analytic continuation of *W**. 2023 (cit. on p. 27).
- [133] Tianyu Zhu and Garnet Kin-Lic Chan. “All-Electron Gaussian-Based G_0W_0 for Valence and Core Excitation Energies of Periodic Systems”. In: *J. Chem. Theory Comput.* 17.2 (2021), pp. 727–741 (cit. on p. 27).
- [134] A Barth and J Schirmer. “Theoretical core-level excitation spectra of N_2 and CO by a new polarisation propagator method”. In: *J. Phys. B: Atom. Mol. Phys.* 18.5 (1985), p. 867 (cit. on pp. 27, 30, 33).
- [135] Jan Wenzel, Michael Wormit, and Andreas Dreuw. “Calculating X-ray Absorption Spectra of Open-Shell Molecules with the Unrestricted Algebraic-Diagrammatic Construction Scheme for the Polarization Propagator”. In: *J. Chem. Theory Comput.* 10.10 (2014), pp. 4583–4598 (cit. on p. 27).
- [136] Jan Wenzel, Michael Wormit, and Andreas Dreuw. “Calculating core-level excitations and x-ray absorption spectra of medium-sized closed-shell molecules with the algebraic-diagrammatic construction scheme for the polarization propagator”. In: *J. Comput. Chem.* 35.26 (2014), pp. 1900–1915 (cit. on p. 27).
- [137] Carlos E. V. de Moura and Alexander Yu. Sokolov. “Simulating X-ray photoelectron spectra with strong electron correlation using multireference algebraic diagrammatic construction theory”. In: *Phys. Chem. Chem. Phys.* 24 (8 2022), pp. 4769–4784 (cit. on p. 27).

- [138]Thomas Fransson and Andreas Dreuw. “Simulating X-ray Emission Spectroscopy with Algebraic Diagrammatic Construction Schemes for the Polarization Propagator”. In: *J. Chem. Theory Comput.* 15.1 (2019), pp. 546–556 (cit. on pp. 27, 76).
- [139]Jan Wenzel, Andre Holzer, Michael Wormit, and Andreas Dreuw. “Analysis and comparison of CVS-ADC approaches up to third order for the calculation of core-excited states”. In: *J. Chem. Phys.* 142.21 (2015), p. 214104 (cit. on pp. 27, 30).
- [140]Young Choon Park, Ajith Perera, and Rodney J. Bartlett. “Equation of motion coupled-cluster for core excitation spectra: Two complementary approaches”. In: *J. Chem. Phys.* 151.16 (2019), p. 164117 (cit. on p. 27).
- [141]Young Choon Park, Ajith Perera, and Rodney J. Bartlett. “Equation of motion coupled-cluster study of core excitation spectra II: Beyond the dipole approximation”. In: *J. Chem. Phys.* 155.9 (2021), p. 094103 (cit. on p. 27).
- [142]Marcel Nooijen and Rodney J. Bartlett. “Description of core-excitation spectra by the open-shell electron-attachment equation-of-motion coupled cluster method”. In: *J. Chem. Phys.* 102.17 (1995), pp. 6735–6756 (cit. on pp. 27, 52).
- [143]Marta L. Vidal, Xintian Feng, Evgeny Epifanovsky, Anna I. Krylov, and Sonia Coriani. “New and Efficient Equation-of-Motion Coupled-Cluster Framework for Core-Excited and Core-Ionized States”. In: *J. Chem. Theory Comput.* 15.5 (2019), pp. 3117–3133 (cit. on pp. 27, 30).
- [144]Daniel R. Nascimento and A. Eugene III DePrince. “Simulation of Near-Edge X-ray Absorption Fine Structure with Time-Dependent Equation-of-Motion Coupled-Cluster Theory”. In: *J. Phys. Chem. Lett.* 8.13 (2017), pp. 2951–2957 (cit. on p. 27).
- [145]Megan Simons and Devin A. Matthews. “Accurate Core-Excited States via Inclusion of Core Triple Excitations in Similarity-Transformed Equation-of-Motion Theory”. In: *J. Chem. Theory Comput.* 18.6 (2022), pp. 3759–3765 (cit. on pp. 27, 76).
- [146]Devin A. Matthews. “EOM-CC methods with approximate triple excitations applied to core excitation and ionisation energies”. In: *Mol. Phys.* 118.21-22 (2020), e1771448 (cit. on pp. 27, 76).
- [147]Christoph Liegener and Hans Ågren. “Electronic spectra of finite polyenes and polyacetylene obtained by electron and polarization propagator calculations”. In: *Theor. Chim. Acta* 89.5-6 (1994), pp. 335–362 (cit. on pp. 27, 76).
- [148]Ulf Ekström, Patrick Norman, Vincenzo Carravetta, and Hans Ågren. “Polarization Propagator for X-Ray Spectra”. In: *Phys. Rev. Lett.* 97 (14 2006), p. 143001 (cit. on p. 27).
- [149]Abdulrahman Y. Zamani and Hrant P. Hratchian. “Assessing the performance of Δ SCF and the diagonal second-order self-energy approximation for calculating vertical core excitation energies”. In: *J. Chem. Phys.* 157.8 (2022), p. 084115 (cit. on p. 27).
- [150]J. Matthias Kahk and Johannes Lischner. “Combining the Δ -Self-Consistent-Field and GW Methods for Predicting Core Electron Binding Energies in Periodic Solids”. In: *J. Chem. Theory Comput.* 19.11 (2023), pp. 3276–3283 (cit. on p. 27).

- [151] Andreas Barth, Robert J. Buenker, Sigrid D. Peyerimhoff, and Werner Butscher. “Theoretical study of the core-ionized and various core-excited and shake-up states of acetylene and ethylene by ab initio MRD-CI methods”. In: *Chem. Phys.* 46.1 (1980), pp. 149–164 (cit. on pp. 27, 30).
- [152] Werner Butscher, Robert J. Buenker, and Sigrid D. Peyerimhoff. “All-electron CI calculations for core-ionized, core-valence excited and shake-up states of N₂”. In: *Chem. Phys. Lett.* 52.3 (1977), pp. 449–456 (cit. on pp. 27, 30).
- [153] T. N. Rescigno and A. E. Orel. “Theoretical study of the 400 eV core-excited valence states of N₂”. In: *J. Chem. Phys.* 70.7 (1979), pp. 3390–3394 (cit. on pp. 27, 30).
- [154] Nariyuki Saito, Nicolas Douguet, Hiroki Sannohe, et al. “Attosecond electronic dynamics of core-excited states of N₂O in the soft x-ray region”. In: *Phys. Rev. Res.* 3 (4 2021), p. 043222 (cit. on p. 27).
- [155] Jeremy P. Coe and Martin J. Paterson. “Multireference X-ray emission and absorption spectroscopy calculations from Monte Carlo configuration interaction”. In: *Theor. Chem. Acc.* 134.5 (2015), p. 58 (cit. on p. 27).
- [156] Scott M. Garner and Eric Neuscamman. “Core excitations with excited state mean field and perturbation theory”. In: *J. Chem. Phys.* 153.15 (2020), p. 154102 (cit. on pp. 27, 30).
- [157] Tarini S. Hardikar and Eric Neuscamman. “A self-consistent field formulation of excited state mean field theory”. In: *The Journal of Chemical Physics* 153.16 (2020), p. 164108 (cit. on p. 27).
- [158] Katherine J. Oosterbaan, Alec F. White, and Martin Head-Gordon. “Non-orthogonal configuration interaction with single substitutions for the calculation of core-excited states”. In: *J. Chem. Phys.* 149.4 (2018), p. 044116 (cit. on pp. 27, 30).
- [159] Katherine J. Oosterbaan, Alec F. White, and Martin Head-Gordon. “Non-Orthogonal Configuration Interaction with Single Substitutions for Core-Excited States: An Extension to Doublet Radicals”. In: *J. Chem. Theory Comput.* 15.5 (2019), pp. 2966–2973 (cit. on p. 27).
- [160] Katherine J. Oosterbaan, Alec F. White, Diptarka Hait, and Martin Head-Gordon. “Generalized single excitation configuration interaction: an investigation into the impact of the inclusion of non-orthogonality on the calculation of core-excited states”. In: *Phys. Chem. Chem. Phys.* 22 (15 2020), pp. 8182–8192 (cit. on p. 27).
- [161] Dimitrios Maganas, Serena DeBeer, and Frank Neese. “A Restricted Open Configuration Interaction with Singles Method To Calculate Valence-to-Core Resonant X-ray Emission Spectra: A Case Study”. In: *Inorg. Chem.* 56.19 (2017), pp. 11819–11836 (cit. on p. 27).
- [162] Dimitrios Maganas, Serena DeBeer, and Frank Neese. “Pair Natural Orbital Restricted Open-Shell Configuration Interaction (PNO-ROCIS) Approach for Calculating X-ray Absorption Spectra of Large Chemical Systems”. In: *J. Phys. Chem. A* 122.5 (2018), pp. 1215–1227 (cit. on p. 27).

- [163]Adam Kubas, Max Verkamp, Josh Vura-Weis, Frank Neese, and Dimitrios Maganas. “Restricted Open-Shell Configuration Interaction Singles Study on M- and L-edge X-ray Absorption Spectroscopy of Solid Chemical Systems”. In: *J. Chem. Theory Comput.* 14.8 (2018), pp. 4320–4334 (cit. on p. 27).
- [164]Paul S. Bagus, Carme Sousa, and Francesc Illas. “Consequences of electron correlation for XPS binding energies: Representative case for C(1s) and O(1s) XPS of CO”. In: *J. Chem. Phys.* 145.14 (2016), p. 144303 (cit. on p. 27).
- [165]Paul S. Bagus, Gianfranco Pacchioni, and Fulvio Parmigiani. “Final state effects for the core-level XPS spectra of NiO”. In: *Chem. Phys. Lett.* 207.4 (1993), pp. 569–574 (cit. on p. 27).
- [166]Meiyuan Guo, Erik Källman, Lasse Kragh Sørensen, et al. “Molecular Orbital Simulations of Metal 1s2p Resonant Inelastic X-ray Scattering”. In: *J. Phys. Chem. A* 120.29 (2016), pp. 5848–5855 (cit. on p. 27).
- [167]Paul S. Bagus and Björn O. Roos. “Bonding and backbonding in NiCO: A MCSCF study”. In: *J. Chem. Phys.* 75.12 (1981), pp. 5961–5962 (cit. on p. 27).
- [168]M. Alagia, E. Bodo, P. Decleva, et al. “The soft X-ray absorption spectrum of the allyl free radical”. In: *Phys. Chem. Chem. Phys.* 15 (4 2013), pp. 1310–1318 (cit. on p. 27).
- [169]L. S. Cederbaum, W. Domcke, and J. Schirmer. “Many-body theory of core holes”. In: *Phys. Rev. A* 22 (1 1980), pp. 206–222 (cit. on p. 27).
- [170]Santosh Ranga and Achintya Kumar Dutta. “A Core–Valence Separated Similarity Transformed EOM-CCSD Method for Core-Excitation Spectra”. In: *J. Chem. Theory Comput.* 17.12 (2021), pp. 7428–7446 (cit. on p. 27).
- [171]Josefine H. Andersen, Kaushik D. Nanda, Anna I. Krylov, and Sonia Coriani. “Cherry-Picking Resolvents: Recovering the Valence Contribution in X-ray Two-Photon Absorption within the Core–Valence-Separated Equation-of-Motion Coupled-Cluster Response Theory”. In: *J. Chem. Theory Comput.* 18.10 (2022), pp. 6189–6202 (cit. on p. 27).
- [172]Michael F. Herbst and Thomas Fransson. “Quantifying the error of the core–valence separation approximation”. In: *J. Chem. Phys.* 153.5 (2020), p. 054114 (cit. on p. 27).
- [173]Pekka Pyykkö. “Relativistic Quantum Chemistry”. In: ed. by Per-Olov Löwdin. Vol. 11. *Adv. Quantum Chem.* Academic Press, 1978, pp. 353–409 (cit. on pp. 27, 35).
- [174]Wenjian Liu. “Ideas of relativistic quantum chemistry”. In: *Mol. Phys.* 108.13 (2010), pp. 1679–1706 (cit. on pp. 27, 35).
- [175]Wenjian Liu. “Essentials of relativistic quantum chemistry”. In: *J. Chem. Phys.* 152.18 (2020), p. 180901 (cit. on pp. 27, 35).
- [176]Joseph M. Kasper, Xiaosong Li, Stosh A. Kozimor, Enrique R. Batista, and Ping Yang. “Relativistic Effects in Modeling the Ligand K-Edge X-ray Absorption Near-Edge Structure of Uranium Complexes”. In: *Journal of Chemical Theory and Computation* 18.4 (2022), pp. 2171–2179 (cit. on p. 27).

- [177]Adam Grofe and Xiaosong Li. “Relativistic nonorthogonal configuration interaction: Application to $L_{2,3}$ -edge X-ray spectroscopy”. In: *Phys. Chem. Chem. Phys.* 24.18 (2022), pp. 10745–10756 (cit. on p. 27).
- [178]Paul S. Bagus, Michel J. Sassi, and Kevin M. Rosso. “Intermediate coupling for core-level excited states: Consequences for X-Ray absorption spectroscopy”. In: *J. Electron Spectrosc. Relat. Phenom.* 200 (2015). Special Anniversary Issue: Volume 200, pp. 174–180 (cit. on p. 27).
- [179]Max Kehry, Yannick J. Franzke, Christof Holzer, and Wim Klopper. “Quasirelativistic two-component core excitations and polarisabilities from a damped-response formulation of the Bethe–Salpeter equation”. In: *Mol. Phys.* 118.21-22 (2020), e1755064 (cit. on p. 27).
- [180]Thomas Fransson, Daria Burdakova, and Patrick Norman. “K- and L-edge X-ray absorption spectrum calculations of closed-shell carbon, silicon, germanium, and sulfur compounds using damped four-component density functional response theory”. In: *Phys. Chem. Chem. Phys.* 18 (19 2016), pp. 13591–13603 (cit. on p. 27).
- [181]Lukas Konecny, Jan Vicha, Stanislav Komorovsky, Kenneth Ruud, and Michal Repisky. “Accurate X-ray Absorption Spectra near L- and M-Edges from Relativistic Four-Component Damped Response Time-Dependent Density Functional Theory”. In: *Inorganic Chemistry* 61.2 (2022), pp. 830–846 (cit. on p. 27).
- [182]Ulf Ekström, Patrick Norman, and Vincenzo Carravetta. “Relativistic four-component static-exchange approximation for core-excitation processes in molecules”. In: *Phys. Rev. A* 73 (2 2006), p. 022501 (cit. on p. 27).
- [183]Tianyuan Zhang, Joseph M. Kasper, and Xiaosong Li. “Chapter Two - Localized relativistic two-component methods for ground and excited state calculations”. In: ed. by David A. Dixon. Vol. 16. *Annual Reports in Computational Chemistry*. Elsevier, 2020, pp. 17–37 (cit. on p. 27).
- [184]Jinghua Guo. “Synchrotron radiation, soft-X-ray spectroscopy and nanomaterials”. In: *Int. J. Nanotechnol.* 1.1-2 (2004), pp. 193–225 (cit. on p. 29).
- [185]Juan-Jesus Velasco-Velez, Cheng Hao Wu, Tod A. Pascal, et al. “The structure of interfacial water on gold electrodes studied by x-ray absorption spectroscopy”. In: *Science* 346.6211 (2014), pp. 831–834 (cit. on p. 29).
- [186]L. M. Oskinova, A. Feldmeier, and W.-R. Hamann. “High-resolution X-ray spectroscopy of bright O-type stars”. In: *MNRAS* 372.1 (2006), pp. 313–326 (cit. on p. 29).
- [187]Michael Odellius, Hirohito Ogasawara, Dennis Nordlund, et al. “Ultrafast Core-Hole-Induced Dynamics in Water Probed by X-Ray Emission Spectroscopy”. In: *Phys. Rev. Lett.* 94 (22 2005), p. 227401 (cit. on p. 29).
- [188]M. S. Schöffler, J. Titze, N. Petridis, et al. “Ultrafast Probing of Core Hole Localization in N_2 ”. In: *Science* 320.5878 (2008), pp. 920–923 (cit. on p. 29).
- [189]L. Weinhardt, E. Ertan, M. Iannuzzi, et al. “Probing hydrogen bonding orbitals: resonant inelastic soft X-ray scattering of aqueous NH_3 ”. In: *Phys. Chem. Chem. Phys.* 17 (40 2015), pp. 27145–27153 (cit. on p. 29).

- [190]P. Glans, K. Gunnelin, P. Skytt, et al. “Resonant X-Ray Emission Spectroscopy of Molecular Oxygen”. In: *Phys. Rev. Lett.* 76 (14 1996), pp. 2448–2451 (cit. on p. 29).
- [191]Alison C. McQuilken, Yang Ha, Kyle D. Sutherlin, et al. “Preparation of Non-heme {FeNO}⁷ Models of Cysteine Dioxygenase: Sulfur versus Nitrogen Ligation and Photorelease of Nitric Oxide”. In: *J. Am. Chem. Soc.* 135.38 (2013), pp. 14024–14027 (cit. on p. 29).
- [192]Yang Ha, Anna R. Arnold, Nicole N. Nuñez, et al. “Sulfur K-Edge XAS Studies of the Effect of DNA Binding on the [Fe₄S₄] Site in EndoIII and MutY”. In: *J. Am. Chem. Soc.* 139.33 (2017), pp. 11434–11442 (cit. on p. 29).
- [193]Iulia Emilia Brumboiu, Dirk R. Rehn, Andreas Dreuw, Young Min Rhee, and Patrick Norman. “Analytical gradients for core-excited states in the algebraic diagrammatic construction (ADC) framework”. In: *J. Chem. Phys.* 155.4 (2021), p. 044106 (cit. on p. 30).
- [194]Rolf H. Myhre, Thomas J. A. Wolf, Lan Cheng, et al. “A theoretical and experimental benchmark study of core-excited states in nitrogen”. In: *J. Chem. Phys.* 148.6 (2018), p. 064106 (cit. on pp. 30, 55, 81).
- [195]Adam E. A. Fouda, Linsey C. Seitz, Dirk Hauschild, et al. “Observation of Double Excitations in the Resonant Inelastic X-ray Scattering of Nitric Oxide”. In: *J. Phys. Chem. Lett.* 11.18 (2020), pp. 7476–7482 (cit. on p. 30).
- [196]Paul S. Bagus, Connie J. Nelin, Eugene S. Ilton, Michel J. Sassi, and Kevin M. Rosso. “Analysis of X-ray adsorption edges: L_{2,3} edge of FeCl₄⁻”. In: *J. Chem. Phys.* 147.22 (2017), p. 224306 (cit. on p. 30).
- [197]Michel Sassi, Carolyn I. Pearce, Paul S. Bagus, Elke Arenholz, and Kevin M. Rosso. “First-Principles Fe L_{2,3}-Edge and O K-Edge XANES and XMCD Spectra for Iron Oxides”. In: *J. Phys. Chem. A* 121.40 (2017), pp. 7613–7618 (cit. on p. 30).
- [198]Jarrett L. Mason, Hassan Harb, Josey E. Topolski, Hrant P. Hratchian, and Caroline Chick Jarrold. “Exceptionally Complex Electronic Structures of Lanthanide Oxides and Small Molecules”. In: *Acc. Chem. Res.* 52.11 (2019), pp. 3265–3273 (cit. on p. 30).
- [199]Caleb Huizenga, Hrant P. Hratchian, and Caroline Chick Jarrold. “Lanthanide Oxides: From Diatomics to High-Spin, Strongly Correlated Homo- and Heterometallic Clusters”. In: *J. Phys. Chem. A* 125.29 (2021), pp. 6315–6331 (cit. on p. 30).
- [200]Nicholas A. Besley, Andrew T. B. Gilbert, and Peter M. W. Gill. “Self-consistent-field calculations of core excited states”. In: *J. Chem. Phys.* 130.12 (2009), p. 124308 (cit. on pp. 30, 76).
- [201]Jason V. Jorstad, Tian Xie, and Christine M. Morales. “ Δ -SCF calculations of core electron binding energies in first-row transition metal atoms”. In: *Int. J. Quantum Chem.* 122.10 (2022), e26881 (cit. on p. 30).
- [202]Yutaka Imamura and Hiromi Nakai. “Analysis of self-interaction correction for describing core excited states”. In: *Int. J. Quantum Chem.* 107.1 (2007), pp. 23–29 (cit. on pp. 30, 41).

- [203]W.H.E. Schwarz, T.C. Chang, U. Seeger, and K.H. Hwang. “Core excitations of symmetrical aromatic molecules. Specific correlations in the valence shell and localization in the core shells”. In: *Chem. Phys.* 117.1 (1987), pp. 73–89 (cit. on pp. 30, 41).
- [204]Diptarka Hait and Martin Head-Gordon. “Highly Accurate Prediction of Core Spectra of Molecules at Density Functional Theory Cost: Attaining Sub-electronvolt Error from a Restricted Open-Shell Kohn–Sham Approach”. In: *J. Phys. Chem. Lett.* 11.3 (2020), pp. 775–786 (cit. on p. 30).
- [205]Leonardo A. Cunha, Diptarka Hait, Richard Kang, Yuezhi Mao, and Martin Head-Gordon. “Relativistic Orbital-Optimized Density Functional Theory for Accurate Core-Level Spectroscopy”. In: *J. Phys. Chem. Lett.* 13.15 (2022), pp. 3438–3449 (cit. on pp. 30, 97).
- [206]Gregory Born, Henry A. Kurtz, and Yngve Öhrn. “Elementary finite order perturbation theory for vertical ionization energies”. In: *J. Chem. Phys.* 68.1 (1978), pp. 74–85 (cit. on pp. 31, 42).
- [207]J. V. Ortiz B. and Yngve Öhrn. “Electron propagator theory of molecular anions”. In: *J. Chem. Phys.* 72.10 (1980), pp. 5744–5751 (cit. on p. 31).
- [208]Hector H. Corzo, Ali Abou Taka, Aurora Pribram-Jones, and Hrant P. Hratchian. “Using projection operators with maximum overlap methods to simplify challenging self-consistent field optimization”. In: *J. Comput. Chem.* 43.6 (2022), pp. 382–390 (cit. on pp. 32, 43, 77).
- [209]P. Lykos and G. W. Pratt. “Discussion on The Hartree-Fock Approximation”. In: *Rev. Mod. Phys.* 35 (3 1963), pp. 496–501 (cit. on pp. 32, 43).
- [210]Louis Noodleman. “Valence bond description of antiferromagnetic coupling in transition metal dimers”. In: *J. Chem. Phys.* 74.10 (1981), pp. 5737–5743 (cit. on pp. 32, 43).
- [211]K. Yamaguchi, F. Jensen, A. Dorigo, and K.N. Houk. “A spin correction procedure for unrestricted Hartree-Fock and Møller-Plesset wavefunctions for singlet diradicals and polyradicals”. In: *Chem. Phys. Lett.* 149.5 (1988), pp. 537–542 (cit. on pp. 32, 43).
- [212]Lee M. Thompson and Hrant P. Hratchian. “On approximate projection models”. In: *Mol. Phys.* 117.9-12 (2019), pp. 1421–1429 (cit. on pp. 32, 43).
- [213]Hans A Bethe and Edwin E Salpeter. *Quantum mechanics of one- and two-electron atoms*. Berlin Heidelberg: Springer Berlin Heidelberg, 1957 (cit. on pp. 33, 51).
- [214]C. L. Pekeris. “Ground State of Two-Electron Atoms”. In: *Phys. Rev.* 112 (5 1958), pp. 1649–1658 (cit. on pp. 33, 51, 81).
- [215]Charles W. Scherr and Jeremiah N. Silverman. “Perturbation Analysis of Two- to Four-Electron Variational Wave Functions”. In: *J. Chem. Phys.* 37.5 (1962), pp. 1154–1156 (cit. on pp. 33, 51, 81).
- [216]Nicholas A. Besley. “Density Functional Theory Calculations of Core–Electron Binding Energies at the K-Edge of Heavier Elements”. In: *J. Chem. Theory Comput.* 17.6 (2021), pp. 3644–3651 (cit. on p. 33).

- [217]Duminda S. Ranasinghe, Johannes T. Margraf, Ajith Perera, and Rodney J. Bartlett. “Vertical valence ionization potential benchmarks from equation-of-motion coupled cluster theory and QTP functionals”. In: *J. Chem. Phys.* 150.7 (2019), p. 074108 (cit. on pp. 33, 53, 81).
- [218]D. P. Chong, O. V. Gritsenko, and E. J. Baerends. “Interpretation of the Kohn–Sham orbital energies as approximate vertical ionization potentials”. In: *J. Chem. Phys.* 116.5 (2002), pp. 1760–1772 (cit. on pp. 33, 53).
- [219]Russel D. Johnson III. *NIST Computational Chemistry Comparison and Benchmark Database NIST Standard Reference Database Number 101. Release 21*. <https://cccbdb.nist.gov/>. (Last accessed on 5 May 2022). 2020 (cit. on pp. 33, 53, 81).
- [220]M. J. Frisch, G. W. Trucks, H. B. Schlegel, et al. *Gaussian Development Version Revision J.15*. Gaussian Inc. Wallingford CT. 2022 (cit. on pp. 33, 53).
- [221]Joseph T. Golab and Danny L. Yeager. “The multiconfigurational spin-tensor electron propagator method for determining vertical principal and shake-up ionization potentials for open shell and highly correlated atoms and molecules”. In: *J. Chem. Phys.* 87.5 (1987), pp. 2925–2944 (cit. on pp. 35, 96).
- [222]V. G. Zakrzewski, J. V. Ortiz, Jeffrey A. Nichols, et al. “Comparison of perturbative and multiconfigurational electron propagator methods”. In: *Int. J. Quantum Chem.* 60.1 (1996), pp. 29–36 (cit. on p. 35).
- [223]Kevin C. Prince, Robert Richter, Monica de Simone, Michele Alagia, and Marcello Coreno. “Near Edge X-ray Absorption Spectra of Some Small Polyatomic Molecules”. In: *J. Phys. Chem. A* 107.12 (2003), pp. 1955–1963 (cit. on pp. 37, 39, 69–72).
- [224]D. Duflot, J.-P. Flament, I. C. Walker, J. Heinesch, and M.-J. Hubin-Franskin. “Core shell excitation of 2-propenal (acrolein) at the O1s and C1s edges: An experimental and ab initio study”. In: *J. Chem. Phys.* 118.3 (2003), pp. 1137–1145 (cit. on pp. 37, 39).
- [225]J. Schirmer, A. B. Trofimov, K. J. Randall, et al. “K-shell excitation of the water, ammonia, and methane molecules using high-resolution photoabsorption spectroscopy”. In: *Phys. Rev. A* 47 (2 1993), pp. 1136–1147 (cit. on pp. 37, 39).
- [226]M. Domke, C. Xue, A. Puschmann, et al. “Carbon and oxygen K-edge photoionization of the CO molecule”. In: *Chem. Phys. Lett.* 173.1 (1990), pp. 122–128 (cit. on pp. 37, 39).
- [227]D. Duflot, J.-P. Flament, A. Giuliani, J. Heinesch, and M.-J. Hubin-Franskin. “Core shell excitation of furan at the O1s and C1s edges: An experimental and ab initio study”. In: *J. Chem. Phys.* 119.17 (2003), pp. 8946–8955 (cit. on pp. 37–40, 53, 69–72).
- [228]G. Remmers, M. Domke, A. Puschmann, et al. “High-resolution K-shell photoabsorption in formaldehyde”. In: *Phys. Rev. A* 46 (7 1992), pp. 3935–3944 (cit. on pp. 37, 39).
- [229]A P Hitchcock and C E Brion. “K-shell excitation of HF and F₂ studied by electron energy-loss spectroscopy”. In: *J. Phys. B: At. Mol. Phys.* 14.22 (1981), pp. 4399–4413 (cit. on pp. 37–40).

- [230]C. Hannay, D. Duflot, J.-P. Flament, and M.-J. Hubin-Franskin. "The core excitation of pyridine and pyridazine: An electron spectroscopy and ab initio study". In: *J. Chem. Phys.* 110.12 (1999), pp. 5600–5610 (cit. on pp. 37–40, 53, 69–72).
- [231]K C Prince, L Avaldi, M Coreno, R Camilloni, and M de Simone. "Vibrational structure of core to Rydberg state excitations of carbon dioxide and dinitrogen oxide". In: *J. Phys. B: At. Mol. Opt. Phys.* 32.11 (1999), pp. 2551–2567 (cit. on pp. 37–40).
- [232]Elizabeth Apen, Adam P. Hitchcock, and John L. Gland. "Experimental studies of the core excitation of imidazole, 4,5-dicyanoimidazole, and s-triazine". In: *J. Chem. Phys.* 97.26 (1993), pp. 6859–6866 (cit. on pp. 37, 39).
- [233]A.P. Hitchcock and C.E. Brion. "Inner shell electron energy loss studies of HCN and C₂N₂". In: *Chem. Phys.* 37.3 (1979), pp. 319–331 (cit. on pp. 37–40).
- [234]M.B. Robin, I. Ishii, R. McLaren, and A.P. Hitchcock. "Fluorination effects on the inner-shell spectra of unsaturated molecules". In: *J. Electron Spectrosc. Relat. Phenom.* 47 (1988), pp. 53–92 (cit. on pp. 37–40).
- [235]G.R. Wight and C.E. Brion. "K-shell excitations in NO and O₂ by 2.5 keV electron impact". In: *J. Electron Spectrosc. Relat. Phenom.* 4.4 (1974), pp. 313–325 (cit. on pp. 37–40, 89, 96).
- [236]G.R. Wight and C.E. Brion. "K-shell excitation of CH₄, NH₃, H₂O, CH₃OH, CH₃OCH₃ and CH₃NH₂ by 2.5 keV electron impact". In: *J. Electron Spectrosc. Relat. Phenom.* 4.1 (1974), pp. 25–42 (cit. on pp. 37, 39).
- [237]A.P. Hitchcock and C.E. Brion. "Carbon K-shell excitation of C₂H₂, C₂H₄, C₂H₆ and C₆H₆ by 2.5 keV electron impact". In: *J. Electron Spectrosc. Relat. Phenom.* 10.3 (1977), pp. 317–330 (cit. on pp. 38, 40).
- [238]George C. King, Frank H. Read, and Michel Tronc. "Investigation of the energy and vibrational structure of the inner shell $(1s)^{-1}(\pi 2p)^1\Pi$ state of the nitrogen molecule by electron impact with high resolution". In: *Chem. Phys. Lett.* 52.1 (1977), pp. 50–54 (cit. on pp. 38, 40).
- [239]Marc Simon, Michel Lavollee, Paul Morin, and Irene Nenner. "Photofragmentation of the Core-Excited s-Tetrazine Molecule Near the Carbon and Nitrogen K Edges". In: *J. Phys. Chem.* 99.6 (1995), pp. 1733–1740 (cit. on pp. 38, 40).
- [240]A. P. Hitchcock, J. A. Horsley, and J. Stöhr. "Inner shell excitation of thiophene and thiolane: Gas, solid, and monolayer states". In: *J. Chem. Phys.* 85.9 (1986), pp. 4835–4848 (cit. on pp. 38, 40).
- [241]R. McLaren, S. A. C. Clark, I. Ishii, and A. P. Hitchcock. "Absolute oscillator strengths from K-shell electron-energy-loss spectra of the fluoroethenes and 1,3-perfluorobutadiene". In: *Phys. Rev. A* 36 (4 1987), pp. 1683–1701 (cit. on pp. 38, 40).
- [242]Yngve Öhrn. "The Calculation of Atomic and Molecular Electron Binding Energies". In: *Excited States in Quantum Chemistry*. Springer Netherlands, 1978, pp. 317–328 (cit. on p. 35).
- [243]Henry A. Kurtz and Yngve Öhrn. "On the calculation of electron binding energies". In: *J. Chem. Phys.* 69.3 (1978), pp. 1162–1167 (cit. on p. 35).

- [244]Lawrence C Snyder. “Core-Electron Binding Energies and Slater Atomic Shielding Constants”. In: *J. Chem. Phys.* 55.1 (1971), pp. 95–99 (cit. on pp. 35, 41, 42, 76).
- [245]L. S. Cederbaum and W. Domcke. “Localized and delocalized core holes and their interrelation”. In: *J. Chem. Phys.* 66.11 (1977), pp. 5084–5086 (cit. on pp. 35, 42).
- [246]Iulia Emilia Brumboiu and Thomas Fransson. “Core-hole delocalization for modeling X-ray spectroscopies: A cautionary tale”. In: *J. Chem. Phys. (in press)* (2022) (cit. on pp. 36, 45, 52).
- [247]Andreas Dreuw and Thomas Fransson. “Using core-hole reference states for calculating X-ray photoelectron and emission spectra”. In: *Phys. Chem. Chem. Phys.* 24 (18 2022), pp. 11259–11267 (cit. on pp. 36, 52, 77).
- [248]L. S. Cederbaum, F. Tarantelli, A. Sgamellotti, and J. Schirmer. “On double vacancies in the core”. In: *J. Chem. Phys.* 85.11 (1986), pp. 6513–6523 (cit. on pp. 41, 42).
- [249]L Hedin and A Johansson. “Polarization corrections to core levels”. In: *J. Phys. B: Atom. Mol. Phys.* 2.12 (1969), pp. 1336–1346 (cit. on p. 42).
- [250]J A D Matthew and R S Perkins. “Variation of relaxation energies with the spatial extent of core holes”. In: *J. Phys. C: Solid State Phys.* 11.14 (1978), pp. L569–L574 (cit. on p. 42).
- [251]Bo Wästberg, Sten Lunell, Christer Enkvist, et al. “1s x-ray-absorption spectroscopy of C₆₀: The effects of screening and core-hole relaxation”. In: *Phys. Rev. B* 50 (17 1994), pp. 13031–13034 (cit. on p. 42).
- [252]D.J. Thouless. *The Quantum Mechanics of Many-Body Systems: Second Edition*. Dover Publications, 2014 (cit. on p. 42).
- [253]Diptarka Hait and Martin Head-Gordon. “Orbital Optimized Density Functional Theory for Electronic Excited States”. In: *J. Phys. Chem. Lett.* 12.19 (2021), pp. 4517–4529 (cit. on p. 42).
- [254]Thomas J. Watson and Rodney J. Bartlett. “Infinite order relaxation effects for core ionization energies with a variational coupled cluster ansatz”. In: *Chem. Phys. Lett.* 555 (2013), pp. 235–238 (cit. on p. 42).
- [255]Saswata Dasgupta, Chandra Shahi, Pradeep Bhetwal, John P. Perdew, and Francesco Paesani. “How Good Is the Density-Corrected SCAN Functional for Neutral and Ionic Aqueous Systems, and What Is So Right about the Hartree–Fock Density?” In: *J. Chem. Theory Comput.* 18.8 (2022), pp. 4745–4761 (cit. on p. 43).
- [256]Kyle R. Bryenton, Adebayo A. Adeleke, Stephen G. Dale, and Erin R. Johnson. “Delocalization error: The greatest outstanding challenge in density-functional theory”. In: *Wiley Interdiscip. Rev. Comput. Mol. Sci.* 13.2 (2023), e1631 (cit. on p. 43).
- [257]Min-Cheol Kim, Eunji Sim, and Kieron Burke. “Understanding and Reducing Errors in Density Functional Calculations”. In: *Phys. Rev. Lett.* 111 (7 2013), p. 073003 (cit. on p. 43).

- [258]Min-Cheol Kim, Eunji Sim, and Kieron Burke. “Ions in solution: Density corrected density functional theory (DC-DFT)”. In: *The Journal of Chemical Physics* 140.18 (2014), 18A528 (cit. on p. 43).
- [259]Stefan Vuckovic, Suhwan Song, John Kozlowski, Eunji Sim, and Kieron Burke. “Density Functional Analysis: The Theory of Density-Corrected DFT”. In: *J. Chem. Theory Comput.* 15.12 (2019), pp. 6636–6646 (cit. on p. 43).
- [260]Rodney J. Bartlett and Yngve Öhrn. “How quantitative is the concept of maximum overlap?” In: *Theor. Chim. Acta* 21.3 (1971), pp. 215–234 (cit. on p. 43).
- [261]Andrew T. B. Gilbert, Nicholas A. Besley, and Peter M. W. Gill. “Self-Consistent Field Calculations of Excited States Using the Maximum Overlap Method (MOM)”. In: *J. Phys. Chem. A* 112.50 (2008), pp. 13164–13171 (cit. on pp. 43, 77).
- [262]Nicholas A. Besley, Andrew T. B. Gilbert, and Peter M. W. Gill. “Self-consistent-field calculations of core excited states”. In: *J. Chem. Phys.* 130.12 (2009), p. 124308 (cit. on p. 43).
- [263]Giovanni Macetti and Alessandro Genoni. “Initial Maximum Overlap Method Embedded with Extremely Localized Molecular Orbitals for Core-Ionized States of Large Systems”. In: *Molecules* 28.1 (2023) (cit. on p. 43).
- [264]Kevin Carter-Fenk and John M. Herbert. “State-Targeted Energy Projection: A Simple and Robust Approach to Orbital Relaxation of Non-Aufbau Self-Consistent Field Solutions”. In: *J. Chem. Theory Comput.* 16.8 (2020), pp. 5067–5082 (cit. on pp. 43, 77).
- [265]Diptarka Hait and Martin Head-Gordon. “Excited State Orbital Optimization via Minimizing the Square of the Gradient: General Approach and Application to Singly and Doubly Excited States via Density Functional Theory”. In: *J. Chem. Theory Comput.* 16.3 (2020), pp. 1699–1710 (cit. on p. 43).
- [266]Hideo Fukutome. “Theory of the Unrestricted Hartree-Fock Equation and Its Solutions.I”. In: *Prog. Theor. Phys.* 45.5 (1971), pp. 1382–1406 (cit. on p. 43).
- [267]Hideo Fukutome. “Theory of the Unrestricted Hartree-Fock Equation and Its Solutions II: Classification and Characterization of UHF Solutions by Their Behavior for Spin Rotation and Time Reversal”. In: *Prog. Theor. Phys.* 52.1 (1974), pp. 115–130 (cit. on p. 43).
- [268]Hideo Fukutome. “Theory of the Unrestricted Hartree-Fock Equation and Its Solutions. III: Classification of Instabilities and Interconnection Relation between the Eight Classes of UHF Solutions”. In: *Prog. Theor. Phys.* 52.6 (1974), pp. 1766–1783 (cit. on p. 43).
- [269]B. N. Plakhutin, E. V. Gorelik, N. N. Breslavskaya, et al. “Anomalous values of $\langle \hat{S}^2 \rangle$ before and after annihilation of the first spin contaminant in UHF wave function”. In: *J. Struct. Chem.* 46.2 (2005), pp. 195–203 (cit. on p. 43).
- [270]Nobuaki Koga, Koichi Yamashita, and Keiji Morokuma. “On incorrect behavior of single annihilation equations of spin-projected UHF and UMP energies”. In: *Chem. Phys. Lett.* 184.4 (1991), pp. 359–362 (cit. on p. 43).

- [271]Ruben Pauncz. *Spin Eigenfunctions: Construction and Use*. Springer US, 1979 (cit. on p. 43).
- [272]Isaiah Shavitt. “The Graphical Unitary Group Approach and Its Application to Direct Configuration Interaction Calculations”. In: *The Unitary Group for the Evaluation of Electronic Energy Matrix Elements*. Ed. by Jürgen Hinze. Berlin, Heidelberg: Springer Berlin Heidelberg, 1981, pp. 51–99 (cit. on p. 43).
- [273]C. R. Sarma, M. A. H. Ahsan, and Sten Rettrup. “A graphical approach to permutation group representations for many-electron systems”. In: *Int. J. Quantum Chem.* 58.6 (1996), pp. 637–643 (cit. on p. 43).
- [274]William I. Salmon. “Genealogical Electronic Spin Eigenfunctions and Antisymmetric Many-Electron Wavefunctions Generated Directly from Young Diagrams”. In: ed. by Per-Olov Löwdin. Vol. 8. *Advances in Quantum Chemistry*. Academic Press, 1974, pp. 37–94 (cit. on p. 43).
- [275]Per-Olov Löwdin. “Angular Momentum Wavefunctions Constructed by Projector Operators”. In: *Rev. Mod. Phys.* 36 (4 1964), pp. 966–976 (cit. on p. 44).
- [276]Terry Amos and Lawrence C. Snyder. “Unrestricted Hartree–Fock Calculations. I. An Improved Method of Computing Spin Properties”. In: *J. Chem. Phys.* 41.6 (1964), pp. 1773–1783 (cit. on p. 44).
- [277]Per-Olov Löwdin and Osvaldo Goscinski. “The exchange phenomenon, the symmetric group, and the spin degeneracy problem”. In: *Int. J. Quantum Chem.* 4.S3B (1969), pp. 533–591 (cit. on p. 44).
- [278]Jr. Smith Vedene H. and Frank E. Harris. “Projection of Exact Spin Eigenfunctions”. In: *J. Math. Phys.* 10.4 (1969), pp. 771–778 (cit. on pp. 44, 144).
- [279]Carlos A. Jiménez-Hoyos, Thomas M. Henderson, Takashi Tsuchimochi, and Gustavo E. Scuseria. “Projected Hartree–Fock theory”. In: *J. Chem. Phys.* 136.16 (2012), p. 164109 (cit. on p. 45).
- [280]Uzi Kaldor. “Calculation of Extended Hartree-Fock Wavefunctions”. In: *J. Chem. Phys.* 48.2 (1968), pp. 835–837 (cit. on p. 45).
- [281]N. Bessis, H. Lefebvre-Brion, and C. M. Moser. “Calculation of Atomic Hyperfine Structure Constants from Projected Unrestricted Hartree-Fock Functions. Constants of F^{19} ”. In: *Phys. Rev.* 130 (4 1963), pp. 1441–1443 (cit. on p. 45).
- [282]A. T. Amos, G. G. Hall, and Harry Jones. “Single determinant wave functions”. In: *Proc. R. Soc. Lond. A* 263.1315 (1961), pp. 483–493 (cit. on p. 45).
- [283]Per-Olov Löwdin. “Expansion Theorems for the Total Wave Function and Extended Hartree-Fock Schemes”. In: *Rev. Mod. Phys.* 32 (2 1960), pp. 328–334 (cit. on pp. 45, 46, 77).
- [284]Nobuhiro Kosugi. “Exchange interaction in core excitation of diatomic systems”. In: *Chem. Phys.* 289.1 (2003). *Decay Processes in Core-excited Species*, pp. 117–134 (cit. on p. 46).

- [285]N. C. Handy, P. J. Knowles, and K. Somasundram. “On the convergence of the Møller-Plesset perturbation series”. In: *Theor. Chim. Acta* 68.1 (1985), pp. 87–100 (cit. on p. 46).
- [286]Uğur Bozkaya and C. David Sherrill. “Orbital-optimized MP2.5 and its analytic gradients: Approaching CCSD(T) quality for noncovalent interactions”. In: *J. Chem. Phys.* 141.20 (2014), p. 204105 (cit. on p. 46).
- [287]Matthias Loipersberger, Luke W. Bertels, Joonho Lee, and Martin Head-Gordon. “Exploring the Limits of Second- and Third-Order Møller–Plesset Perturbation Theories for Noncovalent Interactions: Revisiting MP2.5 and Assessing the Importance of Regularization and Reference Orbitals”. In: *J. Chem. Theory Comput.* 17.9 (2021), pp. 5582–5599 (cit. on p. 46).
- [288]Siba Suliman, Michal Pitoňák, Ivan Cernusak, and Florent Louis. “On the applicability of the MP2.5 approximation for open-shell systems. Case study of atmospheric reactivity”. In: *Comput. Theor. Chem.* 1186 (2020), p. 112901 (cit. on p. 46).
- [289]Uğur Bozkaya. “Accurate Electron Affinities from the Extended Koopmans’ Theorem Based on Orbital-Optimized Methods”. In: *J. Chem. Theory Comput.* 10.5 (2014), pp. 2041–2048 (cit. on p. 46).
- [290]H. Bernhard Schlegel. “Møller-Plesset perturbation theory with spin projection”. In: *J. Phys. Chem.* 92.11 (1988), pp. 3075–3078 (cit. on pp. 46, 49, 77).
- [291]Wei Chen and H. Bernhard Schlegel. “Evaluation of S^2 for correlated wave functions and spin projection of unrestricted Møller–Plesset perturbation theory”. In: *J. Chem. Phys.* 101.7 (1994), pp. 5957–5968 (cit. on pp. 48, 77).
- [292]Jiahua Wang, Axel D. Becke, and Jr. Smith Vedene H. “Evaluation of $\langle S^2 \rangle$ in restricted, unrestricted Hartree–Fock, and density functional based theories”. In: *J. Chem. Phys.* 102.8 (1995), pp. 3477–3480 (cit. on pp. 48, 153).
- [293]H. B. Schlegel. “Spin Contamination”. In: *Encyclopedia of Computational Chemistry*. Ed. by Paul von Ragué Schleyer, Norman L. Allinger, Tim Clark, et al. John Wiley & Sons Ltd, 1998, pp. 2665–2671 (cit. on pp. 49, 77).
- [294]H. Bernhard Schlegel. “Potential energy curves using unrestricted Møller–Plesset perturbation theory with spin annihilation”. In: *J. Chem. Phys.* 84.8 (1986), pp. 4530–4534 (cit. on p. 50).
- [295]R. Krishnan and J. A. Pople. “Approximate fourth-order perturbation theory of the electron correlation energy”. In: *Int. J. Quantum Chem.* 14.1 (1978), pp. 91–100 (cit. on p. 51).
- [296]Delano P. Chong. “Density-functional calculation of core-electron binding energies of C, N, O, and F”. In: *J. Chem. Phys.* 103.5 (1995), pp. 1842–1845 (cit. on pp. 51, 81).
- [297]Germán Cavagliasso and Delano P. Chong. “Accurate density-functional calculation of core-electron binding energies by a total-energy difference approach”. In: *J. Chem. Phys.* 111.21 (1999), pp. 9485–9492 (cit. on p. 51).
- [298]Delano P. Chong. “Localized and delocalized 1s core-holes in DFT calculations”. In: *J. Electron Spectrosc. Relat. Phenom.* 159.1 (2007), pp. 94–96 (cit. on p. 51).

- [299]Xuechen Zheng and Lan Cheng. “Performance of Delta-Coupled-Cluster Methods for Calculations of Core-Ionization Energies of First-Row Elements”. In: *J. Chem. Theory Comput.* 15.9 (2019), pp. 4945–4955 (cit. on pp. 52, 76).
- [300]A.P. Hitchcock and C.E. Brion. “Carbon K-shell excitation of C₂H₂, C₂H₄, C₂H₆ and C₆H₆ by 2.5 keV electron impact”. In: *J. Electron Spectrosc. Relat. Phenom.* 10.3 (1977), pp. 317–330 (cit. on pp. 53, 69–72).
- [301]George C. King, Frank H. Read, and Michel Tronc. “Investigation of the energy and vibrational structure of the inner shell $(1s)^{-1}(\pi 2p)^1\Pi$ state of the nitrogen molecule by electron impact with high resolution”. In: *Chem. Phys. Lett.* 52.1 (1977), pp. 50–54 (cit. on pp. 53, 69–72).
- [302]A P Hitchcock and C E Brion. “K-shell excitation of HF and F₂ studied by electron energy-loss spectroscopy”. In: *J. Phys. B: At. Mol. Phys.* 14.22 (1981), p. 4399 (cit. on pp. 53, 69–72).
- [303]Ph. Parent, F. Bournel, J. Lasne, et al. “The irradiation of ammonia ice studied by near edge x-ray absorption spectroscopy”. In: *J. Chem. Phys.* 131.15 (2009), p. 154308 (cit. on pp. 53, 69–72).
- [304]R. McLaren, S. A. C. Clark, I. Ishii, and A. P. Hitchcock. “Absolute oscillator strengths from K-shell electron-energy-loss spectra of the fluoroethenes and 1,3-perfluorobutadiene”. In: *Phys. Rev. A* 36 (4 1987), pp. 1683–1701 (cit. on pp. 53, 69–72).
- [305]A.P. Hitchcock and C.E. Brion. “Inner shell electron energy loss studies of HCN and C₂N₂”. In: *Chem. Phys.* 37.3 (1979), pp. 319–331 (cit. on pp. 53, 69–72).
- [306]M.B. Robin, I. Ishii, R. McLaren, and A.P. Hitchcock. “Fluorination effects on the inner-shell spectra of unsaturated molecules”. In: *J. Electron Spectrosc. Relat. Phenom.* 47 (1988), pp. 53–92 (cit. on pp. 53, 69–72).
- [307]Paulo Cabral do Couto, Daniel Hollas, and Petr Slavíček. “On the Performance of Optimally Tuned Range-Separated Hybrid Functionals for X-ray Absorption Modeling”. In: *J. Chem. Theory Comput.* 11.7 (2015), pp. 3234–3244 (cit. on pp. 53, 69–72).
- [308]A. P. Hitchcock, D. C. Newbury, I. Ishii, et al. “Carbon K-shell excitation of gaseous and condensed cyclic hydrocarbons: C₃H₆, C₄H₈, C₅H₈, C₅H₁₀, C₆H₁₀, C₆H₁₂, and C₈H₈”. In: *J. Chem. Phys.* 85.9 (1986), pp. 4849–4862 (cit. on pp. 53, 69–72).
- [309]Marc F. Tesch, Ronny Golnak, Felix Ehrhard, et al. “Analysis of the Electronic Structure of Aqueous Urea and Its Derivatives: A Systematic Soft X-Ray–TD-DFT Approach”. In: *Chem. Eur. J.* 22.34 (2016), pp. 12040–12049 (cit. on pp. 53, 69–72).
- [310]I. Ishii, R. McLaren, A. P. Hitchcock, and M. B. Robin. “Inner-shell excitations in weak-bond molecules”. In: *J. Chem. Phys.* 87.8 (1987), pp. 4344–4360 (cit. on pp. 53, 69–72).
- [311]Marc Simon, Michel Lavollee, Paul Morin, and Irene Nenner. “Photofragmentation of the Core-Excited s-Tetrazine Molecule Near the Carbon and Nitrogen K Edges”. In: *J. Phys. Chem.* 99.6 (1995), pp. 1733–1740 (cit. on pp. 53, 69–72).

- [312]F. Sette, J. Stöhr, and A. P. Hitchcock. “Determination of intramolecular bond lengths in gas phase molecules from *K* shell shape resonances”. In: *J. Chem. Phys.* 81.11 (1984), pp. 4906–4914 (cit. on pp. 53, 69–72).
- [313]Rana N.S. Sodhi and C.E. Brion. “High resolution carbon 1s and valence shell electronic excitation spectra of *trans*-1,3-butadiene and allene studied by electron energy loss spectroscopy”. In: *J. Electron Spectrosc. Relat. Phenom.* 37.1 (1985), pp. 1–21 (cit. on pp. 53, 69–72).
- [314]T. Gejo, K. Okada, and T. Ibuki. “Photoabsorption spectrum of ozone in the K-edge region”. In: *Chem. Phys. Lett.* 277.5 (1997), pp. 497–501 (cit. on pp. 53, 69–72).
- [315]E. Rühl and A.P. Hitchcock. “Oxygen K-shell excitation spectroscopy of hydrogen peroxide”. In: *Chem. Phys.* 154.2 (1991), pp. 323–329 (cit. on pp. 53, 69–72).
- [316]S.E. Michelin, K.T. Mazon, F. Arretche, et al. “Comparative study of electron-impact C(1s) core-excitation processes in C₂ and C₂N₂ molecules”. In: *J. Electron Spectrosc. Relat. Phenom.* 171.1 (2009), pp. 30–36 (cit. on pp. 53, 69–72).
- [317]G.R. Wight and C.E. Brion. “K-Shell energy loss spectra of 2.5 keV electrons in CO₂ and N₂O”. In: *J. Electron Spectrosc. Relat. Phenom.* 3.3 (1974), pp. 191–205 (cit. on pp. 53, 69–72).
- [318]Isao H. Suzuki and Norio Saito. “Cation pair formation from acetone following monochromatic soft x-ray absorption”. In: *Int. J. Mass Spectrom.* 198.3 (2000), pp. 165–172 (cit. on p. 53).
- [319]G.R. Wight and C.E. Brion. “K-shell excitations in NO and O₂ by 2.5 keV electron impact”. In: *J. Electron Spectrosc. Relat. Phenom.* 4.4 (1974), pp. 313–325 (cit. on pp. 53, 69–72).
- [320]J. A. Horsley, J. Stöhr, A. P. Hitchcock, et al. “Resonances in the *K* shell excitation spectra of benzene and pyridine: Gas phase, solid, and chemisorbed states”. In: *J. Chem. Phys.* 83.12 (1985), pp. 6099–6107 (cit. on pp. 53, 69–72).
- [321]D C Newbury, I Ishii, and A P Hitchcock. “Inner shell electron-energy loss spectroscopy of some heterocyclic molecules”. In: *Can. J. Chem.* 64.6 (1986), pp. 1145–1155 (cit. on pp. 53, 69–72).
- [322]C. T. Chen, Y. Ma, and F. Sette. “K-shell photoabsorption of the N₂ molecule”. In: *Phys. Rev. A* 40 (11 1989), pp. 6737–6740 (cit. on p. 73).
- [323]G.R. Wight, C.E. Brion, and M.J. Van Der Wiel. “K-shell energy loss spectra of 2.5 keV electrons in N₂ and CO”. In: *J. Electron Spectrosc. Relat. Phenom.* 1.5 (1972), pp. 457–469 (cit. on p. 73).
- [324]M. Nakamura, M. Sasanuma, S. Sato, et al. “Absorption Structure Near the *K* Edge of the Nitrogen Molecule”. In: *Phys. Rev.* 178 (1 1969), pp. 80–82 (cit. on p. 73).
- [325]Benjamin P. Pritchard, Doaa Altarawy, Brett Didier, Tara D. Gibson, and Theresa L. Windus. “New Basis Set Exchange: An Open, Up-to-Date Resource for the Molecular Sciences Community”. In: *J. Chem. Inf. Model.* 59.11 (2019), pp. 4814–4820 (cit. on pp. 53, 81).

- [326]Johanna P. Carbone, Lan Cheng, Rolf H. Myhre, et al. “Chapter Eleven - An analysis of the performance of coupled cluster methods for K-edge core excitations and ionizations using standard basis sets”. In: *State of The Art of Molecular Electronic Structure Computations: Correlation Methods, Basis Sets and More*. Ed. by Lorenzo Ugo Ancarani and Philip E. Hoggan. Vol. 79. Advances in Quantum Chemistry. Academic Press, 2019, pp. 241–261 (cit. on p. 55).
- [327]Ronit Sarangi, Marta L. Vidal, Sonia Coriani, and Anna I. Krylov. “On the basis set selection for calculations of core-level states: different strategies to balance cost and accuracy”. In: *Mol. Phys.* 118.19-20 (2020), e1769872 (cit. on p. 55).
- [328]Maximilien A. Ambroise and Frank Jensen. “Probing Basis Set Requirements for Calculating Core Ionization and Core Excitation Spectroscopy by the Δ Self-Consistent-Field Approach”. In: *J. Chem. Theory Comput.* 15.1 (2019), pp. 325–337 (cit. on p. 55).
- [329]Junichi Adachi, Nobuhiro Kosugi, Eiji Shigemasa, and Akira Yagishita. “Renner–Teller splitting in the $C1s \rightarrow \pi^*$ excited states of CS_2 , OCS , and CO_2 ”. In: *J. Chem. Phys.* 107.13 (1997), pp. 4919–4926 (cit. on p. 56).
- [330]Eva Muchova, Daniel Hollas, David M. P. Holland, et al. “Jahn–Teller effects in initial and final states: high-resolution X-ray absorption, photoelectron and Auger spectroscopy of allene”. In: *Phys. Chem. Chem. Phys.* 25 (9 2023), pp. 6733–6745 (cit. on p. 56).
- [331]Takashi Tsuchimochi and Troy Van Voorhis. “Extended Møller-Plesset perturbation theory for dynamical and static correlations”. In: *J. Chem. Phys.* 141.16 (2014), p. 164117 (cit. on p. 58).
- [332]Takashi Tsuchimochi and Seiichiro L. Ten-no. “Second-Order Perturbation Theory with Spin-Symmetry-Projected Hartree–Fock”. In: *J. Chem. Theory Comput.* 15.12 (2019), pp. 6688–6702 (cit. on p. 58).
- [333]Abdulgani Annaberdiyev, Cody A. Melton, M. Chandler Bennett, Guangming Wang, and Lubos Mitas. “Accurate Atomic Correlation and Total Energies for Correlation Consistent Effective Core Potentials”. In: *J. Chem. Theory Comput.* 16.3 (2020), pp. 1482–1502 (cit. on p. 59).
- [334]Clyde Edmiston and Klaus Ruedenberg. “Localized Atomic and Molecular Orbitals”. In: *Rev. Mod. Phys.* 35 (3 1963), pp. 457–464 (cit. on p. 59).
- [335]S. F. Boys. “Construction of Some Molecular Orbitals to Be Approximately Invariant for Changes from One Molecule to Another”. In: *Rev. Mod. Phys.* 32 (2 1960), pp. 296–299 (cit. on p. 59).
- [336]Andrzej A. Jarzęcki and Ernest R. Davidson. “Does Unrestricted Møller-Plesset Perturbation Theory for Low Spin Converge When the System Has a Triplet Ground State?” In: *The Journal of Physical Chemistry A* 102.24 (1998), pp. 4742–4746 (cit. on p. 59).
- [337]Diana-Gabriela Oprea and Hugh G.A. Burton. “Chapter Fourteen - Convergence of Møller-Plesset perturbation theory for excited reference states”. In: ed. by Philip E. Hoggan. Vol. 88. Advances in Quantum Chemistry. Academic Press, 2023, pp. 249–271 (cit. on p. 59).

- [338] Florian Weigend, Marco Häser, Holger Patzelt, and Reinhart Ahlrichs. “RI-MP2: optimized auxiliary basis sets and demonstration of efficiency”. In: *Chem. Phys. Lett.* 294.1 (1998), pp. 143–152 (cit. on p. 59).
- [339] Uğur Bozkaya. “Orbital-Optimized MP3 and MP2.5 with Density-Fitting and Cholesky Decomposition Approximations”. In: *J. Chem. Theory Comput.* 12.3 (2016), pp. 1179–1188 (cit. on p. 59).
- [340] Wojciech Skomorowski and Anna I. Krylov. “Feshbach–Fano approach for calculation of Auger decay rates using equation-of-motion coupled-cluster wave functions. I. Theory and implementation”. In: *J. Chem. Phys.* 154.8 (2021), p. 084124 (cit. on pp. 60, 96).
- [341] J. V. Ortiz. “Qualitative propagator theory of AX_4 Auger spectra”. In: *J. Chem. Phys.* 81.12 (1984), pp. 5873–5888 (cit. on pp. 60, 96).
- [342] Chunhai Fan and Zhentang Zhao, eds. *Synchrotron Radiation in Materials Science*. Wiley, 2018 (cit. on p. 75).
- [343] Xiaosong Liu, Wanli Yang, and Zhi Liu. “Recent Progress on Synchrotron-Based In-Situ Soft X-ray Spectroscopy for Energy Materials”. In: *Adv. Mater.* 26.46 (2014), pp. 7710–7729 (cit. on p. 75).
- [344] Feng Lin, Yijin Liu, Xiqian Yu, et al. “Synchrotron X-ray Analytical Techniques for Studying Materials Electrochemistry in Rechargeable Batteries”. In: *Chem. Rev.* 117.21 (2017), pp. 13123–13186 (cit. on p. 75).
- [345] Kaushik D. Nanda and Anna I. Krylov. “A simple molecular orbital picture of RIXS distilled from many-body damped response theory”. In: *J. Chem. Phys.* 152.24 (2020), p. 244118 (cit. on pp. 76, 96).
- [346] Kaoru Ohno and Tsubasa Aoki. “Extended quasiparticle approach to non-resonant and resonant X-ray emission spectroscopy”. In: *Phys. Chem. Chem. Phys.* 24 (27 2022), pp. 16586–16595 (cit. on p. 76).
- [347] Hans Ågren, Vincenzo Carravetta, Olav Vahtras, and Lars G. M. Pettersson. “Direct SCF direct static-exchange calculations of electronic spectra”. In: *Theor. Chem. Acc.* 97.1 (1997), pp. 14–40 (cit. on p. 76).
- [348] Carlos A. Marante, Loren Greenman, Cynthia S. Trevisan, et al. “Validity of the static-exchange approximation for inner-shell photoionization of polyatomic molecules”. In: *Phys. Rev. A* 102 (1 2020), p. 012815 (cit. on p. 76).
- [349] Kevin Carter-Fenk, Leonardo A. Cunha, Juan E. Arias-Martinez, and Martin Head-Gordon. “Electron-Affinity Time-Dependent Density Functional Theory: Formalism and Applications to Core-Excited States”. In: *J. Phys. Chem. Lett.* 13.41 (2022), pp. 9664–9672 (cit. on p. 76).
- [350] Marcel Nooijen and Rodney J. Bartlett. “Equation of motion coupled cluster method for electron attachment”. In: *J. Chem. Phys.* 102.9 (1995), pp. 3629–3647 (cit. on p. 76).

- [351] Marcel Nooijen and Rodney J. Bartlett. "Description of core-excitation spectra by the open-shell electron-attachment equation-of-motion coupled cluster method". In: *J. Chem. Phys.* 102.17 (1995), pp. 6735–6756 (cit. on p. 76).
- [352] L. S. Cederbaum and W. Domcke. "Localized and delocalized core holes and their interrelation". In: *J. Chem. Phys.* 66.11 (1977), pp. 5084–5086 (cit. on p. 76).
- [353] David Danovich. "Green's function methods for calculating ionization potentials, electron affinities, and excitation energies". In: *WIREs Comput. Mol. Sci.* 1.3 (2011), pp. 377–387 (cit. on p. 76).
- [354] L. S. Cederbaum and W. Domcke. "Theoretical Aspects of Ionization Potentials and Photoelectron Spectroscopy: A Green's Function Approach". In: *Advances in Chemical Physics* 36 (1977), pp. 205–344 (cit. on p. 76).
- [355] Marcel Nooijen and Jaap G. Snijders. "Coupled cluster Green's function method: Working equations and applications". In: *Int. J. Quantum Chem.* 48.1 (1993), pp. 15–48 (cit. on p. 76).
- [356] H. H. Corzo, Annia Galano, O. Dolgounitcheva, V. G. Zakrzewski, and J. V. Ortiz. "NR2 and P3+: Accurate, Efficient Electron-Propagator Methods for Calculating Valence, Vertical Ionization Energies of Closed-Shell Molecules". In: *J. Phys. Chem. A* 119.33 (2015), pp. 8813–8821 (cit. on p. 77).
- [357] Ernest Opoku, Filip Pawłowski, and J. V. Ortiz. "A new generation of diagonal self-energies for the calculation of electron removal energies". In: *J. Chem. Phys.* 155.20 (2021), p. 204107 (cit. on p. 77).
- [358] Ernest Opoku, Filip Pawłowski, and J. V. Ortiz. "Electron Propagator Self-Energies versus Improved GW100 Vertical Ionization Energies". In: *J. Chem. Theory Comput.* 18.8 (2022), pp. 4927–4944 (cit. on p. 77).
- [359] Ernest Opoku, Filip Pawłowski, and J. V. Ortiz. "Electron Propagator Theory of Vertical Electron Detachment Energies of Anions: Benchmarks and Applications to Nucleotides". In: *J. Phys. Chem. A* 127.4 (2023), pp. 1085–1101 (cit. on p. 77).
- [360] J. V. Ortiz. "An efficient, renormalized self-energy for calculating the electron binding energies of closed-shell molecules and anions". In: *Int. J. Quantum Chem.* 105.6 (2005), pp. 803–808 (cit. on p. 78).
- [361] J. V. Ortiz. "Dyson-orbital concepts for description of electrons in molecules". In: *J. Chem. Phys.* 153.7 (2020), p. 070902 (cit. on p. 78).
- [362] Manuel Díaz-Tinoco, Héctor H. Corzo, Filip Pawłowski, and J. V. Ortiz. "Do Dyson Orbitals resemble canonical Hartree-Fock orbitals?" In: *Mol. Phys.* 117.17 (2019), pp. 2275–2283 (cit. on p. 78).
- [363] Bibek Samal and Vamsee K. Voora. "Modeling Nonresonant X-ray Emission of Second- and Third-Period Elements without Core-Hole Reference States and Empirical Parameters". In: *J. Chem. Theory Comput.* 18.12 (2022), pp. 7272–7285 (cit. on p. 78).

- [364] Vinícius Vaz da Cruz, Sebastian Eckert, and Alexander Föhlisch. “TD-DFT simulations of K-edge resonant inelastic X-ray scattering within the restricted subspace approximation”. In: *Phys. Chem. Chem. Phys.* 23 (3 2021), pp. 1835–1848 (cit. on p. 78).
- [365] L. Triguero, L. G. M. Pettersson, and H. Ågren. “Calculations of X-ray Emission Spectra of Molecules and Surface Adsorbates by Means of Density Functional Theory”. In: *J. Phys. Chem. A* 102.52 (1998), pp. 10599–10607 (cit. on p. 78).
- [366] Rolf Manne. “Molecular Orbital Interpretation of X-Ray Emission Spectra: Simple Hydrocarbons and Carbon Oxides”. In: *J. Chem. Phys.* 52.11 (1970), pp. 5733–5739 (cit. on pp. 78, 94).
- [367] Hans Ågren and Joseph Nordgren. “Ab initio Hartree-Fock calculations of molecular X-ray intensities. Validity of one-center approximations”. In: *Theo. Chim. Acta* 58.2 (1981), pp. 111–119 (cit. on p. 78).
- [368] Kenneth E. Edgecombe and Russell J. Boyd. “Atomic orbital populations and atomic charges from self-consistent field molecular orbital wavefunctions”. In: *J. Chem. Soc., Faraday Trans. 2* 83 (8 1987), pp. 1307–1315 (cit. on p. 78).
- [369] W.H.E. Schwarz and Robert J. Buenker. “Use of the Z+1-core analogy model: examples from the core-excitation spectra of CO₂ and N₂O”. In: *Chem. Phys.* 13.2 (1976), pp. 153–160 (cit. on p. 81).
- [370] M. J. Frisch, G. W. Trucks, H. B. Schlegel, et al. *Gaussian Development Version Revision J.15*. Gaussian Inc. Wallingford CT. 2022 (cit. on p. 81).
- [371] Ankit Rohatgi. *Webplotdigitizer: Version 4.6*. 2022 (cit. on p. 81).
- [372] Hans Ågren, Lennart Selander, Joseph Nordgren, et al. “X-ray spectra and core hole energy curves of some diatomic molecules”. In: *Chem. Phys.* 37.2 (1979), pp. 161–171 (cit. on p. 82).
- [373] Jan-Erik Rubensson, Lennart Petersson, Nial Wassdahl, et al. “Radiative decay of multiply excited core hole states in H₂O”. In: *J. Chem. Phys.* 82.10 (1985), pp. 4486–4491 (cit. on pp. 82, 95).
- [374] Jan-Erik Rubensson, Nial Wassdahl, Ronald Brammer, and Joseph Nordgren. “Local electronic structure in simple alcohols studied in x-ray emission”. In: *J. Electron Spectrosc. Relat. Phenom.* 47 (1988), pp. 131–145 (cit. on pp. 82, 83).
- [375] P Glans, R E La Villa, Y Luo, H Agren, and J Nordgren. “X-ray emission spectroscopy measurements of fluorine substituted methanes”. In: *J. Phys. B: At. Mol. Opt. Phys.* 27.15 (1994), p. 3399 (cit. on pp. 83, 85–87).
- [376] L. O. Werme, J. Nordgren, H. Ågren, C. Nordling, and K. Siegbahn. “X-ray emission spectra of small molecules”. In: *Zeitschrift für Physik A Atoms and Nuclei* 272.2 (1975), pp. 131–141 (cit. on p. 83).
- [377] J Nordgren, H Agren, L O Werme, C Nordling, and K Siegbahn. “X-ray emission spectra of NH₃ and N₂O”. In: *J. Phys. B: At. Mol. Opt. Phys.* 9.2 (1976), p. 295 (cit. on p. 83).

- [378]Razib Obaid, Christian Buth, Georgi L Dakovski, et al. “LCLS in—photon out: fluorescence measurement of neon using soft x-rays”. In: *J. Phys. B: At. Mol. Opt. Phys.* 51.3 (2018), p. 034003 (cit. on p. 83).
- [379]L Pettersson, M Backstrom, R Brammer, et al. “Nitrogen and oxygen K emission spectra of nitrous oxide”. In: *J. Phys. B: At. Mol. Opt. Phys.* 17.9 (1984), p. L279 (cit. on p. 84).
- [380]R. Brammer, L. Pettersson, M. Bäckström, J. Nordgren, and C. Nordling. “The x-ray emission spectrum of gaseous ethene”. In: *Chem. Phys. Lett.* 106.5 (1984), pp. 425–427 (cit. on p. 84).
- [381]Timothy E. Meehan, Josephine McColl, and Frank P. Larkins. “Theoretical X-ray emission spectra for the fluoromethane molecules following carbon *K*-shell ionization”. In: *J. Electron Spectrosc. Relat. Phenom.* 73.3 (1995), pp. 283–292 (cit. on pp. 84–86).
- [382]Robert E. LaVilla. “Carbon and fluorine x-ray emission and fluorine *K* absorption spectra of the fluoromethane molecules, $\text{CH}_{4-n}\text{F}_n$ ($0 \leq n \leq 4$). II”. In: *J. Chem. Phys.* 58.9 (1973), pp. 3841–3848 (cit. on p. 85).
- [383]M. S. Banna, B. E. Mills, D. W. Davis, and D. A. Shirley. “X-ray photoemission molecular orbitals of hydrogen fluoride and the fluorinated methanes”. In: *J. Chem. Phys.* 61.11 (1974), pp. 4780–4786 (cit. on pp. 85, 87).
- [384]D. W. Davis, M. S. Banna, and D. A. Shirley. “Core-level binding-energy shifts in small molecules”. In: *J. Chem. Phys.* 60.1 (1974), pp. 237–245 (cit. on p. 87).
- [385]V. D. Yumatov, A. V. Okotrub, L. N. Mazalov, et al. “X-Ray spectra and electronic structure of the F_2 molecule”. In: *Journal of Structural Chemistry* 27.1 (1986), pp. 157–159 (cit. on p. 87).
- [386]P. Weightman, T. D. Thomas, and D. R. Jennison. “KVV Auger spectrum of F_2 : The importance of hole–hole correlation”. In: *J. Chem. Phys.* 78.4 (1983), pp. 1652–1662 (cit. on p. 87).
- [387]M Tronc, G C King, and F H Read. “Carbon K-shell excitation in small molecules by high-resolution electron impact”. In: *J. Phys. B: At. Mol. Opt. Phys.* 12.1 (1979), pp. 137–157 (cit. on pp. 87, 88, 91).
- [388]A.P. Hitchcock and C.E. Brion. “K-shell excitation spectra of CO , N_2 and O_2 ”. In: *J. Electron Spectrosc. Relat. Phenom.* 18.1 (1980), pp. 1–21 (cit. on p. 88).
- [389]Rana N.S. Sodhi and C.E. Brion. “Reference energies for inner shell electron energy-loss spectroscopy”. In: *J. Electron Spectrosc. Relat. Phenom.* 34.4 (1984), pp. 363–372 (cit. on p. 88).
- [390]R. Püttner, I. Dominguez, T. J. Morgan, et al. “Vibrationally resolved $\text{O } 1s$ core-excitation spectra of CO and NO ”. In: *Phys. Rev. A* 59 (5 1999), pp. 3415–3423 (cit. on p. 88).
- [391]E. Shigemasa, K. Ueda, Y. Sato, T. Sasaki, and A. Yagishita. “Symmetry-resolved *K*-shell photoabsorption spectra of free N_2 molecules”. In: *Phys. Rev. A* 45 (5 1992), pp. 2915–2921 (cit. on pp. 88, 89).

- [392]Y. Ma, C. T. Chen, G. Meigs, K. Randall, and F. Sette. “High-resolution K -shell photoabsorption measurements of simple molecules”. In: *Phys. Rev. A* 44 (3 1991), pp. 1848–1858 (cit. on p. 89).
- [393]G.R. Wight and C.E. Brion. “ K -shell excitation of CH_4 , NH_3 , H_2O , CH_3OH , CH_3OCH_3 and CH_3NH_2 by 2.5 keV electron impact”. In: *J. Electron Spectrosc. Relat. Phenom.* 4.1 (1974), pp. 25–42 (cit. on pp. 89, 90).
- [394]J. Schirmer, A. B. Trofimov, K. J. Randall, et al. “ K -shell excitation of the water, ammonia, and methane molecules using high-resolution photoabsorption spectroscopy”. In: *Phys. Rev. A* 47 (2 1993), pp. 1136–1147 (cit. on pp. 89, 90).
- [395]K C Prince, L Avaldi, M Coreno, R Camilloni, and M de Simone. “Vibrational structure of core to Rydberg state excitations of carbon dioxide and dinitrogen oxide”. In: *J. Phys. B: At. Mol. Opt. Phys.* 32.11 (1999), p. 2551 (cit. on pp. 90, 91).
- [396]Delano P. Chong. “Density functional theory calculation of K -shell excitation of nitrous oxide”. In: *Chem. Phys. Lett.* 441.4 (2007), pp. 209–212 (cit. on p. 91).
- [397]E. Rühl and A.P. Hitchcock. “Oxygen K -shell excitation spectroscopy of hydrogen peroxide”. In: *Chemical Physics* 154.2 (1991), pp. 323–329 (cit. on p. 91).
- [398]Robert E. LaVilla. “ $K \alpha$ Emission Spectrum of Gaseous N_2 ”. In: *J. Chem. Phys.* 56.5 (1972), pp. 2345–2349 (cit. on p. 93).
- [399]A.M. Velasco, C. Lavín, Manuel Díaz-Tinoco, and J.V. Ortiz. “CaH Rydberg series, oscillator strengths and photoionization cross sections from Molecular Quantum Defect and Dyson Orbital theories”. In: *J. Quant. Spectrosc. Radiat. Transf.* 187 (2017), pp. 161–166 (cit. on p. 92).
- [400]H.H. Corzo, A.M. Velasco, C. Lavín, and J.V. Ortiz. “MgH Rydberg series: Transition energies from electron propagator theory and oscillator strengths from the molecular quantum defect orbital method”. In: *J. Quant. Spectrosc. Radiat. Transf.* 206 (2018), pp. 323–327 (cit. on p. 92).
- [401]George C. King, Frank H. Read, and Michel Tronc. “Investigation of the energy and vibrational structure of the inner shell $(1s)^{-1}(\pi 2p)^1\Pi$ state of the nitrogen molecule by electron impact with high resolution”. In: *Chem. Phys. Lett.* 52.1 (1977), pp. 50–54 (cit. on p. 96).
- [402]Per Skytt, Jinghua Guo, Nial Wassdahl, et al. “Probing symmetry breaking upon core excitation with resonant x-ray fluorescence”. In: *Phys. Rev. A* 52 (5 1995), pp. 3572–3576 (cit. on p. 96).
- [403]L.S. Cederbaum, J. Schirmer, W. Domcke, and W. von Niessen. “Complete breakdown of the quasiparticle picture for inner valence electrons”. In: *J. Phys. B: At. Mol. Opt. Phys.* 10.15 (1977), p. L549 (cit. on p. 96).
- [404]J. V. Ortiz. “A nondiagonal, renormalized extension of partial third-order quasiparticle theory: Comparisons for closed-shell ionization energies”. In: *J. Chem. Phys.* 108.3 (1998), pp. 1008–1014 (cit. on pp. 96, 97).

- [405]O. Dolgounitcheva, V. G. Zakrzewski, and J. V. Ortiz. “Electron-propagator calculations on the photoelectron spectrum of ethylene”. In: *J. Chem. Phys.* 114.1 (2001), pp. 130–135 (cit. on p. 96).
- [406]Dirk R. Rehn, Andreas Dreuw, and Patrick Norman. “Resonant Inelastic X-ray Scattering Amplitudes and Cross Sections in the Algebraic Diagrammatic Construction/Intermediate State Representation (ADC/ISR) Approach”. In: *J. Chem. Theory Comput.* 13.11 (2017), pp. 5552–5559 (cit. on p. 96).
- [407]Y. Hori, M. Nishida, F.H. Lim, T. Ida, and M. Mizuno. “Simulation of molecular Auger spectra using a two-electron Dyson propagator”. In: *J. Electron Spectrosc. Relat. Phenom.* 207 (2016), pp. 60–64 (cit. on p. 96).
- [408]Anna Kristina Schnack-Petersen, Torsha Moitra, Sarai Dery Folkestad, and Sonia Coriani. “New Implementation of an Equation-of-Motion Coupled-Cluster Damped-Response Framework with Illustrative Applications to Resonant Inelastic X-ray Scattering”. In: *J. Phys. Chem. A* 127.7 (2023), pp. 1775–1793 (cit. on p. 96).
- [409]J. V. Ortiz. “Qualitative propagator theory of CH_3CN , CH_3NC , and CH_3CCH Auger spectra”. In: *J. Chem. Phys.* 83.9 (1985), pp. 4604–4617 (cit. on p. 96).
- [410]T. Ida and J. V. Ortiz. “Second-order, two-electron Dyson propagator theory: Comparisons for vertical double ionization potentials”. In: *J. Chem. Phys.* 129.8 (2008), p. 084105 (cit. on p. 96).
- [411]Dodi Heryadi, Danny L. Yeager, Joseph T. Golab, and Jeffrey A. Nichols. “Multi-configurational spin tensor electron propagator vertical ionization potentials for O_2 : Comparison to some other forefront methods using the same basis sets and geometries”. In: *J. Chem. Phys.* 102.23 (1995), pp. 9444–9445 (cit. on p. 96).
- [412]J. V. Ortiz. “Approximate Brueckner orbitals in electron propagator calculations”. In: *Int. J. Quantum Chem.* 75.4-5 (1999), pp. 615–621 (cit. on p. 96).
- [413]Masahiro Ehara and Hiroshi Nakatsuji. “Outer- and inner-valence ionization spectra of N_2 and CO : SAC-CI (general-R) compared with full-CI spectra”. In: *Chem. Phys. Lett.* 282.5 (1998), pp. 347–354 (cit. on p. 97).
- [414]I. Martín, A.C. Lavin, M. Velasco, et al. “Quantum defect orbital study of electronic transitions in Rydberg molecules: ammonium and fluoronium radicals”. In: *Chem. Phys.* 202.2 (1996), pp. 307–320 (cit. on p. 97).
- [415]Li Yang, Hans Ågren, Vincenzo Carravetta, and Lars G M Pettersson. “Static exchange and quantum defect analysis of x-ray absorption spectra of carbonyl compounds”. In: *Phys. Scr.* 54.6 (1996), p. 614 (cit. on p. 97).
- [416]J. V. Ortiz, I. Martín, A. M. Velasco, and C. Lavín. “Ground and excited states of NH_4 : Electron propagator and quantum defect analysis”. In: *J. Chem. Phys.* 120.17 (2004), pp. 7949–7954 (cit. on p. 97).
- [417]Wenjian Liu and Daoling Peng. “Exact two-component Hamiltonians revisited”. In: *J. Chem. Phys.* 131.3 (2009), p. 031104 (cit. on p. 97).

- [418] Maria Barysz and Andrzej J. Sadlej. “Two-component methods of relativistic quantum chemistry: from the Douglas–Kroll approximation to the exact two-component formalism”. In: *J. Mol. Struct. THEOCHEM* 573.1 (2001), pp. 181–200 (cit. on p. 97).
- [419] Filip Pawłowski and Joseph Vincent Ortiz. “Relativistic electron detachment energies and spin–orbit splittings from quasiparticle electron propagator calculations”. In: *Mol. Phys.* 118.14 (2020), e1700314 (cit. on p. 97).
- [420] Paul Adrien Maurice Dirac and Ralph Howard Fowler. “Quantum mechanics of many-electron systems”. In: *Proceedings of the Royal Society of London. Series A, Containing Papers of a Mathematical and Physical Character* 123.792 (1929), pp. 714–733 (cit. on p. 139).
- [421] Valerio Magnasco. *Elementary methods of molecular quantum mechanics*. Elsevier, 2006 (cit. on p. 140).
- [422] John E. Harriman. “Natural Expansion of the First-Order Density Matrix for a Spin-Projected Single Determinant”. In: *The Journal of Chemical Physics* 40.10 (1964), pp. 2827–2839 (cit. on p. 144).
- [423] P. A. M. Dirac. “Note on Exchange Phenomena in the Thomas Atom”. In: *Mathematical Proceedings of the Cambridge Philosophical Society* 26.3 (1930), pp. 376–385 (cit. on p. 145).
- [424] Per-Olov Löwdin. “Quantum Theory of Many-Particle Systems. II. Study of the Ordinary Hartree-Fock Approximation”. In: *Phys. Rev.* 97 (6 1955), pp. 1490–1508 (cit. on p. 145).
- [425] Ernest Davidson. *Reduced density matrices in quantum chemistry*. Vol. 6. Elsevier, 1976 (cit. on p. 145).
- [426] M Weissbluth. “Atoms and Molecules”, Acad”. In: *Press, New York* (1978) (cit. on p. 145).
- [427] E. Wigner and F. Seitz. “On the Constitution of Metallic Sodium”. In: *Phys. Rev.* 43 (10 1933), pp. 804–810 (cit. on p. 148).
- [428] J. C. Slater. “A Simplification of the Hartree-Fock Method”. In: *Phys. Rev.* 81 (3 1951), pp. 385–390 (cit. on p. 148).
- [429] Harry F. King, Richard E. Stanton, Hojing Kim, Robert E. Wyatt, and Robert G. Parr. “Corresponding Orbitals and the Nonorthogonality Problem in Molecular Quantum Mechanics”. In: *The Journal of Chemical Physics* 47.6 (1967), pp. 1936–1941 (cit. on p. 153).
- [430] P.J. Knowles and N.C. Handy. “A new determinant-based full configuration interaction method”. In: *Chemical Physics Letters* 111.4 (1984), pp. 315–321 (cit. on p. 154).

List of Figures

1.1	Flowchart for a Hartree-Fock SCF procedure	11
1.2	Table of spin symmetry constraints for RHF, ROHF, UHF, and GHF. . .	13
1.3	A Pople diagram for computational quantum chemistry	14
3.1	Mean absolute errors (eV) of UHF and PUHF for various basis set combinations. ^a	56
3.2	Mean absolute errors (eV) of UMP2 and PUMP2 for various basis set combinations. ^a	57
3.3	Mean absolute errors (eV) of UMP3 and PUMP3 for various basis set combinations. ^a	57
3.4	Mean absolute errors (eV) of UMP2.5 and PUMP2.5 for various basis set combinations. ^a	58
4.1	Model schematic for non-resonant XES with a closed shell reference. .	79
4.2	Model schematic for XAS with a closed shell reference.	80
4.3	Simulated emission spectra for N ₂ . IP _{core} computed with ΔPUMP3. EPT results and relative intensities obtained with a HF/cc-pVTZ reference. Experimental spectrum reprinted from Robert E. LaVilla, <i>J. Chem. Phys.</i> 56 , 2345–2349 (1972), Ref. [398], with the permission of AIP Publishing.	93
4.4	Simulated emission spectra for C ₂ H ₄ . IP _{core} computed with ΔPUMP3. EPT results obtained with a HF/cc-pVTZ reference. Relative intensities are obtained with an extended Hückel reference. Experimental spectrum reprinted from Rolf Manne, <i>J. Chem. Phys.</i> 52 , 5733–5739 (1970), Ref. [366], with the permission of AIP Publishing.	94
4.5	Simulated emission spectra for H ₂ O. IP _{core} computed with ΔPUMP3. EPT results and relative intensities obtained with a HF/cc-pVTZ reference. An alignment shift of -0.9 eV is applied to the simulated spectra. Experimental spectrum reprinted from Jan-Erik Rubensson, Lennart Petersson, Nial Wassdahl, Mats Bäckström, Joseph Nordgren, Olav M. Kvalheim, and Rolf Manne, <i>J. Chem. Phys.</i> 82 , 4486–4491 (1985), Ref. [373], with the permission of AIP Publishing.	95

A.1	Output for a spin-adapted UHF solution: H ₂ at 1.5 Å	157
A.2	Permutation tree for array {1100} with sub-arrays	158

List of Tables

2.1	Δ SCF vertical excitation energies ω_X for the lowest symmetry-allowed core to valence transition.	37
2.2	Mean absolute error (MAE) and root-mean-square error (RMSE) in eV.	37
2.3	Δ SCF + $\Delta\Sigma^{C(2)}$ vertical excitation energies ω_X for the lowest symmetry-allowed core to valence transition.	38
2.4	Mean absolute error (MAE) and root-mean-square error (RMSE) in eV.	38
2.5	Δ SCF + $\Delta\Sigma^{C(2)}$ vertical excitation energies ω_X for the lowest symmetry-allowed core to valence transition.	39
2.6	Mean absolute error (MAE) and root-mean-square error (RMSE) in eV.	39
2.7	Δ SCF vertical excitation energies ω_X for the lowest symmetry-allowed core to valence transition with core localization.	40
2.8	Mean absolute error (MAE) and root-mean-square error (RMSE) in eV.	40
3.1	Set of symmetrical molecules and experimental core-excitation energies at the C, N, O, and F K-edge.	53
3.2	Measure of errors w.r.t. experiment for symmetry-allowed vertical K-edge excitation energies (eV) computed without spin projection using different combinations of the 6-311G(d,p) basis set. ^{a,b}	61
3.3	Measure of errors w.r.t. experiment for symmetry-allowed vertical K-edge excitation energies (eV) computed with spin projection using different combinations of the 6-311G(d,p) basis set. ^{a,b}	62
3.4	Measure of errors w.r.t. experiment for symmetry-allowed vertical K-edge excitation energies (eV) computed without spin projection using different combinations of the 6-311+G(2df) basis set. ^{a,b}	63
3.5	Measure of errors w.r.t. experiment for symmetry-allowed vertical K-edge excitation energies (eV) computed with spin projection using different combinations of the 6-311+G(2df) basis set. ^{a,b}	64
3.6	Measure of errors w.r.t. experiment for symmetry-allowed vertical K-edge excitation energies (eV) computed without spin projection using different combinations of the cc-pVTZ basis set. ^{a,b}	65

3.7	Measure of errors w.r.t. experiment for symmetry-allowed vertical K -edge excitation energies (eV) computed with spin projection using different combinations of the cc-pVTZ basis set. ^{a,b}	66
3.8	Measure of errors w.r.t. experiment for symmetry-allowed vertical K -edge excitation energies (eV) computed without spin projection using different combinations of the aug-cc-pVTZ basis set. ^{a,b}	67
3.9	Measure of errors w.r.t. experiment for symmetry-allowed vertical K -edge excitation energies (eV) computed with spin projection using different combinations of the aug-cc-pVTZ basis set. ^{a,b}	68
3.10	Vertical K -edge excitation energies (eV) using u6-311+G(2df) without spin projection. ^a	69
3.11	Vertical K -edge excitation energies (eV) using u6-311+G(2df) with spin projection. ^a	70
3.12	Vertical K -edge excitation energies (eV) using ucc-pVTZ without spin projection. ^a	71
3.13	Vertical K -edge excitation energies (eV) using ucc-pVTZ with spin projection. ^a	72
3.14	Core-level valence and Rydberg transitions (eV) of N_2 . ^a	73
4.1	Vertical C-N-O-Ne K -edge emission energies \mathcal{E}_X computed with projected, Δ UHF, Δ MP n , and EPT [P3+].	82
4.2	Vertical C-F K -edge emission energies \mathcal{E}_X computed with projected Δ UHF, Δ MP n and EPT [P3+].	84
4.3	Vertical C-N-O K -edge excitation energies ω_X computed with projected Δ UHF, Δ MP n and EPT [P3+].	87

Spin-adapted Configuration State Functions

A.1 Spin Algebra

Let

$$UU^\dagger = U^\dagger U = \mathbf{1} \rightarrow \sum_r U_{rp}^* U_{rq} = \delta_{pq} \quad (\text{A.1})$$

$$\det(UU^\dagger) = \det(U^\dagger U) = \det(\mathbf{1}) = 1 \quad (\text{A.2})$$

$$\det(U^\dagger) \cdot \det(U) = \det(U) \cdot \det(U^\dagger) = 1 \quad (\text{A.3})$$

Here are unitary matrices that satisfy the conditions above

$$U = \begin{pmatrix} \cos \theta & -\sin \theta \\ \sin \theta & \cos \theta \end{pmatrix} \quad U^\dagger = \begin{pmatrix} \cos \theta & \sin \theta \\ -\sin \theta & \cos \theta \end{pmatrix} \quad (\text{A.4})$$

Using Euler's formula it is clear that

$$\det(U) = 1 \quad (\text{A.5})$$

An alternative expression also holds for $\phi \in [0, 2\pi)$. Note that it takes the form of a rotation operator

$$U = e^{i\phi} \quad (\text{A.6})$$

Consider an electronic wavefunction Ψ . Let us rotate the spin components about the z -axis. The unitary operator that generates such a rotation is

$$U_z(\phi) = e^{-i\phi(\mathbf{n}_z \cdot \frac{S_z}{\hbar})} \quad \text{or} \quad U_z(\phi) = e^{-i(\frac{\phi}{2})(\mathbf{n}_z \cdot \sigma_z)} \quad (\text{A.7})$$

The unit vector in the z -direction is \mathbf{n}_z and σ_z is again z Pauli matrix. Using Euler's identity we can expand the operator

$$U_z(\phi) = \cos\left(\frac{\phi}{2}\right) - i\sigma_z \sin\left(\frac{\phi}{2}\right) \quad (\text{A.8})$$

If we do a full 2π rotation about the z -axis, observe the action of $U_z(\phi)$ on $|\Psi\rangle$

$$U_z(2\pi) |\Psi\rangle = (-1) |\Psi\rangle \quad (\text{A.9})$$

We merely have a global phase change

$$|\Psi'\rangle = -|\Psi\rangle \quad (\text{A.10})$$

If we wish to revert back to the original Ψ from the transformed Ψ' , we must perform another 2π rotation

$$U_z(2\pi)U_z(2\pi) |\Psi\rangle = |\Psi\rangle \quad (\text{A.11})$$

After two unitary rotations, we get back Ψ . This is attainable if we restrict the types of unitary matrices to those with determinants equal to 1. This particular subgroup of unitary matrices belongs to the special unitary group $SU(2)$. It just so happens that for fermions, the Pauli matrices are suitable basis representations for $SU(2)$ symmetry. This defines the algebra we use to study the physics of electron spin.

The Pauli matrices, which are Hermitian and unitary, are useful representations of spin symmetry operations

$$\sigma_x = \begin{pmatrix} 0 & 1 \\ 1 & 0 \end{pmatrix} \quad \sigma_y = \begin{pmatrix} 0 & i \\ -i & 0 \end{pmatrix} \quad \sigma_z = \begin{pmatrix} 1 & 0 \\ 0 & -1 \end{pmatrix} \quad (\text{A.12})$$

The related spin operators (in atomic units) are

$$S_x = \frac{1}{2}\sigma_x \quad S_y = \frac{1}{2}\sigma_y \quad S_z = \frac{1}{2}\sigma_z \quad (\text{A.13})$$

With these, the total spin is defined as

$$S = \hat{\mathbf{i}}S_x + \hat{\mathbf{j}}S_y + \hat{\mathbf{k}}S_z \quad (\text{A.14})$$

For use below, we define the product of total spins for a single particle

$$S^2 = S \cdot S \quad (\text{A.15})$$

$$= (\hat{\mathbf{i}}S_x + \hat{\mathbf{j}}S_y + \hat{\mathbf{k}}S_z) \cdot (\hat{\mathbf{i}}S_x + \hat{\mathbf{j}}S_y + \hat{\mathbf{k}}S_z) \quad (\text{A.16})$$

$$= (\hat{\mathbf{i}} \cdot \hat{\mathbf{i}})S_xS_x + (\hat{\mathbf{j}} \cdot \hat{\mathbf{j}})S_yS_y + (\hat{\mathbf{k}} \cdot \hat{\mathbf{k}})S_zS_z \quad (\text{A.17})$$

$$= S_x^2 + S_y^2 + S_z^2 \quad (\text{A.18})$$

The total spin-squared operator is defined in terms of the sum of the total spin of two particles

$$\mathcal{S}^2 = (S_1 + S_2) \cdot (S_1 + S_2) \quad (\text{A.19})$$

$$= S_1^2 + S_2^2 + 2S_1S_2 \quad (\text{A.20})$$

For the term corresponding to the first particle index, we have

$$S_1^2 = S_1 \cdot S_1 \quad (\text{A.21})$$

$$= S_{x_1}^2 + S_{y_1}^2 + S_{z_1}^2 \quad (\text{A.22})$$

Similarly, for the second particle index

$$S_2^2 = S_2 \cdot S_2 \quad (\text{A.23})$$

$$= S_{x_2}^2 + S_{y_2}^2 + S_{z_2}^2 \quad (\text{A.24})$$

It can be shown for each of the squared terms operating on one given index return a scalar and the identity matrix

$$S_x^2 = \frac{1}{4} \begin{pmatrix} 1 & 0 \\ 0 & 1 \end{pmatrix} \quad S_y^2 = \frac{1}{4} \begin{pmatrix} 1 & 0 \\ 0 & 1 \end{pmatrix} \quad S_z^2 = \frac{1}{4} \begin{pmatrix} 1 & 0 \\ 0 & 1 \end{pmatrix} \quad (\text{A.25})$$

Additionally we have:

$$2S_1S_2 = 2(S_{x_1}S_{x_2} + S_{y_1}S_{y_2} + S_{z_1}S_{z_2}) \quad (\text{A.26})$$

Let us apply S^2 on a two electron spin function $|\alpha\beta\rangle$ indexed lexicographically

$$S^2 |\alpha\beta\rangle = S_1^2 + S_2^2 + 2S_1S_2 |\alpha\beta\rangle \quad (\text{A.27})$$

$$= ((S_{x_1}^2 + S_{y_1}^2 + S_{z_1}^2) + (S_{x_2}^2 + S_{y_2}^2 + S_{z_2}^2) + 2(S_{x_1}S_{x_2} + S_{y_1}S_{y_2} + S_{z_1}S_{z_2})) |\alpha\beta\rangle \quad (\text{A.28})$$

For simplicity, we may expand and evaluate the terms separately

$$(S_{x_1}^2 + S_{y_1}^2 + S_{z_1}^2) |\alpha\beta\rangle = \frac{3}{4} |\alpha\beta\rangle \quad (\text{A.29})$$

$$(S_{x_2}^2 + S_{y_2}^2 + S_{z_2}^2) |\alpha\beta\rangle = \frac{3}{4} |\alpha\beta\rangle \quad (\text{A.30})$$

$$2(S_{x_1}S_{x_2} + S_{y_1}S_{y_2} + S_{z_1}S_{z_2})|\alpha\beta\rangle = 2\left[S_{x_1}S_{x_2}|\alpha\beta\rangle + S_{y_1}S_{y_2}|\alpha\beta\rangle + S_{z_1}S_{z_2}|\alpha\beta\rangle\right] \quad (\text{A.31})$$

$$= 2\left[\left(\frac{1}{2}\right)\left(\frac{1}{2}\right)|\beta\alpha\rangle + \left(\frac{i}{2}\right)\left(-\frac{i}{2}\right)|\beta\alpha\rangle + \left(\frac{1}{2}\right)\left(-\frac{1}{2}\right)|\alpha\beta\rangle\right] \quad (\text{A.32})$$

$$= |\beta\alpha\rangle - \frac{1}{2}|\alpha\beta\rangle \quad (\text{A.33})$$

After combining terms, we recover the Dirac identity⁴²⁰

$$\mathcal{S}^2|\alpha\beta\rangle = \frac{3}{4}|\alpha\beta\rangle + \frac{3}{4}|\alpha\beta\rangle + |\beta\alpha\rangle - \frac{1}{2}|\alpha\beta\rangle \quad (\text{A.34})$$

$$= \frac{6}{4}|\alpha\beta\rangle + |\beta\alpha\rangle - \frac{2}{4}|\alpha\beta\rangle \quad (\text{A.35})$$

$$= |\alpha\beta\rangle + |\beta\alpha\rangle \quad (\text{A.36})$$

$$= (\mathbf{1} + \mathcal{P}_{12})|\alpha\beta\rangle \quad (\text{A.37})$$

Observe that the action of \mathcal{S}^2 on $|\alpha\beta\rangle$ is linked to the permutation of spin indices via \mathcal{P}_{12} . Using the expressions defined above, we can recast \mathcal{S}^2 into a more general form

$$\mathcal{S}^2 = \sum_i^N S(i) \cdot S(i) + 2 \sum_{i<j}^N S(i) \cdot S(j) \quad (\text{A.38})$$

$$= \frac{3}{4}N + \sum_{i<j}^N \left(-\frac{1}{2}\mathbb{1} + \mathcal{P}_{ij} \right) \quad (\text{A.39})$$

$$= \frac{3}{4}N + \sum_i^N \left(-\frac{1}{2}\mathbb{1} \right) \sum_j^{N-1} \left(\frac{1}{2}\mathbb{1} \right) + \sum_{i<j}^N \mathcal{P}_{ij} \quad (\text{A.40})$$

$$= \frac{3}{4}N + \left(-\frac{N}{2} \right) \left(\frac{N-1}{2} \right) + \sum_{i<j}^N \mathcal{P}_{ij} \quad (\text{A.41})$$

$$= \frac{3N - N^2 + N}{4} + \sum_{i<j}^N \mathcal{P}_{ij} \quad (\text{A.42})$$

$$= \frac{-N^2 + 4N}{4} + \sum_{i<j}^N \mathcal{P}_{ij} \quad (\text{A.43})$$

$$= \frac{-N(N-4)}{4} + \sum_{i<j}^N \mathcal{P}_{ij} \quad (\text{A.44})$$

which is a recognizable formula for the \mathcal{S}^2 operator.⁴⁰

\mathcal{S}^2 acts on a reference state vector Θ_0

$$\mathcal{S}^2 \Theta_0 = \frac{-N(N-4)}{4} \Theta_0 + \sum_{i<j}^N \mathcal{P}_{ij} \Theta_0 \quad (\text{A.45})$$

This formula is equivalent to more commonly used ladder operator deductions of \mathcal{S}^2 .

A.2 Spin Projection

Spin projection operators can be used to construct spin-adapted configuration state functions (SACSFs).¹ Take the following spin projection operator

¹See P.O. Löwdin *Phys. Rev.* 97, 1509 (1955)³⁰ and *Elementary Methods of Molecular Quantum Mechanics*⁴²¹

$$\mathcal{O}_k = \prod_{s \neq k} \frac{\mathcal{S}^2 - s(s+1)}{k(k+1) - s(s+1)} \quad (\text{A.46})$$

where k is the target spin quantum number, s is the higher spin state quantum number, and \mathcal{S}^2 is the total spin-squared operator. The number of linearly independent SACSFs with S spin is given by the Wigner formula

$$f(N, S) = \frac{(2S+1)N!}{\left(\frac{N}{2} - S\right)! \left(\frac{N}{2} + S + 1\right)!} \quad (\text{A.47})$$

The total number of SACSFs is then

$$2^N = \sum_S [2S+1] f(N, S) \quad (\text{A.48})$$

Recall that

$$\mathcal{S}^2 = \frac{-N(N-4)}{4} + \sum_{i < j}^N \mathcal{P}_{ij} \quad (\text{A.49})$$

where

$$\zeta = \frac{n!}{r!(n-r)!} \quad (\text{A.50})$$

and $r = 2$ for unique pairwise permutations.

Successive application of \mathcal{O}_k on a reference configuration can generate the manifold of normalizable k spin states. When necessary, one can apply Schmidt orthogonalization on the resulting vectors remove to linear dependencies.

For example, take a reference determinant ψ_0 defined as $|\alpha\beta\rangle$. To reiterate, we seek to generate the correct linear combinations of spin configurations that are eigenstates of \mathcal{S}^2 . The one permutation needed is \mathcal{P}_{12} , which gives the configuration

$|\beta\alpha\rangle$. Application of \mathcal{S}^2 will show that the high-spin $M_s = \pm 1$ configurations ($|\alpha\alpha\rangle$ and $|\beta\beta\rangle$) are already triplet eigenstates. The $M_s = 0$ configurations will be spin-adapted into a singlet and triplet upon projection. The SACSFs, denoted by ${}^{2S+1}\Theta_{M_s}$, are then

$${}^3\Theta_1 = |\alpha\alpha\rangle \quad (\text{A.51})$$

$${}^1\Theta_0 = \frac{1}{\sqrt{2}} |\alpha\beta - \beta\alpha\rangle \quad (\text{A.52})$$

$${}^3\Theta_0 = \frac{1}{\sqrt{2}} |\alpha\beta + \beta\alpha\rangle \quad (\text{A.53})$$

$${}^3\Theta_{-1} = |\beta\beta\rangle \quad (\text{A.54})$$

For another example, a reference determinant ψ_0 is defined as $|\alpha\beta\alpha\rangle$.

Each spin eigenfunction is built from components within an M_s block. The 2^N ($N=3$) different spin configurations are

- | | |
|--|--|
| 1. $\alpha\alpha\alpha$ ($M_s = +\frac{3}{2}$) | 5. $\alpha\beta\beta$ ($M_s = -\frac{1}{2}$) |
| 2. $\beta\alpha\alpha$ ($M_s = +\frac{1}{2}$) | 6. $\beta\alpha\beta$ ($M_s = -\frac{1}{2}$) |
| 3. $\alpha\beta\alpha$ ($M_s = +\frac{1}{2}$) | 7. $\beta\beta\alpha$ ($M_s = -\frac{1}{2}$) |
| 4. $\alpha\alpha\beta$ ($M_s = +\frac{1}{2}$) | 8. $\beta\beta\beta$ ($M_s = -\frac{3}{2}$) |

The \mathcal{S}^2 operator for a three electron system is

$$\mathcal{S}^2 = \frac{3}{4}I + \mathcal{P}_{12} + \mathcal{P}_{23} + \mathcal{P}_{13}$$

Operating Eq. A.46 on $|\alpha\beta\alpha\rangle$ yields the following SACSFs

S^2	S	M_s	Spin-Adapted CSFs :: $^{2S+1}\Theta_{M_s}$
3.75	$\frac{3}{2}$	$+\frac{3}{2}$	$^4\Theta_{\frac{3}{2}} = \alpha\alpha\alpha\rangle$
3.75	$\frac{3}{2}$	$+\frac{1}{2}$	$^4\Theta_{\frac{1}{2}} = \frac{1}{\sqrt{3}}(\beta\alpha\alpha\rangle + \alpha\beta\alpha\rangle + \alpha\alpha\beta\rangle)$
3.75	$\frac{3}{2}$	$-\frac{1}{2}$	$^4\Theta_{-\frac{1}{2}} = \frac{1}{\sqrt{3}}(\alpha\beta\beta\rangle + \beta\alpha\beta\rangle + \beta\beta\alpha\rangle)$
0.75	$\frac{1}{2}$	$+\frac{1}{2}$	$^2\Theta_{\frac{1}{2}} = \frac{1}{\sqrt{6}}(\beta\alpha\alpha\rangle + \alpha\beta\alpha\rangle - 2 \alpha\alpha\beta\rangle)$
0.75	$\frac{1}{2}$	$-\frac{1}{2}$	$^2\Theta_{-\frac{1}{2}} = \frac{1}{\sqrt{6}}(\alpha\beta\beta\rangle + \beta\alpha\beta\rangle - 2 \beta\beta\alpha\rangle)$
0.75	$\frac{1}{2}$	$+\frac{1}{2}$	$^2\Theta_{\frac{1}{2}} = \frac{1}{\sqrt{2}}(\beta\alpha\alpha\rangle - \alpha\beta\alpha\rangle)$
0.75	$\frac{1}{2}$	$-\frac{1}{2}$	$^2\Theta_{-\frac{1}{2}} = \frac{1}{\sqrt{2}}(\alpha\beta\beta\rangle - \beta\alpha\beta\rangle)$
3.75	$\frac{3}{2}$	$-\frac{3}{2}$	$^4\Theta_{-\frac{3}{2}} = \beta\beta\beta\rangle$

Alternatively, the S^2 matrix itself can be constructed. For example, the solution to the following matrix element is

$$\begin{aligned}
\langle\alpha\beta\alpha|S^2|\alpha\beta\alpha\rangle &= \langle\alpha\beta\alpha|\frac{3}{4}I + \mathcal{P}_{12} + \mathcal{P}_{23} + \mathcal{P}_{13}|\alpha\beta\alpha\rangle \\
&= \frac{3}{4}\langle\alpha\beta\alpha|\alpha\beta\alpha\rangle + \langle\alpha\beta\alpha|\beta\alpha\alpha\rangle + \langle\alpha\beta\alpha|\alpha\alpha\beta\rangle + \langle\alpha\beta\alpha|\alpha\beta\alpha\rangle \\
&= \frac{3}{4}\langle\alpha|\alpha\rangle\langle\beta|\beta\rangle\langle\alpha|\alpha\rangle + \langle\alpha|\beta\rangle\langle\beta|\alpha\rangle\langle\alpha|\alpha\rangle + \langle\alpha|\alpha\rangle\langle\beta|\alpha\rangle\langle\alpha|\beta\rangle \\
&\quad + \langle\alpha|\alpha\rangle\langle\beta|\beta\rangle\langle\alpha|\alpha\rangle \\
&= \frac{3}{4} + 1 \\
&= \frac{7}{4} \\
&= 1.75
\end{aligned}$$

The entire S^2 matrix can then be generated in a similar fashion

	$\alpha\alpha\alpha$	$\beta\alpha\alpha$	$\alpha\beta\alpha$	$\alpha\alpha\beta$	$\alpha\beta\beta$	$\beta\alpha\beta$	$\beta\beta\alpha$	$\beta\beta\beta$
$\alpha\alpha\alpha$	3.75	0	0	0	0	0	0	0
$\beta\alpha\alpha$	0	1.75	1	1	0	0	0	0
$\alpha\beta\alpha$	0	1	1.75	1	0	0	0	0
$\alpha\alpha\beta$	0	1	1	1.75	0	0	0	0
$\alpha\beta\beta$	0	0	0	0	1.75	1	1	0
$\beta\alpha\beta$	0	0	0	0	1	1.75	1	0
$\beta\beta\alpha$	0	0	0	0	1	1	1.75	0
$\beta\beta\beta$	0	0	0	0	0	0	0	3.75

We can then diagonalize the matrix to obtain the eigenvectors and eigenvalues. The weights for each S^2 eigenvector component are essentially modified Clebsch–Gordan expansion coefficients. Historically, among quantum chemists, these are called Sanibel coefficients as the construction of SACSFs was once a popular topic at the Sanibel Symposium.^{37,278} A SACSF can be expressed as

$$\Theta(S, M, N) = \sum_{j=0}^N C_j(S, M, N) [\alpha^{\mu-j} \beta^j] [\alpha^j \beta^{\nu-j}]$$

where [...] is the sum of all $\alpha\beta$ permutations of that bracket function. Here is one of many formulas to generate the Sanibel coefficients

$$C_j(S, M, n) = \frac{2S+1}{1+n+S} \sum_{k=0}^{S-M} (-1)^{j+S-M-k} \binom{S-M}{k} \binom{S+M}{S-M-k} \binom{n+S}{\mu-j+k}^{-1}$$

where μ is $n\alpha$, and ν is $n\beta$ and n is $\frac{N}{2}$. Furthermore, there is the recursion relation⁴²²

$$C_j(S, M, n) - C_{j+1}(S, M, n) = C_j(S, M, n-1)$$

A.3 Density Matrices and Operators for Many-Body Systems

Density matrices contain information about the probability distributions of many-body quantum systems. Reduced density matrices for many-electron systems enable the solution of expectation values for N -body Hermitian operators.^{40,423–426} Take a Slater determinant constructed with a set of spin orbitals $\{\chi\}$.

$$|\Psi\rangle = \frac{1}{\sqrt{N!}} \begin{vmatrix} \chi_1(\mathbf{x}_1) & \chi_2(\mathbf{x}_1) & \cdots & \chi_N(\mathbf{x}_1) \\ \chi_1(\mathbf{x}_2) & \chi_2(\mathbf{x}_2) & \cdots & \chi_N(\mathbf{x}_2) \\ \vdots & \vdots & \ddots & \vdots \\ \chi_1(\mathbf{x}_N) & \chi_2(\mathbf{x}_N) & \cdots & \chi_N(\mathbf{x}_N) \end{vmatrix} \quad (\text{A.55})$$

The one particle density matrix (1PDM) is defined as

$$\gamma(\mathbf{x}'_1; \mathbf{x}_1) = N \int \Psi^*(\mathbf{x}'_1, \mathbf{x}_2, \mathbf{x}_3, \dots, N) \Psi(\mathbf{x}_1, \mathbf{x}_2, \mathbf{x}_3, \dots, N) d\mathbf{x}_2, \dots, d\mathbf{x}_N \quad (\text{A.56})$$

Above, we perform an integration over all coordinates except \mathbf{x}_1 . Note that these coordinates are separable functions of spin and space

$$\chi(\mathbf{x}) = \phi(\mathbf{r})\sigma(\omega) \quad (\text{A.57})$$

The eigendecomposition of the 1PDM gives natural orbitals and natural orbital occupation numbers between 0 and 1 (inclusive). In this section, we assume binary occupations.

The two particle density matrix (2PDM) is

$$\Gamma(\mathbf{x}'_1 \mathbf{x}'_2; \mathbf{x}_1 \mathbf{x}_2) = \frac{N!}{2!(N-2)!} \int \Psi^*(\mathbf{x}'_1, \mathbf{x}'_2, \mathbf{x}_3, \dots, N) \Psi(\mathbf{x}_1, \mathbf{x}_2, \mathbf{x}_3, \dots, N) d\mathbf{x}_3, \dots, d\mathbf{x}_N \quad (\text{A.58})$$

Here, we integrate over all coordinates except \mathbf{x}_1 and \mathbf{x}_2 and the primes indicate different coordinates. Clearly, we are inspecting two particles ($N = 2$) at a time and can rewrite the 2PDM in an abbreviated form

$$\Gamma(\mathbf{x}'_1 \mathbf{x}'_2; \mathbf{x}_1 \mathbf{x}_2) = \Psi^*(\mathbf{x}'_1, \mathbf{x}'_2) \Psi(\mathbf{x}_1, \mathbf{x}_2) \quad (\text{A.59})$$

Expanding $\Psi^*(\mathbf{x}'_1, \mathbf{x}'_2)$ and $\Psi(\mathbf{x}_1, \mathbf{x}_2)$, we get

$$\Psi^*(\mathbf{x}'_1, \mathbf{x}'_2) = \frac{1}{\sqrt{2}} [\chi_1^*(\mathbf{x}'_1) \chi_2^*(\mathbf{x}'_2) - \chi_1^*(\mathbf{x}'_2) \chi_2^*(\mathbf{x}'_1)] \quad (\text{A.60})$$

and

$$\Psi(\mathbf{x}_1, \mathbf{x}_2) = \frac{1}{\sqrt{2}} [\chi_1(\mathbf{x}_1) \chi_2(\mathbf{x}_2) - \chi_1(\mathbf{x}_2) \chi_2(\mathbf{x}_1)] \quad (\text{A.61})$$

Substitute into $\Gamma(\mathbf{x}'_1 \mathbf{x}'_2; \mathbf{x}_1 \mathbf{x}_2)$

$$\begin{aligned} \Gamma(\mathbf{x}'_1 \mathbf{x}'_2; \mathbf{x}_1 \mathbf{x}_2) &= \frac{1}{2} [\chi_1^*(\mathbf{x}'_1) \chi_2^*(\mathbf{x}'_2) - \chi_1^*(\mathbf{x}'_2) \chi_2^*(\mathbf{x}'_1)] \\ &\quad \times [\chi_1(\mathbf{x}_1) \chi_2(\mathbf{x}_2) - \chi_1(\mathbf{x}_2) \chi_2(\mathbf{x}_1)] \end{aligned} \quad (\text{A.62})$$

$$\begin{aligned} &= \frac{1}{2} [\chi_1^*(\mathbf{x}'_1) \chi_1(\mathbf{x}_1) \chi_2^*(\mathbf{x}'_2) \chi_2(\mathbf{x}_2) - \chi_1^*(\mathbf{x}'_2) \chi_1(\mathbf{x}_1) \chi_2^*(\mathbf{x}'_1) \chi_2(\mathbf{x}_2) \\ &\quad - \chi_1^*(\mathbf{x}'_1) \chi_1(\mathbf{x}_2) \chi_2^*(\mathbf{x}'_2) \chi_2(\mathbf{x}_1) + \chi_1^*(\mathbf{x}'_2) \chi_1(\mathbf{x}_2) \chi_2^*(\mathbf{x}'_1) \chi_2(\mathbf{x}_1)] \end{aligned} \quad (\text{A.63})$$

The 1PDM can be written as a general expansion over spin-orbitals with one-particle coordinates

$$\gamma(\mathbf{x}'_1; \mathbf{x}_1) = \sum_i^N \chi_i^*(\mathbf{x}'_1) \chi_i(\mathbf{x}_1) \quad (\text{A.64})$$

$$\gamma(\mathbf{x}'_2; \mathbf{x}_2) = \sum_i^N \chi_i^*(\mathbf{x}'_2) \chi_i(\mathbf{x}_2) \quad (\text{A.65})$$

$$\gamma(\mathbf{x}'_2; \mathbf{x}_1) = \sum_i^N \chi_i^*(\mathbf{x}'_2) \chi_i(\mathbf{x}_1) \quad (\text{A.66})$$

$$\gamma(\mathbf{x}'_1; \mathbf{x}_2) = \sum_i^N \chi_i^*(\mathbf{x}'_1) \chi_i(\mathbf{x}_2) \quad (\text{A.67})$$

Using the above expressions, the 2PDM can be written in terms of 1PDMs

$$\Gamma(\mathbf{x}'_1 \mathbf{x}'_2; \mathbf{x}_1 \mathbf{x}_2) = \frac{1}{2} [\gamma(\mathbf{x}'_1; \mathbf{x}_1) \gamma(\mathbf{x}'_2; \mathbf{x}_2) - \gamma(\mathbf{x}'_2; \mathbf{x}_1) \gamma(\mathbf{x}'_1; \mathbf{x}_2)] \quad (\text{A.68})$$

For spin-restricted methods, the 1PDM is built from identical α and β orbitals. For example,

$$\gamma(\mathbf{x}'_1; \mathbf{x}_1) = \sum_i^{N/2} \phi_i^*(\mathbf{r}'_1) \phi_i(\mathbf{r}_1) \sigma^*(\alpha'_1) \sigma(\alpha_1) + \sum_i^{N/2} \phi_i^*(\mathbf{r}'_1) \phi_i(\mathbf{r}_1) \sigma^*(\beta'_1) \sigma(\beta_1) \quad (\text{A.69})$$

For spin-unrestricted methods, we use different orbitals for different spins (DODS) to build the 1PDM

$$\gamma(\mathbf{x}'_1; \mathbf{x}_1) = \sum_i^{N_\alpha} \phi_i^*(\mathbf{r}'_1) \phi_i(\mathbf{r}_1) \sigma^*(\alpha'_1) \sigma(\alpha_1) + \sum_{\bar{j}}^{N_\beta} \phi_{\bar{j}}^*(\mathbf{r}'_1) \phi_{\bar{j}}(\mathbf{r}_1) \sigma^*(\beta'_1) \sigma(\beta_1) \quad (\text{A.70})$$

When working with unrestricted orbitals, the 2PDM can be decomposed into its spin components

$$\begin{aligned}
\Gamma(\mathbf{r}'_1\omega'_1\mathbf{r}'_2\omega'_2; \mathbf{r}_1\omega_1\mathbf{r}_2\omega_2) &= \Gamma^{\alpha\alpha;\alpha\alpha}(\mathbf{r}'_1\alpha'_1\mathbf{r}'_2\alpha'_2; \mathbf{r}_1\alpha_1\mathbf{r}_2\alpha_2) \\
&+ \Gamma^{\alpha\beta;\alpha\beta}(\mathbf{r}'_1\alpha'_1\mathbf{r}'_2\beta'_2; \mathbf{r}_1\alpha_1\mathbf{r}_2\beta_2) \\
&+ \Gamma^{\beta\alpha;\beta\alpha}(\mathbf{r}'_1\beta'_1\mathbf{r}'_2\alpha'_2; \mathbf{r}_1\beta_1\mathbf{r}_2\alpha_2) \\
&+ \Gamma^{\beta\beta;\beta\beta}(\mathbf{r}'_1\beta'_1\mathbf{r}'_2\beta'_2; \mathbf{r}_1\beta_1\mathbf{r}_2\beta_2)
\end{aligned} \tag{A.71}$$

The second and third terms correspond to the 2PDMs with off-diagonal spin coordinates. A useful property of integrating over the diagonal indices ($\mathbf{x}'_1 = \mathbf{x}_1$) of the 2PDM is

$$\int \Gamma(\mathbf{x}_1\mathbf{x}_2; \mathbf{x}_1\mathbf{x}_2) d\mathbf{x}_1 d\mathbf{x}_2 = \frac{N(N-1)}{2} \tag{A.72}$$

We also know that the electronic 2PDM is Hermitian and must satisfy the antisymmetry principle. If two indices are equal ($\mathbf{x}_1 = \mathbf{x}_2$), the matrix will be zero^{427,428} (i.e. Fermi or exchange “hole”)

$$\Gamma(\mathbf{x}_1\mathbf{x}_1; \mathbf{x}_1\mathbf{x}_1) = 0 \tag{A.73}$$

For the pair densities $\Gamma^{\alpha\alpha;\alpha\alpha}$ and $\Gamma^{\beta\beta;\beta\beta}$, the inner products of spin functions $\sigma^*(\alpha_1)\sigma(\alpha_1)$, $\sigma^*(\alpha_2)\sigma(\alpha_2)$, $\sigma^*(\beta_1)\sigma(\beta_1)$, and $\sigma^*(\beta_2)\sigma(\beta_2)$ integrate to unity. In a similar manner as the total 2PDM, integrating over the remaining spatial indices yields:

$$\int \Gamma^{\alpha\alpha;\alpha\alpha}(\mathbf{r}_1\mathbf{r}_2; \mathbf{r}_1\mathbf{r}_2) d\mathbf{r}_1 d\mathbf{r}_2 = \frac{N_\alpha(N_\alpha-1)}{2} \tag{A.74}$$

and

$$\int \Gamma^{\beta\beta;\beta\beta}(\mathbf{r}_1\mathbf{r}_2; \mathbf{r}_1\mathbf{r}_2) d\mathbf{r}_1 d\mathbf{r}_2 = \frac{N_\beta(N_\beta-1)}{2} \tag{A.75}$$

We shall see that the 2PDM and its (spatial) diagonal elements are sufficient for describing real-space expectation values for linear Hermitian operators. One may expand an N -body operator \mathcal{O} into the following series:

$$\mathcal{O} = \mathcal{O}_0 + \sum_i^N \mathcal{O}_i + \frac{1}{2!} \sum_{i \neq j}^N \mathcal{O}_{ij} + \frac{1}{3!} \sum_{i \neq j \neq k}^N \mathcal{O}_{ijk} + \dots \quad (\text{A.76})$$

Each additional index, starting at i , augments the order of \mathcal{O} . For a two-body operator, its expectation value for a normalized quantum state Ψ is given by:

$$\langle \mathcal{O}_{ij} \rangle = \int \Psi^*(\mathbf{x}'_1, \mathbf{x}'_2, \mathbf{x}'_3, \dots, N) \left[\frac{1}{2!} \sum_{i \neq j}^N \mathcal{O}_{ij} \right] \Psi(\mathbf{x}_1, \mathbf{x}_2, \mathbf{x}_3, \dots, N) d\mathbf{x} \quad (\text{A.77})$$

Invoke the interchange theorem

$$\langle \mathcal{O}_{ij} \rangle = \frac{1}{2!} \sum_{i \neq j}^N \int \Psi^*(\mathbf{x}'_1, \mathbf{x}'_2, \mathbf{x}'_3, \dots, N) \mathcal{O}_{ij} \Psi(\mathbf{x}_1, \mathbf{x}_2, \mathbf{x}_3, \dots, N) d\mathbf{x} \quad (\text{A.78})$$

$$= \frac{1}{2} \sum_i^N \sum_j^{N-1} \int \Psi^*(\mathbf{x}'_1, \mathbf{x}'_2, \mathbf{x}'_3, \dots, N) \mathcal{O}_{ij} \Psi(\mathbf{x}_1, \mathbf{x}_2, \mathbf{x}_3, \dots, N) d\mathbf{x} \quad (\text{A.79})$$

Let us take the example where \mathcal{O} operates on particles with indices \mathbf{x}_1 and \mathbf{x}_2 only.

$$\langle \mathcal{O}_{12} \rangle = \frac{1}{2} N(N-1) \int \Psi^*(\mathbf{x}'_1, \mathbf{x}'_2) \mathcal{O}_{12} \Psi(\mathbf{x}_1, \mathbf{x}_2) d\mathbf{x}_1 d\mathbf{x}_2 (d\mathbf{x}_3, \dots, d\mathbf{x}_N) \quad (\text{A.80})$$

From our definition of the 2PDM, we can reformulate this expression

$$\langle \mathcal{O}_{12} \rangle = \int \mathcal{O}_{12} \Gamma(\mathbf{x}'_1 \mathbf{x}'_2; \mathbf{x}_1 \mathbf{x}_2) d\mathbf{x}_1 d\mathbf{x}_2 \quad (\text{A.81})$$

After applying the action of operator \mathcal{O}_{12} , we set the primed coordinates of the bra-space equal to those of the ket-space ($\mathbf{x}'_1 = \mathbf{x}_1, \mathbf{x}'_2 = \mathbf{x}_2$) as we are, for

now, concerned only the diagonal elements (in spatial coordinates) of the density operator.

\mathcal{S}^2 is a two-body operator. It is composed of an integer term and a summation over all unique permutations over electrons or spin labels. We will use the pairwise spin permutation operator \mathcal{P}_{ij}^σ

$$\mathcal{S}^2 = \frac{-N(N-4)}{4} + \sum_{i < j}^N \mathcal{P}_{ij}^\sigma \quad (\text{A.82})$$

Its expectation value, in Dirac notation:

$$\langle \mathcal{S}^2 \rangle = \langle \Psi | \mathcal{S}^2 | \Psi \rangle \quad (\text{A.83})$$

$$\begin{aligned} \langle \mathcal{S}^2 \rangle &= \int \Psi^*(\mathbf{x}'_1, \mathbf{x}'_2, \mathbf{x}'_3, \dots, N) \left[\frac{-N(N-4)}{4} \right] \Psi^*(\mathbf{x}_1, \mathbf{x}_2, \mathbf{x}_3, \dots, N) d\mathbf{x} \\ &+ \int \mathcal{P}_{12}^\sigma \Gamma(\mathbf{x}_1 \mathbf{x}_2; \mathbf{x}_1 \mathbf{x}_2) d\mathbf{x}_1 d\mathbf{x}_2 \end{aligned} \quad (\text{A.84})$$

$$\begin{aligned} &= \frac{-N(N-4)}{4} \int \Psi^*(\mathbf{x}'_1, \mathbf{x}'_2, \mathbf{x}'_3, \dots, N) \Psi^*(\mathbf{x}_1, \mathbf{x}_2, \mathbf{x}_3, \dots, N) d\mathbf{x} \\ &+ \iint \mathcal{P}_{12}^\sigma \Gamma(\mathbf{r}'_1 \omega'_1 \mathbf{r}'_2 \omega'_2; \mathbf{r}_1 \omega_1 \mathbf{r}_2 \omega_2) d\mathbf{r}_1 d\omega_1 d\mathbf{r}_2 d\omega_2 \end{aligned} \quad (\text{A.85})$$

$$= \frac{-N(N-4)}{4} + \iint \Gamma(\mathbf{r}_1 \omega_1 \mathbf{r}_2 \omega_2; \mathbf{r}_1 \omega_2 \mathbf{r}_2 \omega_1) d\mathbf{r}_1 d\omega_1 d\mathbf{r}_2 d\omega_2 \quad (\text{A.86})$$

The primes are dropped after applying the permutation operator which swaps the spin labels for the ket-side coordinates. Spin is then integrated out for \mathbf{x}_1 and \mathbf{x}_2 . Since we can conveniently work in an orthogonal basis and the wavefunction Ψ is normalized, we have $\langle \Psi | \Psi \rangle = 1$. Thus, the integer term remains. Now the total spin-squared expectation value becomes

$$\langle \mathcal{S}^2 \rangle = \frac{-N(N-4)}{4} + \int \Gamma^{\sigma\sigma; \sigma\sigma}(\mathbf{r}_1 \mathbf{r}_2; \mathbf{r}_1 \mathbf{r}_2) d\mathbf{r}_1 d\mathbf{r}_2 \quad (\text{A.87})$$

Decomposition of the permuted 2PDM into its spin components gives us a clearer interpretation of what quantities are needed for computing an \mathcal{S}^2 matrix element

$$\begin{aligned} \langle \mathcal{S}^2 \rangle = & \frac{-N(N-4)}{4} + \int \left[\Gamma^{\alpha\alpha;\alpha\alpha}(\mathbf{r}_1\mathbf{r}_2; \mathbf{r}_1\mathbf{r}_2) + \Gamma^{\alpha\beta;\beta\alpha}(\mathbf{r}_1\mathbf{r}_2; \mathbf{r}_1\mathbf{r}_2) \right. \\ & \left. + \Gamma^{\beta\alpha;\alpha\beta}(\mathbf{r}_1\mathbf{r}_2; \mathbf{r}_1\mathbf{r}_2) + \Gamma^{\beta\beta;\beta\beta}(\mathbf{r}_1\mathbf{r}_2; \mathbf{r}_1\mathbf{r}_2) \right] d\mathbf{r}_1 d\mathbf{r}_2 \end{aligned} \quad (\text{A.88})$$

Due to the following property of Hermitian matrices, we can show that $\Gamma^{\alpha\beta;\beta\alpha}$ and $\Gamma^{\beta\alpha;\alpha\beta}$ are equivalent

$$\Gamma(\mathbf{x}'_1\mathbf{x}'_2; \mathbf{x}_1\mathbf{x}_2) = \Gamma^*(\mathbf{x}_1\mathbf{x}_2; \mathbf{x}'_1\mathbf{x}'_2) \quad (\text{A.89})$$

Recall solutions to the integrals over the pair densities $\Gamma^{\alpha\alpha;\alpha\alpha}$ and $\Gamma^{\beta\beta;\beta\beta}$. Also recall that $N = N_\alpha + N_\beta$ with $N_\alpha \geq N_\beta$. We will now proceed with some tedious algebra

$$\begin{aligned} \langle \mathcal{S}^2 \rangle = & \frac{-(N_\alpha + N_\beta)((N_\alpha + N_\beta) - 4)}{4} + \frac{N_\alpha(N_\alpha - 1)}{2} + \frac{N_\beta(N_\beta - 1)}{2} \\ & + 2 \int \Gamma^{\alpha\beta;\beta\alpha}(\mathbf{r}_1, \mathbf{r}_2; \mathbf{r}_1, \mathbf{r}_2) d\mathbf{r}_1 d\mathbf{r}_2 \end{aligned} \quad (\text{A.90})$$

Expand

$$\begin{aligned} \langle \mathcal{S}^2 \rangle = & -\frac{N_\alpha^2}{4} - \frac{2N_\alpha N_\beta}{4} + \frac{4N_\alpha}{4} - \frac{N_\beta^2}{4} + \frac{4N_\beta}{4} + \frac{N_\alpha^2 - N_\alpha}{2} + \frac{N_\beta^2 - N_\beta}{2} \\ & + 2 \int \Gamma^{\alpha\beta;\beta\alpha}(\mathbf{r}_1, \mathbf{r}_2; \mathbf{r}_1, \mathbf{r}_2) d\mathbf{r}_1 d\mathbf{r}_2 \end{aligned} \quad (\text{A.91})$$

Separate terms the last two terms before the integral and find common denominators

$$\begin{aligned} \langle \mathcal{S}^2 \rangle = & -\frac{N_\alpha^2}{4} - \frac{2N_\alpha N_\beta}{4} + \frac{4N_\alpha}{4} - \frac{N_\beta^2}{4} + \frac{4N_\beta}{4} + \frac{2N_\alpha^2}{4} - \frac{2N_\alpha}{4} + \frac{2N_\beta^2}{4} - \frac{2N_\beta}{4} \\ & + 2 \int \Gamma^{\alpha\beta;\beta\alpha}(\mathbf{r}_1, \mathbf{r}_2; \mathbf{r}_1, \mathbf{r}_2) d\mathbf{r}_1 d\mathbf{r}_2 \end{aligned} \quad (\text{A.92})$$

Simplify and group terms, leaving an extra N_β

$$\langle S^2 \rangle = \frac{N_\alpha^2}{4} + \frac{N_\beta^2}{4} - \frac{2N_\alpha N_\beta}{4} + \frac{N_\alpha}{2} - \frac{N_\beta}{2} + N_\beta + 2 \int \Gamma^{\alpha\beta;\beta\alpha}(\mathbf{r}_1, \mathbf{r}_2; \mathbf{r}_1, \mathbf{r}_2) d\mathbf{r}_1 d\mathbf{r}_2 \quad (\text{A.93})$$

Notice some terms are factorable

$$\langle S^2 \rangle = \frac{N_\alpha - N_\beta}{2} \left(\frac{N_\alpha - N_\beta}{2} + 1 \right) + N_\beta + 2 \int \Gamma^{\alpha\beta;\beta\alpha}(\mathbf{r}_1, \mathbf{r}_2; \mathbf{r}_1, \mathbf{r}_2) d\mathbf{r}_1 d\mathbf{r}_2 \quad (\text{A.94})$$

And for collinear spin

$$S_z = \frac{N_\alpha - N_\beta}{2} \quad (\text{A.95})$$

Rendering

$$\langle S^2 \rangle = S_z (S_z + 1) + N_\beta + 2 \int \Gamma^{\alpha\beta;\beta\alpha}(\mathbf{r}_1, \mathbf{r}_2; \mathbf{r}_1, \mathbf{r}_2) d\mathbf{r}_1 d\mathbf{r}_2 \quad (\text{A.96})$$

This is an expression for S^2 matrix elements between the same determinant. The integrand will vary depending on orbital differences between determinants used to calculate matrix elements—following the Slater-Condon rules for two-electron operators.

A.4 S^2 Matrix Elements

Let's demonstrate this by defining three Slater determinants which we will use to derive the different expressions for diagonal and off-diagonal elements of the S^2 matrix. These determinants will also aid in the construction of generalized 1PDMs and 2PDMs.

$$|\Psi\rangle = \frac{1}{\sqrt{N!}} |\cdots pq \cdots| \quad (\text{A.97})$$

$$|\Phi\rangle = \frac{1}{\sqrt{N!}} |\cdots pr \cdots| \quad (\text{A.98})$$

$$|\Xi\rangle = \frac{1}{\sqrt{N!}} |\cdots rs \cdots| \quad (\text{A.99})$$

MOs labeled p, q, r and s can be from the orthonormal set of $\alpha \{i, k, m, o, q, s, \dots\}$ or $\beta \{\bar{j}, \bar{l}, \bar{n}, \bar{p}, \bar{r}, \bar{t}, \dots\}$ orbitals.

Two additional items to consider. There is a phase factor related to the number of permutations required to align the orbitals between determinants. We assume the wavefunctions are normalized:

$$(-1)^P \langle \cdots \chi_k \chi_l \cdots | \mathcal{S}^2 | \cdots \chi_k \chi_l \cdots \rangle \quad (\text{A.100})$$

Also, determinants built from the exact same orthonormal basis but differ by one or more orbitals (α or β) will lead to a determinantal overlap of zero.⁴²⁹

There are three main cases to consider when solving the \mathcal{S}^2 matrix elements.²⁹² The determinants can be the same, differ by one α or β orbital, or differ by one α and β orbital. Matrix elements between determinants that differ by two α or β orbitals will be zero. Also, differences of three or more orbitals will be zero.

Case I: No Difference

$$\langle \Psi | \mathcal{S}^2 | \Psi \rangle = S_z (S_z + 1) + N_\beta - \sum_{i\bar{j}}^{N_{occ}} \mathbb{S}_{ji} \mathbb{S}_{i\bar{j}} \quad (\text{A.101})$$

$$= S_z (S_z + 1) + N_\beta - \sum_{i\bar{j}}^{N_{occ}} |\mathbb{S}_{i\bar{j}}|^2 \quad (\text{A.102})$$

Case IIA: 1 α Difference

$$\langle \Psi | \mathcal{S}^2 | \Phi \rangle = -(-1)^{\mathbf{p}_i + \mathbf{p}_k} \sum_{\bar{j}}^{N_{occ}^\beta} \mathbb{S}_{k\bar{j}} \mathbb{S}_{\bar{j}i} \quad (\text{A.103})$$

Case IIB: 1 β Difference

Same procedure as IIA. The sum will run over i to N_{occ}^α ; orbitals common to $\langle \Psi |$ and $| \Phi \rangle$.

Case IIIAB: 1 α and 1 β Difference

$$\langle \Psi | \mathcal{S}^2 | \Xi \rangle = -(-1)^{\mathbf{p}_i + \mathbf{p}_k + \mathbf{p}_j + \mathbf{p}_l} \mathbb{S}_{i\bar{l}} \mathbb{S}_{\bar{j}k} \quad (\text{A.104})$$

This is a unique element with no sum.

So far, we have assumed the electrons reside in hydrogenic orbitals where the spatial overlaps are 0 or 1. Molecular orbitals are delocalized and the overlap integrals must be calculated. In RHF, the α and β MO coefficients are the same, so the result is “perfect pairing” with δ_{ij} overlaps. In spin-polarized or UHF calculations, the α and β MO coefficients are not necessarily the same and the $\alpha\beta$ MO overlaps are not simply zero or unity. In this case, the third term in Eq. A.101 will not cancel completely with N_β . This is where spin contamination in single reference UHF calculations originates. The recoupling of angular momentum (including L and J) through spin adaption is needed to alleviate the ambiguity in spin state assignments.

A.5 Implementation

Configuration interaction (CI) can be performed in a spin-adapted basis. To define a data structure, we use occupation number representation⁴³⁰ to create α and β string determinants that each have a leading dimension of nBasis. For both α and β strings, we assign occupied orbitals with 1 and virtual orbitals with 0.

Molecular orbitals (MOs) with α spin are denoted as $\{i, k, m, o, q, s, \dots\}$ and those with β spin as $\{\bar{j}, \bar{l}, \bar{n}, \bar{p}, \bar{r}, \bar{t}, \dots\}$.

$$|\psi\rangle = |110 : \overline{100}\rangle \longrightarrow |ik\bar{j}\rangle$$

Overlaps between same-spin MOs equate to δ_{pq} . For example, $\mathbb{S}_{ii} = 1$ whereas $\mathbb{S}_{ik} = 0$. Elements of the $\alpha\beta$ MO overlap matrix ($\mathbb{S}_{\alpha\beta}$) will be in the range of $[-1, 1]$.

Full configuration interaction (FCI) effectively scales $\mathcal{O}(N!)$ and can quickly become an intractable feat. Instead, a feasible truncated approximation is desired. We can start by utilizing the CI *ansatz* to selectively construct a basis of singly (S) and doubly (D) substituted determinants given a reference electronic state ψ_0 , such as a converged unrestricted Hartree-Fock (UHF) solution. The S^2 matrix would then be

$$\mathcal{S}_{SD}^2 = \begin{bmatrix} \langle \psi_0 | \mathcal{S}^2 | \psi_0 \rangle & \langle \psi_0 | \mathcal{S}^2 | \psi_i^a \rangle & \cdots & \langle \psi_0 | \mathcal{S}^2 | \psi_{ij}^{ab} \rangle & \cdots & \langle \psi_0 | \mathcal{S}^2 | \psi_{yz}^{mn} \rangle \\ \langle \psi_i^a | \mathcal{S}^2 | \psi_0 \rangle & \langle \psi_i^a | \mathcal{S}^2 | \psi_i^a \rangle & \cdots & \langle \psi_i^a | \mathcal{S}^2 | \psi_{ij}^{ab} \rangle & \cdots & \langle \psi_i^a | \mathcal{S}^2 | \psi_{yz}^{mn} \rangle \\ \vdots & \vdots & \ddots & \vdots & \vdots & \vdots \\ \langle \psi_{ij}^{ab} | \mathcal{S}^2 | \psi_0 \rangle & \langle \psi_{ij}^{ab} | \mathcal{S}^2 | \psi_i^a \rangle & \cdots & \langle \psi_{ij}^{ab} | \mathcal{S}^2 | \psi_{ij}^{ab} \rangle & \cdots & \langle \psi_{ij}^{ab} | \mathcal{S}^2 | \psi_{yz}^{mn} \rangle \\ \vdots & \vdots & \vdots & \vdots & \ddots & \vdots \\ \langle \psi_{yz}^{mn} | \mathcal{S}^2 | \psi_0 \rangle & \langle \psi_{yz}^{mn} | \mathcal{S}^2 | \psi_i^a \rangle & \cdots & \cdots & \cdots & \langle \psi_{yz}^{mn} | \mathcal{S}^2 | \psi_{yz}^{mn} \rangle \end{bmatrix}$$

The size of the \mathcal{S}^2 matrix depends on the number of determinants.

Singles and Doubles:

$$\begin{aligned} nDet = & \left(N_{occ}^\alpha * N_{virt}^\alpha \right) + \left(N_{occ}^\beta * N_{virt}^\beta \right) + \left(\binom{N_{occ}^\alpha}{2} * \binom{N_{virt}^\alpha}{2} \right) \\ & + \left(\binom{N_{occ}^\beta}{2} * \binom{N_{virt}^\beta}{2} \right) + \left(\left(N_{occ}^\alpha * N_{virt}^\alpha \right) * \left(N_{occ}^\beta * N_{virt}^\beta \right) \right) \end{aligned}$$

Full Space:

$$nDet = \frac{N_{basis}!}{N_{occ}^{\alpha}! N_{virt}^{\alpha}!} * \frac{N_{basis}!}{N_{occ}^{\beta}! N_{virt}^{\beta}!}$$

With the increasing amount of substituted determinants used, the time and space complexity of the problem grows immensely with the number of electrons and basis functions. Let us examine the simple case of the H₂ molecule at 1.5 Å with a minimal basis where a broken symmetry UHF solution is used. The \mathcal{S}^2 matrix in the space of singles and doubles is

$${}_{H_2}\mathcal{S}_{SD}^2 = \begin{bmatrix} \langle \psi_0 | \mathcal{S}^2 | \psi_0 \rangle & \langle \psi_0 | \mathcal{S}^2 | \psi_i^k \rangle & \langle \psi_0 | \mathcal{S}^2 | \psi_j^{\bar{l}} \rangle & \langle \psi_0 | \mathcal{S}^2 | \psi_{ij}^{k\bar{l}} \rangle \\ \langle \psi_i^k | \mathcal{S}^2 | \psi_0 \rangle & \langle \psi_i^k | \mathcal{S}^2 | \psi_i^k \rangle & \langle \psi_i^k | \mathcal{S}^2 | \psi_j^{\bar{l}} \rangle & \langle \psi_i^k | \mathcal{S}^2 | \psi_{ij}^{k\bar{l}} \rangle \\ \langle \psi_j^{\bar{l}} | \mathcal{S}^2 | \psi_0 \rangle & \langle \psi_j^{\bar{l}} | \mathcal{S}^2 | \psi_i^k \rangle & \langle \psi_j^{\bar{l}} | \mathcal{S}^2 | \psi_j^{\bar{l}} \rangle & \langle \psi_j^{\bar{l}} | \mathcal{S}^2 | \psi_{ij}^{k\bar{l}} \rangle \\ \langle \psi_{ij}^{k\bar{l}} | \mathcal{S}^2 | \psi_0 \rangle & \langle \psi_{ij}^{k\bar{l}} | \mathcal{S}^2 | \psi_i^k \rangle & \langle \psi_{ij}^{k\bar{l}} | \mathcal{S}^2 | \psi_j^{\bar{l}} \rangle & \langle \psi_{ij}^{k\bar{l}} | \mathcal{S}^2 | \psi_{ij}^{k\bar{l}} \rangle \end{bmatrix}$$

$${}_{H_2}\mathcal{S}_{SD}^2 = \begin{bmatrix} 1 - |\mathbb{S}_{ij}^{\bar{l}}|^2 & -\mathbb{S}_{k\bar{j}}\mathbb{S}_{\bar{j}i} & -\mathbb{S}_{\bar{j}i}\mathbb{S}_{i\bar{l}} & -\mathbb{S}_{i\bar{l}}\mathbb{S}_{k\bar{j}} \\ -\mathbb{S}_{k\bar{j}}\mathbb{S}_{\bar{j}i} & 1 - |\mathbb{S}_{k\bar{j}}|^2 & -\mathbb{S}_{i\bar{j}}\mathbb{S}_{k\bar{l}} & -\mathbb{S}_{k\bar{l}}\mathbb{S}_{k\bar{j}} \\ -\mathbb{S}_{\bar{j}i}\mathbb{S}_{i\bar{l}} & -\mathbb{S}_{i\bar{j}}\mathbb{S}_{k\bar{l}} & 1 - |\mathbb{S}_{i\bar{l}}|^2 & -\mathbb{S}_{k\bar{l}}\mathbb{S}_{i\bar{l}} \\ -\mathbb{S}_{i\bar{l}}\mathbb{S}_{k\bar{j}} & -\mathbb{S}_{k\bar{l}}\mathbb{S}_{k\bar{j}} & -\mathbb{S}_{k\bar{l}}\mathbb{S}_{i\bar{l}} & 1 - |\mathbb{S}_{k\bar{l}}|^2 \end{bmatrix}$$

The $\alpha\beta$ MO overlap is

$${}_{H_2}\mathbb{S}_{\alpha\beta} = \begin{bmatrix} \mathbb{S}_{i\bar{j}} & \mathbb{S}_{i\bar{l}} \\ \mathbb{S}_{k\bar{j}} & \mathbb{S}_{k\bar{l}} \end{bmatrix} = \begin{bmatrix} 0.552363547 & 0.833603386 \\ 0.833603386 & -0.552364588 \end{bmatrix}$$

Evaluation yields

$${}_{H_2}\mathcal{S}_{SD}^2 = \begin{bmatrix} 0.6948945 & -0.4604521 & -0.4604521 & -0.6948945 \\ -0.4604521 & 0.3051054 & 0.3051054 & 0.4604521 \\ -0.4604521 & 0.3051054 & 0.3051054 & 0.4604521 \\ -0.6948945 & 0.4604521 & 0.4604521 & 0.6948945 \end{bmatrix}$$

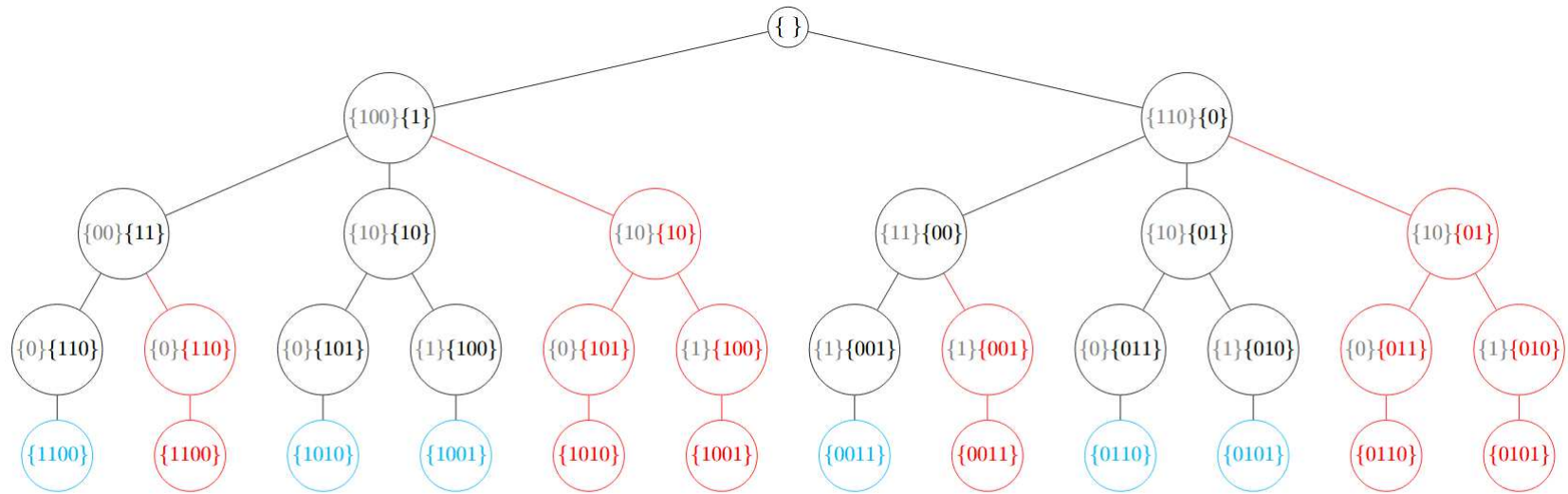
Note the spin contamination reflected in the $\langle \psi_0 | \mathcal{S}^2 | \psi_0 \rangle$ matrix element. One can find the eigenvalues and eigenvectors of \mathcal{S}^2 matrix with standard linear algebra packages (e.g. LAPACK). Singular value decomposition (SVD) is applied here.

```

=====
Performing SVD
=====
Singular (Sigma) Eigenvalues of S^2 matrix in descending order:
      1      2      3      4
  1  2.000000  0.000000  0.000000  0.000000
  2  0.000000  0.000000  0.000000  0.000000
  3  0.000000  0.000000  0.000000  0.000000
  4  0.000000  0.000000  0.000000  0.000000
Left (U) eigenvectors of S^2 matrix:
      1      2      3      4
  1 -0.589446 -0.778919  0.044961 -0.209325
  2  0.390581 -0.454472 -0.662860  0.448908
  3  0.390581 -0.359774  0.747311  0.399418
  4  0.589446 -0.239381 -0.010999 -0.771446

```

Fig. A.1.: Output for a spin-adapted UHF solution: H_2 at 1.5 \AA



Unique Path. Unique Permutation. Duplicate Path/Permutation. Sub-Array of Remaining Elements.

Note: Select the leftmost index of the sub-array and stack its corresponding element to the right of the unique path array.

Fig. A.2.: Permutation tree for array {1100} with sub-arrays

Colophon

This thesis was typeset with $\text{\LaTeX}2_{\epsilon}$. It uses the *Clean Thesis* style developed by Ricardo Langner. The design of the *Clean Thesis* style is inspired by user guide documents from Apple Inc.

Download the *Clean Thesis* style at <http://cleanthesis.der-ric.de/>.

Curriculum Vitae

Education

University of California, Merced

Ph.D. Chemistry

Merced, California

Aug 2018 – Dec 2023

La Sierra University

B.S. Biochemistry

Riverside, California

Aug 2014 – Jun 2017

Riverside City College

Riverside, California

Jun 2012 – Jun 2014

Research Experience

UC Merced | Department of Chemistry and Biochemistry

Jun 2018 – Present

Graduate Student Researcher | Advisor: Hrant P. Hratchian

La Sierra University | Department of Chemistry and Biochemistry

Jun 2015 – Jun 2017

Undergraduate Student Researcher | Advisor: Marco M. Allard

Publications

A.Y. Zamani and H.P. Hratchian. " Δ -based composite models for calculating X-ray absorption and emission energies." *J. Chem. Phys.* Accepted (2023)

A.Y. Zamani and H.P. Hratchian. "Estimating vertical core excitation energies from Møller Plesset theory with spin projection." *in prep* (2023)

H.H. Corzo, A.E. Hillers-Bendtsen, A. Barnes, A.Y. Zamani, F. Pawlowski, J. Olsen, P. Jørgensen, K.V. Mikkelsen and D. Bykov. "Coupled Cluster Theory on Modern Heterogeneous Supercomputers." *Front. Chem.* **11**, 1154526 (2023)

A.Y. Zamani and H.P. Hratchian. "Assessing the performance of Δ SCF and the diagonal second-order self-energy approximation for calculating vertical core excitation energies." *J. Chem. Phys.* **157**, 084115 (2022)

Presentations

West Coast Theoretical Chemistry Meeting | Davis, CA | Poster

May 2023

Advanced Light Source User Meeting | Virtual | Poster

Aug 2022

10th Conference on Molecular Quantum Mechanics | Blacksburg, VA | Poster

Jun 2022

ACS National Meeting | San Diego, CA | COMP: Contributed Talk

Mar 2022

ACS National Meeting | San Diego, CA | COMP & Sci-Mix Poster

Aug 2019

Selected Honors and Awards

Chemistry and Chemical Biology Summer Research Fellowship | UC Merced

2019 - 2020

Chemistry Graduate Student Travel Award Fellowship UC Merced	2019
Competitive Edge Summer Bridge Fellowship UC Merced	2018
Leland Wilson Memorial Chemistry & Biochemistry Scholarship La Sierra U.	2017
Greater Riverside Dollars for Scholars Scholarship	2012

Teaching Experience

UC Merced Department of Chemistry and Biochemistry	<i>Aug 2018 – Present</i>
Graduate Teaching Assistant	
<ul style="list-style-type: none"> ○ CHEM 001 – Preparatory Chemistry ○ CHEM 002, 010 – General Chemistry I, II ○ CHEM 112 – Quantum Chemistry and Spectroscopy 	
La Sierra University Department of Chemistry and Biochemistry	<i>Jun 2015 – Jun 2017</i>
Undergraduate Teaching Assistant	
<ul style="list-style-type: none"> ○ CHEM 281L, 282L, 283L – Organic Chemistry I, II, III Laboratory 	

Service Activities

Competitive Edge Summer Bridge Program Graduate Mentor	<i>Jul 2022 – Aug 2022</i>
Assisting incoming students with their transition into graduate studies at UC Merced	
ACS National Meeting San Diego, CA COMP Session Presider	<i>Aug 2019</i>
Symposium – <i>Exploring Transition Metal Chemistry & Spectroscopy with Quantum Chemistry</i>	
Science Outreach Volunteer	<i>May 2017 – May 2019</i>
Chemistry demonstrations at CA elementary schools – Weaver USD (May 2017), Alvord USD (May 2019); Science Fair Volunteer – Donn B. Chenoweth Elementary School (Nov 2018)	